

Copyright

by

Fernando Valentin Ulloa Barbaran

2002

**COMPOSITE STRUCTURAL MEMBERS FOR  
SHORT SPAN HIGHWAY BRIDGES**

by

**Fernando Valentin Ulloa Barbaran, B.S., M.S.**

**Dissertation**

Presented to the Faculty of the Graduate School of  
the University of Texas at Austin  
in Partial Fulfillment  
of the Requirements  
for the Degree of

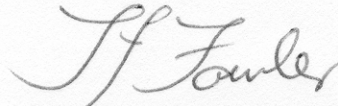
**Doctor of Philosophy**

The University of Texas at Austin  
May 2002

The Dissertation Committee for Fernando Valentin Ulloa Barbaran  
Certifies that this is the approved version of the following dissertation:

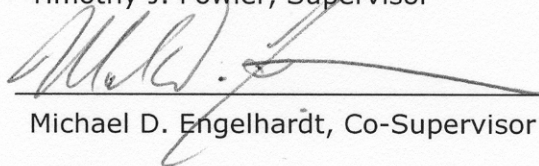
**COMPOSITE STRUCTURAL MEMBERS FOR  
SHORT SPAN HIGHWAY BRIDGES**

**Committee:**



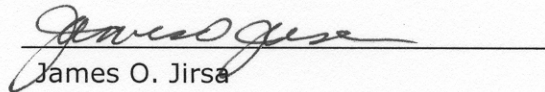
---

Timothy J. Fowler, Supervisor



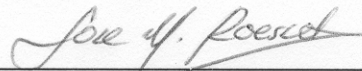
---

Michael D. Engelhardt, Co-Supervisor



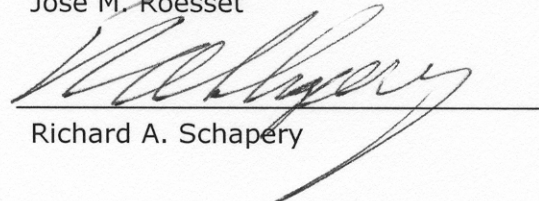
---

James O. Jirsa



---

José M. Roesset



---

Richard A. Schapery

## **Dedication**

*To my parents, my wife and my daughter*

## **Acknowledgements**

I wish to express my gratitude and appreciation to Professor Timothy Fowler, for his guidance, friendship and support throughout the course of this research. Working under his supervision has been a very unique learning experience. His patience and great sense of humor always helped, especially during difficult times. I also thank his wife Marie for all the attentions throughout this time.

I wish to express my thanks to Dr. Roesset and Dr. Engelhardt, both provided advice, help and encouragement at critical times during the course of this research. I thank Dr. Jirsa and Dr. Schapery for their help along the way.

Financial support for this project was provided by the Texas Department of Transportation. Special thanks to Ronald Medlock and Mike Smith for all the encouragement received during this time.

I also wish to acknowledge the technical support received from the following people:

Ethan A., Love and Frank Mayfield of Fibergrate.

Frank Pickering and Jim Justis of I.K.G.

Glenn Barefoot of Strongwell.

Hossein Arian and Bob Currie of Fiber Glass Systems.

Jess A. Richter of Tankinetics.

Bert Kriekemans of Structural Composites Inc.

Mac Puckett of Dow Chemical and Carol Manheim of Vetrotex CertainTeed.

Professor Paul Ziehl, my best friend, you were always there in good times and bad. Thanks a lot for all the support throughout this time. I wish you the very best and more.

Professor Charles Bowen, your support is greatly appreciated.

Nat, it is good to know that the future of AE and NN is in very capable hands.

Blake Stassney, Wayne Fontenot, Mike Bell, Ray Madonna and all the helpful and friendly staff at the FSEL, your help is greatly appreciated.

My friends at the FSEL, the list is too long to mention everyone.

I am indebted to my wife Akemi, for her constant love, endless support and understanding. I have always been able to count on you.

To my daughter Kristie, for all the happiness she brought home when she "moved in" a year ago. You have been a source of continuous inspiration ever since.

To my parents, I wish I could be as good a parent as you both are.

Fernando Ulloa

May 2002

# **COMPOSITE STRUCTURAL MEMBERS FOR SHORT SPAN HIGHWAY BRIDGES**

Publication No. \_\_\_\_\_

Fernando Valentin Ulloa Barbaran, Ph.D.  
The University of Texas at Austin, 2002

Supervisor: Timothy J. Fowler  
Co-Supervisor: Michael D. Engelhardt

This research focused on the development of a structural system composed of a reinforced concrete (RC) deck and fiber reinforced plastic (FRP) girders and arches. The deck and the girders were designed to carry the load by means of composite action. This system can be used in applications such as short span bridges. The research study involved both experimental and analytical work.

In all, six full-scale specimens were tested. Each specimen was composed of an RC deck and an FRP component, i.e. girder, arches. The length of each specimen was 30 ft, with a clear span between supports of 28.5 ft. The RC deck had an average width of 4 ft., and a thickness of 6 in. Both short and long term loading was considered.

Pultruded and contact molded FRP girders were utilized. A pair of arches assembled with filament wound FRP pipes also was studied as an alternative to the girders.

Based on the experimental results, the structural system proposed was found to be suitable for short span bridge applications. Furthermore, the excellent corrosion resistance of the FRP makes this system ideal for applications in corrosive environments.

Finally, the experimental data was used to develop design recommendations for the proposed structural system.



# Table of Contents

<b>Chapter 1: Introduction</b>	<b>1</b>
1.1 Overview	1
1.2 Objective of Research	2
1.3 Structural Plastics	2
1.4 Scope of Research	5
1.5 Chapters Outline	6
1.6 References	8
<b>Chapter 2: Literature Review</b>	<b>9</b>
2.1 Overview	9
2.2 Historical Background	9
2.3 Applications	14
2.3.1 Bridges	14
2.3.1.1 Footbridges	15
2.3.1.2 Road Bridges	21
A. Road Bridges	21
B. FRP Tendons	25
2.3.1.3 Decks	26
2.3.2 Repair and Retrofit	29
2.3.2.1 Sheets	29
2.3.2.2 Column Wrap	30
2.3.2.3 Patching	31
2.3.3 Nonstructural Applications	32
2.3.3.1 Markers and Barriers	33
2.3.3.2 Signs	33
2.3.4 Reinforcing Bars and Prestressing Tendons	33
2.3.4.1 Reinforcing Bars	33
2.3.4.2 Cables, Tendons	34
2.3.5 Pipes and Manholes	35

2.3.5.1 Pipes	35
2.3.5.2 Manholes	36
2.3.6 Secondary Structures (flagpoles, light poles, guard rail, sign supports, traffic signals, etc.)	36
2.3.6.1 Flagpoles	36
2.3.6.2 Light Poles	37
2.3.7 Other Applications	37
2.3.7.1 Transportation Equipment	37
A. Aircraft Industry	38
B. Mass Transit	38
C. Trucks	38
D. Cars	39
E. Trains	39
F. Recreational	39
2.3.7.2 Pressure Vessels, Tanks	39
2.3.7.3 Stacks	39
2.3.7.4 Oil Platforms	40
2.3.7.5 Industrial	40
2.3.7.6 Medical	40
2.3.7.7 Sporting Goods	40
2.3.7.8 Enclosures	41
2.4 Glossary	41
<b>Chapter 3: Experimental Procedures</b>	<b>50</b>
3.1 Overview	50
3.2 Materials	50
3.2.1 RC Deck	51
3.2.2 FRR Components	51
3.3 Specimens	52
3.4 Data Acquisition System and Instrumentation	54
3.4.1 Data Acquisition System (DAS)	55

3.4.2 Instrumentation	58
3.4.2.1 Strain Gages (SG)	58
3.4.2.2 Linear Potentiometers (LP)	60
3.4.2.3 Load Cells (LC)	61
3.4.2.4 Acoustic Emission (AE) Sensors.	63
3.5 Test Setup	63
3.6 Summary	66
<b>Chapter 4: Isophthalic Polyester Pultruded Fiber Reinforced Plastic Girder</b>	<b>67</b>
4.1 Overview	67
4.2 General Description	67
4.3 Material Properties	77
4.3.1 FRP Pultruded Girder	77
4.3.2 RC Deck	88
4.4 Structural Analysis and Design	89
4.5 Instrumentation	90
4.6 Loading	93
4.7 Results and Discussion	93
4.8 Significant Findings	102
4.9 Summary	103
<b>Chapter 5: Isophthalic Polyester Pultruded Fiber Reinforced Plastic Girder With Carbon Fiber Reinforced Plastic Strip</b>	<b>104</b>
5.1 Overview	104
5.2 General Description	104
5.3 Material Properties	108
5.3.1 FRP Pultruded Girder	108
5.3.2 RC Deck	109
5.3.3 CFRP Strip	109
5.4 Structural Analysis and Design	109

5.5 Instrumentation	110
5.6 Loading	110
5.7 Results and Discussion	113
5.7.1 Specimen with Tubes on Girder Bottom Flange	113
5.7.2 Specimen with Tubes on Girder Bottom Flange Removed	120
5.8 Significant Findings	122
5.9 Summary	122
<b>Chapter 6: Vinyl Ester Pultruded Fiber Reinforced Plastic Girder</b>	<b>124</b>
6.1 Overview	124
6.2 General Description	124
6.2.1 Specimen IKG1	126
6.2.2 Specimen IKG2	130
6.3 Material Properties	130
6.3.1 FRP Pultruded Girder	132
6.3.2 RC Deck	141
6.4 Structural Analysis and Design	144
6.5 Instrumentation	145
6.6 Loading	145
6.7 Test Results	150
6.8 Significant Findings	153
6.9 Summary	154
<b>Chapter 7: Vinyl Ester Pultruded Hybrid Fiber Reinforced Plastic Girder</b>	<b>155</b>
7.1 Overview	155
7.2 General Description	155
7.2.1 Specimen SW1	157
7.2.2 Specimen SW2	158

7.3 Material Properties	160
7.3.1 FRP Pultruded Girder	161
7.3.2 RC Deck	171
7.4 Structural Analysis and Design	171
7.5 Instrumentation	178
7.6 Loading	178
7.7 Test Results	184
7.8 Significant Findings	187
7.9 Summary	187
<b>Chapter 8: Vinyl Ester Fiber Reinforced Plastic Contact Molded Girder</b>	<b>189</b>
8.1 Overview	189
8.2 General Description	189
8.3 Material Properties	196
8.3.1 FRP Pultruded Girder	196
8.3.2 FRP Pipe	198
8.3.3 RC Deck	198
8.4 Structural Analysis and Design	198
8.5 Instrumentation	200
8.6 Loading	203
8.7 Results and Discussion	203
8.7.1 Load Deflection Behavior	203
8.7.2 Failure	207
8.7.3 Strain Behavior	213
8.8 Significant Findings	223
8.9 Summary	223
<b>Chapter 9: Tied Arch Fabricated From Epoxy FRP Pipes</b>	<b>225</b>
9.1 Overview	225

9.2 General Description	225
9.3 Material Properties	237
9.3.1 FRP Pipes	237
9.3.2 RC Deck	242
9.4 Structural Analysis and Design	243
9.5 Instrumentation	244
9.6 Loading	245
9.7 Results and Discussion	248
9.8 Significant Findings	262
9.9 Summary	262
<b>Chapter 10: Design Of Fiber Reinforced Plastic Structural Members</b>	<b>264</b>
10.1 Overview	264
10.2 Structural Analysis	264
10.3 Failure Criteria	266
10.3.1 Maximum Strain Criterion	266
10.3.2 Maximum Stress Criterion	268
10.3.3 Tsai-Wu Criterion	269
10.4 Viscoelastic Behavior	271
10.4.1 Creep	271
10.4.2 Relaxation	271
10.4.3 Viscoelastic Models	272
10.4.3.1 Spring-Dashpot Models	272
10.4.3.2 Findley's Model	275
10.4.3.3 Boltzmann's Superposition Principle	277
10.5 Stability	279
10.5.1 Overall	279
10.5.2 Creep Buckling	279
10.5.3 Local Buckling	279
10.6 ASTM Testing Methods	280

10.7 Allowable Design Factors	281
10.8 Summary	285
<b>Chapter 11: Summary, Conclusions, and Recommendations</b>	<b>286</b>
11.1 Overview	286
11.2 Objective of Research Study	286
11.3 Experimental Program Summary	286
11.4 Conclusions and Recommendations	287
11.5 Design Recommendations	290
11.6 Other Observations	291
11.7 Future Research	292
<b>References</b>	<b>293</b>
<b>Vita</b>	<b>301</b>

# **Chapter 1**

## **Introduction**

### **1.1 Overview**

The state of the bridge infrastructure in the U.S. is of major concern. Over a third of the nation's bridges are in serious disrepair or functionally obsolete. A large number of these bridges need to be strengthened, retrofitted, or simply replaced with a new structure (Saadatmanesh, 1998). Many of the proposed solutions are only temporary and few of them address the underlying problem of long term corrosion or degradation, which is inherent to the conventional materials used in bridge construction, i.e. reinforced concrete, steel, and timber. In addition, most of the suggested remedies tend to increase installation and maintenance costs. Clearly new alternatives are to be sought.

Development of new bridge technology that provides durable bridges at reasonable cost is a research topic of great interest to a wide range of researchers in the civil engineering field. A number of solutions have been suggested. Among them is the use of fiber reinforced plastics (FRP) materials. Extensive research on the use of FRP in repairing and strengthening of bridges has been done in recent years. One typical way of using FRP in strengthening bridges is by attaching FRP plates to the tension face of RC girders and decks. These FRP plates provide an increase in stiffness and load capacity of the structure.

Although limited, some work has been reported on bridges having FRP components as part of its structural system. These FRP components have been used as girders and decks mainly for short span bridges.



## **1.2 Objective of Research**

Investigate, by literature review and experimental studies, the technical feasibility of utilizing structural plastic materials for the primary structural members in an economically viable short span highway bridge.

## **1.3 Structural Plastics**

The American Society of Civil Engineers (ASCE) defines a structural plastic as "Any load-carrying member or assembly where plastics, plain or reinforced, undergo computable stress, either as a single material or as an element in conjunction with other materials". Approximately 77 billion pounds of plastic were manufactured in the United States in 1996. Under the broad ASCE definition, approximately 2/3 of this production was used as a structural plastic. It is estimated that 12 billion pounds were used by the construction industry.

Plastics are a large, complex, constantly developing group of materials, which present the structural engineer with a combination of often unfamiliar and unique advantages and limitations. These synthetic organic high polymers range in strength and stiffness from soft and flexible to hard and rigid. They may be used in their pure unaltered states, or they may be modified by additives and reinforcements that profoundly change their characteristics. They may be expanded into lightweight foams. On a strength-to-weight basis, composites can provide the most efficient structural materials available to the engineer. Conversely, they may easily fail if not properly designed and employed.

The largest portion of the 12 billion pounds of plastic used in construction is for pipe applications. In this category, sewer, gas, water, and drainage pipe, electrical conduit, and bathroom and sanitary fittings are the

most important uses. Other applications of plastics in construction are siding, insulation, flooring, windows and doors, wallboard, prefabricated homes, and security and other types of glazing. None of these uses are classic structural engineering applications. Other disciplines have used composites as the principal structural material. In the transportation field weight is a very important factor, and composites are used for the primary structure in items such as mass transit vehicles, stealth fighter aircraft, and commercial airliners. Sports equipment such as skis, tennis rackets, golf clubs, and fishing poles is almost entirely made from structural plastics. In corrosive environments of the type found in industry, composite tanks, pressure vessels, and other containers are common.

Structural plastics are among the most promising and potentially useful materials available to the engineering profession, yet they also represent a major unresolved challenge. It is generally acknowledged that these relatively new materials have not come near to realizing their great potential in structural applications where they would be both efficient and cost effective. Even though they are now in wide and successful use elsewhere, structural applications tend to be specialized and scattered. A number of reasons have been suggested for the slow rate of acceptance of composites in structural engineering applications.

- The structural behavior of plastics reflects a number of characteristics different from those of the usual metal, lumber, and concrete materials familiar to the structural engineer.
- A bewildering array of materials encompassed by the terms plastics. The American Society for Testing and Materials (ASTM) Standard D 1600 list over 100 different plastic materials. Each one of these plastics is a separate material with distinct and unique properties. In addition, ASTM D 1600 lists 40 blends and alloy of plastics. Most plastics have a number of different grades, can be reinforced with

fibers or particulates, and can be used in combination with various fillers. The result is that the structural engineer is faced with over 1000 different materials to choose from.

- Technical information is not available in a form that structural engineers can use for design. A particularly important issue is the lack of codes, standards, and design guides.
- Structural plastics have not proved themselves in broad service and still represent a venture each time used.
- There is insufficient economic incentive to plastics materials suppliers to develop products. Structural engineering products require a long lead time for development and proof testing and represent a relatively small increment in total plastics sales.

The issues listed above have been addressed by a number of organizations. ASCE has made a particularly strong effort to address the first three items through the work of the Structural Plastic Research Council (SPRC) and the Structural Composites and Plastics Technical Committee (SCAP) of the Materials Engineering Division. A review of the literature on the use of composites for structural engineering applications shows that one reference, ASCE Manual No. 63, Structural Plastics Design Manual, stands well above the rest in importance. The manual, which was developed under the auspices of SPRC, was funded by the Federal Highway Administration, the Urban Mass Transportation Administration, and the U.S. Department of Housing and Urban Development, together with a number of major plastics manufacturers. The manual addresses material behavior, design criteria, analytical techniques, design methods, and structural systems, and serves as the principal reference for design of composite structures. Two additional ASCE documents, Manual No. 66, Structural Plastic Selection Manual, and "A Report on Current Practice in Structural Plastic Connections" complement the Design Manual.

Federal Government research funding has attempted to address the last two items listed above. The National Institute of Standards and Technology (NIST), the National Science Foundation (NSF), and the Department of Defense, Advanced Research Projects Agency (ARPA) have all funded major programs in the area of composites. These programs are primarily aimed at demonstrating the technology. Of particular interest is ARPA funding for development of a highway bridge by Lockheed Martin Missile and Space Company. Under this project a prototype highway bridge was built and tested at Lockheed's facility at Palo Alto, CA. NSF has funded a Center of Excellence at the University of Delaware. NIST has funded a number of defense conversion programs to translate aerospace composite technology to civilian applications. The Ferguson Structural Engineering Laboratory participated with Northrop Grumman to develop an offshore deep-water drilling riser.

#### **1.4 Scope of Research**

This research presents development of a structural system composed of a reinforced concrete (RC) deck and a fiber reinforced plastic (FRP) component. This structural system can be used in short span highway bridge applications. The FRP component features two configurations: girders and arches. The FRP components were pultruded and contact molded for the girders and filament wound for the arches.

The structural system combine conventional reinforced concrete and new reinforced polymeric materials. The objective is a long lasting and efficient solution that can be utilized for short span bridge applications.

In all, six full-scale specimens were considered. The specimens had an RC deck with an average width of 4 ft. The average depth of the specimens was 20 in., and the overall length was 30 ft. Five of these specimens were

designed to have the RC deck and the FRP girder working in composite action. For the remaining specimen, composite action was not considered in its design.

Both short and long-term loading was considered. The long-term loading was considered in order to study the creep behavior of the structural system.

In addition to the six full-scale specimens, a number of other smaller specimens were tested in order to determine properties of specific FRP components. These tests ranged from a four-point bending of a 30 ft. long girder without an RC deck to compression tests on FRP pipes of short length.

The experimental study was conducted at the Ferguson Structural Engineering Laboratory at the University of Texas at Austin. Funding was provided by the Texas Department of Transportation (TxDOT) under research project 0-1773.

## **1.5 Chapters Outline**

Chapter 2 presents a summary of applications using FRP structural members in bridge design. Other civil engineering FRP applications are also presented.

Chapter 3 describes the experimental program. The instrumentation, data acquisition system, and test setup.

Chapters 4 and 5 describe specimens FG1 and FG2. The FRP component for both specimens was very similar in geometry and materials. The FRP girder for specimen FG2 had a carbon fiber reinforced plastic (CFRP) strip attached to its bottom flange, and additional shear connectors, with

respect to specimen FG1, placed on its top flange. Both specimens were tested under short term loading in four-point bending.

Chapter 6 describes specimen IKG1. This specimen was similar in geometry to specimens FG1 and FG2. The pultruded FRP girder was composed of different materials. Specimen IKG1 was tested under sustained loading for a period of seven months.

Chapter 7 describes specimen SW1. The pultruded FRP girder for this specimen had a cross section with an unconventional geometry. It featured a double web specially designed to resist buckling. Also, the flanges of the FRP girder were composed of a mixture of carbon and glass fiber reinforcement, increasing thus its flexural stiffness. Specimen SW1 was tested under a sustained loading for a period of seven months.

Chapter 8 describes specimen TK1. The FRP component for this specimen was a contact molded FRP girder with a trapezoidal cross section constant in the middle third, and with the end portions tapered from the middle toward each end. Specimen TK1 was tested under short term loading in four-point bending.

Chapter 9 describes specimen FGS12. This specimen featured an RC deck and two FRP arches, the RC deck rested on the arches and composite action was not considered. The arches were made from FRP pipes used in the oil industry. Specimen FGS1 was tested under short term loading in four-point bending.

Chapter 10 presents design guidelines for the structural system developed in this research. These design guidelines are based on the results from the experimental program.

Chapter 11 briefly summarizes the results and findings on this research. It also recommends issues for future research associated with this kind of structural systems for applications in short span bridge design.

## **1.6 Summary**

This chapter presented an overview, objective and a scope of research for this study. It also presented a comprehensive description of structural plastic materials used for various structural applications.

## **Chapter 2**

### **Literature Review**

#### **2.1 Overview**

The civil engineering profession has an interest in the use of fiber reinforced plastics (FRP) materials. This interest is particularly strong in both the government and commercial sectors of the industry. FRP materials are of special interest to bridge engineering since there are a great number of bridges that need to undergo major maintenance or to be replaced by new structures. The use of FRP materials for either of these tasks is very attractive since these materials offer a number of advantages with respect to traditional materials such as reinforced concrete (RC) and steel.

FRP materials, however, have inherent disadvantages. Thus the design of structural systems featuring FRP structural shapes becomes an engineering challenge. The currently used design approach combines knowledge of composite materials from applications in aerospace engineering and structural engineering. Cost is a significant factor in bridge design but less so in aircraft systems. Affordable manufacturing and assembly methods are needed to produce efficient civil engineering applications.

This chapter will present a number of applications that have been reported to date. These applications are mainly in the field of bridge engineering, however, other civil engineering applications are also presented.

#### **2.2 Historical Background**

The earliest applications of structural plastics for civil engineering structures date back to the late 1950s. A "House of the Future" designed



entirely with structural plastics was presented by Whittier (1957) as part of an exhibit built at Disneyland in Anaheim, California, see Figure 2.1. Two years later, structural plastics were used for the construction of the U.S. Pavillion as part of the American Exhibition in Moscow (Dietz, 1969, *Modern Plastics*, 1959), see Figure 2.2. A comprehensive review of early structural applications of structural plastics is contained in the ASCE Manual of Engineering Practice No. 47 (ASCE, 1967)

However, the use of FRP materials for civil engineering applications has been limited due to the lack of comprehensive design guidelines (ASCE, 1984). In order to be accepted in the civil engineering profession, composites must be competitive in cost with conventional materials. The improved corrosion resistance and other advantageous properties of composites add value to the product. However, this additional value may be relatively small. This contrasts with the aerospace industry, which places emphasis on weight reductions. The need to reduce costs in civil structures has a major influence in design and fabrication methods. One of the early civil engineering structures using FRP was a footbridge designed and built in 1977 at the University of Virginia (McCormick, 1986). This bridge used a low cost winding process to fabricate the triangular truss structure. Figures 2.3 and 2.4 show the Virginia footbridge.

For pressure vessels and piping applications, where corrosion protection is a primary concern, FRP materials have also been used extensively (ASME, 1992 and 1998). FRP vessels provide an economical means for storage of many chemicals, which are highly corrosive to metals, and for other fluid storage applications where external environments are corrosive (Heger, 1970).

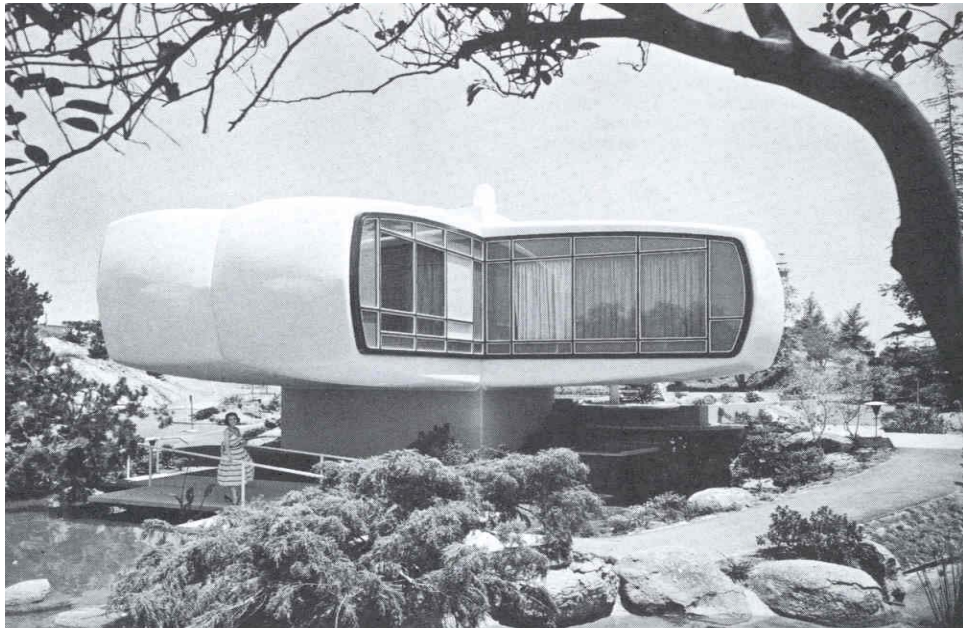


**Figure 2.1.** House of the Future (Dietz, 1969).



**Figure 2.2.** American Exhibition in Moscow, 1959 (Dietz, 1969).



**Figure 2.3.** Virginia Footbridge. Set in Place (McCormick, 1986).

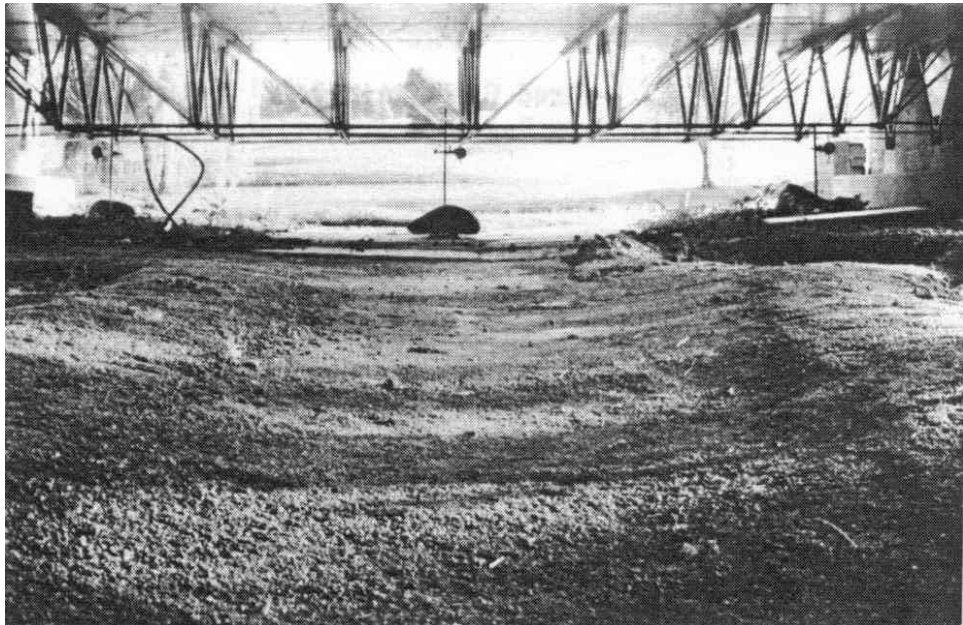


**Figure 2.4.** Virginia Footbridge. Finished (McCormick, 1986).

The first tanks were installed in process plants in the 1950s. In the mid 1990s, one of these tanks was still operating as designed in a St. Louis plant (Fowler, 2002).

Fiber reinforced composites have been consistently used in other fields of engineering since the late 1960s. In aerospace and automotive industries, the widespread use of high strength, lightweight materials results in significant fuel savings and the possibility of increasing the payload. Airplane and automobile parts that were traditionally fabricated using steel and aluminum are being replaced with composites (Mallick, 1993). Other fields such as the boating industry and sporting goods industry have also benefited from the use of FRP materials. The many structural applications include wind turbine blades, manlift beams, ladders, and sewer pipe.

In civil engineering, the use of composites is only beginning to gain acceptance because composite materials have not been economically competitive with traditional building materials such as steel and concrete. The use of these materials for the repair and strengthening of the aging infrastructure provides an interesting alternative to traditional methods, because of their high strength-to-weight ratio, corrosion resistance, and excellent fatigue performance. Although the technology of the use of composites in the aerospace industry has advanced significantly over the last 30 years, methods for their application to strengthen existing structures are still being researched.

To assess the applicability of composite materials for the bridge infrastructure in the United States, the Federal Highway Administration conducted a scanning tour of the United Kingdom, Switzerland, Germany, and Japan, where composites had already been used to strengthen existing bridges (FHWA, 1997). During this survey, applications that did not require modification for use in the United States were identified. In addition, areas

where further research was needed before the technology could be implemented in field applications were highlighted.

A useful source of technical data on composites, manufacturing techniques, and applications in civil engineering structures is given in *Composites for Infrastructure* by Hazen and Bassett (1998). Dufton (1997) also gives a comprehensive review of the use of polymers in building and construction.

## **2.3 Applications**

### **2.3.1 Bridges**

Presently, there is a potential market for FRP bridges because of the need to replace many of the nation's highway bridges, which have deteriorated through age, lack of maintenance, and typical wear for these kind of structures. At the present time, there are approximately 580,000 bridges in the U.S., and between 150 and 200 collapse partially or completely each year (ICCI 98, Vol. II, 1998).

Deterioration and structural safety of reinforced concrete (RC), timber, and steel bridges and the cost of their rehabilitation and repair have become a major concern among the structural engineering community. RC bridge deterioration is caused mainly by corrosion of reinforcing steel resulting from its exposure to highly humid climates, salt water environments, and deicing chemicals. The same agents also cause deterioration in steel bridge components. Several alternatives have been proposed as solutions to this problem. Among them, and perhaps the most promising alternatives involve the use of composites.

Several bridge applications have been developed using FRP composites as the primary material component. At this time (2002), there is no

information on the long term performance of these structures. These applications can be placed in two main groups: footbridges and road bridges.

Currently, composite materials such as FRP are being developed as possible replacements to conventional prestressing steel tendons and reinforcing steel bars. Glass fiber reinforced plastics (GFRP) composites were first used for prestressing experimental bridges about ten years ago in Germany. Other FRP composites using aramid fiber reinforced plastic (AFRP) and carbon fiber reinforced plastic (CFRP) are also being developed.

### **2.3.1.1 Footbridges**

Most of the applications of composites in bridges have been devoted to footbridge applications. These applications have a wide range of span lengths, and a variety of member shapes and arrangements. Many of the early footbridges were demonstration projects. Composite materials were chosen because the lighter weight results in less disruption to the environment. For example, construction of the bridge in Westminster Cathedral and the National Parks needed to be accomplished with minimum damage and disruption to the environment. Some of these applications are listed below.

1. Westminster Cathedral, London, UK, 1970 <sup>(ICCI 98, Vol. I, 1998)</sup>.  
Materials: E-glass/polyester.  
Description: two spans with U-shaped cross section.  
Dimensions: 80 ft.
2. Virginia, Virginia, U.S., 1977 <sup>(McCormick, 1985, 1986)</sup>. Figures 2.3, 2.4.  
Materials: E-glass/polyester.  
Description: triangular trussed girders connected by a top cover plate.  
Dimensions: 16 ft. long, 7 ft. wide.
3. Adolf Kiepert, Berlin, Germany, late 1980s <sup>(ICCI 98, Vol. I, 1998)</sup>.  
Materials: E-glass/polyester.  
Description: the superstructure has partial external prestressing without bond. Double-T cross section.  
Dimensions: 90.6 ft.

4. Lunen'sche Gasse, Dusseldorf, Germany, 1980 <sup>(ICCI 98, Vol. I, 1998)</sup>.  
 Materials: E-glass/polyester.  
 Description: single span with tendons. Tendons installed without bond.  
 Dimensions: 21.5 ft.
5. Chongqing cable-stayed, Chongqing, China, 1986 <sup>(ICCI 98, Vol. I, 1998)</sup>.  
 Materials: E-glass/polyester.  
 Description: contains GFRP box girder with cover plates.  
 Dimensions: 90 ft.
6. Guanyinqiao, Chongqing, China, 1988 <sup>(ICCI 98, Vol. I, 1998)</sup>.  
 Materials: E-glass/polyester.  
 Description: GFRP deck girders suspended from reinforced concrete rigid frames by high strength wires.  
 Dimensions: 515 ft.
7. Nagatsugawa, Chiba, Japan, 1989 <sup>(ICCI 98, Vol. I, 1998)</sup>.  
 Materials: Carbon/vinyl ester.  
 Description: simple slab 8.2 ft. wide and 26.2 ft. long, pretensioned with CFRP.  
 Dimensions: 26 ft. long, 8 ft. wide.
8. Dupont Country Club, Wilmington, Delaware, 1990 <sup>(ICCI 98, Vol. I, 1998)</sup>.  
 Materials: pressure-treated lumber, FRP and AFRP.  
 Description: bridge deck.  
 Dimensions: 30 ft.
9. Birdie, Mito, Japan, 1990 <sup>(WTEC, 2001)</sup>. Figure 2.5.  
 Materials: Carbon/vinyl ester.  
 Description: post-tensioned concrete suspended slab bridge. CFRP, AFRP suspension cables.  
 Dimensions: 178 ft. long, 6.5 ft. wide.
10. Hakui Kenmin, Ishikawa, Japan, 1992 <sup>(WTEC, 2001)</sup>.  
 Materials: Carbon/vinyl ester.  
 Description: hollow-slab pretensioned with CFRP tendons.  
 Dimensions: 24 ft. long, 11.5 ft. wide.
11. Aberfeldy, River Tay, Scotland, 1992 <sup>(Johansen, 1995, FHWA, 1997)</sup>. Figures. 2.6, 2.7.  
 Materials: Aramid FRP cables, Isophthalic polyester/GFRP box sections.  
 Description: World's first cable-stayed footbridge built entirely with composites. It has two A-shaped towers.  
 Dimensions: 370 ft. long, 207 ft. midspan, 7 ft. wide.



**Figure 2.5.** Birdie Footbridge (WTEC, 2001).

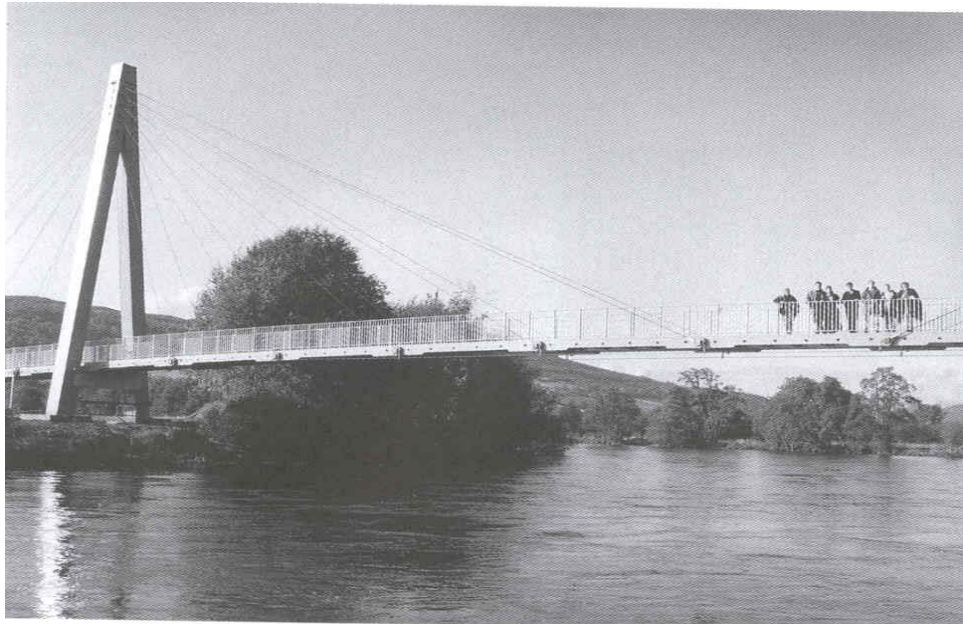


**Figure 2.6.** Aberfeldy Golf Club Footbridge (Johansen, 1995, FHWA, 1997).





**Figure 2.7.** Aberfeldy Golf Club Footbridge (Johansen, 1995, FHWA, 1997).

12. Olympic National Park (Washington), 1995 (Schwartz, 1996; CFI, 1998).  
 Materials: FRP E-glass/polyester pultruded shapes.  
 Description: X-braced FRP space frame supports a wooden deck.  
 Dimensions: 75 ft. long, 4 ft. wide.
13. Haleakala National Park, Maui, Hawaii, 1995 (Hull, 1996). Figure 2.8.  
 Materials: E-glass/polyester.  
 Description: pultruded channels and square tubes support the bridge every 10 ft.  
 Dimensions: 80 ft.
14. Daniel Boone Nat. Park, Bath County, Kentucky, 1997<sup>(SPI, 1996)</sup>. Figure 2.9.  
 Materials: E-glass, Carbon/Vinyl ester pultruded girders.  
 Description: The bridge is supported by E-glass/Vinyl ester rods and also uses 24 in. deep hybrid girders.  
 Dimensions: 60 ft.
15. Public Works, Tsukuba City, Japan, 1997 (FHWA, 1997, CFI 1998). Figure 2.10.  
 Materials: E-glass/vinyl ester, 70% reinforcement.  
 Description: Cable stayed bridge.  
 Dimensions: 65.6 ft. long, 6.6 ft. wide.



**Figure 2.8.** Haleakala Footbridge (Hull, 1996).



**Figure 2.9.** Daniel Boone National Park Footbridge (SPI, 1996).



**Figure 2.10.** Tsukuba Public Works Footbridge (FHWA, 1997, CFI 1998).



**Figure 2.11.** Kolding Bridge (CFI, 1998).

16. Kolding's, Kolding, Denmark, 1997 <sup>(CFI, 1998)</sup>. Figure 2.11.  
 Materials: E\_glass/polyester, 60%.  
 Description: Truss towers at third span hold FRP deck, composed of molded grating with FRP plates.  
 Dimensions: 131 ft. long, 10 ft. wide.
17. Greensbranch trail, Smyrna, Delaware, 1999 <sup>(Hardcore Tech. Lit., 2001)</sup>.  
 Materials: E\_glass/Epoxy.  
 Description: Self supported FRP deck.  
 Dimensions: 32 ft. long, 6 ft. wide.

### **2.3.1.2 Road Bridges**

The applications in this area are not as numerous as for the footbridges. Nevertheless, interesting applications have been reported and are presented below. It is expected that confidence in this type of structural system will build upon the success of the footbridges. The applications can be divided in two groups.

#### **A. Road Bridges**

1. Ginzi highway, Ginzi, Bulgaria, 1982 <sup>(Hollaway, 2001)</sup>. Figure 2.12.  
 Materials: Chop strand mat/resin.  
 Description: GFRP-I simply supported beams.  
 Dimensions: 33 ft. long.
2. Miyun highway, China, 1982 <sup>(Hollaway, 2001)</sup>.  
 Materials: GFRP.  
 Description: simply supported box girders with a honeycomb core.  
 Dimensions: 68 ft. long.
3. A19 Tees-Viaduct, Middlesbrough, England, 1989 <sup>(ICCI 98, Vol. I, 1998)</sup>.  
 Materials: GFRP.  
 Description: viaduct enclosure.  
 Dimensions: 384 ft. long.
4. Bonds Mill, Stonehouse, UK, 1994 <sup>(FHWA, 1997)</sup>. Figures 2.13, 2.14.  
 Materials: E-glass/epoxy.  
 Description: bascule vehicular traffic bridge. Six cell-box pultruded FRP girders were used.  
 Dimensions: 27 ft. long, 15 ft. wide, 2.8 ft. deep.

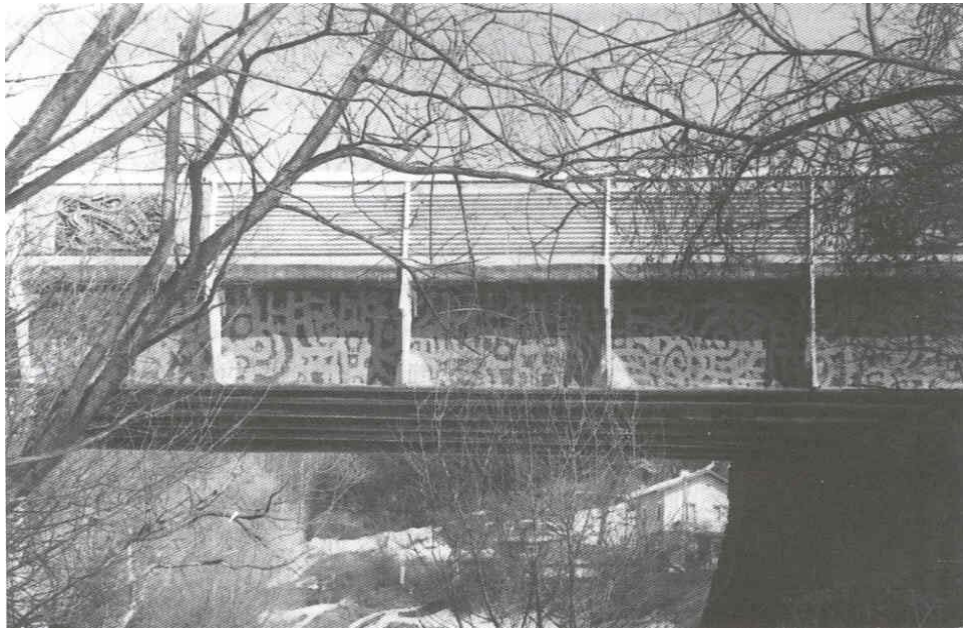


**Figure 2.12.** Ginzi Bridge (Hollaway, 2001).



**Figure 2.13.** Bonds Mill Bridge (FHWA, 1997).



**Figure 2.14.** Bonds Mill Bridge (FHWA, 1997).

4. Tom's Creek, Blacksburg, Virginia, 1997 (Lesko, Hayes, 1998). Figures. 2.15, 2.16.  
Materials: E-glass, Carbon/Vinyl ester.  
Description: FRP hybrid I-beams pultruded and wooden deck.  
Dimensions: 20 ft. long, 24 ft. wide.
6. Butler County, Ohio, 1997 (Scott, Wheeler, 2001, Foster, D.C., 1998).  
Materials: E-glass/polyester.  
Description: DursSpan™ deck: pultruded tubes FRP sheets. Deck and girders are bonded together.  
Dimensions: 33 ft. long, 24 ft. wide.
7. Buffalo Creek, McKinleyville, W. Virginia, 1997 (FHWA, 1997).  
Materials: E-glass/Epoxy.  
Description: FRP rebars in concrete deck.  
Dimensions: 178 ft. long (3 span continuous), 2 lanes of traffic.
8. Bennett's, West Union, New York, 1998 (Hardcore, Tech. Lit, 2001).  
Materials: E-glass/resin.  
Description: Self supported FRP bridge.  
Dimensions: 32 ft. long, 33 ft. wide.



**Figure 2.15.** Tom's Creek Bridge (Before Repair) (Lesko, Hayes, 1998).



**Figure 2.16.** Tom's Creek Bridge (After Repair) (Lesko, Hayes, 1998).

## B. FRP Tendons

1. Ulenborgstrasse, Dusseldorf, Germany, 1986 <sup>(FHWA, 1997)</sup>. Figure 2.17.  
Materials: GFRP.  
Description: deck with GFRP prestressing tendons.  
Dimensions: 84 ft.
2. Shinmiya highway, Ishikawa, Japan, 1988 <sup>(WTEC, 2001)</sup>.  
Materials: CFRP.  
Description: pretensioned concrete slab, pretensioned I-girders.  
Dimensions: 20 ft. long, 23 ft wide.
3. Bachi River highway, Kitakyushu, Japan, 1989 <sup>(WTEC, 2001)</sup>.  
Materials: CFRP.  
Description: post-tensioned and pretensioned girders.  
Dimensions: 117.5 ft. long, 40 ft. wide.
4. Oststrasse, Ludwigshafen, Germany, 1989 <sup>(ICCI 98, Vol. I, 1998)</sup>.  
Materials: CFRP.  
Description: two straight and two curved spans, post-tensioned.  
Dimensions: 279 ft. long.



**Figure 2.17.** Ulenborgstrasse Bridge <sup>(FHWA, 1997)</sup>.



5. Shieffersstrasse, Leverkusen, Germany, 1990 <sup>(FHWA, 1997)</sup>.  
Materials: GFRP.  
Description: pretensioned solid concrete slab with GFRP tendons.  
Dimensions: 174 ft. long.
6. Notsch road, Karnten, Austria, 1990 <sup>(ICCI 98, Vol. I, 1998)</sup>.  
Materials: GFRP.  
Description: pretensioned concrete slab with GFRP tendons.  
Dimensions: 144 ft.
7. Nasu, Nasu, Japan, 1990 <sup>(ICCI 98, Vol. I, 1998)</sup>.  
Materials: AFRP.  
Description: pretensioned concrete slab with AFRP tendons.  
Dimensions: 118 ft. long.
8. Southfield, Michigan, U.S., 1996 <sup>(ICCI 98, Vol. II, 1998, Herakovich, 1998)</sup>.  
Materials: GFRP.  
Description: pretensioned concrete slab with GFRP tendons.  
Dimensions: 144.4 ft.
9. Sumitomo, Tochigi, Japan, 1996 <sup>(WTEC, 1999)</sup>.  
Materials: GFRP.  
Description: pretensioned, postensioned box girder with GFRP tendons.  
Dimensions: 80 ft., 40 ft. long, 13 ft. wide.

### **2.3.1.3 Decks**

Another very active area of research is the development of FRP bridge decks, as well as the rehabilitation and repair of RC and steel bridge decks. FRP decks are lightweight, easy to transport and install, non-corroding, and fatigue resistant. Except for a few particular cases, replacing a bridge is a rather expensive endeavor. Normally, rehabilitation of the deck results in lower cost, and, with the right choice of materials, the live-load capacity and the service life of the structure can be improved. (ICCI 98, Vol. 1, 1998)

1. Washington Schoolhouse, Cecil County, Maryland, 1997 <sup>(Hardcore, Tech. Lit, 2001)</sup>.  
Materials: E-glass/Epoxy.  
Description: FRP deck.  
Dimensions: 20 ft. long, 25 ft. wide.

2. Laurel Lick Bridge, Lewis County, West Virginia, 1997<sup>(IPWEA, 2001)</sup>.  
Figure 2.18.  
Materials: Superdeck™, FRP WF girders.  
Description: Deck supported on FRP WF pultruded girders.  
Dimensions: 20 ft. long, 16 ft. wide.
3. Wickwire Run Bridge, Taylor County, West Virginia, 1998<sup>(IPWEA, 2001)</sup>.  
Figure 2.19.  
Materials: Superdeck™, steel I girders.  
Description: Deck supported on steel I girders.  
Dimensions: 30 ft. long, 32 ft. wide.
4. No Name Creek (Russell, Kansas) <sup>(CFI, 1998)</sup>.  
Materials: Chopped glass/isophthalic resin.  
Description: Sandwich deck with FRP honeycomb core.  
Dimensions: 23 ft. long, 27 ft. wide.
5. Wilson's, Chester County, Pennsylvania, 1998 <sup>(Hardcore, Tech. Lit, 2001)</sup>.  
Materials: E-glass/resin.  
Description: FRP deck.  
Dimensions: 65 ft. long, 16 ft. wide.
6. Troutville Weigh Station, Virginia, 1999 <sup>(IPWEA, 2001, Halloway, 2001)</sup>.  
Materials: E-glass, Carbon/Vinyl ester.  
Description: EXTREN<sup>R</sup> shapes and FRP plates deck supported on steel I girders.  
Dimensions: 15 ft. long, 15 ft. wide.
7. Mill Creek, Wilmington, Delaware, 1999 <sup>(IPWEA, 2001, Hardcore, Tech. Lit, 2001)</sup>.  
Materials: GFRP.  
Description: GFRP Hardcore composite deck on steel girders.  
Dimensions: 39 ft. long, 17 ft. wide.
8. Bentley's creek, Elmira, New York, 1999 <sup>(Hardcore, Tech. Lit, 2001)</sup>.  
Materials: GFRP.  
Description: GFRP Hardcore composite deck on steel girders.  
Dimensions: 140 ft. long (six panels), 25 ft. wide.



**Figure 2.18.** Laurel Lick Bridge (IPWEA, 2001).

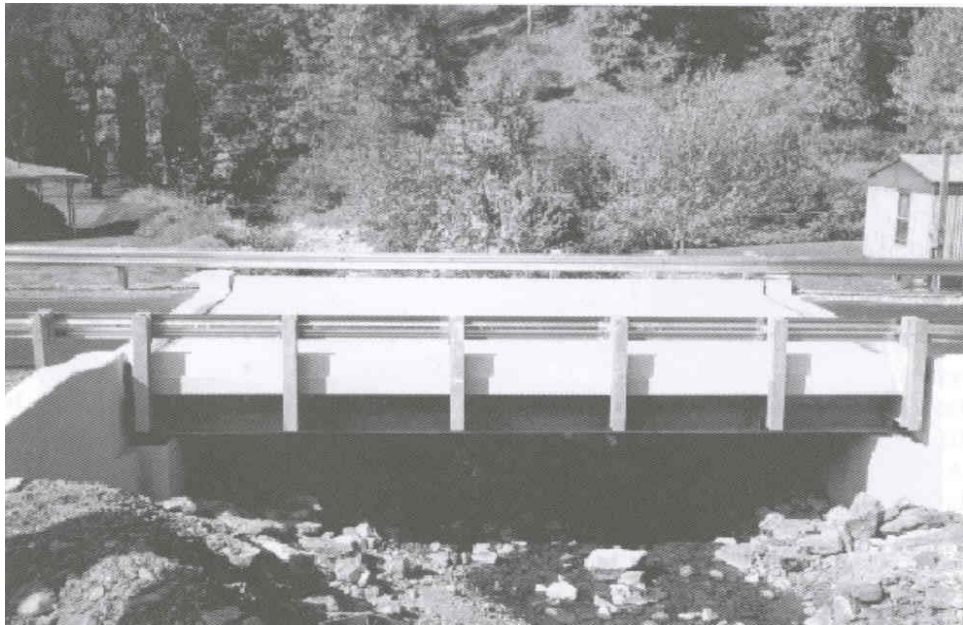


**Figure 2.19.** Wickwire Run Bridge (IPWEA, 2001).

### **2.3.2 Repair and Retrofit**

Traditional repair methods are being challenged by this new technology, which promises to lower the total installed cost of the repair. In fact, there are over 1000 field installations, worldwide, of FRP composite repair or strengthening systems with no reported failures. These installations are in Great Britain, Canada, France, Germany, Greece, Italy, Japan, Sweden, Switzerland, and the United States on such structures as beams, columns, decks/slabs, walls, arches, and tunnels. Many of these repairs were made to highway structures, buildings, and historical monuments (SPI Composites Institute, 1996). Teng (2002) gives a throughout coverage of the different techniques currently available for strengthening of RC structures with FRP.

#### **2.3.2.1 Sheets**

Strengthening by externally bonded FRP sheets is a relatively new technology. Its ease and speed of installation makes it very attractive in the repair of deteriorating civil structures. FRP sheets bonded to the tension face of RC beams supporting bridge decks increase the ultimate strength and stiffness of the repaired structural member (ICCI 98, Vol. 1, 1998).

University of Dayton Research Institute (UDRI) researchers have taken a set of 1000 pound, 8 ft. long steel-RC beams and determined their bending strength. Then, they have taken similar beams, glued graphite epoxy sheets weighing about a pound to their tension sides and have conducted the same tests. The result: a layer of graphite epoxy promoted a 65 percent increase in the strength of these concrete beams (University of Dayton News, 1995).

Repair of aging bridges is not the only application for this technique. For example, the University of Dayton suggests that the application of these composites could include the reinforcement of building walls to protect occupants from explosions or earthquakes (University of Dayton News, 1995). Obviously, this technique opens up many potential applications.

Recent research on the use of composites to repair aging bridges has been performed at the University of Texas at Austin (Breña, 2000).

### **2.3.2.2 Column Wrap**

A rather familiar sight these days is the deterioration of concrete pillars supporting bridges over heavily traveled highways. Dampness and exhaust fumes in the environment are the primary causes of steel reinforcement deterioration. Replacement of the columns can be very costly and complicated. In contrast, a method of enveloping the columns in a composite wrap has been shown to work remarkably well (ICCI 98, Vol. I, 1998).

One of the most difficult aspects of bridge maintenance is coping with the long-term structural effects of weather. After 20 to 30 years, the combination of road deicing chemicals and freeze/thaw cycles can wreak havoc on bridges, resulting in cracks, rebar corrosion, and concrete spalling. XXsys Technologies has developed Robo-Wrapper™, a hoop-wrapped jacketing system that uses a carbon fiber composite to retrofit corroded and structurally unfit bridges. After it is cured, the composite is three times stronger than steel but weighs less, strengthening and stiffening bridge columns to protect them from failure during earthquakes. Carbon fiber has very high strength. Carbon composites are not affected by water and alkalis and do not corrode. In several demonstrations, both in the field and in laboratory tests at the University of Utah and Utah State University, the technology has been shown to upgrade the load-carrying capacity of deteriorated and underdesigned bridges. In addition, numerous laboratory tests in the United States, Japan, and Europe have shown that strength and stiffness can be significantly increased in reinforced concrete members through the external application of very thin carbon-fiber composite plies (Liu, Silva, Nanni, 2001). Essentially, the carbon fiber wrap acts as an external stirrup, effectively increasing the diameter of the column.

### 2.3.2.3 Patching

Patching is a localized repair carried out on damaged structures. The method is widely used for bituminous and concrete roads. This includes the filling of potholes. When small areas of the road surface are badly cracked or sunken, patching repairs are carried out to provide a smooth surface and to prevent further damage by the action of traffic or water. Also, applications in this area include FRP patching for aesthetic reasons, repair of concrete cover, and structural upgrading. Some of these applications are presented below.

1. Foulk Road Bridge, 1995 (Hull, 1996) .  
Materials: CFRP sheets.  
Description: Rehabilitation of severely damaged bridge.
2. Alamo Cement Co., 1997 (Hull, 1996). Figure 2.20.  
Materials: Epoxy wrap  
Description: Rehabilitation of aging smokestacks.



**Figure 2.20.** Alamo Cement Co. Stacks (Hull, 1996).  
Repaired Stacks (Left), Top of Stack Before Repair (Right).

3. Caltrans bridge seismic retrofit program, 1997 <sup>(Hull, 1996)</sup>. Figure 2.21.  
Materials: CFRP strips.  
Description: Retrofit of various bridge elements to their original capacity.
4. Staunton route 4, 1997 <sup>(Hull, 1996)</sup>  
Materials: CFRP sheets  
Description: Rehabilitation of severely damaged bridge.

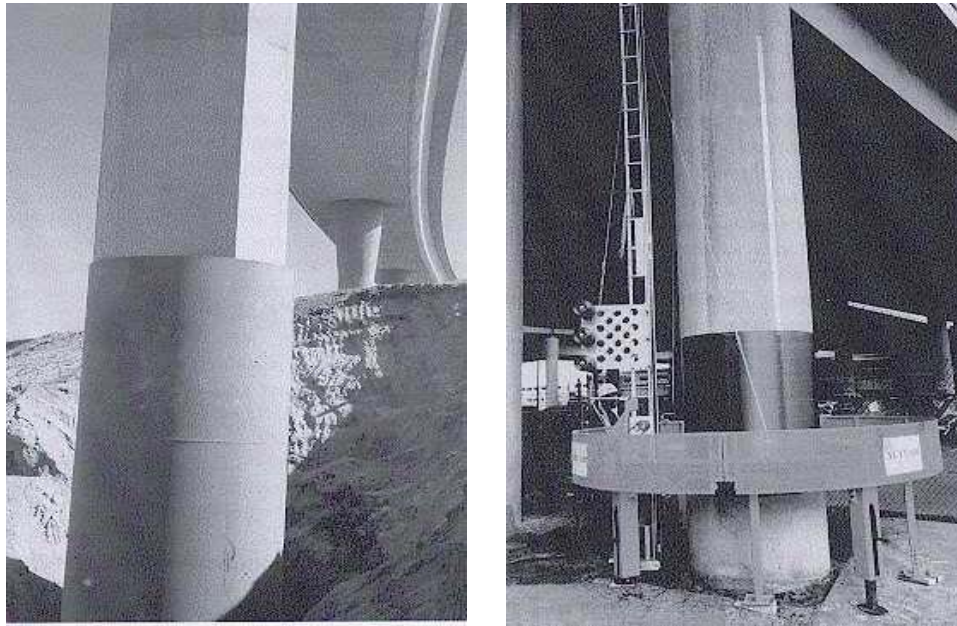


**Figure 2.21.** Caltrans Bridge Pier Retrofit <sup>(Hull, 1996)</sup>.

### **2.3.3 Nonstructural Applications**

There are numerous civil engineering applications of composites and plastics, although they do not necessarily qualify as structural components. Perhaps the most popular of this group are the cones and the barrels used as markers and barriers.

Most of these items are made from unreinforced engineering thermoplastics such as high density polyethylene, polyvinyl chloride, and polyurethane.

### **2.3.3.1 Markers and Barriers**

Different types of markers are currently in use. Mostly they are used to divert traffic on areas under construction or subject to maintenance. The most popular markers are cones and barrels. In addition, composite barrels and other devices are used as shock absorbers in potentially dangerous areas along highways. Typical locations are at the end of bridge abutments and guard rails, and against other obstructions at the edge of the right of way. Temporary composite barriers are also widely used. Some of these are water filled to provide mass.

### **2.3.3.2 Signs**

A variety of signs made out of composites and plastics are currently in use. These signs range from permanent to temporary and are seen all around, along roads under maintenance, construction sites, airports, etc. They are lightweight, which allows for easy transport and setup, and are corrosion resistant with a long life.

## **2.3.4 Reinforcing Bars and Prestressing Tendons**

### **2.3.4.1 Reinforcing Bars**

Compared to steel, composite reinforcing bars (rebars) for concrete are light in weight and inherently resist the destructive effects of moisture and deicing chemicals. The manufacturing process combines pultrusion and compression molding.

One popular type of rebar currently available in the market has a core of low-cost glass fiber-reinforced polyester. The outer skin is a urethane-modified vinyl ester with excellent resistance to moisture and chemicals, including the alkaline concrete mix. Because the outer skin is molded, it can include design features that improve the mechanical bond between the rebar



and concrete. Compared to epoxy-coated steel rebar, composite rebars have twice the tensile strength at one-fourth their weight.

#### **2.3.4.2 Cables, Tendons**

Tension cables are the main structural elements of cable-stayed bridges. Unlike many other bridge types, these components are completely exposed to environmental conditions. It is thus important to make these cables as corrosion resistant as possible. Advanced composites such as carbon or aramid fiber reinforced plastics offer properties like high specific strength and stiffness, and high fatigue and corrosion resistance. They can be an excellent alternative to conventional steel by extending service life, reducing maintenance and simplifying installation. The advantages of the materials include superior abrasion resistance, excellent moisture resistance, and exceptional property retention over a broad ranges of temperature and chemical environments. Furthermore, due to the lightweight, high strength and high stiffness, they allow the construction of more efficient long-span bridges.

Steel tensioning tendons (typically threaded bars or seven-wire strands) used to post-tension bridge decks can lose up to 65 percent of the initial imposed tension due to the shrinkage of concrete with time. Due to this high loss, the relevant American Association of State Highway and Transportation Officials (AASHTO) specification for stress-laminated bridge decks requires high initial levels of post-tension, up to 2.5 times the minimum required tension. Furthermore, the tendons must be retensioned to the initial prestress level during the second week after initial deck lamination and again between the fifth and eighth weeks after lamination.

Tendons made of glass fiber reinforced plastics (GFRP) strands need no retensioning after completing the initial post-tension. This is because the low stiffness of the GFRP strands. The modulus of elasticity is approximately

one-fourth that of steel. The low modulus of these strands means that they can accommodate the concrete contraction with only a small loss of prestress. GFRP cables retain approximately 80 percent of that tension over the long term.

Faster post-tensioning is another advantage of GFRP strands. To attain the specified initial tension, only two tensioning passes are needed. Each strand along the bridge deck is tensioned once: then all strands are tensioned a second time to reach final prestress. Depending on the size of the deck, initial prestressing typically takes only one or two hours. In contrast, steel tendons typically require five or more tensioning passes before reaching initial design prestress. Again, the difference is due to the difference in modulus of the two materials.

## **2.3.5 Pipes and Manholes**

### **2.3.5.1 Pipes**

Advantages of composites and structural plastics (unreinforced thermoplastics such as PVC, ABS, and HDPE) for piping are the inherent corrosion resistance, lighter weight, ease of fabrication, lower maintenance costs, and lower life cycle costs when compared to concrete or steel pipe. Additional advantages are reduced problems with plugging of fire lines, reduced hot work from welding, better flow characteristics allowing increased flow capacity for the same diameter pipe, reduction in structural support sizes and reduction in the material handling during construction. The use of composites and structural plastics has been held back by the lack of engineering knowledge and experience by the owners and designers, and by the lack of standardization of materials between manufactures. Composite piping is widely used in the petroleum and chemical industry because of its corrosion resistance. It is also being considered for high pressure piping and for a variety of structural applications such as tethers and production risers

(Ramirez, 1999). This kind of piping is commonly designed and built to handle operating temperatures up to 250°F and pressures to 500 psig. Composite pipes have been shown to behave remarkably well under these severe conditions (Broutman, 1969). Composites and structural plastics are particularly well suited to use in sewer lines because of their resistance to corrosion.

### **2.3.5.2 Manholes**

There are several applications in this area, including the complete manhole, which is lightweight, and not subject to corrosion. Other applications include a lightweight hinged fiberglass cover with hasp for locking, concentric manway reducer for use with steel cover suitable for H-20 highway loading, concentric reducer with aluminum watertight (gas tight) lid for non-traffic loads. Composites and structural plastics in these applications have some particularly valuable characteristics. They are watertight, and the FRP bottom completely seals the manhole and eliminates infiltration. They are lightweight, weighing less than 10% of comparable concrete structures. This feature permits fast and easy installation. They are extremely resistant to numerous chemicals, salt water, corrosive soil conditions, ground water and electrolysis. The smooth interior provides a clean non-abrasive working place inside the manhole.

### **2.3.6 Secondary Structures (flagpoles, light poles, guard rail, sign supports, traffic signals, etc.)**

#### **2.3.6.1 Flagpoles**

Available in standard heights from 20–40 feet and customized to any length, composite flagpoles have found widespread use. By using high-strength composite laminates and building the poles in large tapered sections, current products can fly larger flags than similarly sized metal or wooden poles. With a weight of 20% the weight of a similar wood pole, 40% the

weight of a similar steel pole, and 10% the weight of a similar concrete pole, the shipping and handling advantage is obvious. An additional advantage of composites is that the flagpoles are available in a wide range of integral colors.

### **2.3.6.2 Light Poles**

Composite light poles are widely used in Europe. In North America, where timber is more plentiful, they are used less. FRP poles are lightweight and are easily molded to accommodate electrical components. Centrifugal casting is a common fabrication method.

One of the leading manufacturers is Direct Burial Fiberglass Light Poles. The company's literature states that the poles "save time and money due to:

- Lower installation labor
- Lower construction equipment costs associated with pole installation
- Reduced or eliminated need for lifting equipment
- Reduced traffic interruption and required traffic management costs
- Faster, simpler, easier, less expensive site preparation
- No concrete foundations required
- Ideal for underground wiring"

### **2.3.7 Other Applications**

#### **2.3.7.1 Transportation Equipment**

The transportation area has the largest number of applications among all other current areas of use (Composites Design & Applications, 1996). For transportation applications, lightweight is very important. Any saving in weight of the structure translates into more cargo that can be carried. The less dead weight that has to be hauled on each trip the better in terms of

energy saving, infrastructure support, etc. The following are some of these applications.

### **A. Aircraft Industry**

Starting in 1940, aircraft structural applications have grown steadily in both variety and quantity. Composites have been used extensively in radomes, rotor blades, floors, doors, control surfaces, empennages, wings, and fuselages all of them with very auspicious results (ICCI 98, Vol. 1, 1998). It should be pointed out that most of the initial applications were military designs. The advent of stealth technology has also accelerated the use of composites in military applications. In commercial aircraft, the use of composites has been rather conservative mainly due to safety concerns (Kaw, 1997).

In recent years, however, the use of composites has grown significantly. Modern commercial aircraft such as the Boeing 777 and the most recent Airbus use composites for large portions of the aircraft including the control surfaces, and empennage.

### **B. Mass Transit**

About 50% of the takeoff weight of large-scale passenger aircraft, is the passengers and cargo, and the structural weight is about 30%. A reduction in structural weight leads directly to a reduction in fuel consumption and allows the downsizing of engines, wings, and so on, which produce a snowball effect resulting in further reduction.

### **C. Trucks**

Body panels made from hybrid composites have a reduced weight with an increase in strength and toughness. Hybrid panels weigh 20 to 30% of steel panels. Hybrids are 50–100% stronger than fiberglass. As a result, the truck burns less fuel.

## **D. Cars**

A modern car contains approximately 320 lbs. of plastic. Use of plastic reduces weight, which leads to improved fuel consumption and replaces parts that can corrode with non corrosive materials.

## **E. Trains**

The factors normally considered when selecting candidate materials for transit cars are initial costs, maintenance costs, and weight (Broutman, 1969). Insulated composite boxcars made from reinforced composites have been successfully built. These boxcars have fewer joints compared to steel boxcars, and provide more optimal insulation with heat transfer reduced approximately 60% (ICCI 98, Vol. 1, 1998). Refrigerated boxcars make extensive use of composites.

## **F. Recreational**

Recreational vehicles such as two-, three-, and four-wheeled scooters, snowmobiles, boats, and water jet craft make extensive use of composites and structural plastics.

### **2.3.7.2 Pressure Vessels, Tanks**

As noted previously composite tanks are excellent devices for storing highly corrosive chemicals, including even concentrated hydrochloric acid. As such, filament-wound FRP offer an economical alternative to metallic vessels.

### **2.3.7.3 Stacks**

The lightweight and excellent chemical resistance of reinforced-polyester composite material makes it a logical choice for stacks. Such stacks are permitted to handle chemical fumes and temperatures up to 180°F, and in many cases, higher. There are many stacks in service now over 100 ft in height and a few over 200 ft. (Broutman, 1969).

#### **2.3.7.4 Oil Platforms**

Offshore oil platforms are another significant area for the use of composite materials. The drilling structure, helicopter deck, process and utility equipment, tether, and risers are potential applications for advanced composites.

#### **2.3.7.5 Industrial**

Composites are used throughout industry to reduce costs by prolonging working life as well as by improving performance. Examples of longer life applications include drive and conveyor belts, hoses, tear and puncture resistant fabrics, rotor vanes, mandrels, ropes, and cables. Composite flywheels have the potential for performance not attainable with traditional materials because of the higher speeds possible (Herakovich, 1998).

#### **2.3.7.6 Medical**

Composites are used in a variety of medical applications. They have been used to reduce weight and extend durability. Lightweight wheelchairs and crutches offer an obvious advantage to the user (Herakovich, 1998).

#### **2.3.7.7 Sporting Goods**

One of the most popular applications, bicycles use hybrid construction of graphite/epoxy composites wound on either an aluminum tubing or chopped S-glass-reinforced urethane foam. Composites, also allow frames to consist of one piece, which improves fatigue life and avoids stress concentration found in metallic frames at their joints. Other applications such as golf clubs shafts, tennis and racquetball rackets, ice hockey sticks, fishing rods, skis, etc. also have been developed (Kaw, 1997).

### **2.3.7.8 Enclosures**

Fiberglass enclosures combine the strength and corrosion resistance of compression molded fiberglass with clean styling. Enclosures of this type have multiple applications in today's industry. Enclosures are also made of reinforced PVC, which are meant to be a permanent cover. They are available in different colors and textures. An important application is the light vehicle industry.

## **2.4 Glossary**

### **Acoustic Emission**

The elastic energy released by materials when they undergo deformation. Rapid release of energy results in transient elastic waves that propagate through the material. In composites, acoustic emission is typically associated with matrix cracking, fiber breakage, fiber debonding or delamination. Acoustic emission can be monitored to detect damage and is the basis of an important nondestructive test method.

### **AFRP**

Aramid fiber reinforced plastic.

### **CFRP**

Carbon fiber reinforced plastic (includes graphite fiber reinforced plastic).

### **C-Glass**

A glass that is used for its chemical stability in corrosive environments.

### **Chopped Strand Mat**

A fiberglass reinforcement that utilizes continuous rovings that are cut into short strands, arranged in a random pattern and held together with a binder.



**Composite**

A combination of one or more materials differing in form or composition on a macroscale. The constituents retain their identities; i.e. they do not dissolve or merge completely into one another, although they act in concert. Normally, the components can be physically identified and exhibit an interface between one another. In this dissertation the term composite refers to a polymer matrix reinforced with fibers. (See also FRP Composite)

**Compression Molding**

A composite manufacturing technique whereby thermoset composite materials are compressed between matched die molds using hydraulic pressure and heated until the materials are cured to its final form

**Contact Molding**

A process for molding reinforced plastics in which reinforcement and resin are placed on a mold. Cure is either at room temperature using a catalyst system or by heating in an oven, without additional pressure.

**Continuous Roving**

Parallel filaments coated with sizing, drawn together into single or multiple strands and wound into a cylindrical package.

**Corrosion Resistance**

The ability of a material to withstand contact with ambient natural factors or those of a particular artificially created atmosphere, without degradation or change in properties.

**Creep**

The change in dimension of a material under sustained load over a period of time, not including the material's initial elastic deformation. The time-dependent part of strain resulting from an applied load. Most polymers exhibit

viscoelastic properties and the time-dependant strain is recoverable when load is removed. (See also Viscoelastic)

### **Debonding**

The separation of bonded surfaces, usually unplanned.

### **Delamination**

A separation of the layers of a material in a laminate, either local or covering a wide area. Can occur in the cure or during the life of a product. In flexural members, delamination can occur as the result of shear stress or direct tensile stress (peel).

### **E-Glass**

A family of glasses with a calcium alumina borosilicate composition and a maximum alkali content of 2.0%. A general purpose fiber that is most often used in reinforced plastics, and is suitable for electrical laminates because of its high resistivity.

### **Empennage**

The tail assembly of an airplane.

### **Epoxy**

A polymerizable thermoset polymer containing one or more epoxide groups and curable by reaction with amines, alcohols, phenols, carboxylic acids, acid anhydrides, and mercaptans.

### **Fabric**

Arrangement of fibers held together in two dimensions. A fabric may be woven, nonwoven, or stitched.

**Fabric, nonwoven**

Material formed from fibers or yams without interlacing. This can be stitched, knit or bonded.

**Fabric, woven**

Material constructed of interlaced yams, fibers, or filaments.

**Fiber**

General term for a filamentary material. The single unit of substance that is broken into parts fit to form threads to be woven; a filament. Any material whose length is at least 100 times its diameter.

**Fiber Architecture**

The design of the reinforcement; the arrangement of the fibers to achieve specific results. Examples include braiding, fabrics (stitched and woven), rovings, mats, etc.

**Fiber Content**

The amount of fiber present in a composite. This is usually expressed as a percentage volume fraction or weight fraction of the composite.

**Fiber Direction**

The orientation or alignment of the longitudinal axis of the fiber with respect to a stated reference axis.

**Fiberglass Reinforcement**

Major material used to reinforce plastic. Available as a mat, roving, fabric, etc.

**Fiber Pattern**

Visible fibers on the surface of laminates or molding. The thread size and weave of glass cloth.

**Fiber-Reinforced Plastic or Fiber Reinforced Plastic (FRP)**

A general term for a composite that is reinforced with cloth, mat, strands, or any other fiber form.

**Filament**

Smallest unit of a fibrous material. A fiber made by spinning or drawing into one long continuous entity.

**Filament Winding**

A process for fabricating a composite structure in which continuous reinforcements (filament, wire, yarn, tape, or other), either previously impregnated with a matrix material or impregnated during the winding, are placed over a rotating and removable form or mandrel in a prescribed way to meet certain stress conditions. Generally, the shape is a surface of revolution and may or may not include end closures. When the required number of layers is applied, the wound form is cured and the mandrel removed.

**FRP**

Fiber reinforced polymer (plastic).

**FRP Composite**

A polymer matrix, either thermoset or thermoplastic, reinforced with a fiber or other material with a sufficient aspect ratio (length to thickness) to provide a discernable reinforcing function in one or more directions (see composites).

**Hand Lay-Up**

A contact molding fabrication method in which reinforcement layers, pre-impregnated or coated afterwards, are placed in a mold by hand, then cured to the formed shape.

**Hybrid**

A composite laminate consisting of laminae of two or more composite material systems. A combination of two or more different fibers, such as carbon and glass or carbon and aramid, into a structure.

**Infusion Molding**

Method of forming a plastic to the desired shape by forcibly injecting the polymer into the mold. The most popular infusion molding is known as SCRIMP (Seamann Composite Resin Infusion Molding Process).

**Interlaminar Shear**

Shearing force that produces a relative displacement between two laminae along their interface.

**Lamina**

A single layer of fiber bound together in a resin matrix.

**Laminate**

Two or more layers of fiber bound together in a resin matrix.

**Lay-Up**

The reinforcing material placed in position in the mold. The process of placing the reinforcing material in position in the mold.

**Mat**

A fibrous reinforcing material comprised of chopped filaments (for chopped-strand mat) or swirled filaments (for continuous-strand mat) with a binder to maintain form; available in blankets of various widths, weights, and lengths.

**Matrix**

The essentially homogeneous resin or polymer material in which the fiber

system of a composite is imbedded. Both thermoplastic and thermoset resins may be used, as well as metals, ceramics, and glasses.

### **Mechanical Properties**

The properties of a material such as compressive and tensile strengths and modulus that are associated with elastic and inelastic reaction when force is applied. The relationship between stress and strain.

### **Open Molding**

The general term used to describe composites manufacture whereby resin and reinforcement are placed on an open mold. See also hand lay up and spray up.

### **Plastic**

A material that contains as a essential ingredient an organic polymer of large molecular weight, hardeners, fillers, reinforcements, and so forth; is solid in its finished state; and at some stage in its manufacture of its processing into finished articles, can be shaped by flow.

### **Pultrusion**

A continuous process for manufacturing composites that have a constant cross section. The process consists of pulling a fiber-reinforcing material through a resin impregnation bath and through a shaping die, where the resin is subsequently cured.

### **Polyester**

Resin produced by the polycondensation of dihydroxy derivatives and dibasic organic acids or anhydrides yielding resins that can be compounded with vinyl.

**Random Fiber Mat**

A fibrous material for reinforced plastic consisting of randomly oriented chopped filaments, short fibers (with or without a carrier fabric), or swirled continuous filaments loosely held together with a binder.

**Reinforcement**

Strong materials bonded to or into a matrix to improve mechanical properties. Materials, ranging from short fibers through complex textile forms that are combined with a resin to provide the composite with enhanced mechanical properties.

**Resin**

The term "resin" is frequently used to describe the polymer matrix.

**Roving**

A number of yarns, strands, tows, or ends collected into a parallel bundle with little or no twist.

**S-Glass**

A magnesium alumina silicate composition that is especially designed to provide very high tensile strength glass filaments.

**Spray-up**

Technique in which a spray gun is used as an applicator tool. In reinforced plastics, for example, fibrous glass can be cut and mixed with resin and can be simultaneously deposited in a mold.

**Thermoplastic**

A resin that can be remelted and reformed.

**Thermoset**

A thermoset cannot be melted and reformed.

**Tow**

An untwisted bundle of continuous filaments. Commonly used in referring to man-made fibers, particularly carbon and graphite, but also glass and aramid. A tow designated as 140K has 140,000 filaments.

**Vinyl Esters**

A class of thermosetting resins containing ester of acrylic and/or methacrylic acids, many of which have been made from epoxy resin.

**Viscoelasticity**

Mechanics: a condition of a liquid or solid that exhibits viscosity but also memory of past deformation, with the ability to store energy elastically and to dissipate energy due to viscosity of the medium; exhibiting features of hysteresis, relaxation, and creep. Materials Science: the typical manifestation of this quality in a polymer; the shear viscosity is expressed by the relaxation time, which is the ratio of the viscous to the elastic characteristics in the determinant property.

**Woven Fabric**

A material constructed by interlacing yarns, fibers or filaments to form specific fabric patterns.

**Woven Roving**

A heavy glass fiber fabric made by weaving roving.



## **Chapter 3**

### **Experimental Procedures**

#### **3.1 Overview**

This chapter describes the experimental program associated with this research project. Six full-scale specimens were studied, four of them under short-term loading and two under long-term loading. Description of materials, instrumentation and testing setup is presented. The section on materials presents an overview of the resins and fibers for the fiber reinforced plastic (FRP) structural components; the section on the instrumentation summarizes the measurement devices used in the testing; and the section on the testing setup describes the loading frame and the safety frames used while testing the different specimens.

The experimental program was designed to contribute to the overall objective of the research study, which is to investigate the technical feasibility of using structural plastic materials for the primary structural members in short span highway bridges. Commonly used fabrication procedures and resins were evaluated. Emphasis was placed on lower cost reinforcements and conventional bridge construction techniques.

#### **3.2 Materials**

The full scale specimens considered in this experimental program were composed of a reinforced concrete (RC) deck and fiber reinforced plastic (FRP) structural members. Four specimens were tested under short term load, and two were tested under sustained load. A number of smaller specimens, without the concrete deck, were tested in order to examine specific structural characteristics.

The RC deck material components: concrete and reinforcing steel were the same for all specimens. The material components for the FRP members on the other hand varied, also, three manufacturing processes were considered for the FRP members: pultrusion, contact molded, and filament wound.

### **3.2.1 RC Deck**

All the RC decks in this project have the same thickness, 6 in., and an average width of 4 ft. These dimensions were selected as representative of a single beam in a typical short span bridge. The concrete in these decks is a normal concrete type with a nominal compressive strength of 5 ksi. The concrete strength of each deck was measured with cylinder tests and the modulus of elasticity was calculated using the formula given in the American Concrete Institute (ACI) code. The deck was reinforced in both longitudinal and transverse directions by #4 Grade 60 rebars spaced at 12 in.

### **3.2.2 FRP Components**

Pultruded FRP structural shapes were used in the first four specimens. A contact molded FRP shape was used in the fifth specimen, and filament wound FRP pipes were used to assemble a pair of arches for the sixth specimen.

Polyester, vinyl ester, and epoxy resins are widely used in FRP construction. In general, polyester has excellent corrosion resistance, but tends to have less elongation to failure and can be difficult to fabricate. Epoxy is easy to fabricate, but has less corrosion resistance. Vinyl ester provides a balance between these two resins. All three are candidate materials for bridge construction and are evaluated as part of this research. Historically, the resins tend to be used for specific applications and this experience was used for the components in this study. Pipes were fabricated

with epoxy, pultruded girders were fabricated with isophthalic polyester and vinyl ester, and contact molded girders were made with vinyl ester.

The reinforcement for the pultruded shapes was mainly E-glass, however the third specimen tested under long-term loading, had both E-glass and carbon fibers in its flanges, and E-glass in its web. A mixture of fibers is called hybrid reinforcement.

### **3.3 Specimens**

In all, six full-scale specimens were considered. The specimens had an RC deck with an average width of 4 ft. The average depth of the specimens was 20 in., and the overall length was 30 ft. Five of these specimens were designed to have the RC deck and the FRP girder working in composite action. For the remaining specimen, composite action was not considered in its design.

For the specimens designed to work in composite action pultruded and contact molded structural shapes were utilized. These structural shapes were joined to the RC deck by shear connectors, needed to develop composite action. The structural shapes had various cross sections and material configurations, which will be described in the chapters covering each particular specimen.

The specimen designed to work in non-composite action had a pair of arches assembled from filament wound FRP pipes. The RC deck was simply supported on these arches.

**Table 3.1. Summary of Test Program.**

<b>Specimen</b>	<b>FRP Girder Fabricator</b>	<b>FRP Girder Resin</b>	<b>FRP Girder Fiber</b>	<b>Loading</b>	<b>Related Smaller Specimens</b>
FG1 (FRP Girder / RC Deck)	Fibergrate (Pultrusion)	Isophthalic polyester	Glass	Short term	<ul style="list-style-type: none"> <li>• 2 Samples from girder, web and flanges cutouts, flexural test.</li> <li>• 4 Dogbone coupons, tensile test.</li> </ul>
FG2 (FRP Girder / RC Deck)	Fibergrate (Pultrusion)	Isophthalic polyester	Glass/Carbon	Short term	
IKG1 (FRP Girder / RC Deck)	IKG (Pultrusion)	Vinyl ester	Glass	Long term	
IKG2 (FRP Girder only)	IKG (Pultrusion)	Vinyl ester	Glass		<ul style="list-style-type: none"> <li>• 1 Sample from girder, web and flanges cutouts, flexural test.</li> <li>• 4 Dogbone coupons, tensile test.</li> </ul>
SW1 (FRP Girder / RC Deck)	Strongwell (Pultrusion)	Vinyl ester	Glass/Carbon	Long term	
SW2 (FRP Girder only)	Strongwell (Pultrusion)	Vinyl ester	Glass/Carbon		<ul style="list-style-type: none"> <li>• Whole girder, 1 sample from girder, flexural test.</li> <li>• 3 Dogbone coupons, tensile test.</li> <li>• 3 pieces from girder, web buckling test.</li> </ul>
FGS12 (FRP Arches / RC Deck)	Fiber Glass Systems (Filament winding)	Epoxy	Glass	Short term	<ul style="list-style-type: none"> <li>• 4 short length pipes, compression test.</li> </ul>
TK1 (FRP Girder / RC Deck)	Tankinetics (Contact Molding)	Vinyl ester	Glass	Short term	<ul style="list-style-type: none"> <li>• Whole girder, flexural test.</li> <li>• 2 samples from web, bolt bearing test.</li> </ul>

The pultruded FRP girders and the filament wound FRP arches are commercially available in a wide range of sizes and geometries covering particular design needs. On the other hand, the contact molded FRP girder was specifically designed and fabricated for this project.

Both short and long-term loading was considered. The long-term loading was used to study the creep behavior of the structural system. Four specimens were loaded in four-point bending short-term loading; the remaining two specimens were loaded under a long-term loading. The long-term was applied by a number of concrete blocks placed along the length of each specimen. The long-term loading was applied for seven months.

In addition to the six full-scale specimens, a number of other smaller specimens were tested in order to determine properties of specific FRP components. These tests ranged from a four-point bending of a 30 ft. long girder without an RC deck to compression tests on FRP pipes of short length. A summary of the test program is show in Table 3.1.

The specimens tested under long-term loading, were loaded under the action of concrete blocks with the nominal dimensions of 12 x 16 x 23 in. The average measured weight was 400 lbs. These blocks were placed uniformly along the specimen and the number of blocks was increased with time. The minimum number of blocks used was five, and was gradually increased to nine, eighteen, and up to a maximum of thirty seven blocks.

### **3.4 Data Acquisition System and Instrumentation**

The instrumentation used consisted of three types of measurement devices: strain gages (SG), linear potentiometers (LP), and load cells (LC), used to measure strains, displacements, and load respectively, at specific locations on each the specimens. These devices were connected to the data

acquisition system (DAS) currently used at the Ferguson structural engineering laboratory (FSEL) at the University of Texas at Austin.

### **3.4.1 Data Acquisition System (DAS)**

The data acquisition system (DAS) consists of a personal computer (PC) and an analog to digital converter. The PC controls the converter, also known as a scanner; records, interprets, and displays the information it receives from the scanner. The scanner converts voltage (analog signal), produced by the measurement device attached to the specimen, to its numeric representation (digital format) and relays it to the PC.

The DAS supports two categories of measurements, namely, full bridge and quarter bridge categories. The full bridge handles LC and LP, whereas the quarter bridge handles single active arm SG. Throughout the rest of this chapter, and in other related chapters, the term gage will be used to refer to any of the measurement devices above. Figure 3.1 shows a sketch of a DAS and some connections to different types of instrumentation.

Each gage is activated by DC voltage referred to as the "excitation voltage". The gage then produces a certain amount of volts, proportional to the changes in the specimen, referred to as the "output" or "signal". The voltage output of a measurement gage, whether full or quarter bridge, is fed to an input channel of the scanner. Each gage signal is fed to the scanner via a "front end box" described next. The number of channels in a typical DAS ranges from 60 to 140.

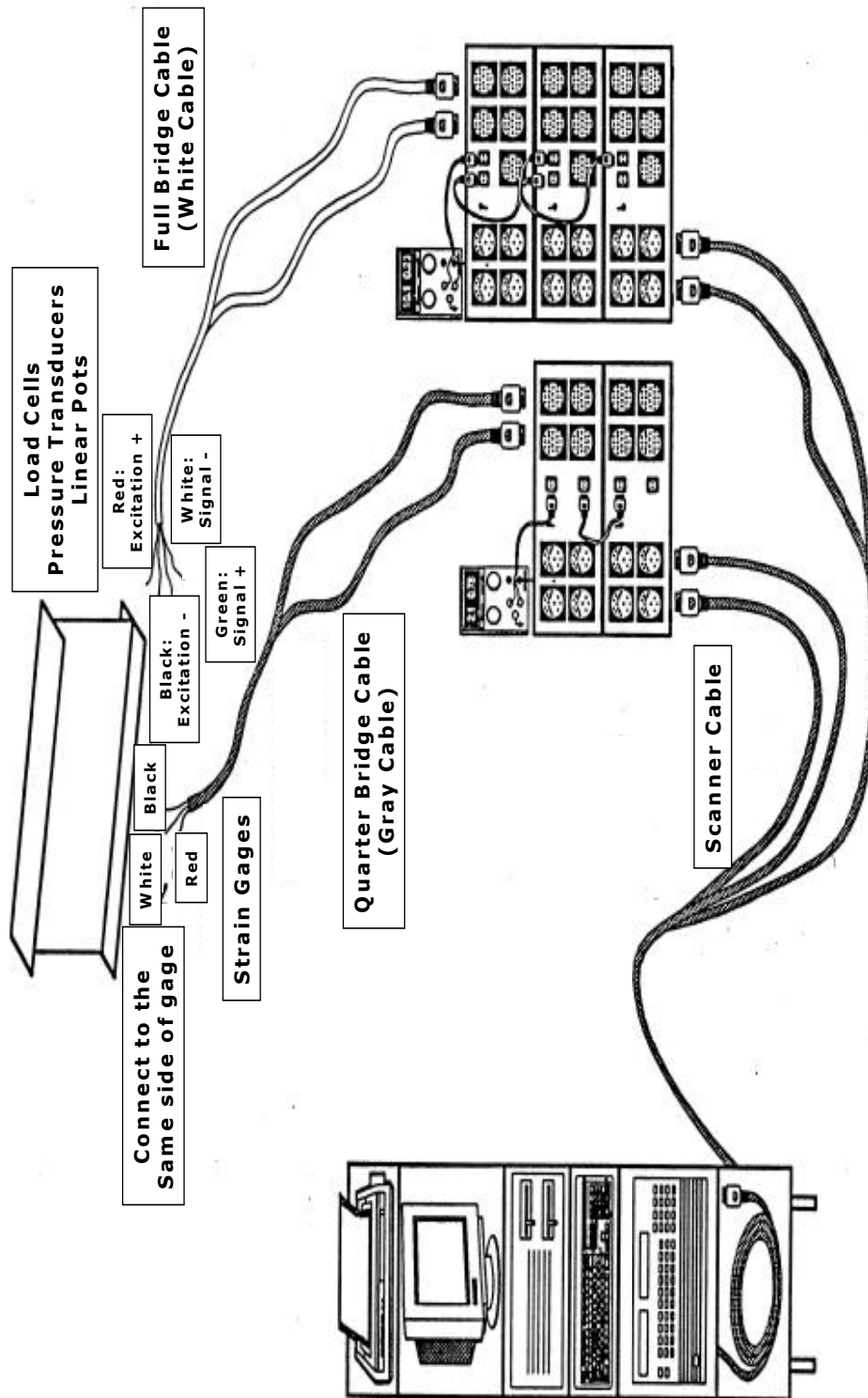


Figure 3.1. DAS and Instrumentation Sketch.

Quarter bridge end boxes connect SG to the DAS. The input connectors (4 per box) have in all 20 channels (5 per connector) of input from the specimen. These channels are fed to the scanner via the output connectors. Two connectors provide connections for the excitation voltage supplied by an external power supply. Normally the excitation level is set to 2 volts. Higher voltages may cause heating of the gages.

Full bridge end boxes connect LC and LP to the DAS. The input connectors (5 per box) provide 20 channels (4 per connector) of input from the specimen. These channels are also fed to the scanner via the output connectors. Two connectors provide connections for the excitation voltage supplied by an external power supply. Normally the excitation level is set to 10 volts.

Four single wires are used to connect a full bridge gage to the system. Two wires carry the excitation voltage, often 10 volts, from the front-end box to the gage and two wires carry the "signal" or "output" of the gage back to the front-end box. One wire is for excitation or output positive and one for excitation or output negative. LC provide 4 connecting wires for this purpose. However, a LP provides only 3 wires since excitation negative and output negative are the same and therefore share the same wire.

The SG use 3 wires to connect to the system. Normally the SG have a small resistance (120 Ohms). To avoid introducing the resistance of the connecting wires, two wires are connected to one side of the SG and a single wire to the other side.

The current DAS software used at the FSEL is a National Instruments Win/NT Measure, which uses an interactive spreadsheet for displaying the test output as the test progresses (FSEL-DAS, 1993).



### 3.4.2 Instrumentation

#### 3.4.2.1 Strain Gages (SG)

Strain gages, are measurement devices used to measure the strains in the specimen as a result of applied stresses (loading). There is a variety of SG commercially available for all kinds of applications and needs. For this experimental program two types of SG were selected, according to the surface on which the gage was to be used: plastic, or concrete.

The SG used on plastic surfaces were of the type CEA gages, a general-purpose family of constant SG widely used in experimental stress analysis. These SG are supplied with a fully encapsulated grid and exposed copper-coated integral solder tabs. These SG have a length is 1/8 in. Figure 3.2 shows a picture of a set of this type of gage.

Table 3.2 shows some properties for this type of gage. These gages have a strain limit of approximately 5% for gage length 1/8 in and larger; approximately 3% for gage lengths under 1/16 in.

**Table 3.2.** CEA Gage Properties

Type	Resistance at 75°F, Ohms	Gage Factor at 75°F	Transverse sensitivity at 75°C	Temperature range
CEA-06-250UW-120	120.0 ± 0.3%	2.065 ± 0.5%	(+0.4 ± 0.2)%	-100°F to +350°F

Fatigue life is a marked function of solder joint formation. With 30-AWG leads directly attached to gage tabs, fatigue life will be  $10^5$  cycles at  $\pm 1500\mu$  in/in ( $\mu$ in/in) using M-Line 361 A solder (Measurements Group, Inc, 1997).

These SG were bonded onto the plastic surfaces with the M-Bond AE-10 Adhesive. The M-Bond AE-10 Adhesive is a 100%-solids epoxy systems for use with strain gages and special-purpose sensors. AE-10 will cure at +70

°F (+20 °C) in 6 hours, with approximately 6% elongation capability and essentially creep-free performance. Elongation capability of approximately 10% can be obtained by extending the cure time to 24 to 48 hours at +75 °F (+24 °C) (Instruction Bulletin B-137-16, 1997).



**Figure 3.2.** Strain Gages Used on Plastic Surfaces.

The SG used on concrete surfaces were of the type FLA gages, a general-purpose family of constant SG widely used in experimental stress analysis. These gages are supplied with a fully encapsulated grid and exposed copper-coated integral solder tabs. The gages length is ¼ in. Figure 3.3 shows a picture of this type of gage.

Table 3.3 shows some properties for this type of gage. (Tokyo Sokki Kenkyujo Co., Ltd., 1999).

These SG were bonded onto the concrete surface with the M-Bond 200 Adhesive. Micro-Measurements certified M-Bond 200 is an excellent general-purpose laboratory adhesive because of its fast room-temperature cure and ease of application. When properly handled and used with the appropriate strain gage, M-Bond 200 can be used for high-elongation tests in excess of 60000  $\mu$  in/in, for fatigue studies, and for one-cycle proof tests to over +200° F (+95° C) or below -300° F (-185° C) (Instruction Bulletin B-127, 1997).

### 3.4.2.2 Linear Potentiometers (LP)

Linear potentiometers, otherwise known as contact transducers are measurement devices exclusively used to measure deflections at certain locations on the specimen under testing. An LP is a variable resistor with three leads. Two leads connect to the ends of the resistor, so the resistance between them is fixed. The third connects to a slider or wiper that travels along the resistor and the resistance between it and each of the other two connections varies.

**Table 3.3.** CEA gage properties

Type	Resistance at 75°F, ohms	Gage Factor at 75°F	Transverse sensitivity at 75°F	Temperature range
FLA-6-11-3LT	119.5 ± 0.5 %	2.12 ± 1 %	0.0 %	73.4 °F

There are several types of LP, each specifically designed for a particular situation. The LP used in this experimental program were of the same type with 2 in. and 6 in. stroke lengths respectively. Figure 3.4 shows LP with 2 in. and 6 in. stroke length.

The LP were located at midspan, and each end of the specimens, they were also used to measure relative slippage between the RC deck and FRP

girders. Actual locations will be given for each particular specimen in its corresponding chapter.

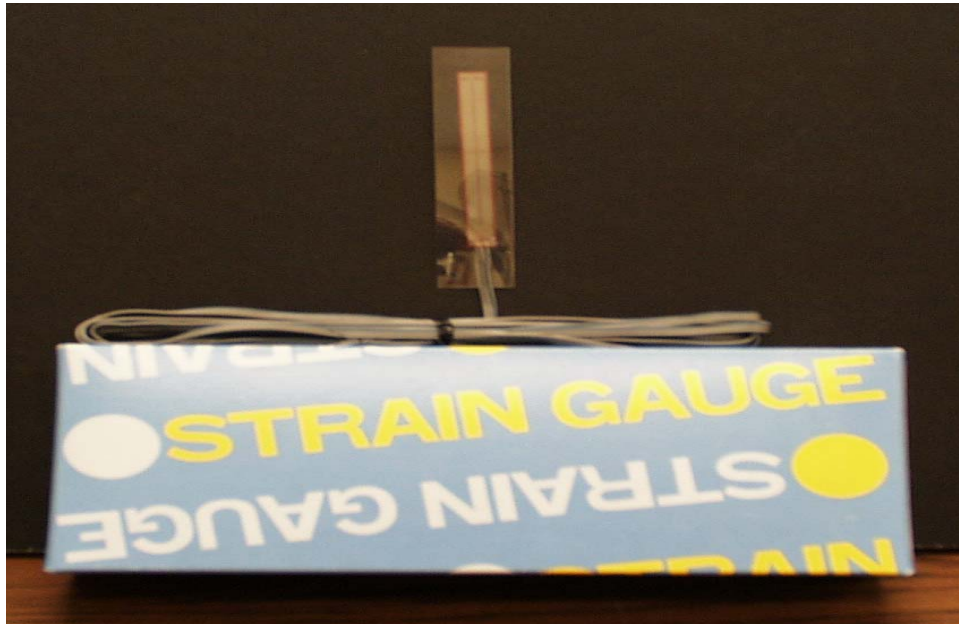


**Figure 3.3.** Strain Gages Used on Concrete Surfaces.

#### **3.4.2.3 Load Cells (LC)**

Load cells, are devices used to measure the magnitude of load being applied onto the specimen under testing. There is a wide range of LC available for a variety of applications. The main factor considered in selecting an LC is its capacity (maximum load the LC can handle). Figure 3.5 shows a typical LC used in this experimental program with a capacity of 50 kips.

The load on the specimens was applied by means of a hydraulic jack. A manual pump was used to drive the jack. The pump had attached a dial gage, showing the oil pressure applied into the jack. The ram area of the hydraulic jack was 13.14 in<sup>2</sup>. The jack then applied the load on the LC, whose gage measured the magnitude of the applied load and transmitted it to the DAS, where the value was recorded. Figure 3.6 shows a picture of a hydraulic jack, it also shows the oil hoses.

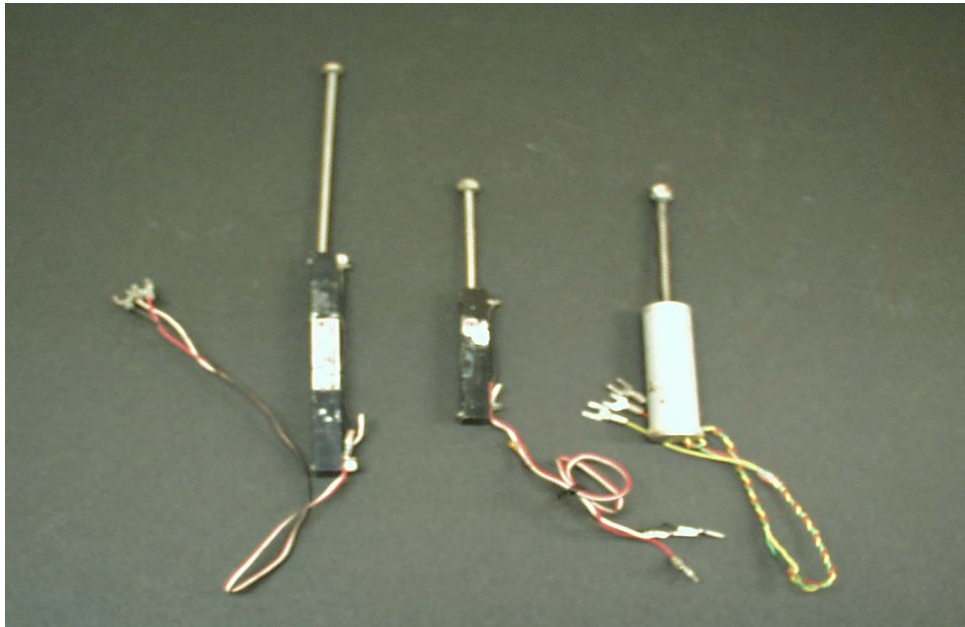


**Figure 3.4.** Linear Potentiometers 6 in. and 2 in. Stroke Length.



**Figure 3.5.** Load Cell, Capacity 50 kips.



**Figure 3.6.** Hydraulic Jack and Hose System.

#### **3.4.2.4 Acoustic Emission (AE) Sensors**

Acoustic emission (AE) sensors were also used to monitor the specimen during testing. These sensors were placed at locations of major stress. The AE research is not part of this project and the findings and conclusions of the AE study will be published separately.

### **3.5 Test setup**

The specimens were supported on elastomeric bearings whose dimensions were 2 in. x 9 in. x 14 in. The bearing was oriented with the 9 in. side parallel to the length of the specimen. Figure 3.7 shows a picture of a typical elastomeric bearing. These bearings in turn rested on reinforced concrete pedestals. The specimens then could be considered as simply supported.

The test setup for the short-term loading consisted of a steel frame whose girder held the hydraulic jack at its midspan. The frame was bolted to the testing slab by steel rods. The frame was designed to handle a maximum load of 200 kips. Figure 3.8 shows the loading frame used in this experimental program, it also shows the hydraulic jack attached to its girder.



**Figure 3.7.** Elastomeric Bearing Support.

All the specimens in this experimental program were full-scale. Each specimen had a length of 30 ft. and a width of 4 ft. Handling and testing a specimen of these dimensions involves some sort of hazard. Of special concern was the possibility of the specimens accidentally overturning under load. To prevent this from happening lateral support by means of triangular steel frames was provided. These frames were placed at the specimen midspan and at each end, on both sides of the specimen. It should be noted that these frames were never in contact with the specimen; they were just placed close enough in case the specimen moved and needed to be held in place to prevent accidental overturning. Figure 3.9 shows a pair of such frames.



**Figure 3.8.** Loading Frame.



**Figure 3.9.** Lateral Support Frames.



The specimens tested under long-term loading, were loaded under the action of concrete blocks with the nominal dimensions of 12 x 16 x 23 in. The average measured weight was 400 lbs. These blocks were placed uniformly along the specimen and the number of blocks was increased with time. The minimum number of blocks used was five, and was gradually increased to nine, eighteen, and up to a maximum of thirty seven blocks.

### **3.6 Summary**

This chapter presented a general description of the DAS and instrumentation utilized in the testing of the specimens in this experimental program. Materials, test setup, and a general description of the specimens considered in this research study were also presented. Additional details on the DAS, instrumentation, and test setup, will be given in the chapters covering each particular specimen.

## **Chapter 4**

# **Isophthalic Polyester Pultruded Fiber Reinforced Plastic Girder**

### **4.1 Overview**

Specimen FG1 was the first prototype tested in this experimental program. This chapter covers its design, instrumentation, and testing. Specimen FG1 was a structural system composed of a reinforced concrete (RC) deck and a fiber reinforced plastic (FRP) pultruded girder. The girder was fabricated with isophthalic polyester resin. The deck and girder were designed to carry the load by means of composite action. The specimen was designed to meet AASHTO HS20 standards.

### **4.2 General Description**

Specimen FG1 had a nominal length of 30 ft., and was composed of an RC deck and an FRP pultruded girder, designed to sustain the applied load by means of deck-girder composite action. The clear span between supports was 28.5 ft.

The FRP pultruded girder was supplied by Fibergrate Composite Structures Inc., Stephenville, Texas, but was actually manufactured by Strongwell Corporation, Bristol Virginia. It was selected from a set of structural shapes commercially known as Dynaform®. These structural shapes are available in a wide range of sizes and shapes, and combine a high strength-to-weight ratio with very good corrosion resistance. These FRP members are typically used in corrosive environments and offer a number of significant features including: (Fibergrate Composite Structures Inc., 1997)

- Lightweight, high strength fiberglass/resin construction.
- High corrosion resistance.
- Ease of fabrication.
- Choice of ISO (Isophthalic polyester), ISOFR (Fire Retardant grade of isophthalic polyester) and VEFR (Fire Retardant Vinyl Ester) resin systems.

Since most structural engineers lack a formal training in composites design, a good way of introducing the design of structural systems with FRP components is following the steel design approach; technically, however it is a bad idea. Structural plastics are in general anisotropic, but in practice they can be considered as isotropic; steel on the other hand for practical purposes is considered as isotropic materials. This difference in material properties has a major influence in the design process. Differences between these two ways of designing structural systems are discussed below.

1. For many years Strongwell and their predecessor company, Morrison Molded Fiber Glass corporation, has marketed a range of pultruded structural shapes.
2. The shapes are similar to those available in the steel industry: angles, wide flange shapes, structural tubes (rectangular and square), channels, and I beams. No structural Tee's are available.
3. The tables of properties and load carrying capacity tables were similar to those for steel, which are very familiar to civil engineers (Strongwell Design manual).
4. The orientation of the fibers in a pultruded structural member is primarily longitudinal. Some woven cloth is included to provide strength in the transverse direction.
5. FRP contrasts with steel in at least two important aspects.
  - The modulus of elasticity of FRP is an order of magnitude less.

- FRP is not isotropic and its properties are very different in different directions.
6. Failure of an FRP structural member under compressive stresses due to bending will nearly always be governed by buckling because of its low modulus. The lack of strength (delamination) perpendicular to the fibers contributes to this failure.
  7. Poor shear strength is also a problem especially near supports and load points, and also at bolt holes locations.
  8. Finally, connecting FRP structural components is very challenging.

The FRP girder had a length of 30 ft., and a cross section composed of a wide flange (WF) section 12 in. width, 12 in. depth, and ½ in. thick. On the top flange 2 in. equal leg angles, ¼ in. thick, each 6 in. long, were placed in pairs as shear connectors across the flange, spaced at 12 in. A pair of angles was used because the top flange of the FRP girder was not flat, but bowed downwards from the web. In addition, two 3 in. structural square tubes, ¼ in. thick, were attached to the bottom flange, one at the tip of each flange. This is shown in Figures 4.1 and 4.2. The C-clamps shown in the figures were used to hold the angles in place during bonding.

The structural square tubes, were initially designed to be 30 ft. long. During fabrication however, the fabricator decided to use two pieces of 20 ft., and 10 ft. lengths instead. The two tubes were joined and reinforced to form a continuous member using conventional industry practice. A detail of this splice is shown in Figure 4.3.

The angles at the top flange were intended to transfer the shear stresses at the interface between the RC deck and the FRP girder. The square tubes were added to increase the bending stiffness of the FRP girder.

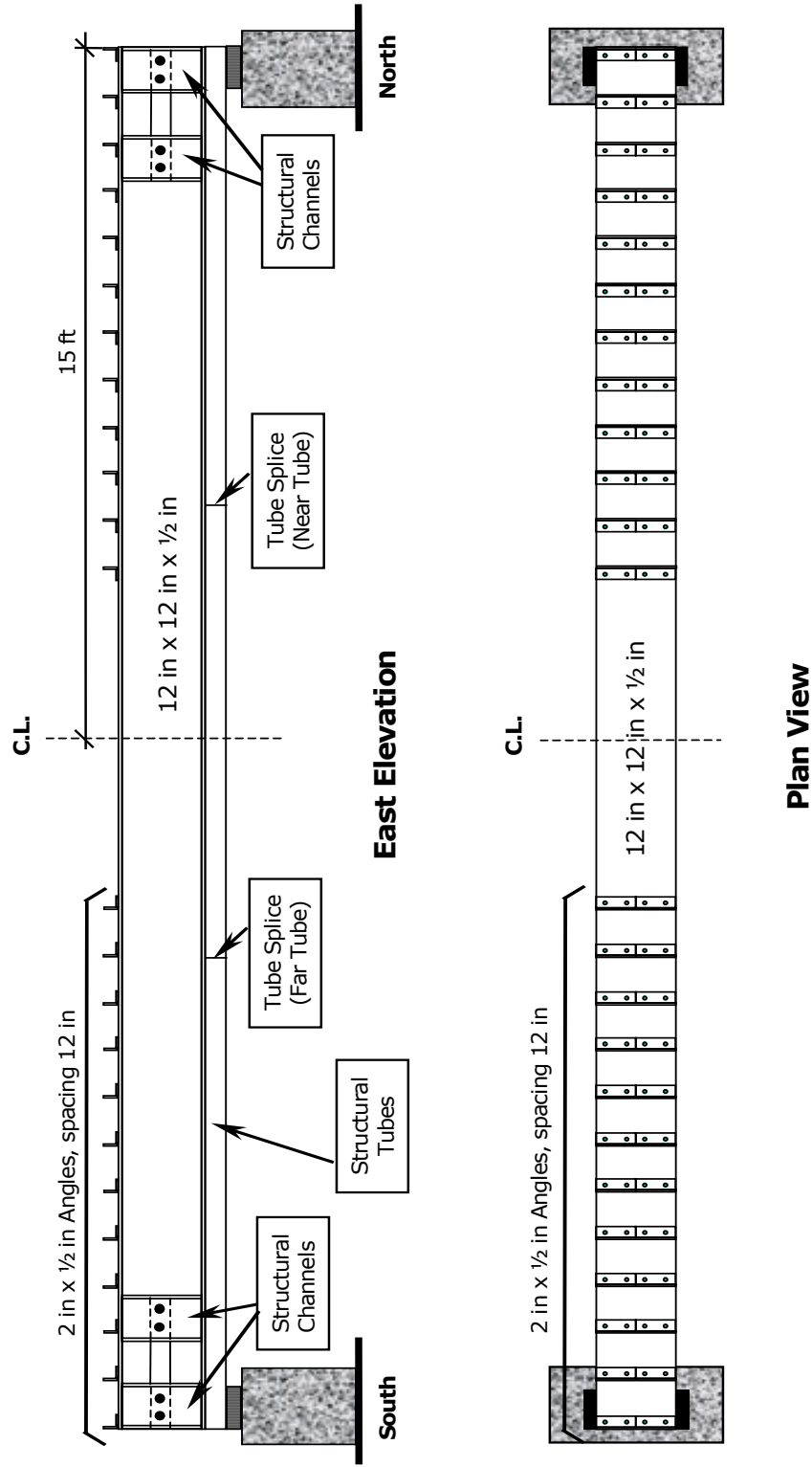


**Figure 4.1.** FRP Pultruded Girder.

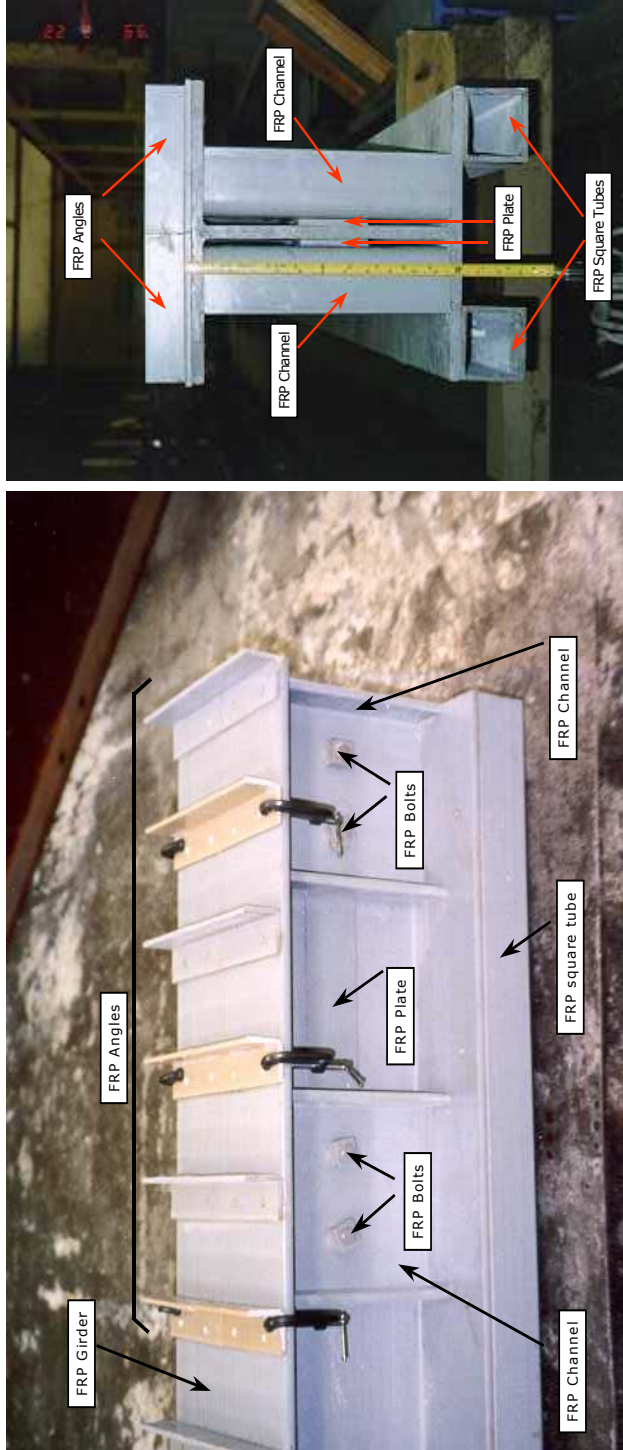


**Figure 4.2.** FRP Pultruded Girder End View.

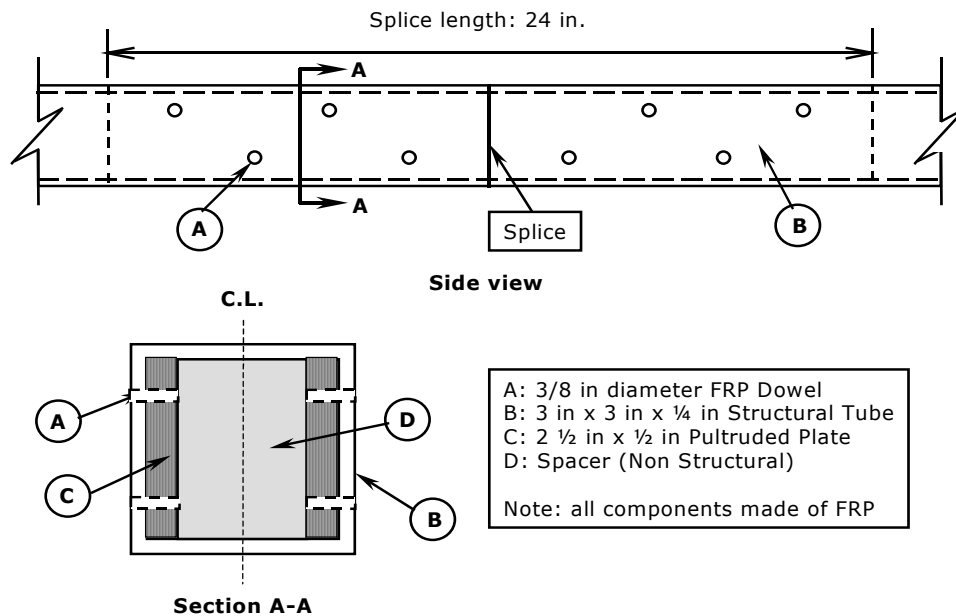


**Figure 4.3.** Square Tubes Splice Detail.

Additionally, a pair of channels 10 in. x 11 in. x 1/2 in. was added at each end on both sides of the girder's web. The purpose of these channels was to prevent local buckling due to high concentrations of shear and compression forces at each end of the girder (supports). See Figure 4.2.

The square tubes and angles added to the original cross section were bonded onto the flanges with epoxy, and then the bond was additionally secured by means of 1 in. long, 3/8 in. diameter FRP dowels, running through the thickness of both the flanges and the tubes. The structural tubes, shear connectors, and channels were attached to the girder by Fibergrate Composite Structures, as shown in Figures 4.3 and 4.4. A picture of the FRP girder is shown in Figure 4.5.

The RC deck was 4 ft. width, 6 in. thick, and 30 ft. long, placed on the FRP girder top flange. Standard forms were used for the RC deck cast as shown in Figure 4.6. Steel reinforcement was placed in two layers of #4

Grade 60 rebars spaced at 12 in. longitudinally and 18 in. transversely; these layers were 3 ½ in. apart. Figure 4.7 shows the bottom reinforcement layer during placing. The forms were removed 3 weeks after casting the slab. During casting of the deck the FRP girder was supported with three shores as shown in Figure 4.8, this shoring was left in place and was removed just prior to testing.

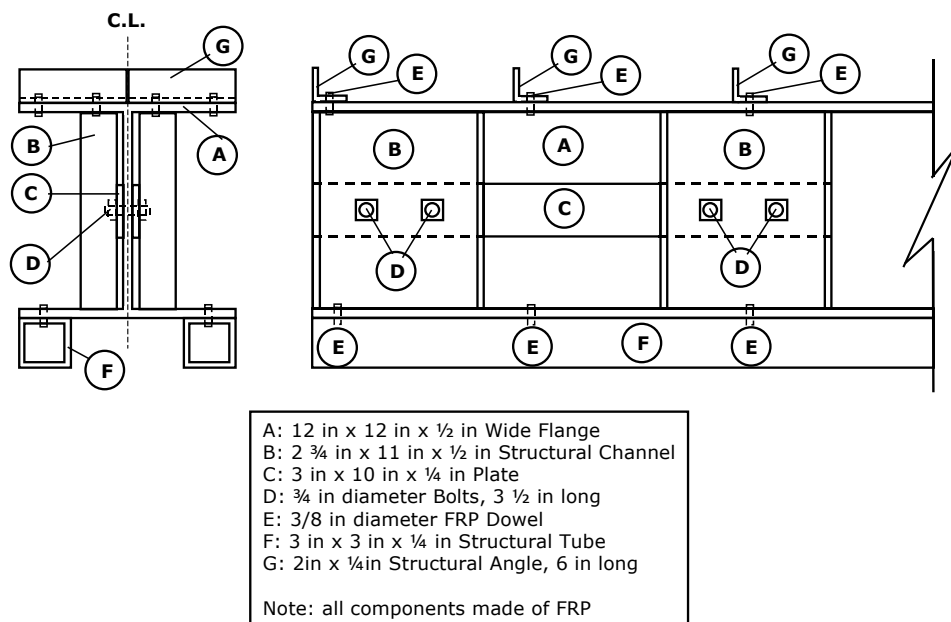


**Figure 4.4.** Pultruded Girder End Detail.

The specimen was supported at each end on the bottom flange in an area between the structural tubes that is just under the girder's web. A ½ in. thick elastomeric pad was placed in between the flange and a 3 in. thick steel plate. This steel plate in turn was welded onto another steel plate whose thickness was ¾ in. Finally this whole arrangement rested on an elastomeric bearing whose dimensions were approximately 3 in. x 11 in. x 20 in. The bearing was oriented with the 11 in. dimension parallel to the axis of the beam. RC blocks were used as a bottom support, these blocks rested on RC pedestals as shown in Figures 4.8, 4.9, and 4.10. The specimen clear span was 28.5 ft. Figure 4.11 shows specimen FG1 prior to testing.





**Figure 4.5.** FRP Pultruded Girder.

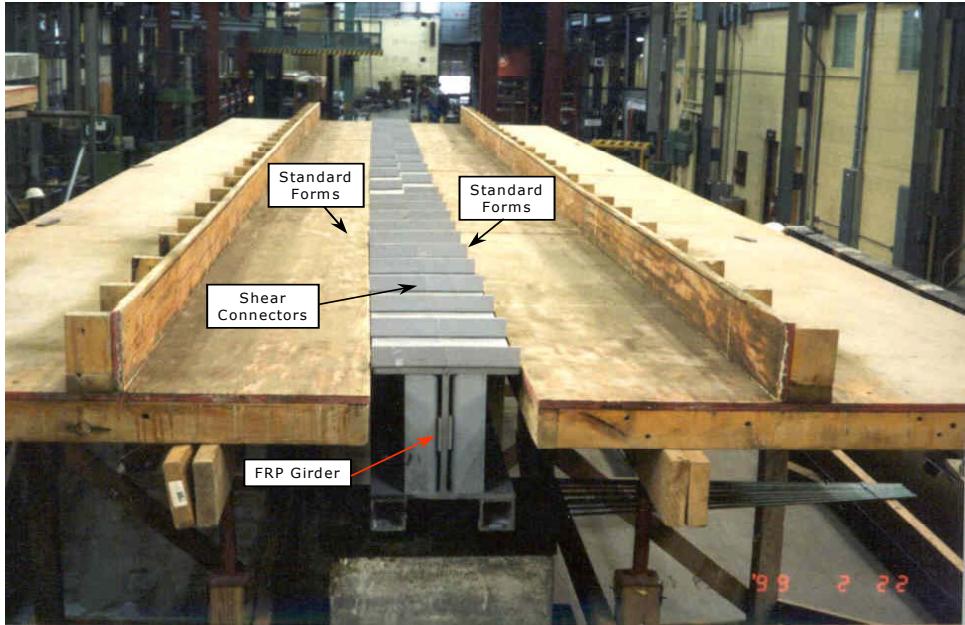


**Figure 4.6.** FRP Pultruded Girder, Forms.

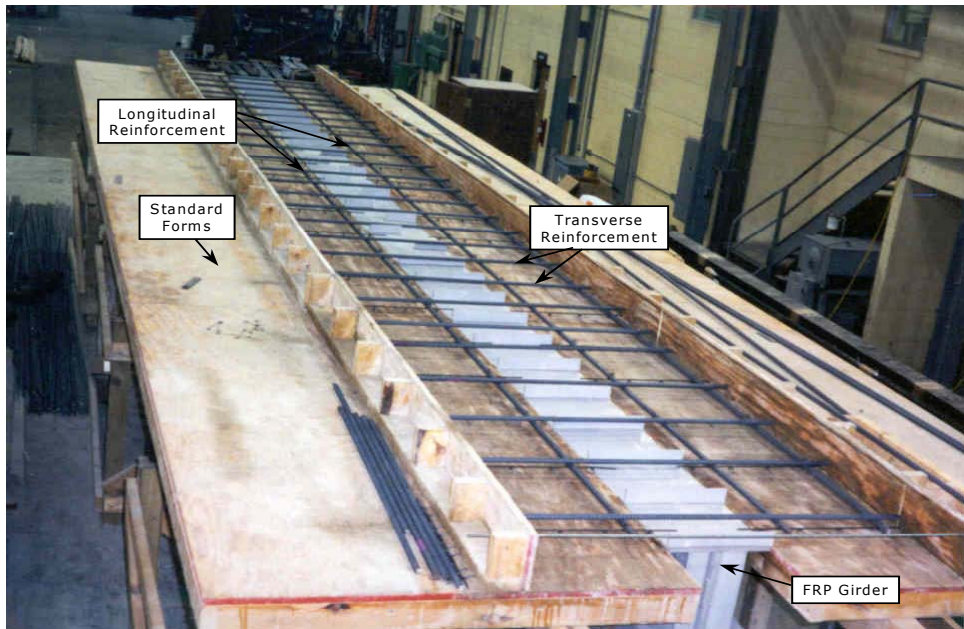


**Figure 4.7.** RC Deck Bottom Reinforcement Layer.



**Figure 4.8.** Specimen FG1.

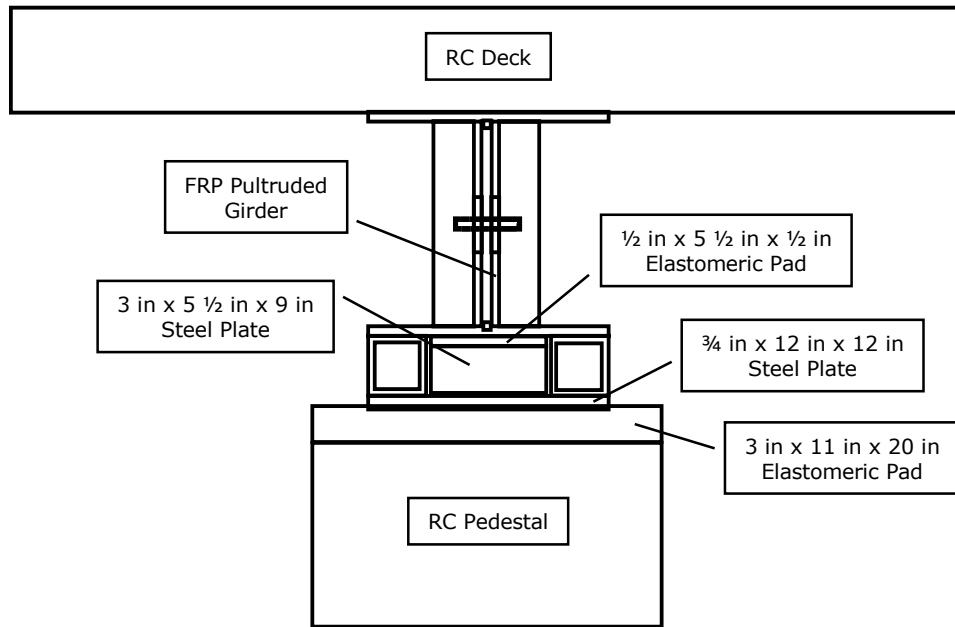


**Figure 4.9.** Support Detail.



**Figure 4.10.** South End Support View.

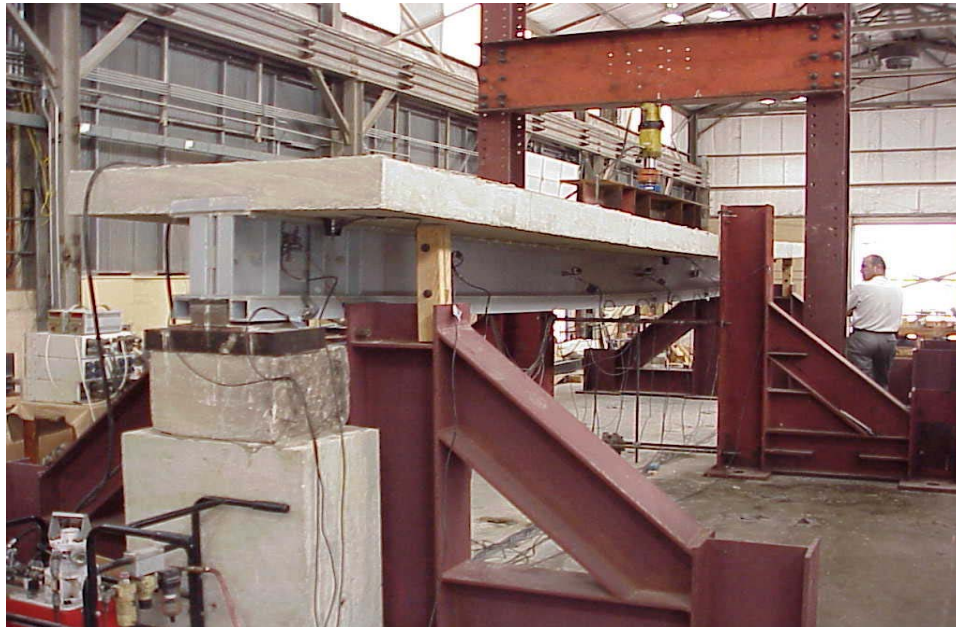


**Figure 4.11.** Specimen FG1 Prior to Testing.

### **4.3 Material Properties**

The materials used in specimen FG1 were thermosetting isophthalic polyester resin, and E-Glass reinforcement in an amount of 50% by weight. The resin was a fire resistant grade Iso-FR gray, which is a commodity plastic available from a number of resin suppliers. Material mechanical properties were found by testing samples from both components: the RC deck and the FRP girder.

#### **4.3.1 FRP Pultruded Girder**

A tensile test on a coupon taken from one of the flanges of the FRP girder was performed. The dimensions of the coupon were 19 ½ in. length, 5 ¼ in. width, and ½ in. thick machined into a dog-bone shape. Three strain gages (SG) were used to monitor the strains during testing, one oriented parallel to the loading, and two oriented transverse to the loading.

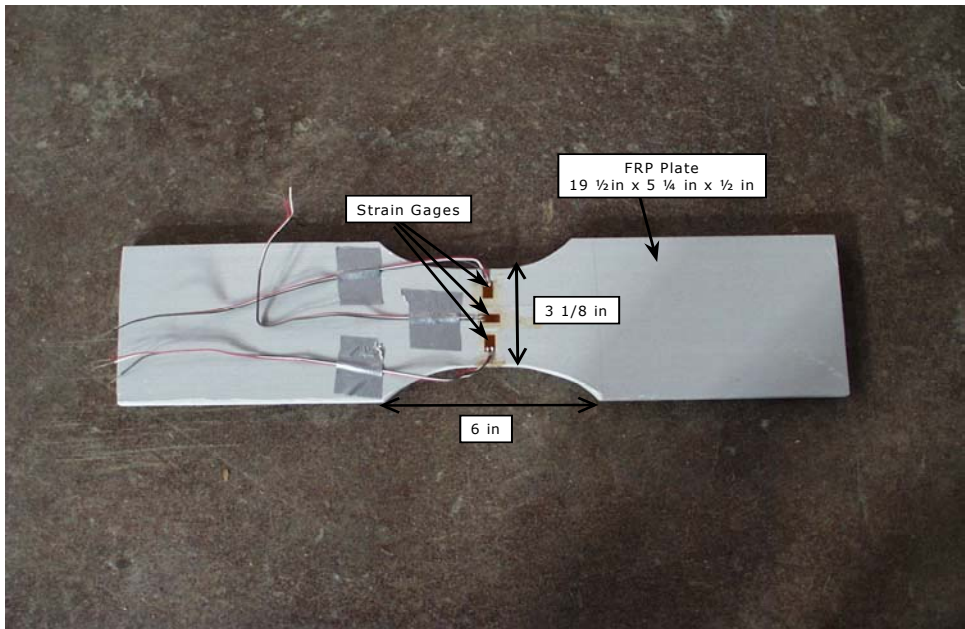


**Figure 4.12.** FRP Girder Coupon Before Test.

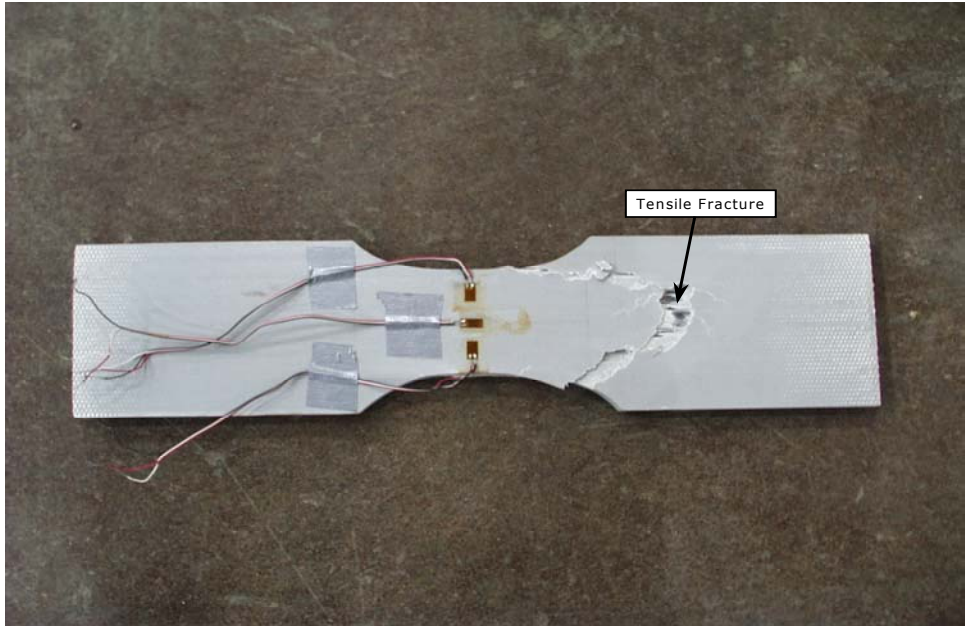


**Figure 4.13.** FRP Girder Coupon at Failure.

The coupon cross section at the location of interest was 3 1/8 in. x 1/2 in. See Figure 4.12.

Loading was applied along the longitudinal axis of the specimen. The load was applied monotonically up to failure. The specimen failed by tensile fracture as shown in Figure 4.13.

A plot of the applied stress vs. measured strain is shown in Figure 4.14. The maximum applied stress was 24 ksi. The behavior exhibited was essentially linear for both axial and transverse directions until close to failure. Based on this response a longitudinal elastic modulus of  $E_{L1} = 3850$  ksi, for stresses less than 8 ksi; and  $E_{L1} = 3500$  ksi, for stresses over 8 ksi. A Poisson ratio of  $\nu_{LT} = 0.17$  was determined. The fabricator listed a value for the elastic modulus of  $E_L = 2800$  ksi.

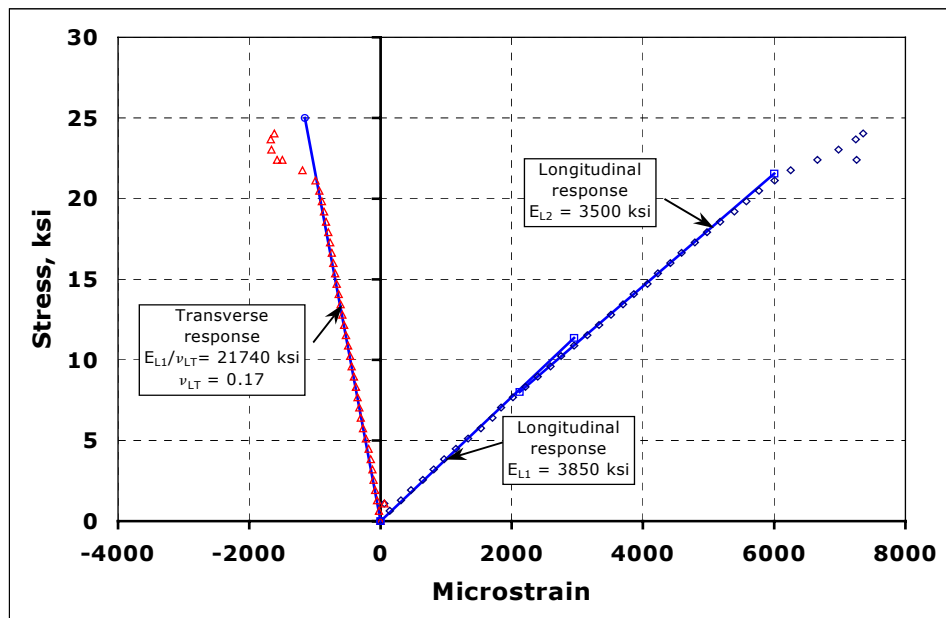


**Figure 4.14.** Tensile Test Stress-Strain Curves.

In addition to this tensile coupon a sample from the FRP girder was tested under four point bending conditions. Two tests were performed. The objective of these tests was to find the capacity of the girder under bending loading. The limitations imposed by the compressive stresses and the tension stresses were investigated.

The specimen had a 98 in. length, and a cross section corresponding to the FRP girder WF 12 in. x 12 in. x ½ in. Part of the bottom flange was removed symmetrically at midspan. Also, a 4 in. diameter hole was cut out from the web as shown in Figure 4.15. These alterations to the cross section were intended to reduce the strength of the flange so that it reached its tensile capacity at a load similar to the load that caused the top flange to buckle.

The specimen also had the web at each end reinforced to prevent it from buckling. Structural channels were used on both sides of the web, and FRP plates also were placed so as to have the web supported at its mid height, increasing thus the capacity of the web against compressive stresses. See Figures 4.1 and 4.2. This sample was taken from the FRP girder of specimen FG1 after this specimen had been tested.

The instrumentation for this sample consisted of strain gages (SG), linear pots (LP), and a load cell (LC). In addition, acoustic emission (AE) sensors were also used. SG were used on both flanges and the web. LP were used at midspan and close to each support. AE sensors were placed at midspan on top and bottom flanges, and on the web. See Figures 4.16 and 4.17.

Load was applied by means of a hydraulic jack as shown on Figures 4.18 and 4.19. The spreader beam distributed the applied load to points at 18 in. spacing.

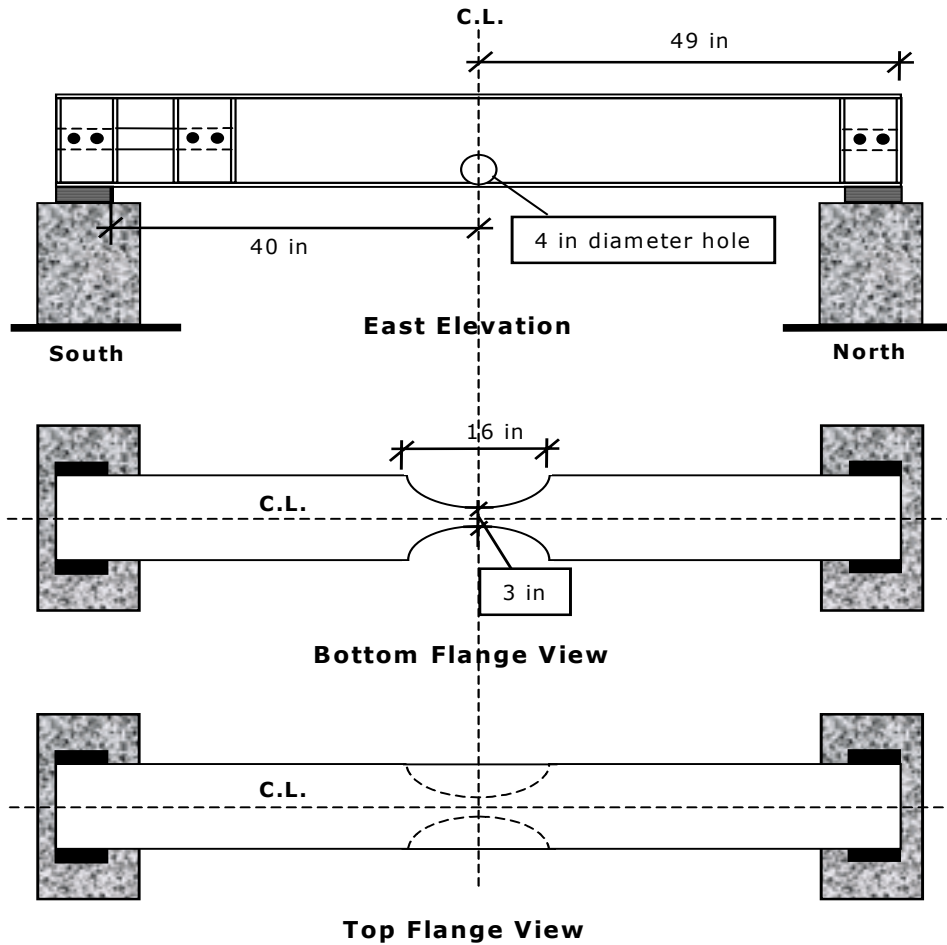


**Figure 4.15.** Four-Point Bending Test Specimen.

In the first test the top flange buckled. Figure 4.20 shows the buckling of the top flange. The response was essentially linear until buckling of the top flange. Figure 4.21 shows the load deflection curve at midspan for this test. The straight line on this figure is used to define a stiffness, hence the elastic moduli of the FRP. Based on this curve a value for the effective elastic modulus was found as  $E_{FRPgirder} = 3425$  ksi.



Since the objective of the test was to find the tensile strength of the FRP material, additional modifications on the specimen were performed in an attempt to induce flange tensile failure, instead of buckling failure of the top flange.

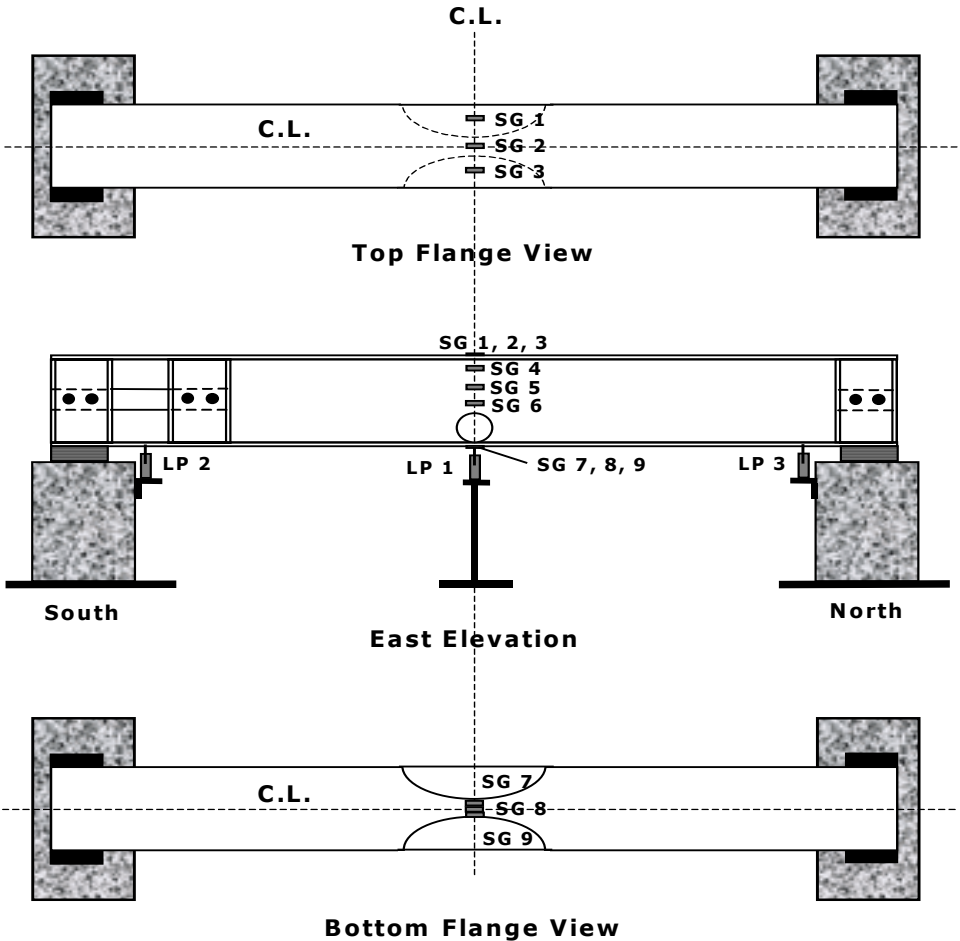


**Figure 4.16.** Four-Point Bending Test Specimen. Instrumentation.

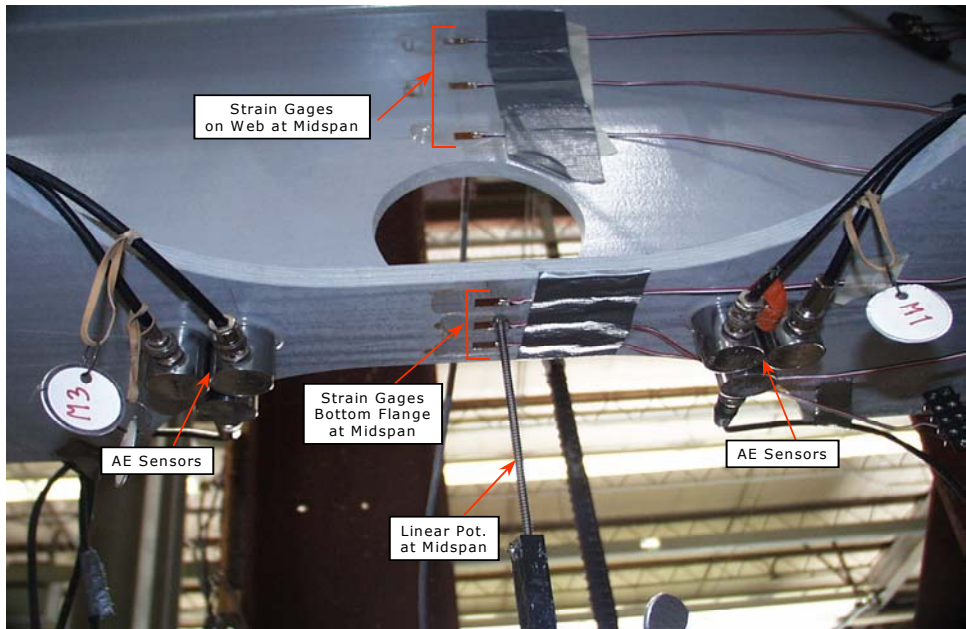


**Figure 4.17.** Midspan Instrumentation.

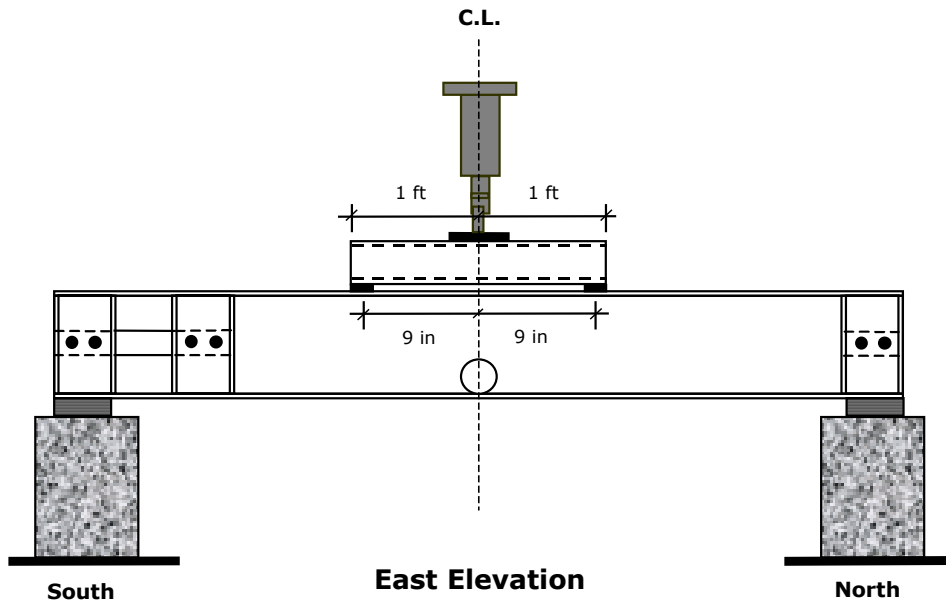


**Figure 4.18.** Four-Point Bending Test Loading.

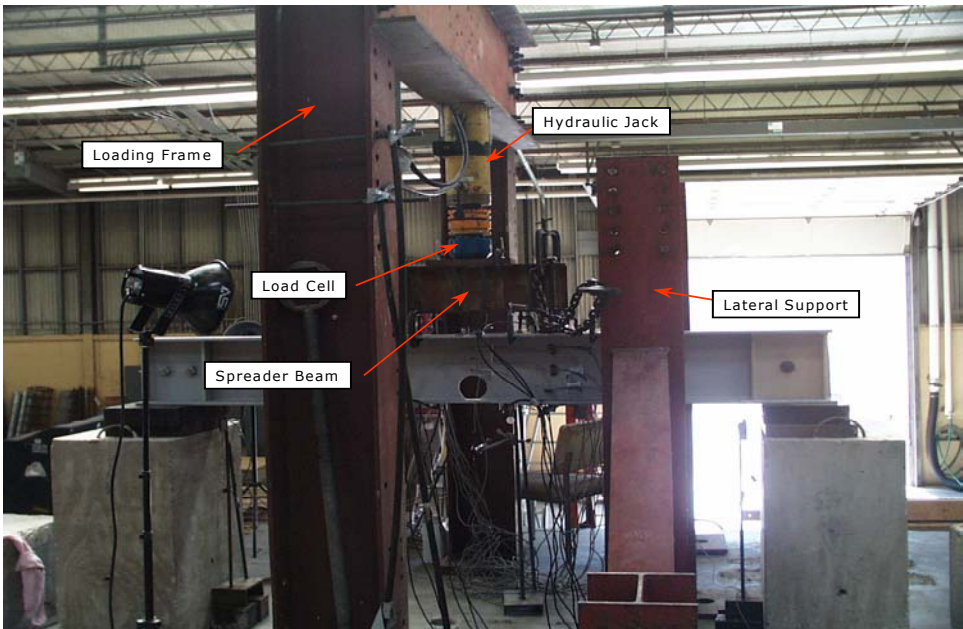


**Figure 4.19.** Test Setup.



**Figure 4.20.** Buckling of Top Flange.

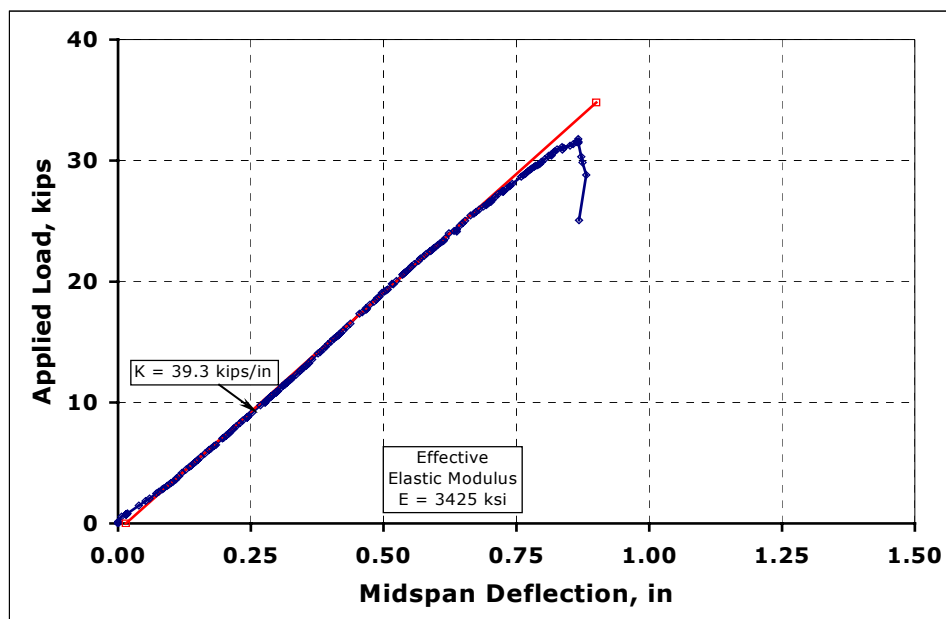


**Figure 4.21.** Load Deflection Response at Midspan.

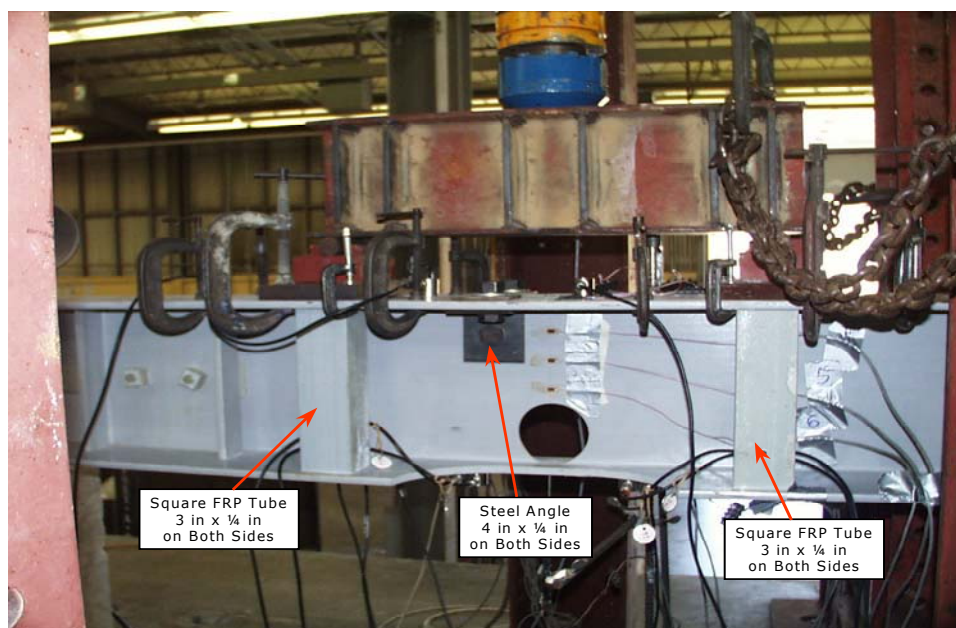


**Figure 4.22.** Second Specimen with Increased Buckling Resistance.

These changes mainly consisted of using square FRP tubes 3 in. x 1/4 in. right under the ends of the spreader beam on both sides of the web. This essentially shortened the effective length of the specimen. A pair of steel angles 4 in. x 1/4 in. were also used on both sides of the web at the juncture of the top flange and the web, their purpose was to support the top flange against buckling. The resulting configuration is shown in Figure 4.21.

With these changes the specimen failed by tensile fracture of the bottom flange as intended. Figures 4.22 and 4.23 show the tensile fracture at the bottom flange and on the web right at the top and the bottom of the circular hole.

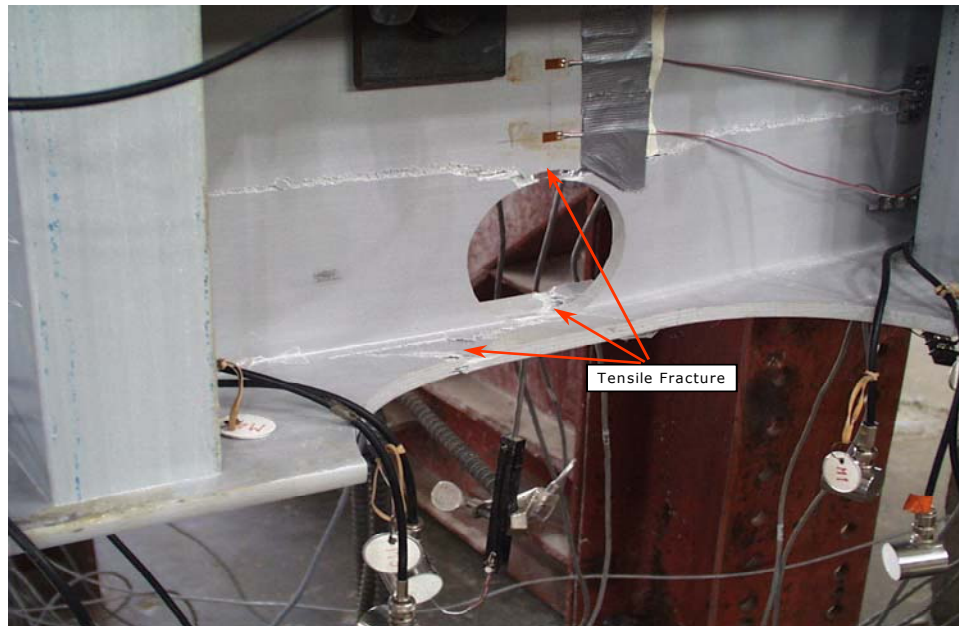


**Figure 4.23.** Tensile Fracture.

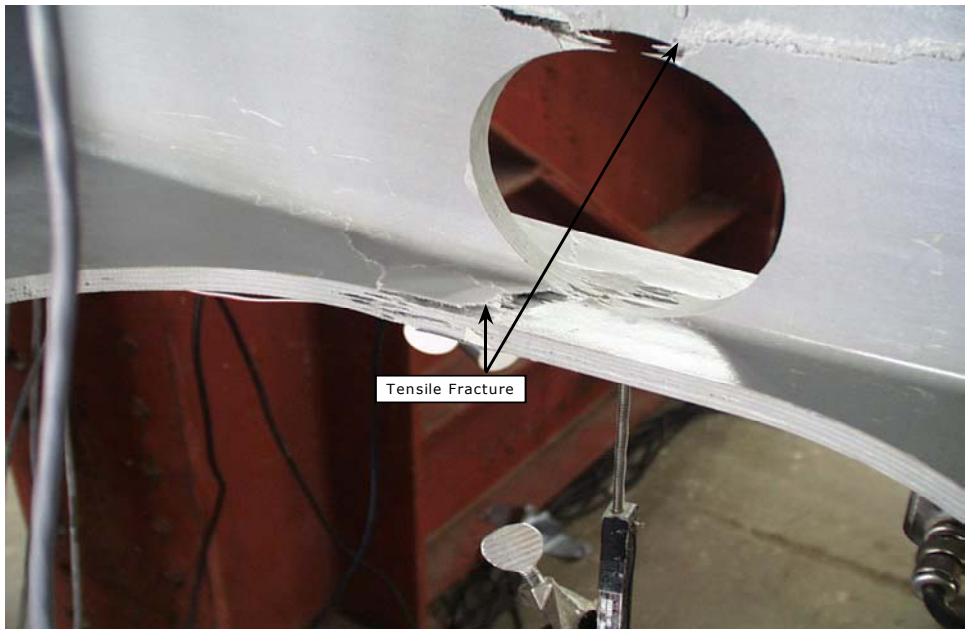


**Figure 4.24.** Tensile Fracture.

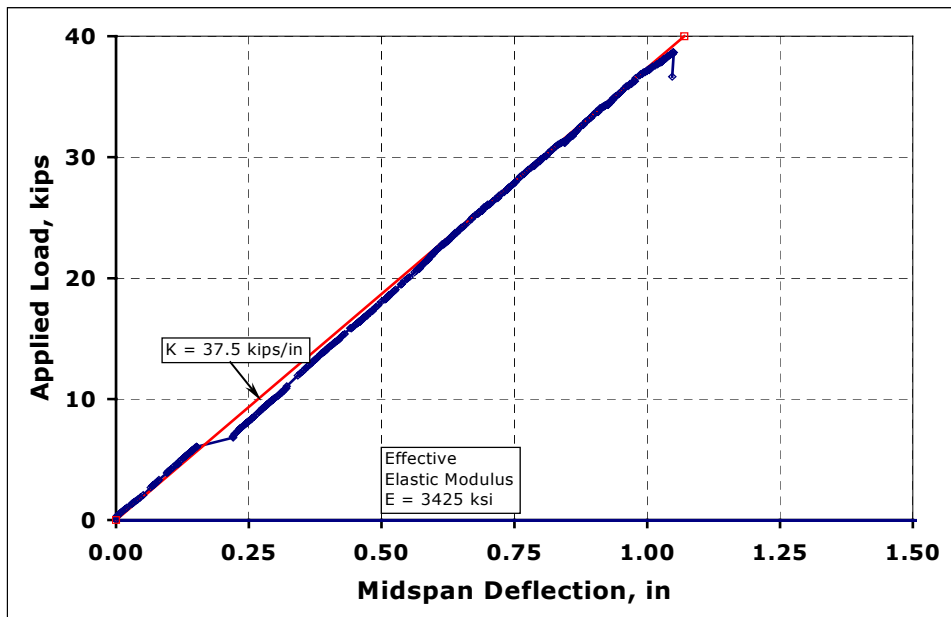


**Figure 4.25.** Load Deflection Response at Midspan.

The response for this test is shown in Figure 4.25. Again it is seen that the response is essentially linear up to failure. The straight line on this figure is used to define a stiffness, which then is used to calculate an effective elastic modulus of the FRP. Based on this curve a value for the elastic modulus was found to be  $E_{FRPgirder} = 3425$  ksi.

Based on the results of both tests, which are plotted on Figures 4.21 and 4.25, the ultimate load for the second test ( $\sigma_u = 38.6$  ksi) is 20% higher than for the first test ( $\sigma_u = 31.5$  ksi). As described above, major modifications were made to the specimen in order to have it reach its tensile strength at the bottom flange. On the modified section, the material carrying the tensile stresses is about 25% of the material carrying the compressive stresses. The tests confirm that the wide flange type of cross section is a very inefficient way of distributing the material in the cross section. Since composite materials have a very low modulus, they are very susceptible to buckling under compressive stress, which will always control for cross sections such as wide flanges and I shapes. It can be concluded that a more efficient cross section is a Tee shaped section, with the larger flange being subjected to compressive stresses.

This inefficient use of material in the FRP girder section, is a compelling reason to develop a structural system combining both the excellent tensile strength of the FRP girder with the compressive strength of the RC deck, furthermore, the ideal combination will have them both working under composite action.

#### **4.3.2 RC Deck**

Concrete cylinders made during casting of the RC deck were tested at 3, 7, 14, 21, and 28 days, to determine the compressive strength of the concrete. The nominal strength was 5000 psi, whereas the measured

compressive strength was 4980 psi. The corresponding elastic modulus using the ACI formula for normal weight concrete was  $E_{\text{concrete}} = 4020$  ksi.

#### **4.4 Structural Analysis and Design**

Specimen FG1 was designed for AASHTO HS20 loading. The resulting structural system consisted of an FRP pultruded girder and an RC deck, both working under composite action.

With this loading, a linear elastic structural analysis was carried out to determine the bending moments, and shear forces developed in the structure. The software used was LEAF (1996). The maximum bending moments, and shear forces developed in the structure were  $M_{\text{max}} = 91.6$  k-ft, at the girder midspan, and  $V_{\text{max}} = 12.8$  kips, close to the girder supports. These values were used for design.

The primary concern during the design of the cross section was finding a way to overcome the low elastic modulus of the FRP, which results in the system undergoing undesirable large deflections. A way to deal with this situation is to consider composite action between the RC deck and the FRP beam. By considering composite action the stiffness of the system increases from  $EI = 6 \times 10^6$  k-in<sup>2</sup> to  $EI = 15 \times 10^6$  k-in<sup>2</sup>, 2.5 times. Hence, the deflection is reduced by the same factor.

Another potential problem caused by the low FRP elastic modulus is buckling. Of particular interest is buckling of the web and top flange. Buckling of the web cross section can occur due to shear stresses acting on it, and diagonal compression (strut action) near the supports, whereas buckling of the top flange is caused by the normal flexural compressive stresses acting on the cross section.



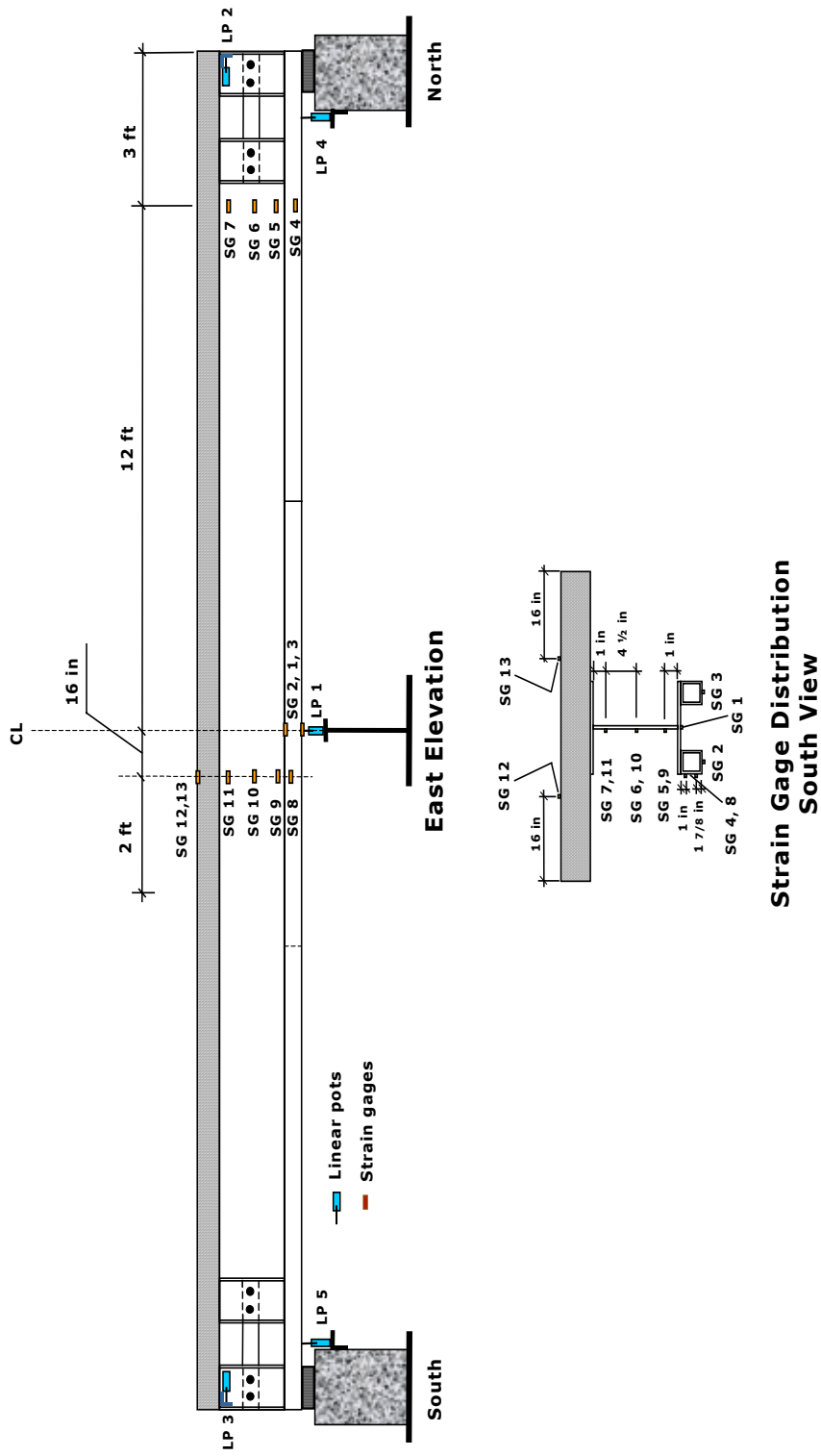
The design also relied on the capacity of the shear connectors at the top flange to carry the shear stresses developed at the deck-girder interface. This part of the design was essential, since the shear connectors were instrumental to the behavior of the system, both for sustaining the load and reducing the level of deflection of the whole system. A general design procedure of FRP thin-walled cross sections is covered in Chapter 10.

#### **4.5 Instrumentation**

Strain gages (SG) were placed on the FRP girder at a section 3 ft. from the south end, and on the FRP girder and the RC deck at a section 16 in. from midspan. These gages were oriented longitudinally with respect to the specimen.

Linear potentiometers (LP) were used to measure the deflections at both ends of the girder near the elastomeric bearings, and at midspan. Differential horizontal displacement between the girder and the deck close to each end was also measured. Figures 4.26 through 4.28 show the distribution of SG and LP for this specimen.

A load cell (LC) was used to measure the magnitude of the applied load on the specimen. See Figure 4.29.



**Strain Gage Distribution South View**

**Figure 4.26.** Specimen FG1, Strain Gages and Linear Pots.

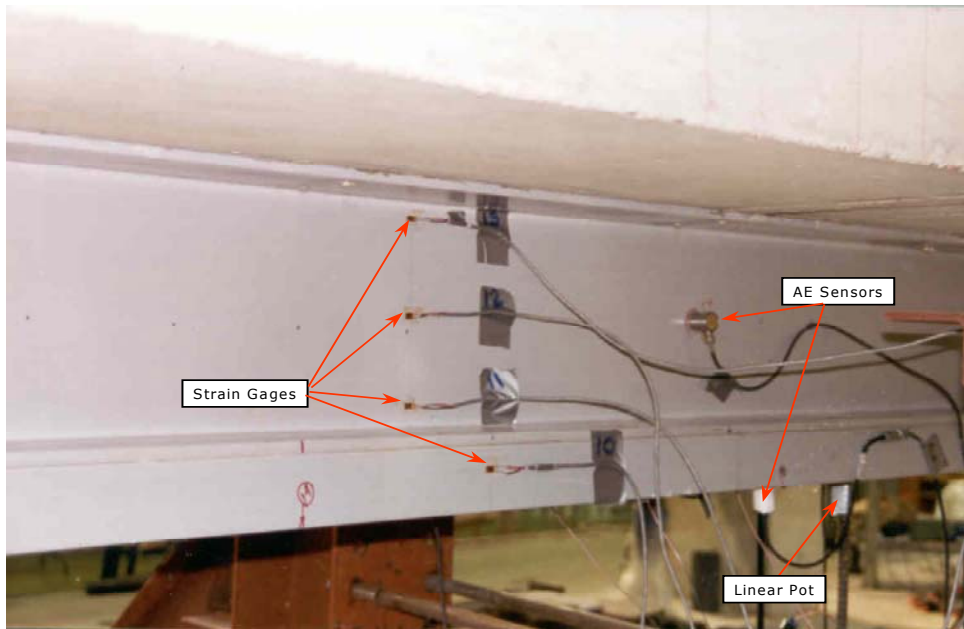


**Figure 4.27.** Instrumentation, Strain Gages, AE Sensors.



**Figure 4.28.** Instrumentation, Linear Potentiometer, AE Sensors.

## 4.6 Loading

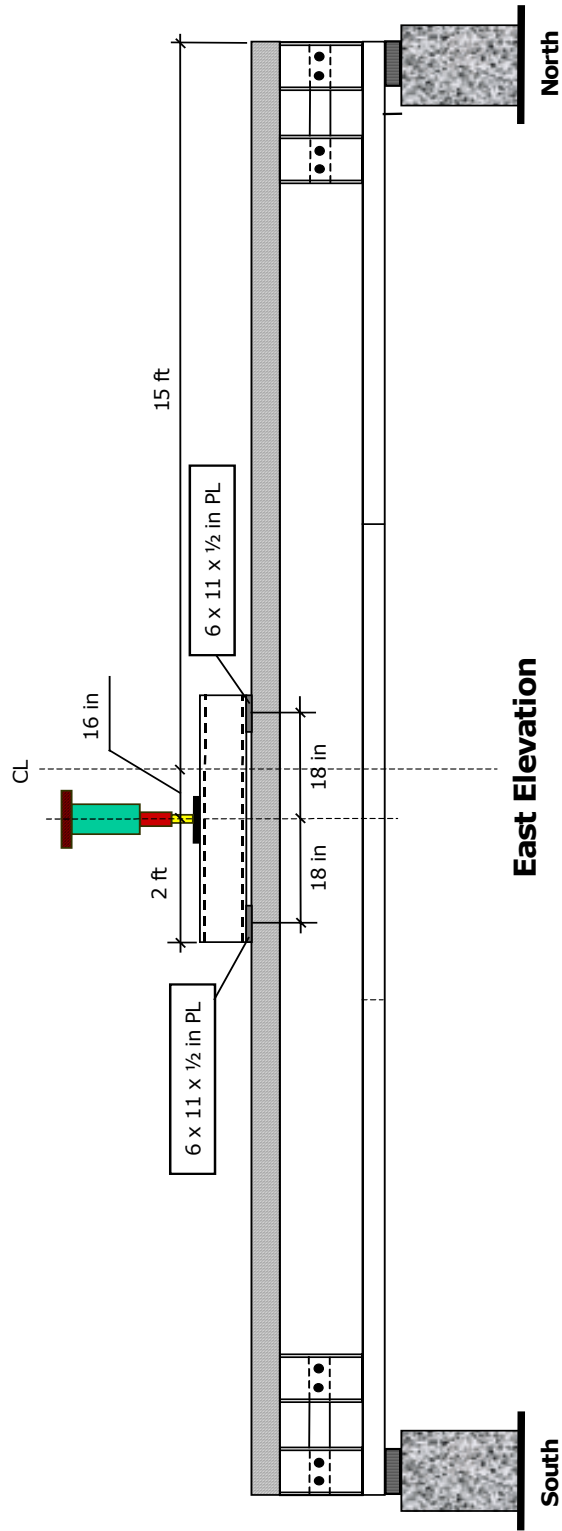
The test setup was described in Chapter 3. A sketch of the loading system is shown in Figure 4.29 and Figure 4.30 shows the loading frame with specimen FG1.

Load was applied to the specimen through a spreader beam on top of the slab. This beam distributed the applied load so as to achieve a four point bending load. The spreader beam was 4 ft. long, with its web stiffened to prevent local buckling. The applied load then was actually applied as two loads 3 ft. apart.

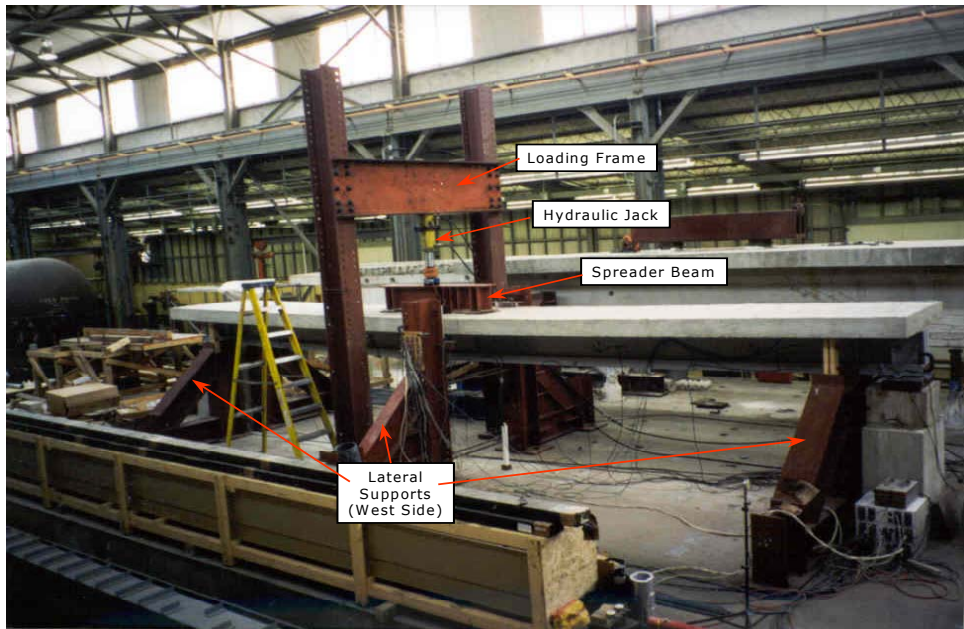
The load was gradually applied to the spreader beam. Except for the initial load, load was applied in increments of 3 kips. Since AE data was being collected for each increment of load a loading–unloading cycle was performed with a waiting period between increments. The specimen was initially loaded up to 4 kips total load, then unloaded to 1 kip, next it was loaded to 7 kips, and then unloaded to 4 kips and so forth. Details are shown in Figure 4.31.

## 4.7 Results and Discussion

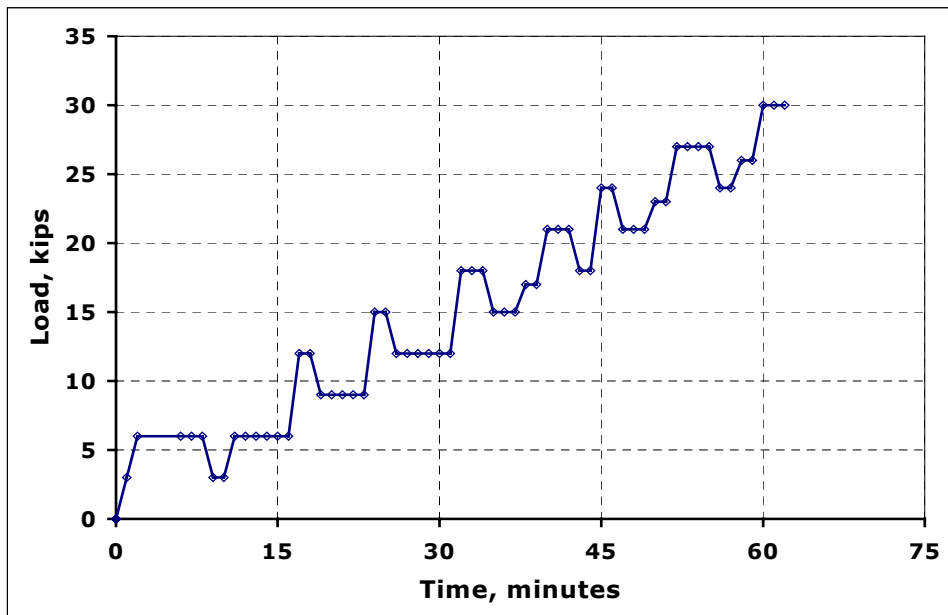
Figure 4.32 shows the experimental load deflection (midspan) curve for this specimen. This deflection already subtracts out the deflection of the elastomeric bearings at each end of the specimen. A theoretical line corresponding to a full composite action is shown in this figure. Also shown is the design load for this structural system cross section due to bending  $M_{\max} = 91.6 \text{ k-ft}$  ( $P = 14.4 \text{ kips}$ ).



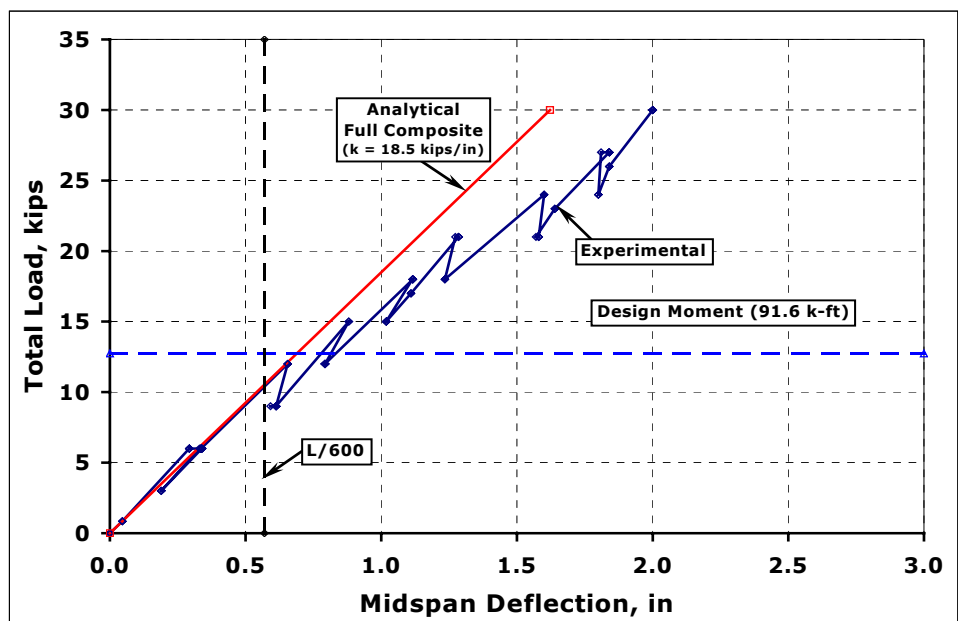
**Figure 4.29.** Specimen FG1, Loading.



**Figure 4.30.** Loading Frame and Lateral Supports.



**Figure 4.31.** Load Schedule.



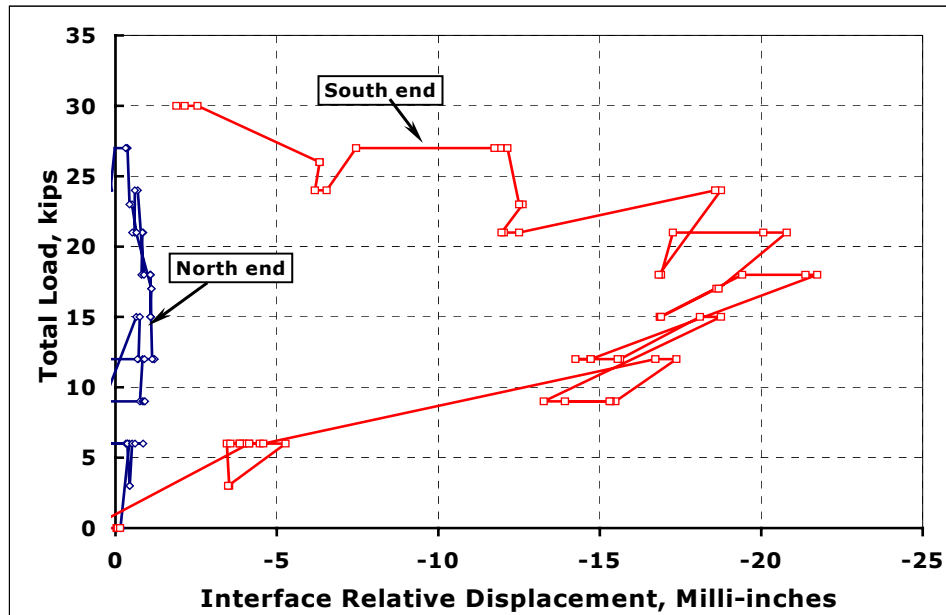
**Figure 4.32.** Specimen FG1, Load-Deflection Curve.

Figure 4.33 shows a plot corresponding to the relative horizontal displacement at the deck-girder interface. The values plotted correspond to measurements at both ends. This figure shows that most of the displacement took place at the south end of the specimen.

Figure 4.32 shows the specimen had an initial stiffness close to the theoretical value for the full composite action of 18.3 kip/in. The stresses began to deteriorate as the level of load was increased. The system response was predicted very closely by the model, for levels of load below 15 kips. As the applied load increased over 15 kips, the system stiffness began to decay. Figure 4.33 shows that at this level, the horizontal relative displacement approached its maximum value. The average stiffness of the system was about 76% of the initial stiffness, that is 13 kips/in.

As the applied load approached 30 kips the system was still working under composite action, although, it was no longer a full composite action

state, instead the cross section carried the loading through partial composite action, as some shear connectors (specifically the ones close to south end), stopped effectively transferring the shear stresses at the deck-girder interface.



**Figure 4.33.** Deck-Girder Relative Horizontal Displacement at each End.

Failure took place at 30 kips, with a corresponding midspan deflection of about 2 in. Failure occurred when the shear connectors completely sheared off, mainly on the south half. Once this happened the system composite action was seriously affected. At this point, the system still had some load carrying capacity, although it clearly experienced large deflections. Specimen FG1 sustained 2.35 times the design load before failure.

As stated earlier, failure started to develop at the south end. Figures 4.34 and 4.35 show the specimen after failure. These figures show that the south half of the FRP girder sheared off from the RC deck. Also, Figure 4.35



shows the slippage of the deck-girder interface as a result of composite action being lost.

The shear connectors failed in three different well defined patterns. The first pattern shows the shearing off of the angle leg embedded in the RC deck, as shown in Figure 4.36. This type of failure occurs parallel to the fibers, which are aligned along the length of the angle. The fiber orientation means that the angle is very weak in this direction.

The second pattern observed shows slippage of the leg embedded in the RC deck. The angle appears to peel from the girder, indicating a good bond with the deck as shown in Figure 4.37. Finally, the third pattern is the failure of the leg bonded to the girder flange through the FRP dowels, also shown in Figure 4.37. This suggests a poor bond between the angle and girder. These last two patterns only take place after some shear connectors had sheared off, and the deck and girder are forced to pry each other open.

Based on the experimental response, it is observed that initially the system effectively developed composite action. As the loading increased the shear connectors began bearing against the surrounding RC deck concrete to transfer shear. Eventually, reaching the shear capacity of the FRP angles. These FRP angles have an inherent low shear capacity in the transverse direction, hence providing little shear capacity where it was needed the most. Also the lack of proper adherence of the shear connectors to the deck and girder compounded the problem and caused composite action to deteriorate. Hence, as soon as the shear connectors failed by shear, the system's stiffness was severely compromised.

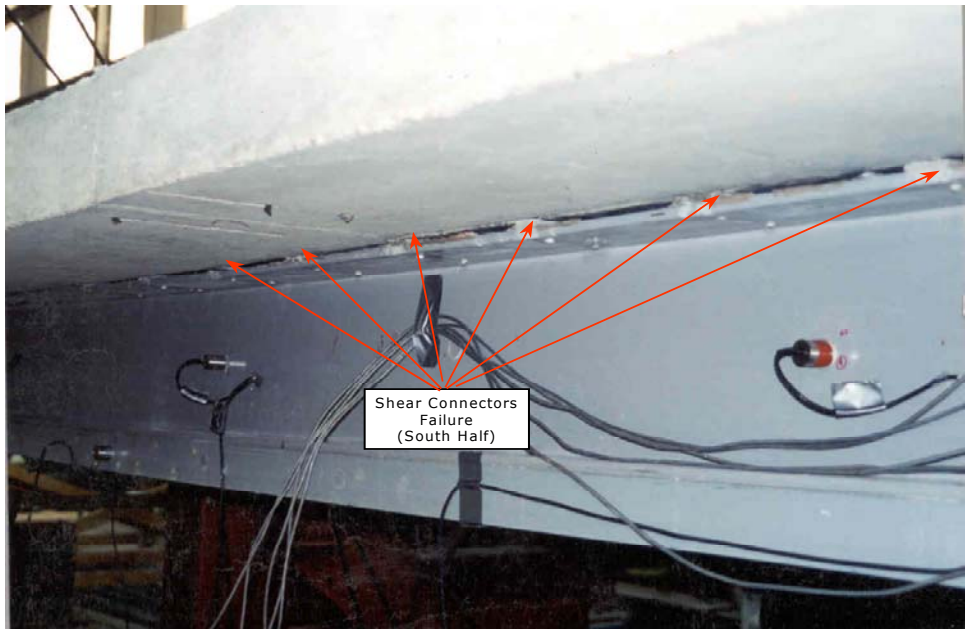


**Figure 4.34.** Failure of Shear Connectors (South Half).

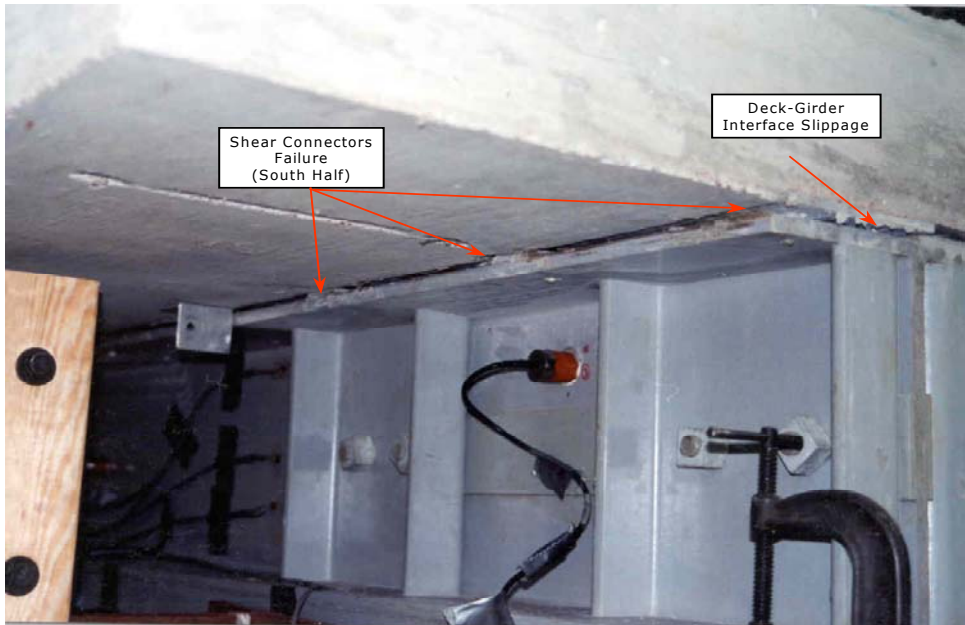


**Figure 4.35.** Failure of Shear Connectors (South End).

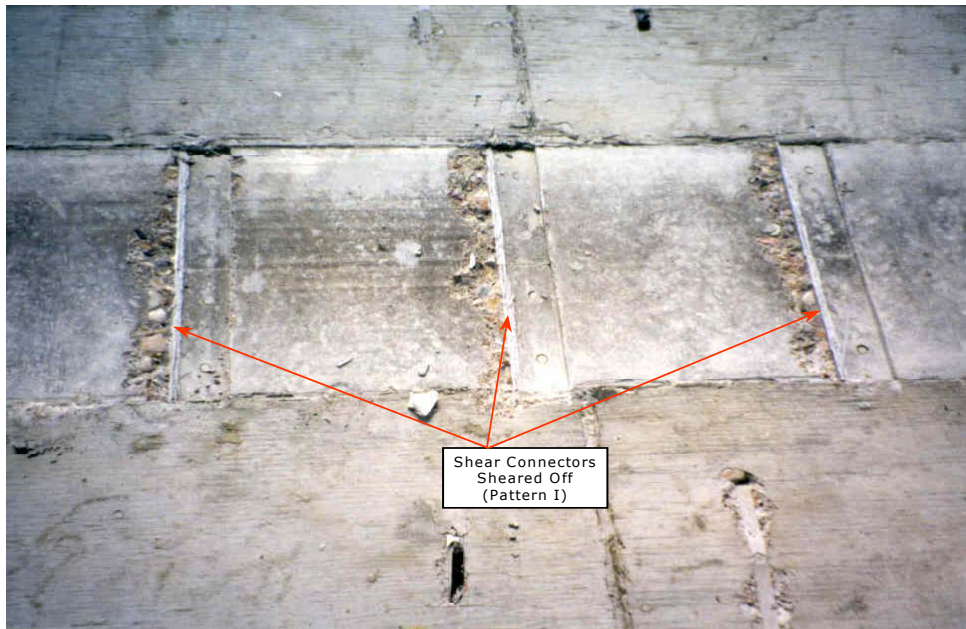


**Figure 4.36.** Shear Connectors Failure: Pattern one.

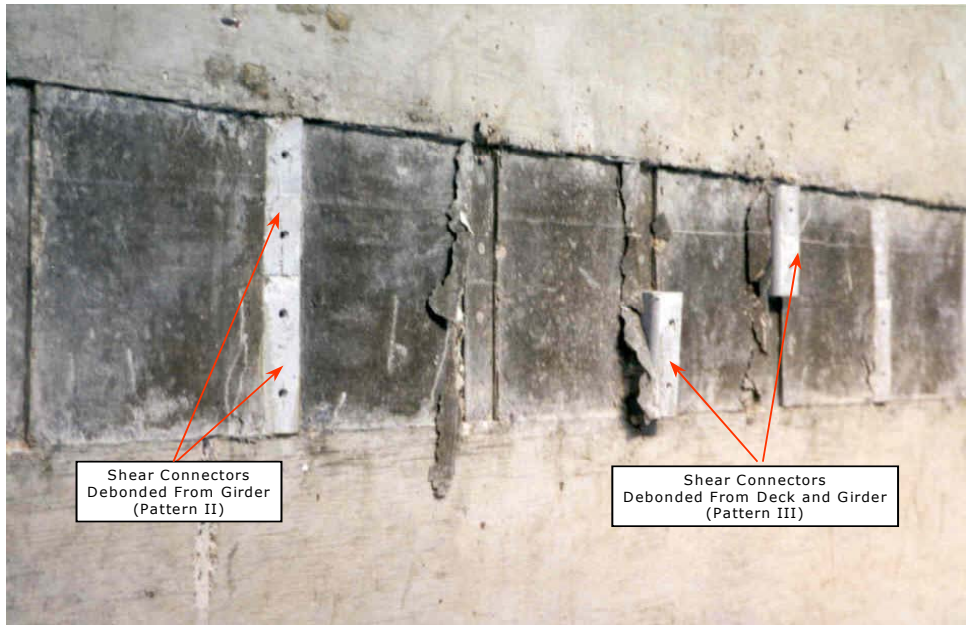


**Figure 4.37.** Shear Connectors Failure: Patterns two and three.

It should be emphasized though, that loss of composite action did not result in a complete collapse of the structural system. The system still was able to carry additional load and certainly its self-weight.

Throughout the test no signs of buckling were observed. The areas that were carefully monitored were the girder web at the supports, and the girder top flange. It appears that the design for buckling was appropriate.

Finally, the strain profiles shown in Figures 4.38 and 4.39 indicate that plane sections do not remain plane. This is more noticeable for the section at midspan, where it appears as if the upper part of the section has a different curvature as compared with lower part, in fact the ratio of curvatures from upper part of the section to the lower part of the section varies from 2 to 2.6.

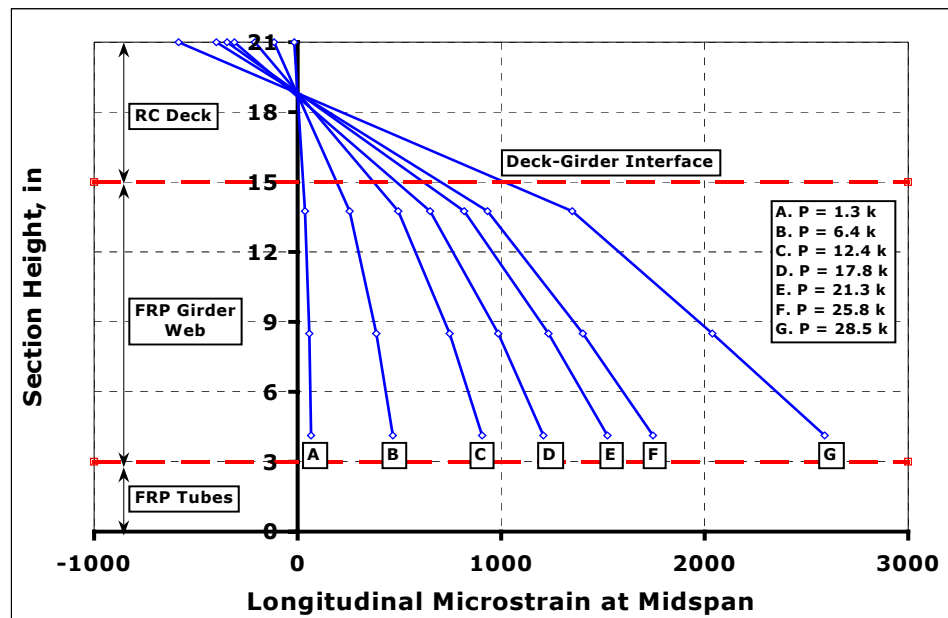


**Figure 4.38.** Longitudinal Strains at Midspan Section.

The fact that plane sections do not remain plane can be attributed to the fact the composite action was not achieved to the level it was expected.

Since development of composite action is closely related to the appropriate behavior of the shear connectors, it is expected that an improved design will greatly improve the behavior of the structural system.

At the section closer to the support shear stresses dominate the behavior and plane sections do not remain plane. This is particularly true for pultruded sections because most fibers are in the longitudinal direction and horizontal shear is carried by the resin. At this section the ratio of curvatures varies from 0.08 to 0.12.

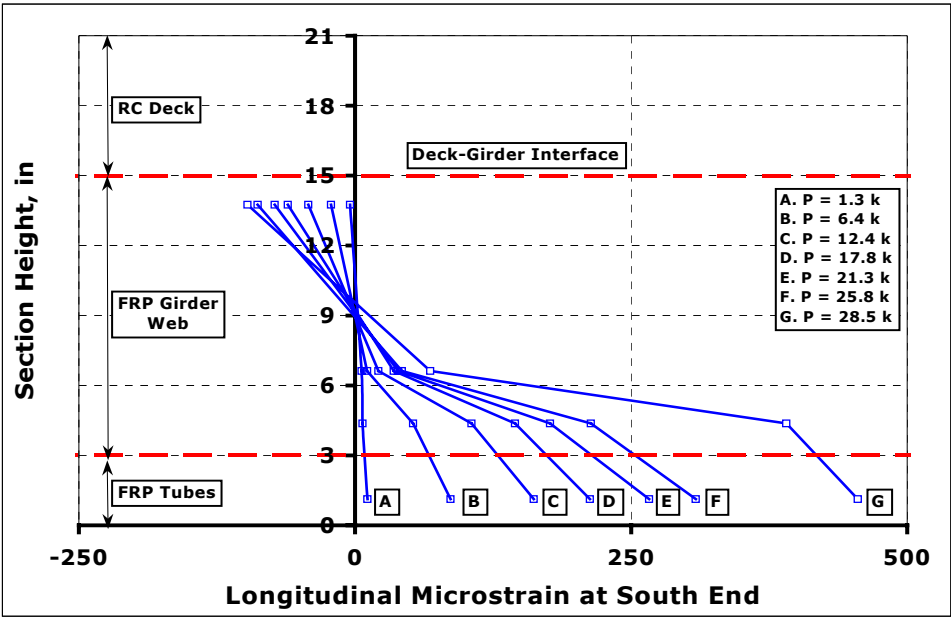


Figure 4.39. Longitudinal Strains at a Section Close to the South End.

### 4.8 Significant Findings

Specimen FG1 behaved as expected. Based on the experimental results, it seems that its structural design was appropriate. A short span bridge based on this structural system is feasible. This design, however, can

be improved by increasing the number of shear connectors in order to develop full composite action.

The method of bonding the shear connectors onto the top flange of the FRP was not adequate. The shear connectors were cut from pultruded angles and the strength was not adequate because the shear stresses were applied on the plane of weakness perpendicular to the fibers.

#### **4.9 Summary**

This chapter described specimen FG1. This specimen had an RC deck together with an FRP pultruded girder, and the resulting structural system sustained load by means of composite action. Composite action was achieved through shear connectors composed of FRP angles attached to the FRP girder top flange.

The specimen sustained loads up to the level it was designed to. The system failed at its weakest link: the shear connectors. When this happened the stiffness of the system was seriously compromised, as a result large deflections took place. It should be emphasized that even when composite action was lost over nearly half the specimen, stability of the system was not an issue. In other words, the system did not experience a catastrophic type of failure.

The system showed great potential for applications in short span bridges, and it is expected that by providing adequate means of handling the shear transfer between the RC deck and the FRP girder, the structural behavior of the system will be greatly improved.

## **Chapter 5**

# **Isophthalic Polyester Pultruded Fiber Reinforced Plastic Girder with Carbon Fiber Reinforced Plastic Strip**

### **5.1 Overview**

This chapter covers specimen FG2. Specimen FG2 was similar to specimen FG1 with the addition of a carbon fiber reinforced plastic (CFRP) strip bonded onto the bottom flange, symmetrically placed between the structural tubes. This CFRP strip was intended to give additional stiffness to the structural system. Additional shear connectors were placed on the top flange, to prevent a failure similar to that which occurred in specimen FG1. This specimen also was designed to meet AASHTO HS20 standards.

### **5.2 General Description**

Specimen FG2 had a nominal length of 30 ft., with a clear span between supports of 28.5 ft. It was composed of a 6 in. thick RC deck and an FRP pultruded girder both of them described in Chapter 4. Figure 5.1 shows details on the FRP girder.

Due to the large deflections experienced by specimen FG1, it was clear that the stiffness of the specimen needed to be increased. In order to increase the stiffness a CFRP strip bonded to the bottom flange of the girder along its entire length was utilized.

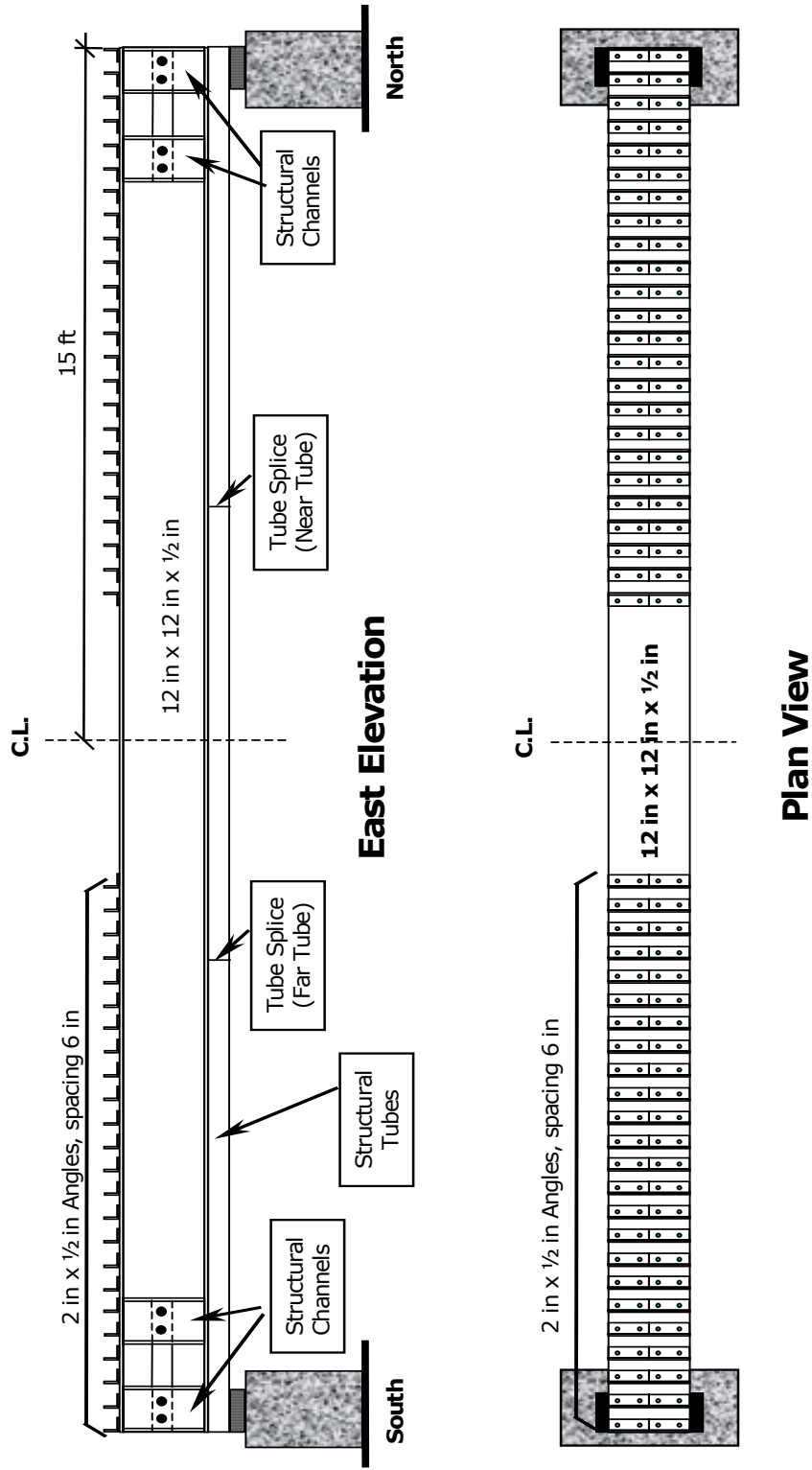


**Figure 5.1.** FRP Pultruded Girder.



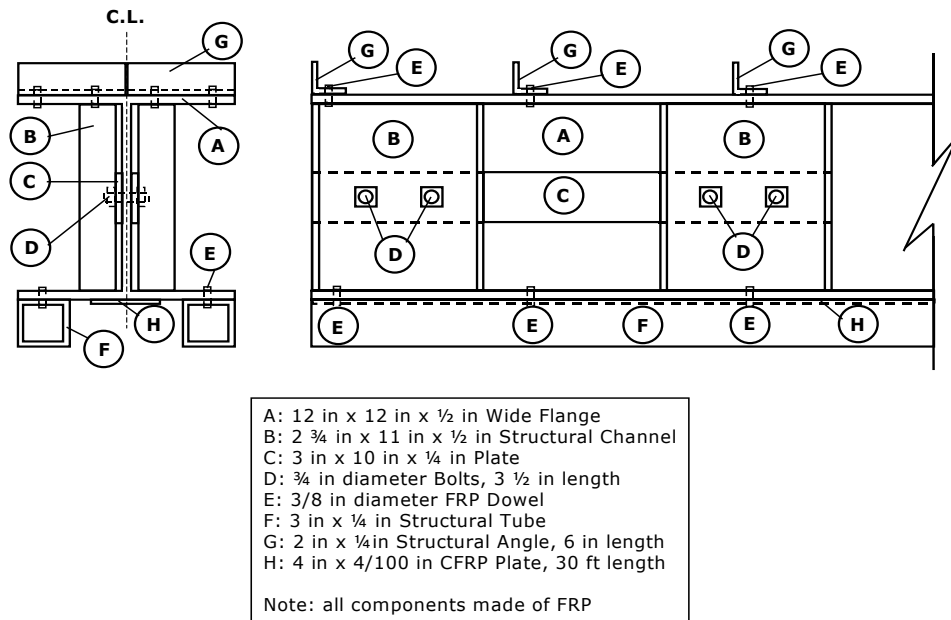


**Figure 5.2.** FRP Pultruded Girder End View and Elevation.

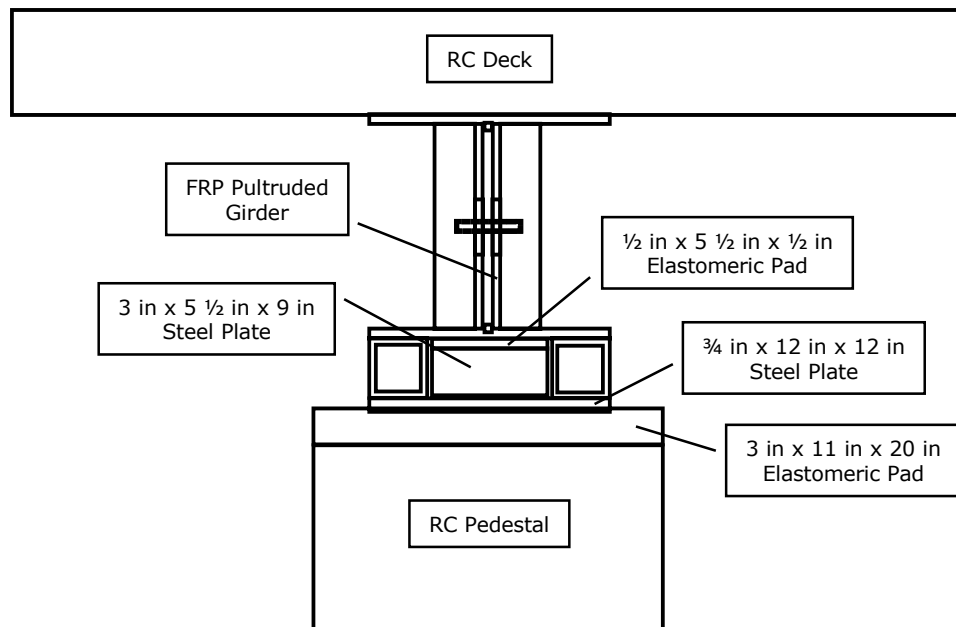


**Figure 5.3.** Support Detail.

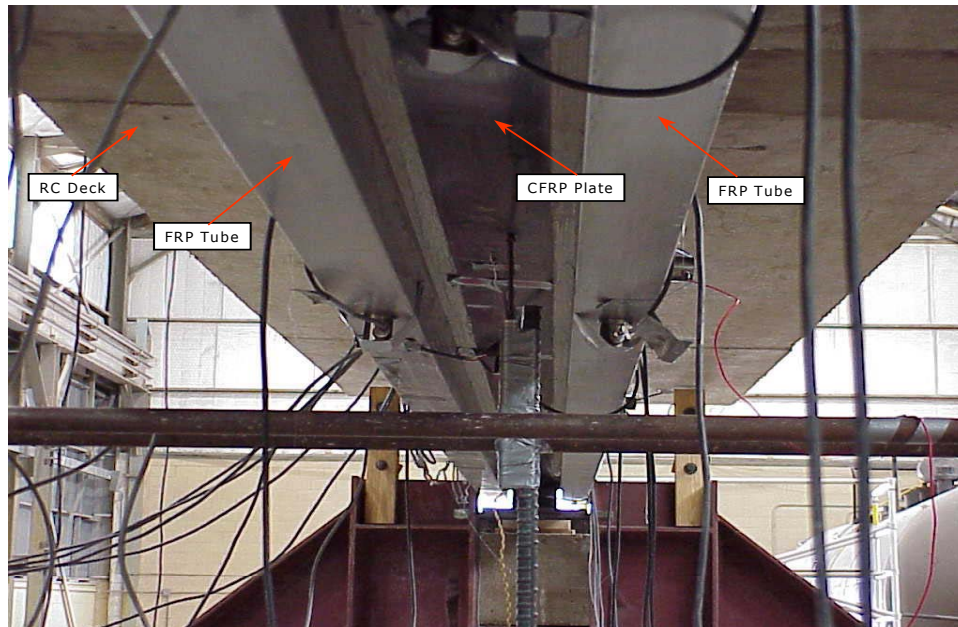


**Figure 5.4.** CFRP strip on Bottom FLange.

The CFRP strip had a 4 in. width and a thickness of 0.055 in. The bonding was performed using standard epoxy. No FRP dowels or other types of additional fasteners were utilized. See Figures 5.2 through 5.4.

Another difference with respect to specimen FG1 was the use of additional shear connectors on the top flange of the girder. Compared to specimen FG1, the number was doubled decreasing the spacing from 12 in. to 6 in.

Lateral support for the specimen was provided as described in Chapter 3. Figure 5.5 shows specimen FG2 prior to testing.



**Figure 5.5.** Specimen FG2 Prior to Testing.

### **5.3 Material Properties**

The materials used in specimen FG2 were thermosetting isophthalic polyester resin, and E-Glass reinforcement in an amount of 50% by weight. Actual material properties were found by testing samples from the RC deck concrete and from a similar FRP girder, specimen FG1.

#### **5.3.1 FRP Pultruded Girder**

A tensile test on a coupon taken from specimen FG1 was performed. The results from this test were discussed in Chapter 4. Based on this results a longitudinal elastic modulus of  $E_L = 3600$  ksi, and a Poisson ratio of  $\nu_{LT} = 0.165$  were determined. A value  $E_L = 2800$  ksi was given by the fabricator.

### **5.3.2 RC Deck**

Concrete cylinders made during casting of the RC deck were tested at 3, 7, 14, 21, and 28 days, to determine the compressive strength of the concrete. The nominal strength was 5000 psi, whereas the actual compressive strength from testing was 5360 psi. The corresponding 28 days elastic modulus using the ACI formula for normal weight concrete was  $E_{\text{concrete}} = 4175 \text{ ksi}$ .

### **5.3.3 CFRP Strip**

The CFRP strips are pultruded laminates commercially available from Structural Composites Inc., and were provided for this specimen by BK International. The mechanical properties provided by the manufacturer are:  $E_{\text{CFRP}} = 30 \text{ Msi}$ ,  $\sigma_{\text{CFRP}} = 300 \text{ ksi}$  (tensile), with reinforcement volume of 70% by volume (Structural Composites Inc., 2000).

## **5.4 Structural Analysis and Design**

As stated earlier Specimen FG2, basically had the same design as Specimen FG1. Hence the design presented in Chapter 4, applies here as well. The influence of the CFRP strip bonded to the girder's bottom flange was not an original design requirement. The plate was added in order to evaluate the effect of this reinforcement on the overall behavior of the structural system. Design calculations actually showed that a thicker CFRP strip would significantly improve the stiffness deficiency of the specimen. The supplier recommended against stacking additional sheets because of concerns about the bond. In a practical application, a greater thickness would be required. A standard 0.04 in. strip was used and it did increase the stiffness of the section by 10%.

It should be recalled that Specimen FG2 was designed for AASHTO HS20 loading. The bending moment, and shear force requirements were  $M_{\max} = 91.6$  k-ft, at the girder midspan, and  $V_{\max} = 12.8$  kips at the supports.

## **5.5 Instrumentation**

Strain gages (SG) were placed on the FRP girder at sections 3 ½ ft., and 8 ½ ft., from the south end, and at midspan. These gages were oriented longitudinally with respect to the specimen.

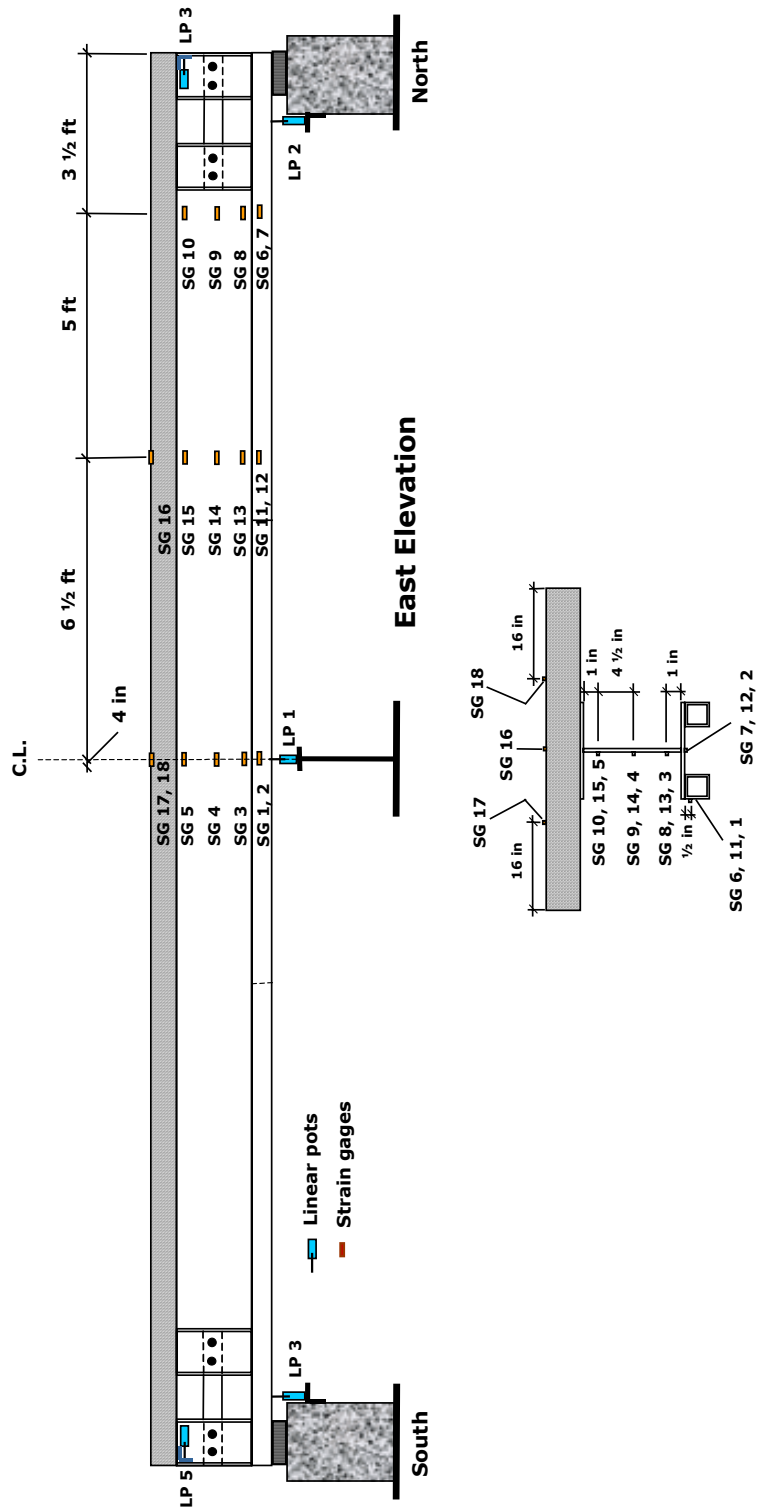
Linear potentiometers (LP) were used to measure the deflections at both ends of the girder near the elastomeric bearings, and at midspan. Horizontal displacement between the girder-deck interface close to each end was also measured. Figures 5.6 through 5.8 show the instrumentation for this specimen.

A load cell (LC) was used to measure the magnitude of the applied load on the specimen.

## **5.6 Loading**

The same loading frame used on Specimen FG1 was used. It was set up with the centerline of the load 4 in. off midspan as shown in Figure 5.9. Load was applied to the specimen through a spreader beam on top of the slab.

This beam distributed the applied load so as to achieve a four point bending load. The spreader beam was 8 ft. long, properly stiffened to prevent local buckling. The effective length between the two loads was 7 ft. as shown in Figure 5.9.



**Strain gages distribution South View**

**Figure 5.6.** Specimen FG2, Strain Gages and Linear Pots.

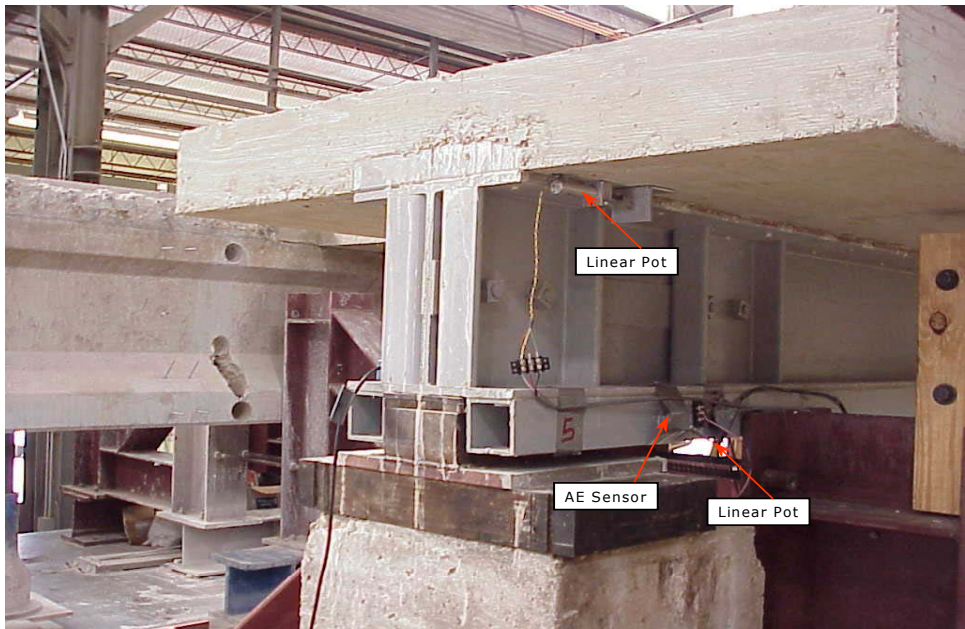


**Figure 5.7.** Instrumentation, South End.

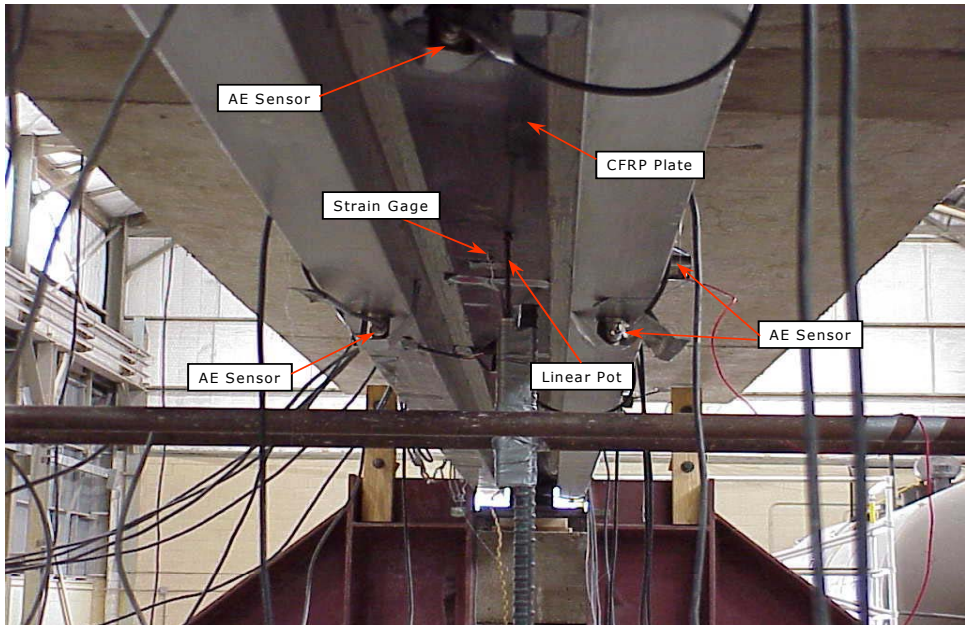


**Figure 5.8.** Instrumentation, Bottom View.

The load was gradually applied to the spreader beam, in increments of 3 kips. Since AE data was being collected simultaneously, for each increment of load a loading–unloading cycle was performed, with a waiting period in between increments. For instance the specimen was initially loaded up to 4 kips total load, then unloaded to 1 kip, next it was loaded to 7 kips, and then unloaded to 4 kips and so forth. See Figure 5.10.

## **5.7 Results and Discussion**

### **5.7.1 Specimen With Tubes on Girder Bottom Flange**

Figure 5.11 shows the experimental load deflection (midspan) curve for this specimen. This deflection already subtracts out the deflection of the elastomeric bearings at each end of the specimen. On this figure also are shown theoretical lines corresponding to a full composite action with the tubes at the bottom flange on, and full composite action with the tubes at the bottom flange removed. Also shown is the design load for this structural system bending  $M_{\max} = 91.6$  k-ft ( $P = 14.4$  kips).

Figure 5.12 shows a plot corresponding to the horizontal relative displacement at the deck-girder interface. The values plotted correspond to measurements near both ends. Figure 5.12 shows the relative displacements at the north end of the specimen were larger than those at the other end. However, the actual value of these displacements was very small. Compared with Specimen FG1, these relative displacements for Specimen FG2 were smaller by a factor of 10.



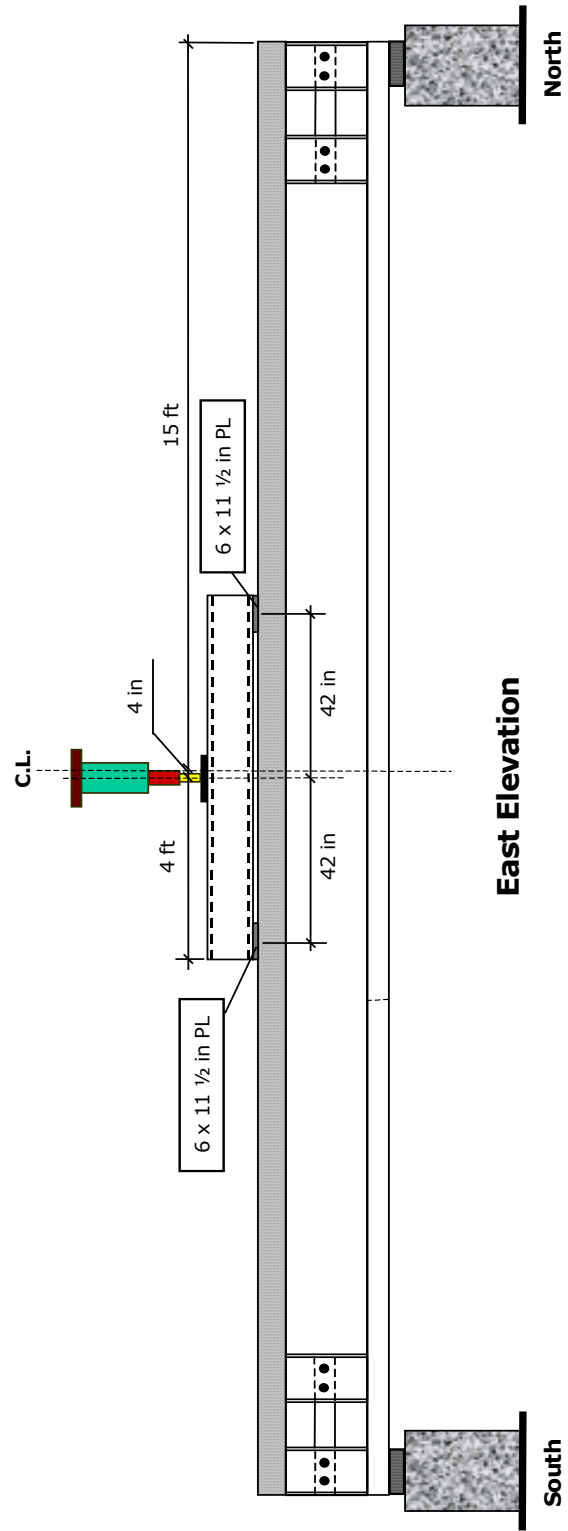


**Figure 5.9.** Specimen FG2, Loading.

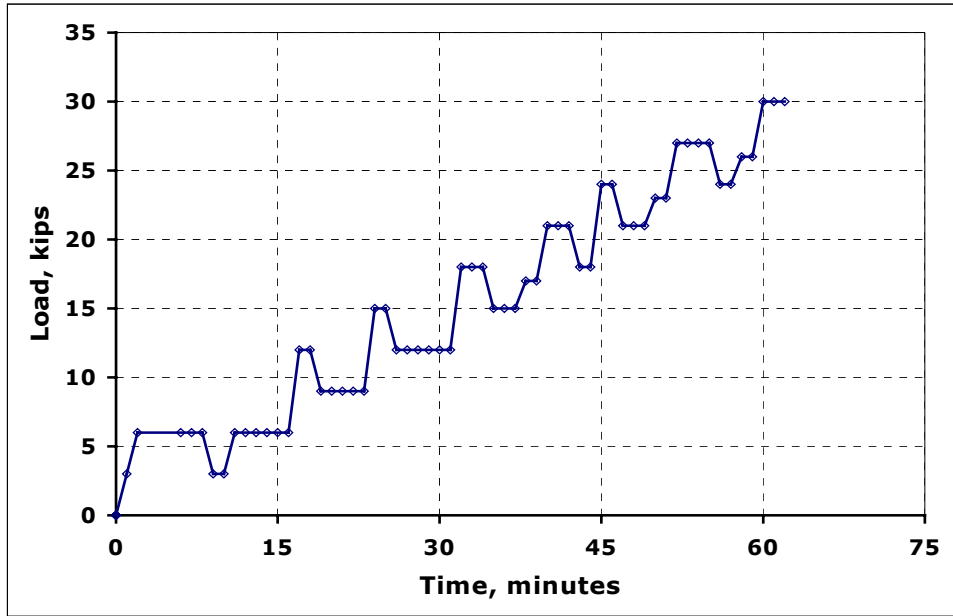


Figure 5.10. Load Schedule.

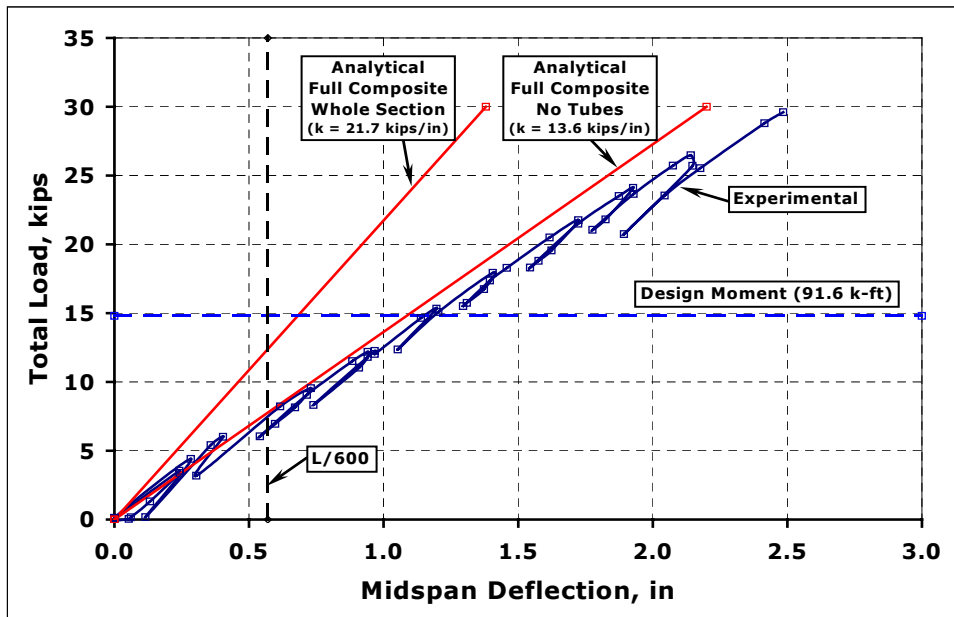
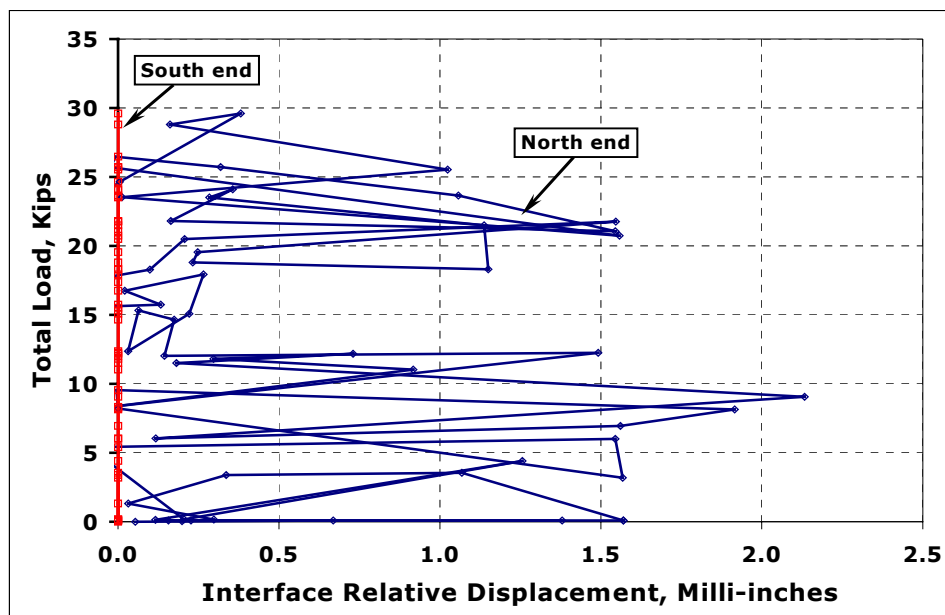


Figure 5.11. Specimen FG2, Load-Deflection Curve.

Figure 5.11 shows the specimen had an initial stiffness of about 15 kip/in, which began to deteriorate very early as the load was applied. By the time the applied load exceeded 6 kips, the system lost almost 20 % of its initial stiffness, down from 15 kips/in to 12 kips/in. The stiffness of 12 kips/in remains almost constant up to failure. The main reason for this unexpected behavior was the early debonding of the tubes on the bottom flange. AE data from the specimen showed that debonding of the tubes began early during the test. Visually it was not possible to see this taking place.



**Figure 5.12.** Deck-Girder Interface Horizontal Displacement at each End.

The specimen response was as though the section did not have the tubes bonded to the bottom flange of the girder, thus having its stiffness seriously affected as shown by the predicted responses on Figure 5.11, which shows that the specimen response was close to the predicted behavior of a specimen having the FRP girder with no tubes on its bottom flange.

Failure took place at 30 kips, with a corresponding midspan deflection of about 2.5 in. Failure occurred when the tube on the west side on the bottom flange came off. It completely debonded from the midspan towards the south end. See Figures 5.13 and 5.14. This was the most significant damage. A visual inspection, showed the shear connectors had suffered some damage, similar to that with specimen FG1. Specimen FG1 sustained 2.0 times the design load before failure.

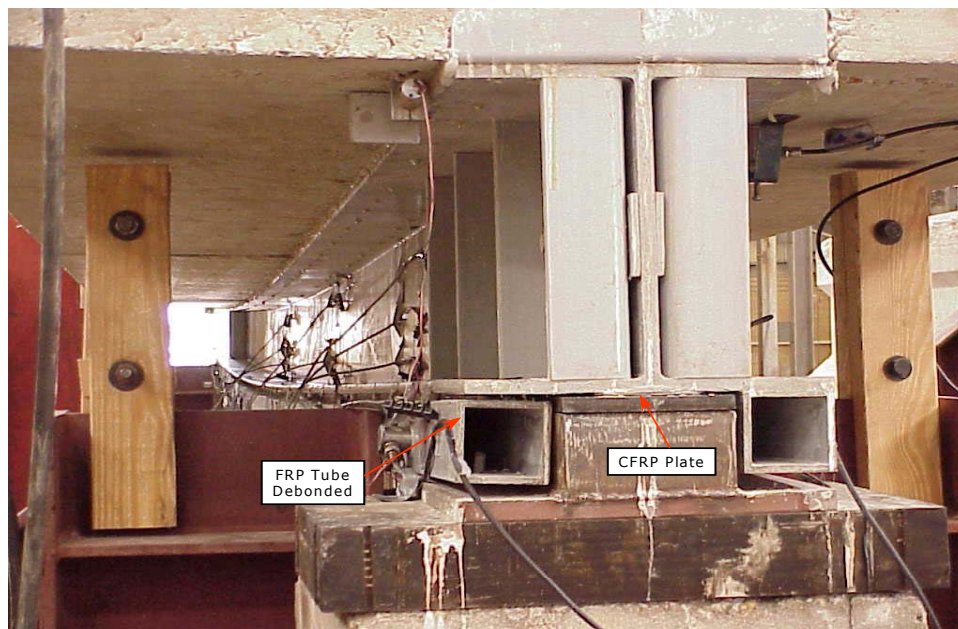


**Figure 5.13.** West Side Tube Debonded, View From South End.

The reasons for the debonding of the tube are not clear. It could have been caused by poor initial fabrication. Damage to the specimen in the bonding area, might have also been caused during transit. The failure is unsettling, because the same basic specimen (specimen FG1) had a completely different behavior.

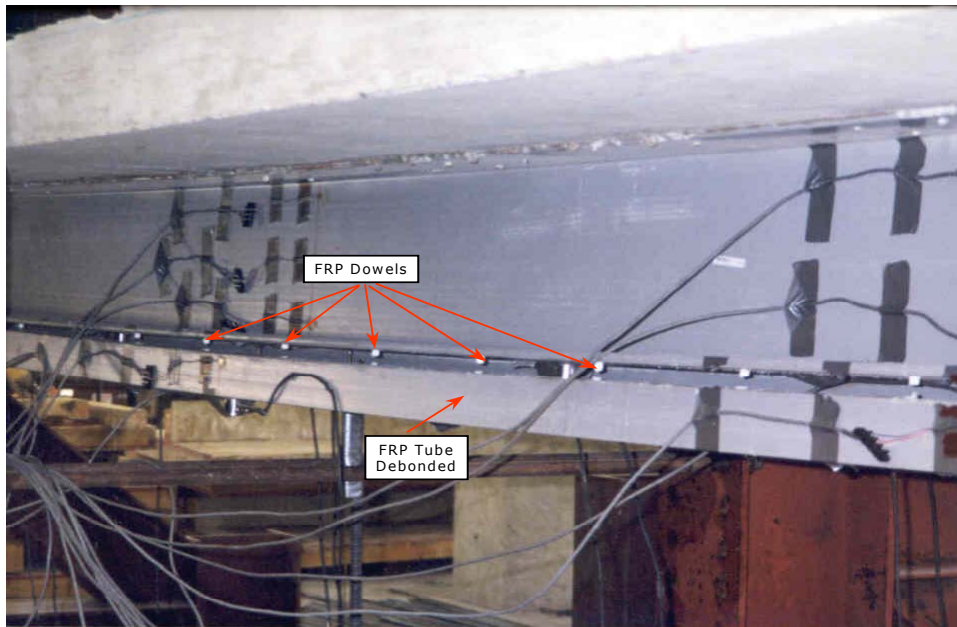


**Figure 5.14.** West Side Tube Debonded, View From West Side.

In Chapter 4, the strain profile at two sections along the specimen was presented, and it was shown that plane sections did not remain plane as the load was applied. It was speculated that this was caused by inadequate composite action development, and it was suggested that improving the behavior of the shear connectors the section would deform more uniformly.

Specimen FG2 featured an increased number of shear connectors. The strain profiles for sections at similar locations as specimen FG1 are shown in Figures 5.15 and 5.16. These figures show the longitudinal strain distribution along the depth at midspan and at a section 3.5 ft. from the south end.

It is seen in these figures that the sections now experienced a more uniform curvature, specially the section at midspan. The section at the south end still shows some inconsistencies, but it is to be expected since at this location the shear forces control the behavior of the section as opposed to the section at midspan where bending controls.

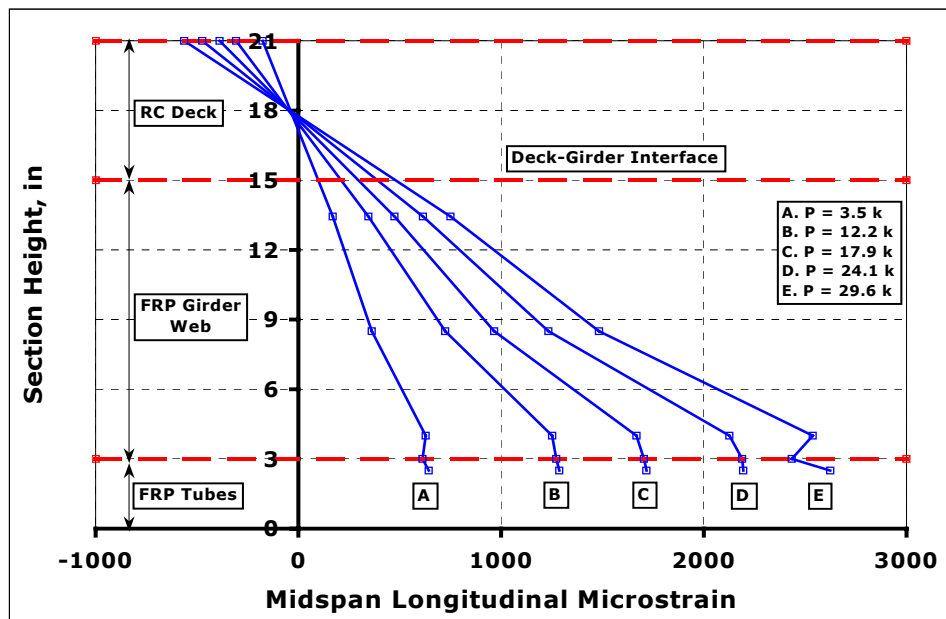


Figure 5.15. Longitudinal Strain at Midspan.

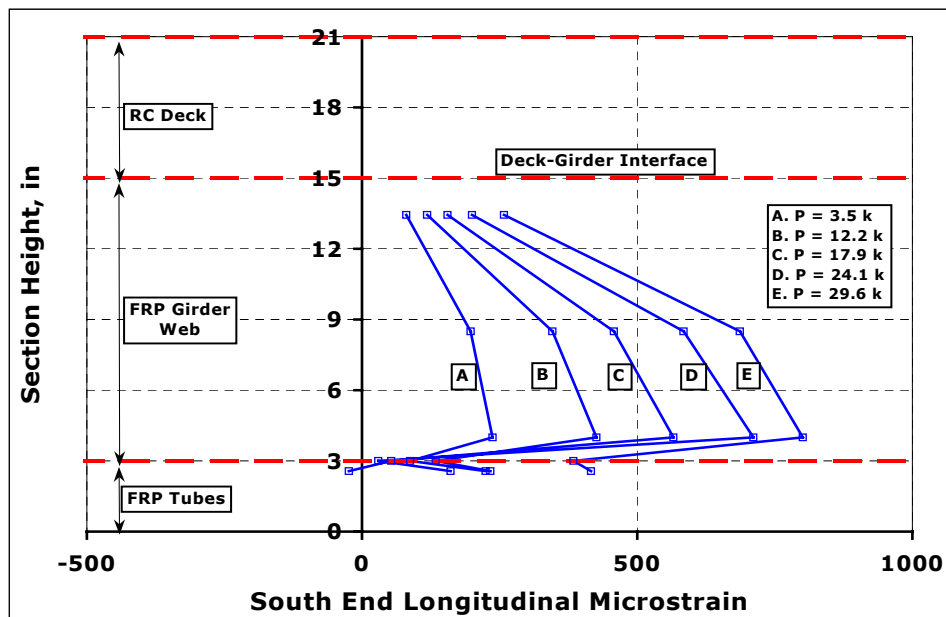


Figure 5.16. Longitudinal Strains at 3.5 ft. From South End.

Also, it is seen on these figures that the strains in the tubes at the bottom flange do not follow the profile of the rest of the section. The section close to the south end shows it very clearly. These strains show that the tubes were slipping at early stages of loading, suggesting that the bond between the tubes and the bottom flange was not transferring the shear forces at that interface.

### **5.7.2 Specimen With Tubes on Girder Bottom Flange Removed**

It was decided to remove both tubes on the bottom flange of the specimen and continue the test. Figure 5.17 shows the specimen during testing. It can be observed that large deflections are taking place. Eventually, the test was stopped because of the excessive deflections that the specimen developed. A post-test visual inspection revealed that the shear connectors failed in some areas, although not as many as with specimen FG1. Thus the increase in the number of shear connectors actually helped to enhance the shear capacity at the interface.

The results of this test are shown in Figure 5.18. Initially the results are close to the theoretical values, but eventually deviate from it. This deviation from the theoretical curve might have been caused by the shear connectors on the top flange beginning to experience some damage. As the test progressed, this deviation increased.

Throughout the test no signs of buckling were observed. The areas that were carefully monitored were the girder web at the supports, and the girder top flange.



**Figure 5.17.** Specimen Without Tubes, Excessive Deflections.

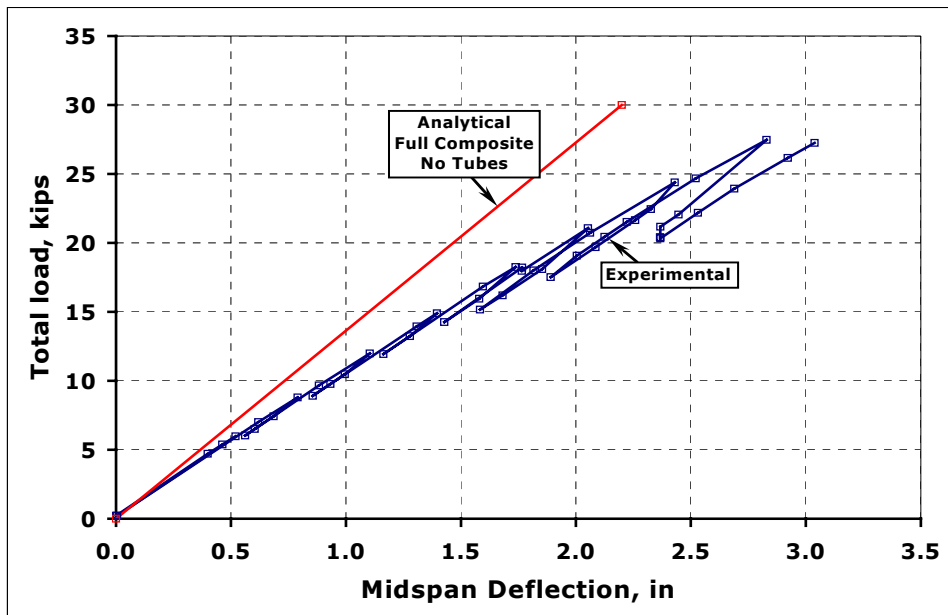


**Figure 5.18.** Load deflection Curve. Specimen FG2 without Bottom Tubes.



## **5.8 Significant Findings**

The increase in number of shear connectors improved the development of composite action, because shear failure at the deck-girder interface was not observed.

The debonding of the tubes on the bottom flange of the FRP girder was now a clear indication that adhesive bonding of composite components is not reliable. Other ways of connecting structural members should be explored.

The influence of the CFRP on the bottom flange of the girder could not be fully assessed, because of the early debonding of the tubes. Within this limitation, the CFRP laminate behaved as expected and remained bonded to the bottom flange.

Wide flange and I shaped pultruded structural members are not very efficient for structural applications when acting alone. This is because the compression flange controls the behavior of the member. The limit imposed by the compression flange is one quarter of the limit of the tension flange.

## **5.9 Summary**

This chapter described specimen FG2. This specimen had a RC deck attached to a FRP pultruded girder, and the resulting structural system sustained load by means of composite action. In addition this specimen had a CFRP strip bonded to the bottom flange of the FRP girder. Composite action was achieved through shear connectors composed of FRP angles attached to the girder top flange.

Except for the CFRP strip and the shear connectors, Specimens FG1 and FG2 were identical. They both were fabricated in the same shop, and

were visually inspected upon arrival at the FSEL. No indication of damage or different quality of bond between tubes and girder was observed. Nevertheless, the behavior of specimen FG2 was significantly different from specimen FG1, as one of the tubes on the bottom flange debonded at low level of applied load. This very different behavior of similar FRP components, points the need for using NDT methods to inspect the integrity of secondary bonds, before the structural member is used as part of the structural system. The NDT techniques are ideal for this kind of application.

The addition of shear connectors at the deck-girder interface improved the development of composite action and hence the behavior of the sections along the specimen length behaved much better than the corresponding sections in specimen FG1. In Specimen FG1, it was shown that the assumption that plane sections remain plane was not realistically met.

Also the influence of the addition of the CFRP strip on the bottom flange could not be assessed due to the early debonding of the bottom tubes. Once this happened, there was no way of comparing specimens FG1 and FG2, since their configuration changed. Theoretically the addition of the CFRP strip increased the stiffness of the section by 10%, experimentally though it was not possible to verify this increase in stiffness.

Otherwise, the system showed great potential for applications in short span bridges, but for the system to behave more reliably, additional research is needed on an efficient way of bonding the shear connectors to the FRP girder and the RC deck. The other alternative is to use mechanical fasteners instead. The study of this option is obviously a topic for future research.

## **Chapter 6**

# **Vinyl Ester Pultruded Fiber Reinforced Plastic Girder**

### **6.1 Overview**

This chapter describes experimental work performed on specimens IKG1 and IKG2. Specimen IKG1 had a configuration similar to specimen FG1 discussed in Chapter 4; its structural system was composed of a built-up FRP girder and an RC deck working under composite action. The FRP girder was similar in geometry to the girders in Specimens FG1 and FG2, but it had different material components. The girder was fabricated with vinyl ester. Specimen IKG1 was subjected to a long-term loading to study its creep behavior. Specimen IKG2 consisted of the FRP girder alone and was tested under short term loading to establish its bending, shear, and buckling properties.

### **6.2 General Description**

Specimen IKG1 had a nominal length of 30 ft., with a clear span between supports of 28.5 ft. It was composed of a built-up fiber reinforced plastic (FRP) girder and a reinforced concrete (RC) deck designed to carry loading by means of composite action. The FRP girder was similar in geometry to the FRP girders used in Specimens FG1 and FG2 described in Chapters 4 and 5.

The original FRP girders were developed and commercialized by IKG Fiberglass Systems, Nashville, Tennessee. These girders have a typical length of 30 ft., and the dimensions of the cross section are 12 in. width, 12 in. depth, with an average thickness of ½ in.

The built-up section consisted of the original FRP girder with the addition of a pair of FRP tubes onto its bottom flange, and a set of channels at each end to increase the stability of the web.

The girders, structural tubes, channels, and angles were fabricated for IKG by Bedford Reinforced Plastics, Inc., Bedford, Pennsylvania. Figure 6.1 shows a picture of the original FRP girder, whereas Figure 6.2 shows a picture of the finished built-up FRP girder.

Specimen IKG2 was a sample taken from one of the original FRP girders. It was tested to find the material properties of the FRP girders. Special attention must be paid to the shear, bending, and buckling behavior of these kinds of structural shapes.



**Figure 6.1.** Original FRP Girder.

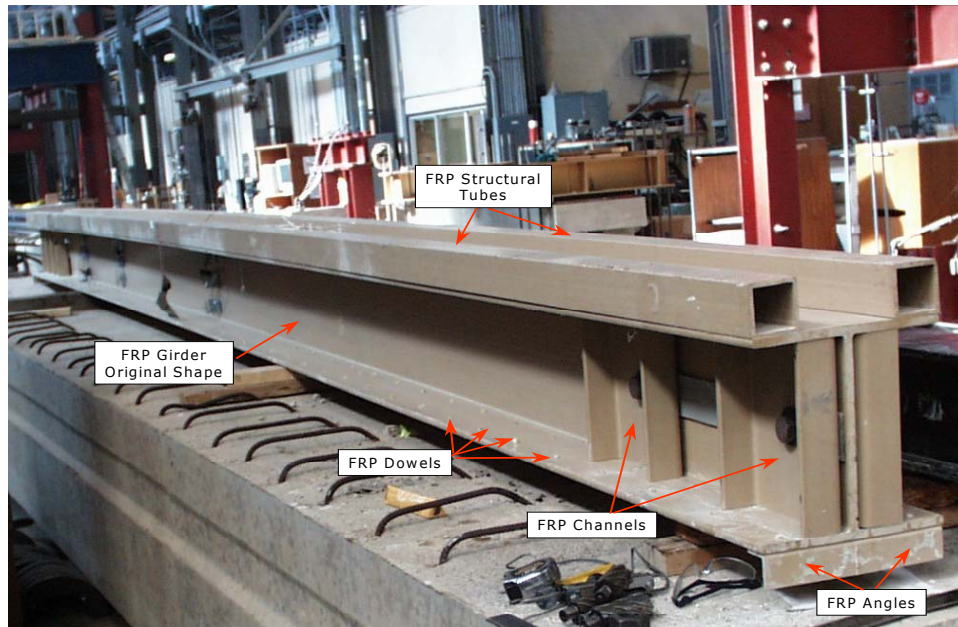


**Figure 6.2.** FRP Girder Built-up Cross Section (Upside Down).

### 6.2.1 Specimen IKG1

Specimen IKG1 was composed of a built-up FRP girder and an RC deck. This structural configuration was intended to have the girder and the deck working under composite action. This specimen was similar in geometry to specimens FG1 and FG2 described in Chapters 4 and 5.

FRP structural angles and FRP structural square tubes were added to the top and bottom flanges of the original wide flange section respectively. The FRP square tubes were intended to increase the stiffness of the original section, whereas pairs of angles across the top flanges were added to work as shear connectors necessary to develop composite action between the FRP girder and the RC deck. These shear connectors had one of their legs bonded to the top flange of the FRP girder and the other leg embedded in the RC deck. Shear connectors were not added over the midspan. Both tubes and angles were first bonded onto the flanges and then further secured by

means of FRP dowels. The procedure was similar to the one used for the built-up FRP girders in specimens FG1 and FG2 discussed in Chapters 4 and 5. In addition, FRP channels were attached to both sides of the web at each end of the girder tightly secured by steel bolts; they were designed to provide lateral stiffening to the girder web. Attachment of the shear connectors, structural tubes, and channels was done at the University of Texas. Figure 6.3 shows a detail of the built-up girder end, and Figure 6.4 shows the finished built-up girder.

The RC slab had a 4 ft. width, 6 in. thickness and 30 ft. length. Number 4 Grade 60 rebars were used 12 in. apart both longitudinally and transversely. Figure 6.5 shows specimen IKG1 typical dimensions and Figure 6.6 shows the finished specimen still with the shoring in place. The specimen clear span was 28.5 ft.

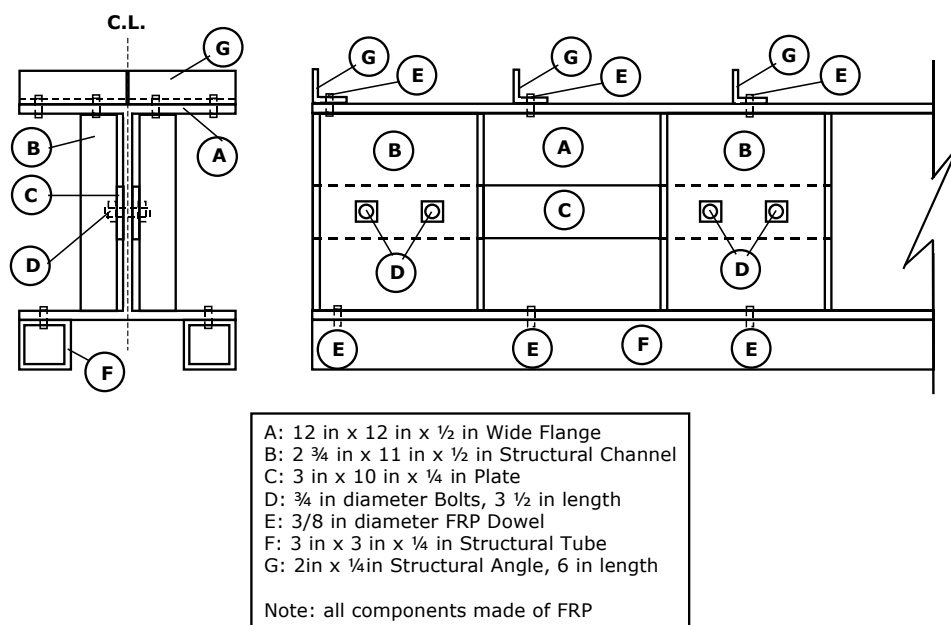


**Figure 6.3.** Pultruded Girder End Detail.

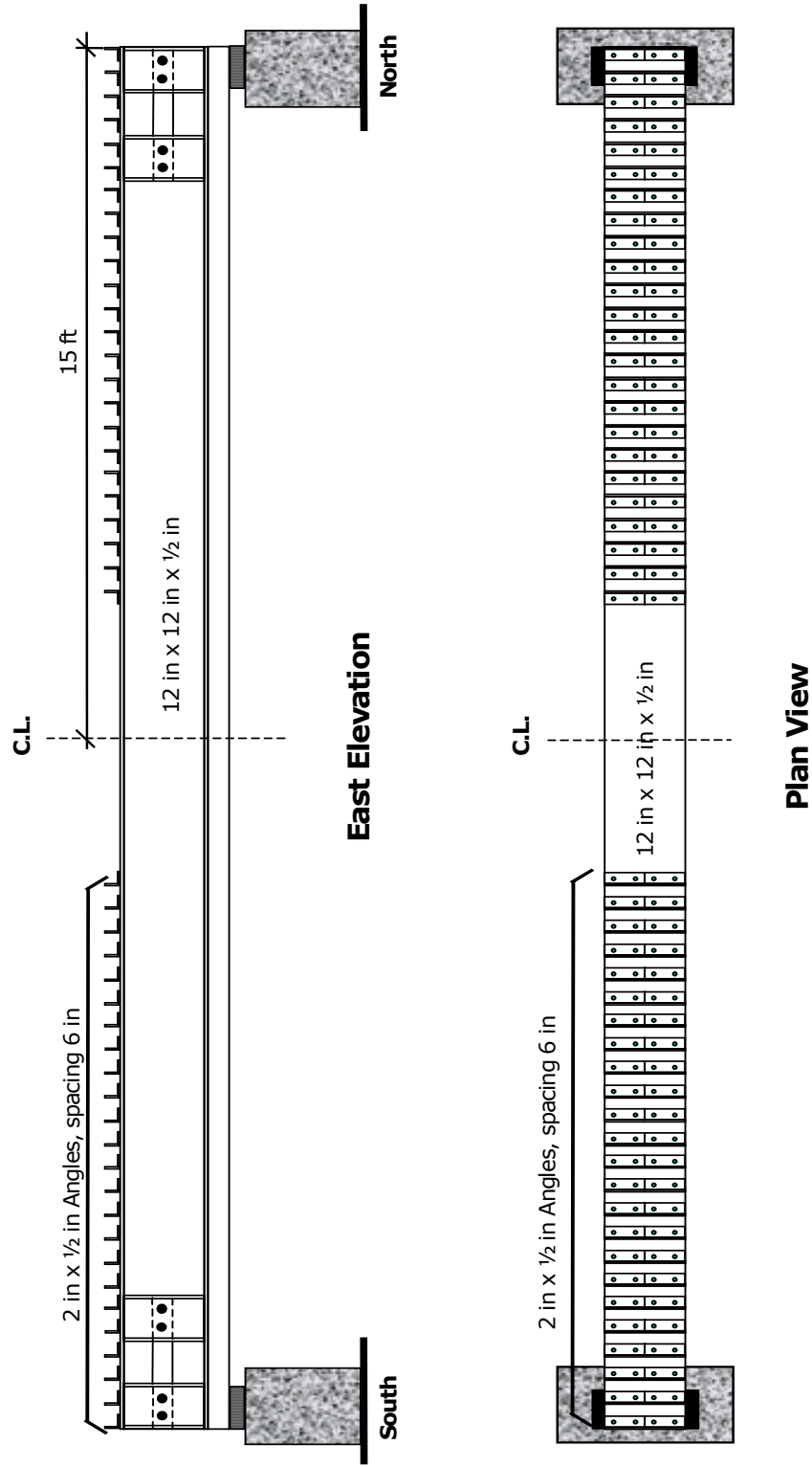


**Figure 6.4.** Specimen IKG1 - FRP girder.

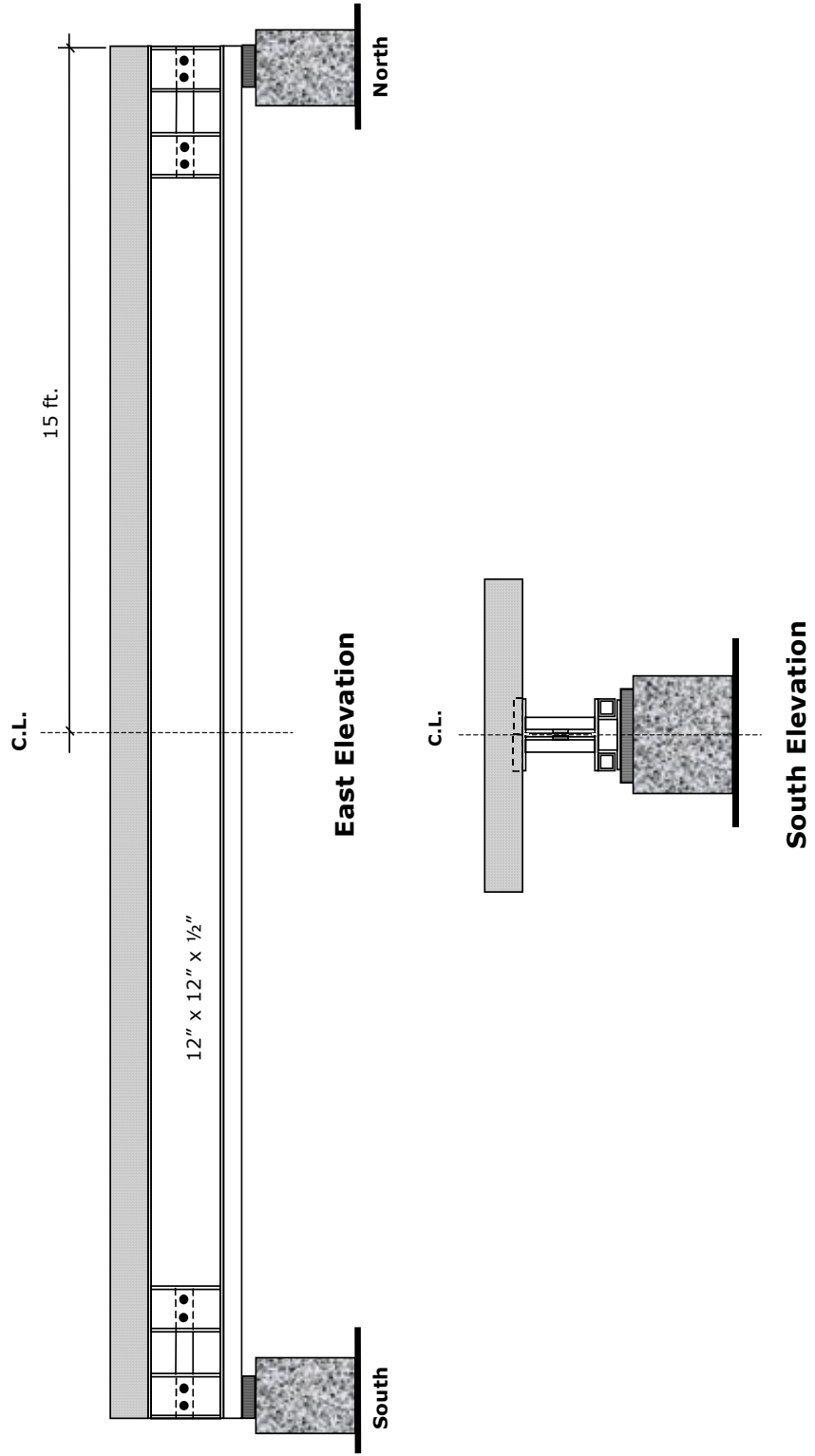


**Figure 6.5.** Specimen IKG1.



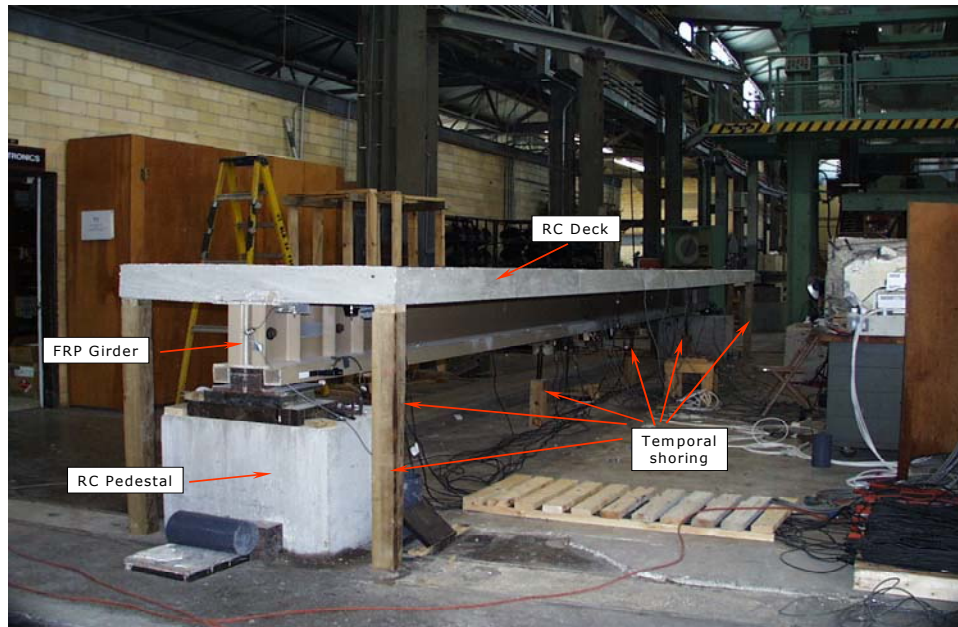


**Figure 6.6.** Specimen IKG1 finished.

### **6.2.2 Specimen IKG2**

Specimen IKG2 was taken from an original FRP girder, and had a length of 98 in. It featured some geometry modifications on its web and bottom flanges aimed at inducing tensile failure of the bottom flange, rather than compressive failure of the top flange. The modifications to the web and bottom flange were performed at an independent shop and are discussed in Section 6.3. This specimen was tested under four point bending to find the overall mechanical properties of the girder alone.

### **6.3 Material Properties**

The materials components for the FRP girder, tubes, angles and channels, were vinyl ester resin, and E-glass reinforcement in an amount of 50% by weight. Derakane 510C vinyl ester manufactured by Dow Chemical

Company was chosen for the resin. Actual material properties were found by testing samples taken from the FRP girder (Specimen IKG2) and the RC deck.

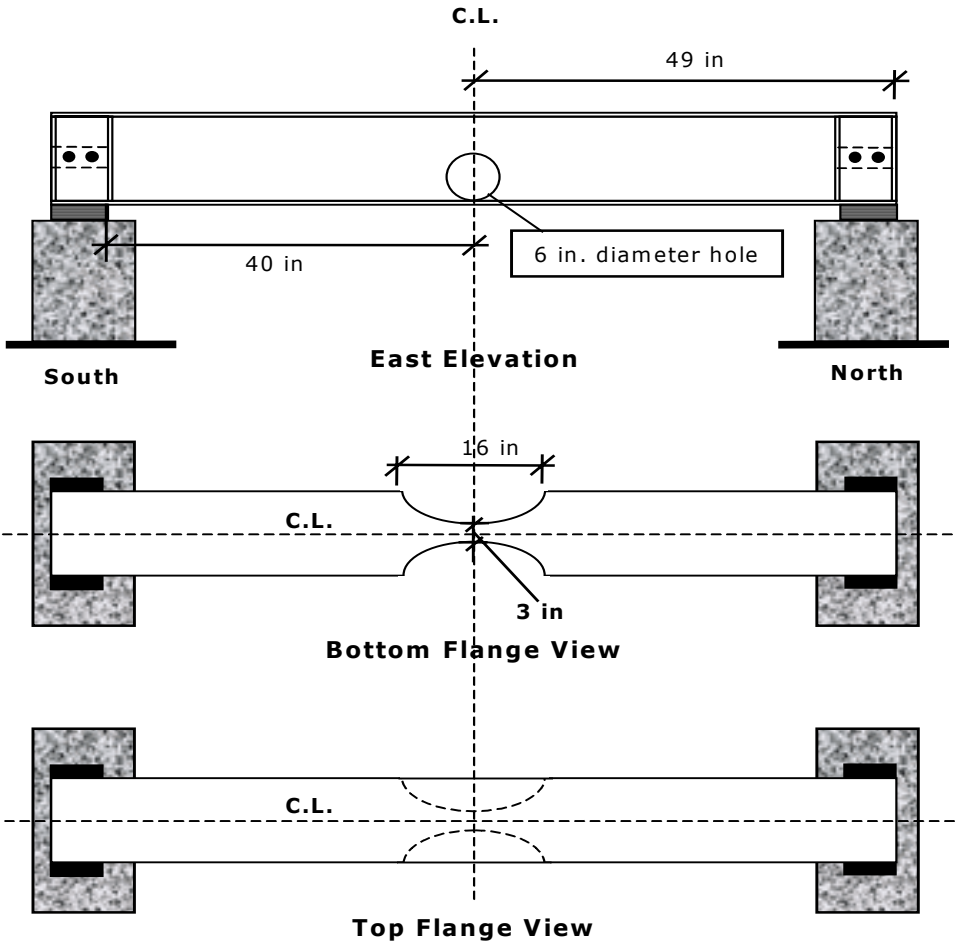


**Figure 6.7.** Specimen IKG2.



**Figure 6.8.** Specimen IKG2.

### **6.3.1 FRP Pultruded Girder**

A schematic of Specimen IKG2 is shown in Figure 6.7, and a picture of the actual specimen is shown in Figure 6.8.

The specimen also had its web at each end reinforced to prevent it from buckling. Structural channels were used on both sides of the web. FRP plates were placed between the web and the channels so as to have the web supported at its mid height as shown in Figure 6.8.

The instrumentation for Specimen IKG2 consisted of strain gages (SG), linear pots (LP), and a load cell (LC). In addition, AE sensors were also used. Longitudinal strains were measured at the midspan section on both flanges and the web, whereas deflections were measured at midspan, and at points close to both ends as shown in Figure 6.9. AE sensors were placed at midspan on the top and bottom flanges and on the web.

Specimen IKG2 was subjected to a four point bending loading with a span of 18 in. for the constant moment span. Load was applied by means of a hydraulic jack as shown on Figure 6.10. The spreader beam distributed the applied load to loading points spaced 18 in apart.

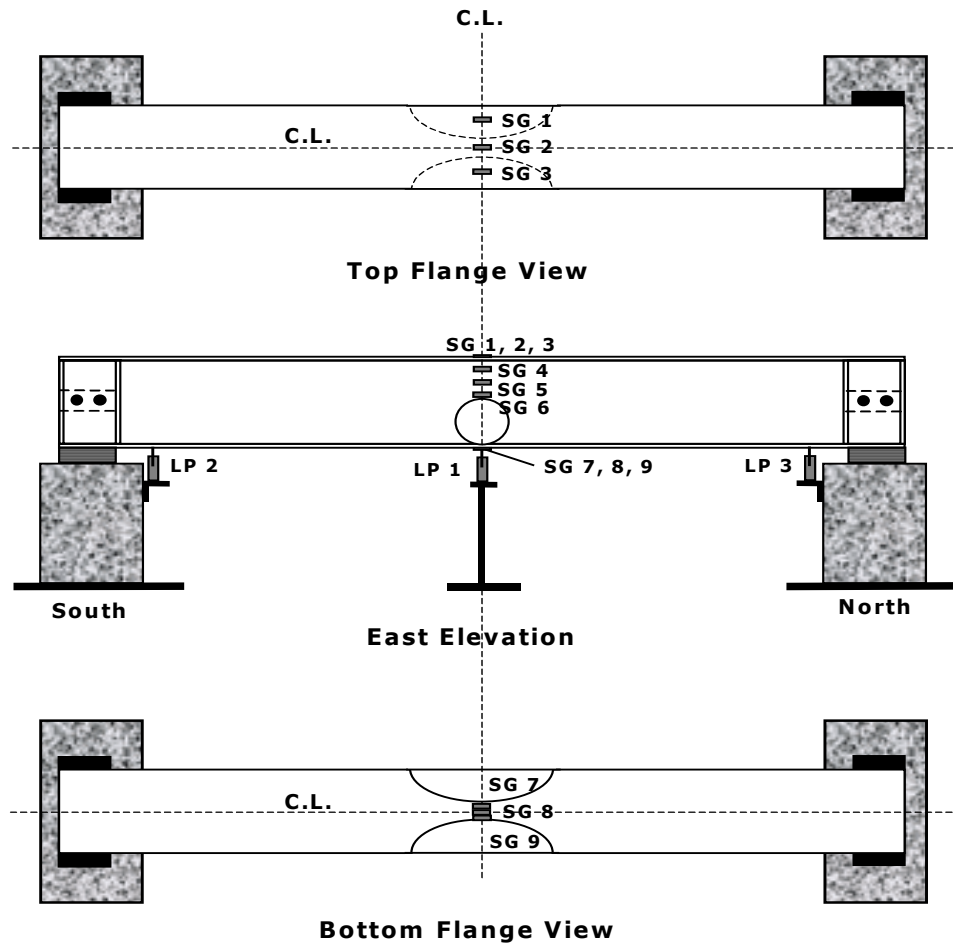


**Figure 6.9.** Specimen IKG2 - Instrumentation.

It should be noted that in order to prevent buckling of the top flange, additional restraining was added by means of FRP tubes placed between both flanges right below the supports of the spreader beam on both sides of the

web. Figure 6.11 shows the tubes on the specimen's West side, these tubes were fitted between the flanges with no special bonding.

The applied loading and the symmetry of the specimen cross section away from the web hole and flange cut out allowed for both flanges to fail at essentially the same load, with the top and bottom flanges being subject to compressive and tensile stresses respectively. Figures 6.12 and 6.13 show the specimen before and during testing respectively.

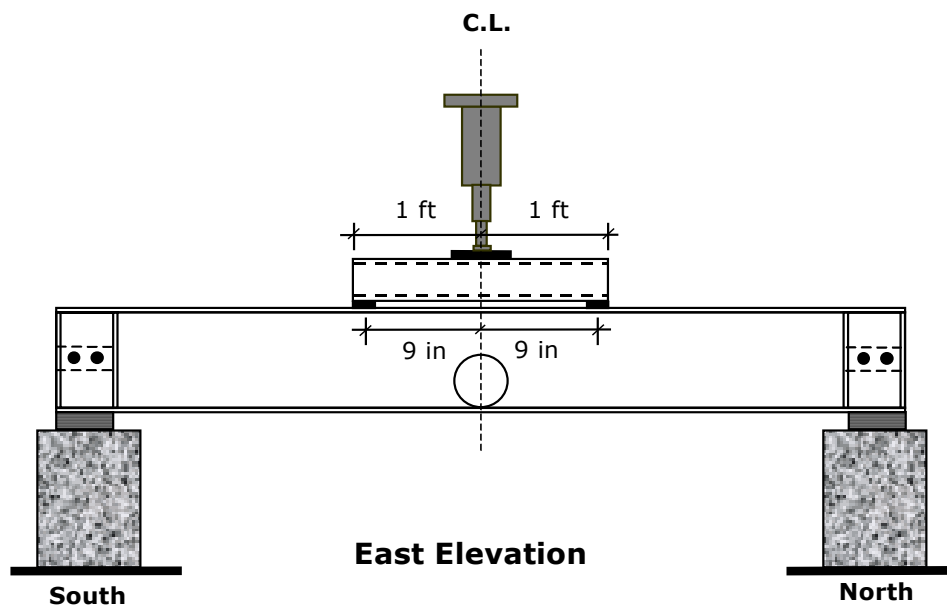


**Figure 6.10.** Specimen IKG2 - Loading.

The specimen failed at a maximum total load of 51 kips, corresponding to a midspan deflection of 1.4 in. The specimen failed when the bottom flange of the section at midspan experienced a longitudinal shear failure. The failure appeared to be caused by shear transfer due to the reduced cross section, this failure is shown in Figures 6.14 and 6.15. It developed at the section with the smallest width at the junction of the web and flange, and propagated longitudinally towards the North end.

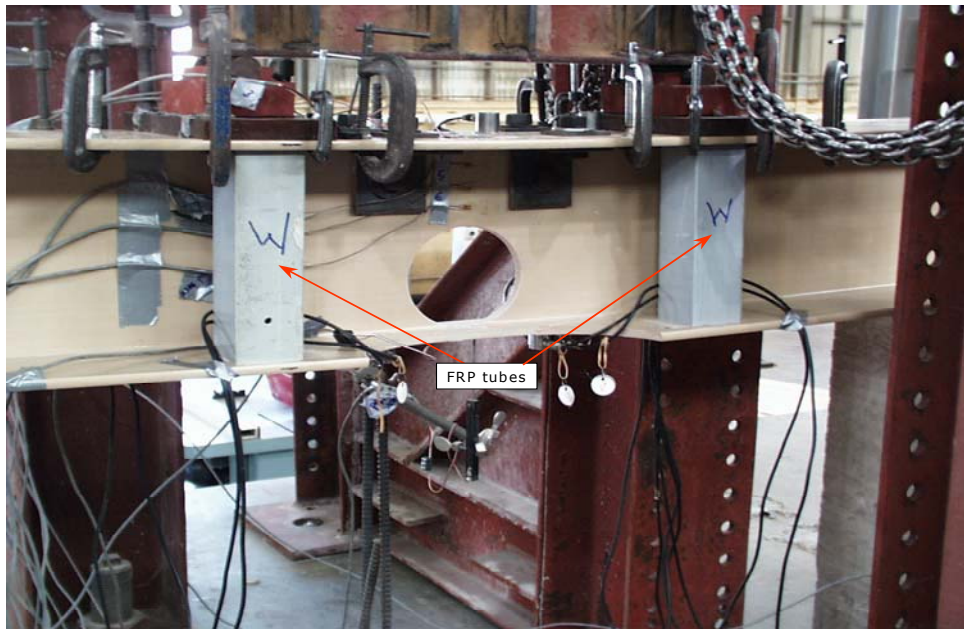


**Figure 6.11.** FRP Structural Tubes Restraining the Flanges.

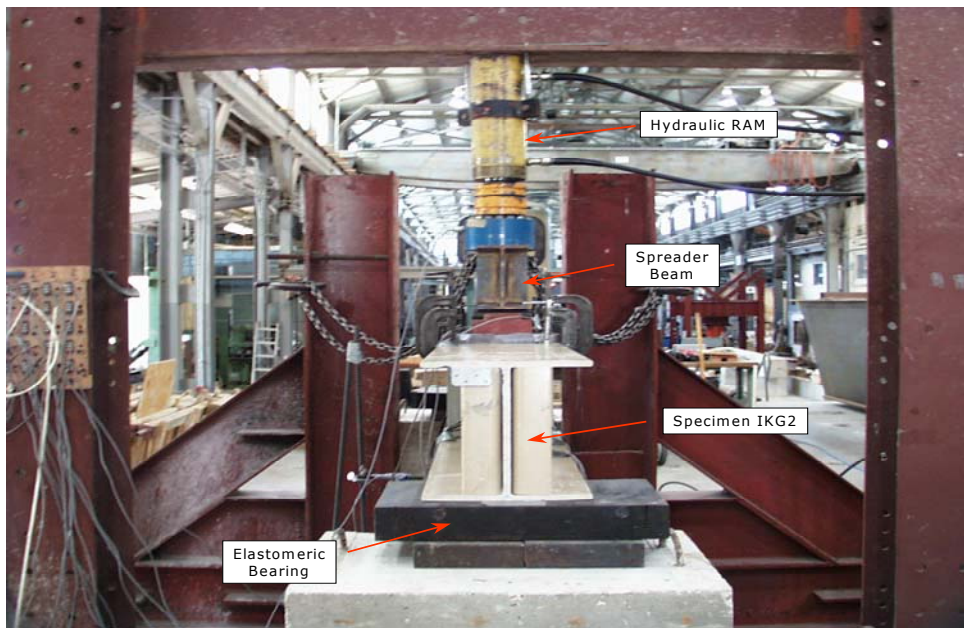


**Figure 6.12.** Specimen IKG2 Before Testing.



**Figure 6.13.** Specimen IKG2 During Testing.

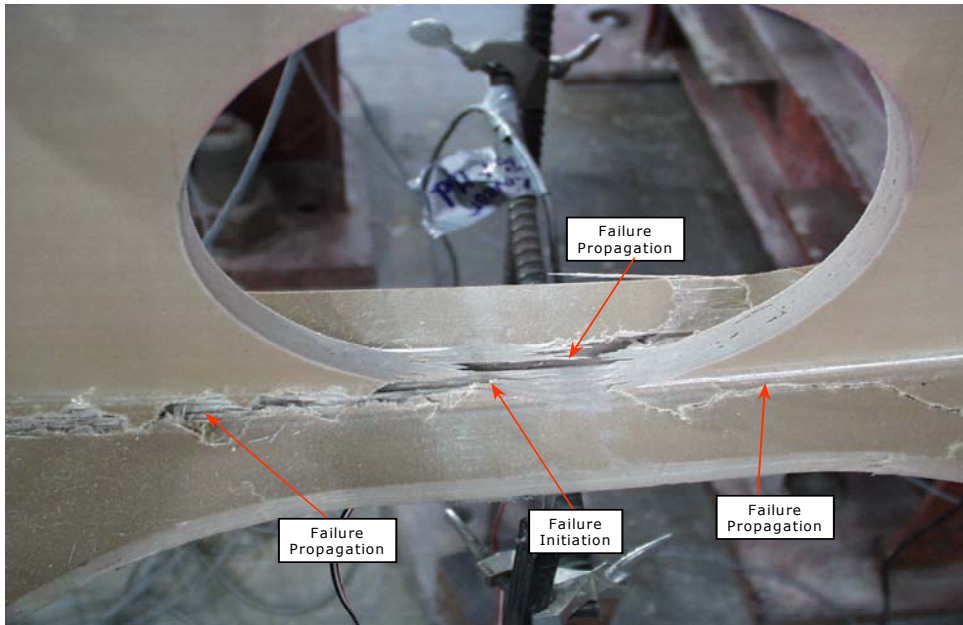


**Figure 6.14.** Specimen IKG2 Failure of Bottom Flange.

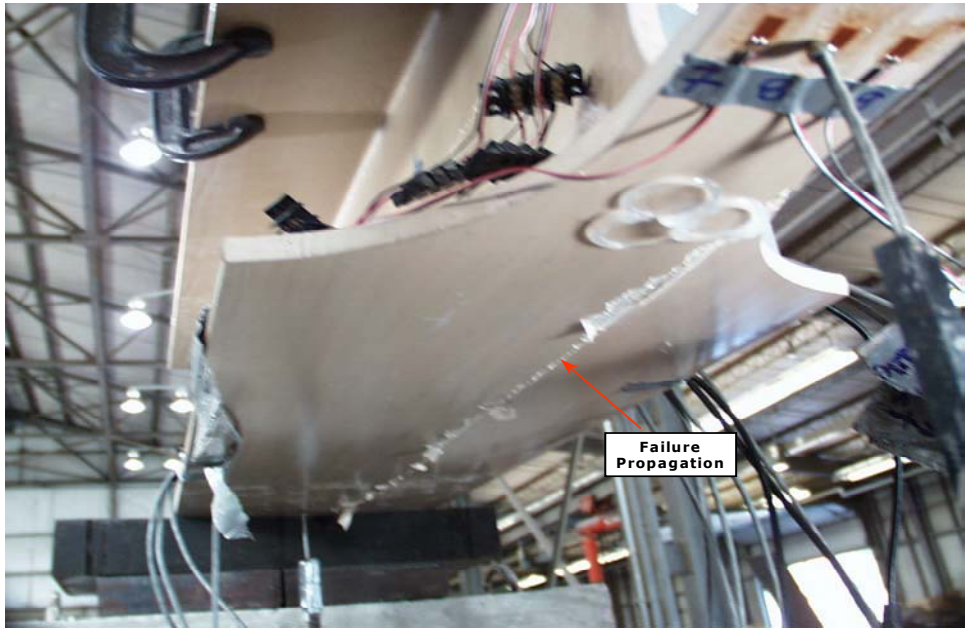


**Figure 6.15.** Specimen IKG2 Bottom View of Failure.

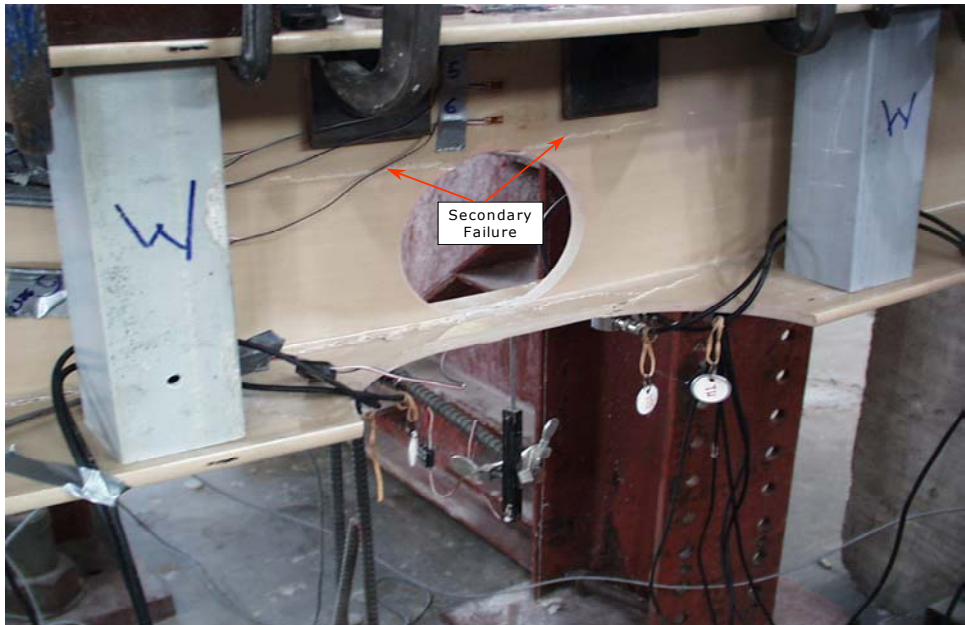


**Figure 6.16.** Specimen IKG2 Failure of Web.



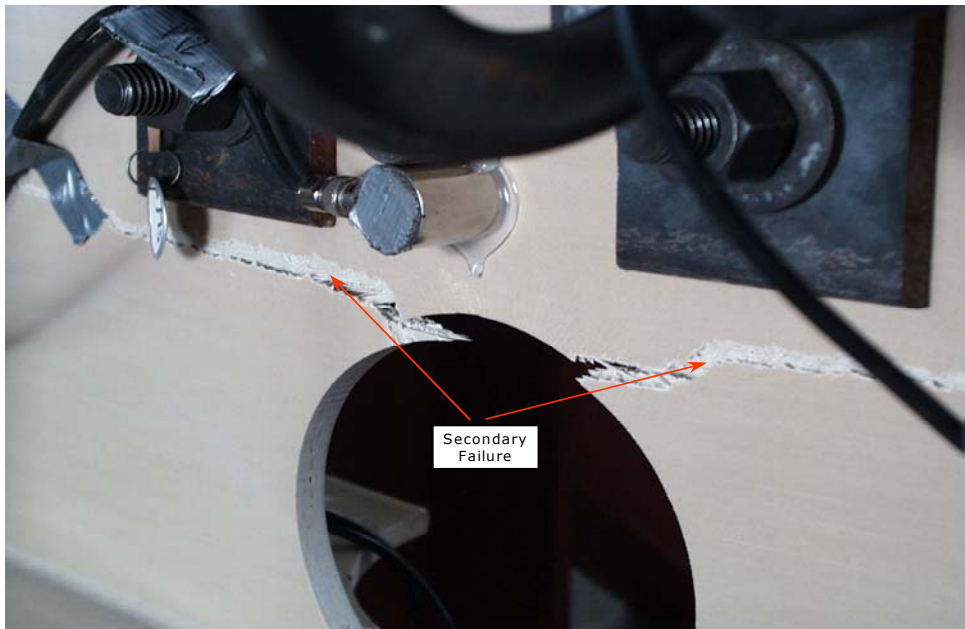


**Figure 6.17.** Specimen IKG2 Details of Failure of Web.

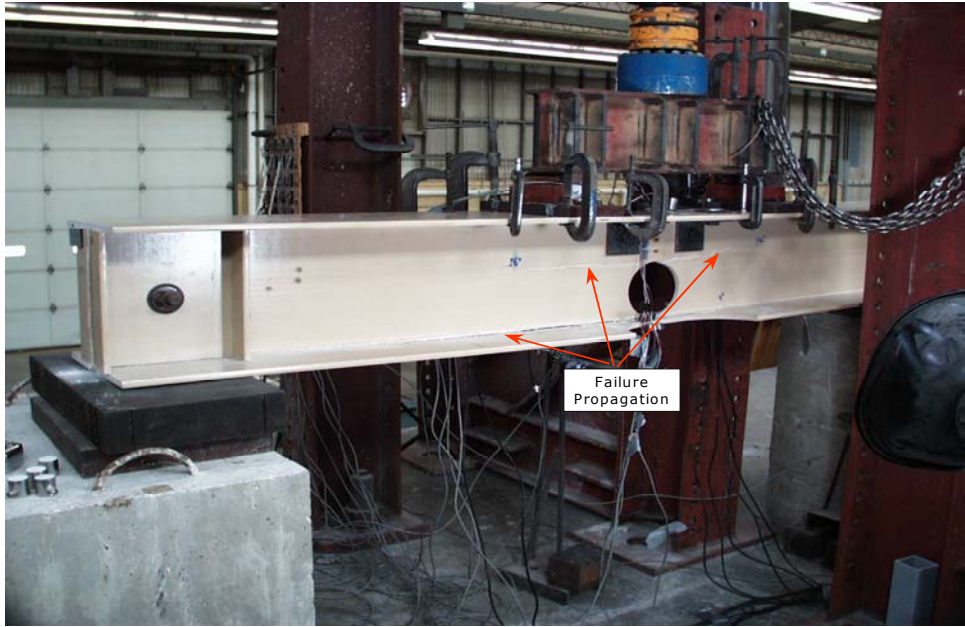


**Figure 6.18.** Specimen IKG2 After Testing.

As the load was increased the next failure developed at the top of the circular hole on the web. This failure is shown in Figures 6.16 and 6.17. Figure 6.18 is an overall view of the specimen after testing. It is observed from Figures 6.14 through 6.18 that the failure propagated a significant distance.

Figure 6.19 shows the load-deflection curve corresponding to the midspan of the specimen. It is seen in this figure that the behavior of the specimen is linear up to an applied load of 30 kips. A gradual loss of stiffness is observed beyond this point. At a load of 46 kips, failure at the bottom flange takes place, and as the applied load is increased, failure on the web begins to develop. It is the failure in the web that finally causes the system's failure when the applied load reaches a value of 52 kips. The straight lines on this figure are used to define the stiffness of the system as the test progressed. These values of stiffness are used to calculate a value for the longitudinal elastic modulus of the FRP girder.

Based on this curve a value for the effective longitudinal elastic modulus was found as  $E_{LFRPgirder} = 4255$  ksi. The analytical response considered only bending deflections since at midspan only bending stresses are acting on the specimen.

Figure 6.20 shows the average of the strain measurements at midspan on the bottom and top flanges respectively. It is seen that the magnitude of the strains acting on the bottom flange are 3.5 times greater than the magnitude of the strains taking place on the top flange. Also it is seen that the strains on the bottom flange (under tensile stress) is highly nonlinear. This can be explained by the very abrupt change in geometry on the bottom flange at midspan, this idea is supported by the strain distribution on the top flange where it is seen that the behavior is fairly linear.

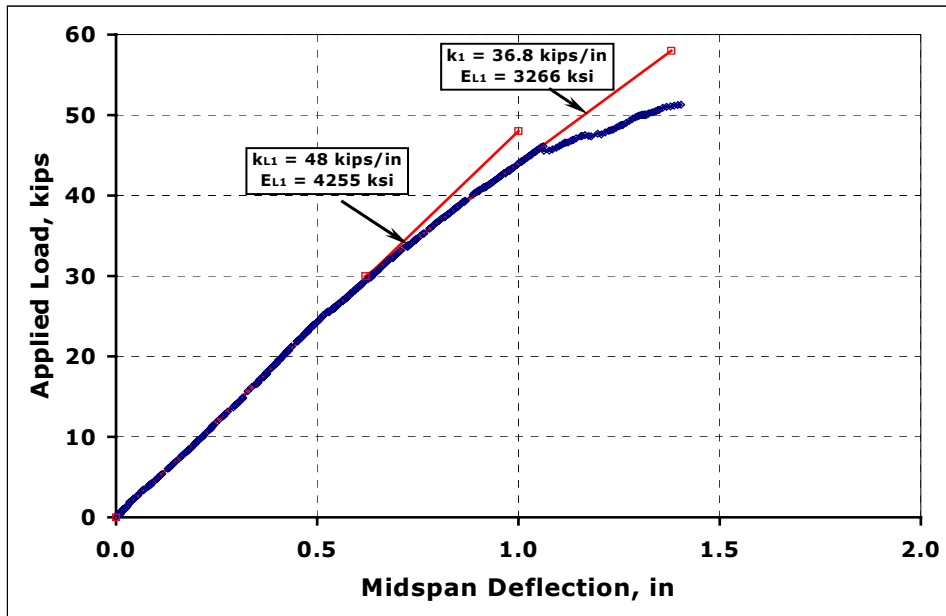


**Figure 6.19.** Specimen IKG2 Midspan Load-Deflection Curve.

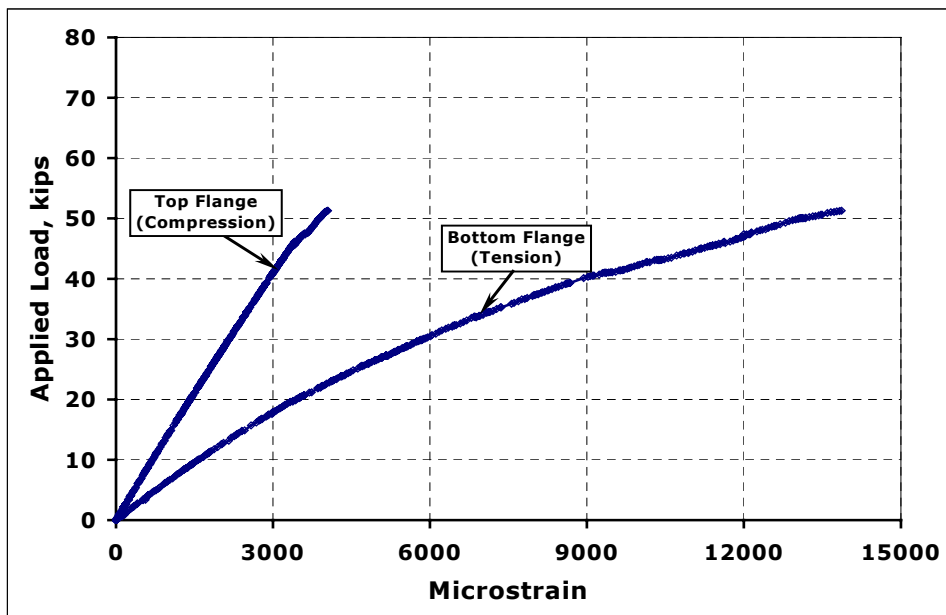


**Figure 6.20.** Specimen IKG2 Bottom Flange Average Strain.

In order to confirm the overall tensile behavior of the material, additional tensile coupons were tested. They were taken from the same girder as Specimen IKG2 and were shaped and tested in both longitudinal and transverse directions with respect to the reinforcing fibers. Figure 6.21 shows a tensile coupon after testing. This coupon was taken from the flange aligned in the longitudinal direction. Figure 6.22 shows a coupon taken from the web and aligned transversely to the fiber direction.

Figure 6.23 shows the response of a tensile test on a coupon with the fibers oriented longitudinally with respect to length of the specimen and loading direction. The response is very much linear. Based on this response a value for the longitudinal elastic modulus can be inferred as  $E_{LFRPgirder} = 4255$  ksi. This value is exactly the same value obtained from the test on Specimen IKG2, which shows a good correlation.

Figure 6.24 shows the response of a tensile test coupon but in this case the fibers are oriented transversely to the length of the specimen and the loading direction. The response in this case is also linear up to a 50% of the applied load. Beyond this point the material still behaves linearly but with a smaller stiffness. Based on this response a value for the transverse elastic modulus can be inferred as  $E_{TFRPgirder} = 1800$  ksi.

### **6.3.2 RC Deck**

Concrete cylinder samples taken during casting of the RC deck were tested at 3, 7, 14, 21, and 28 days, to determine the compressive strength of the concrete. The nominal 28 days strength was 5000 psi, whereas the actual compressive strength from testing was 5200 psi. The corresponding elastic modulus using the ACI formula for normal weight concrete was found to be  $E_{concrete} = 4110$  ksi.



**Figure 6.21.** Tensile Test Coupon, Longitudinal Direction.



**Figure 6.22.** Tensile Test Coupon, Transverse Direction.

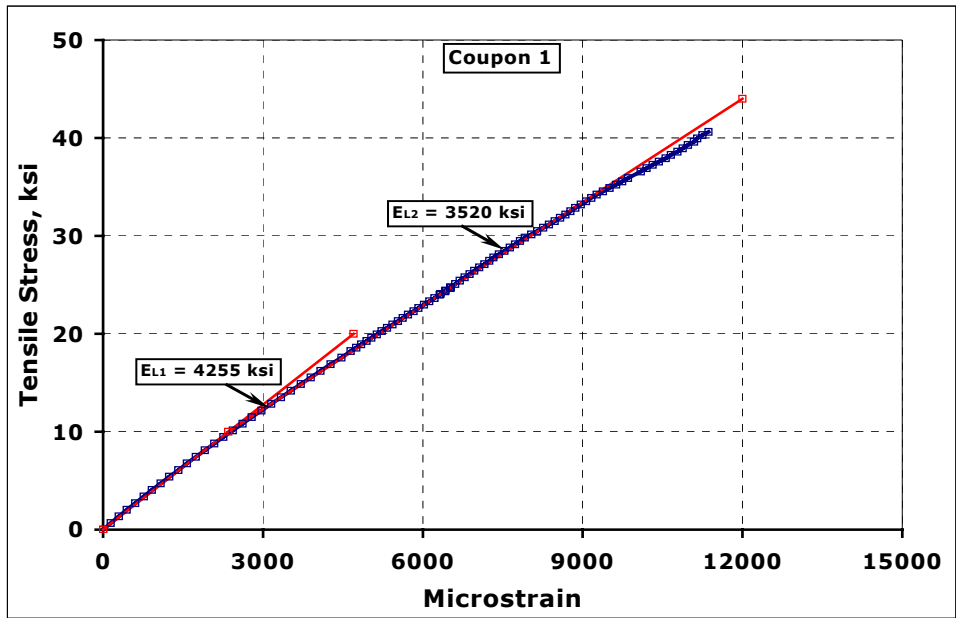


Figure 6.23. Tensile Test Response, Longitudinal Direction.

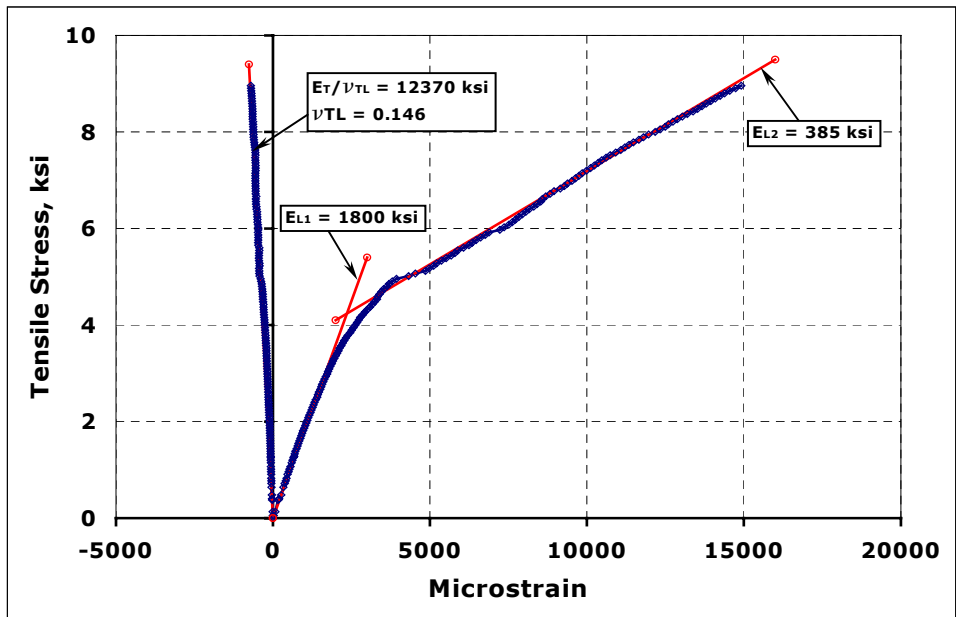


Figure 6.24. Tensile Test Response, Transverse Direction.

## 6.4 Structural Analysis and Design

Specimen IKG1 was designed for AASHTO HS20 loading. The resulting structural system consisted of an FRP hybrid girder and an RC deck, both working under composite action.

With this loading a linear elastic structural analysis was carried out to determine the bending moments, and shear forces developed in the structure. The software used was LEAF (1996). The maximum bending moments, and shear forces developed in the structure where  $M_{\max} = 91.6$  k-ft, at the girder midspan, and  $V_{\max} = 12.8$  kips, close to the girder supports. These values were used for design.

Again the emphasis was placed on a composite design for the RC deck and the FRP girder, due to the low elastic modulus of the FRP. By considering composite action the stiffness of the system increases from  $EI = 6.5 \cdot 10^6$  k-in<sup>2</sup> to  $EI = 17.1 \cdot 10^6$  k-in<sup>2</sup>, 2.6 times. Hence, the level of deflections is reduced by the same factor. Furthermore the use of an RC slab enhances the behavior of the FRP girder, since in this case the RC deck will be carrying the bulk of the compressive load.

Another potential problem caused by the low FRP elastic modulus is buckling. Of particular interest is buckling of the web and top flange. Buckling of the cross section web can occur due to shear stresses acting on it, and diagonal compression (strut action) near the supports, whereas buckling of the top flange is caused by the normal compressive stresses acting on the cross section. Figure 6.3 shows a detail of the cross section at each end.

## **6.5 Instrumentation**

Strain gages (SG) were placed on the FRP girder at sections 4 ft., and 8 ft. from the south end, and at midspan on the FRP girder, and on the RC deck at the same sections. All sections considered for instrumentation had SGs longitudinally oriented.

Linear potentiometers (LP) were used to measure the deflections at both ends of the girder near the elastomeric bearings, and at midspan. Horizontal displacement between the girder-deck interface close to each end was also measured. Figure 6.25 shows the instrumentation for this specimen.

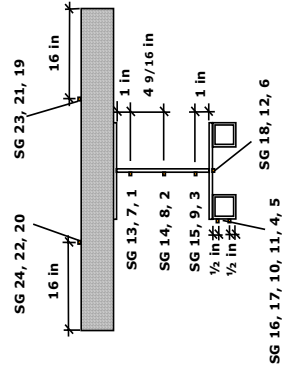
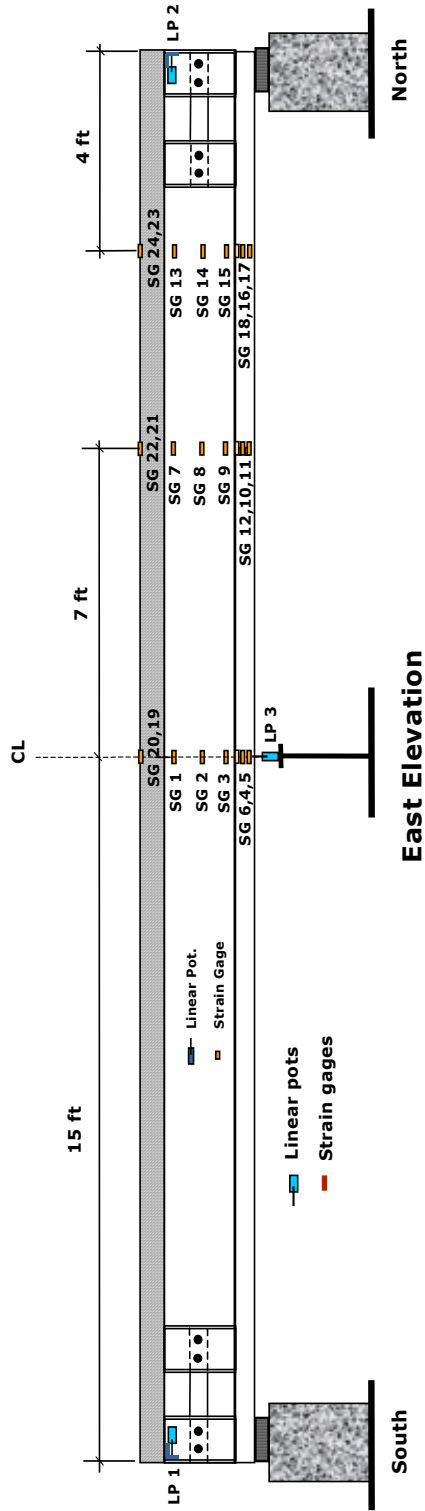
Acoustic emission (AE) sensors were also used to monitor the specimen during testing. These sensors were placed at locations of major stress. The AE research is not part of this project the findings and conclusions of this study will be published separately.

The specimen was supported at each end using elastomeric bearings as described in Chapter 3. The specimen clear span was 28.5 ft. Figure 6.25 shows the distribution of SG and LP on the specimen.

## **6.6 Loading**

Specimen IKG1 was subjected to long-term loading. The loading was provided by a number of concrete blocks uniformly placed along its length. Each concrete block was 400 pounds weight, and was placed on top of the deck resting on elastomeric bearings 1 in. thick as shown in Figure 6.26.





**Strain gages location South View**

**Figure 6.25.** Specimen IKG1 Strain Gages and Linear Pots.

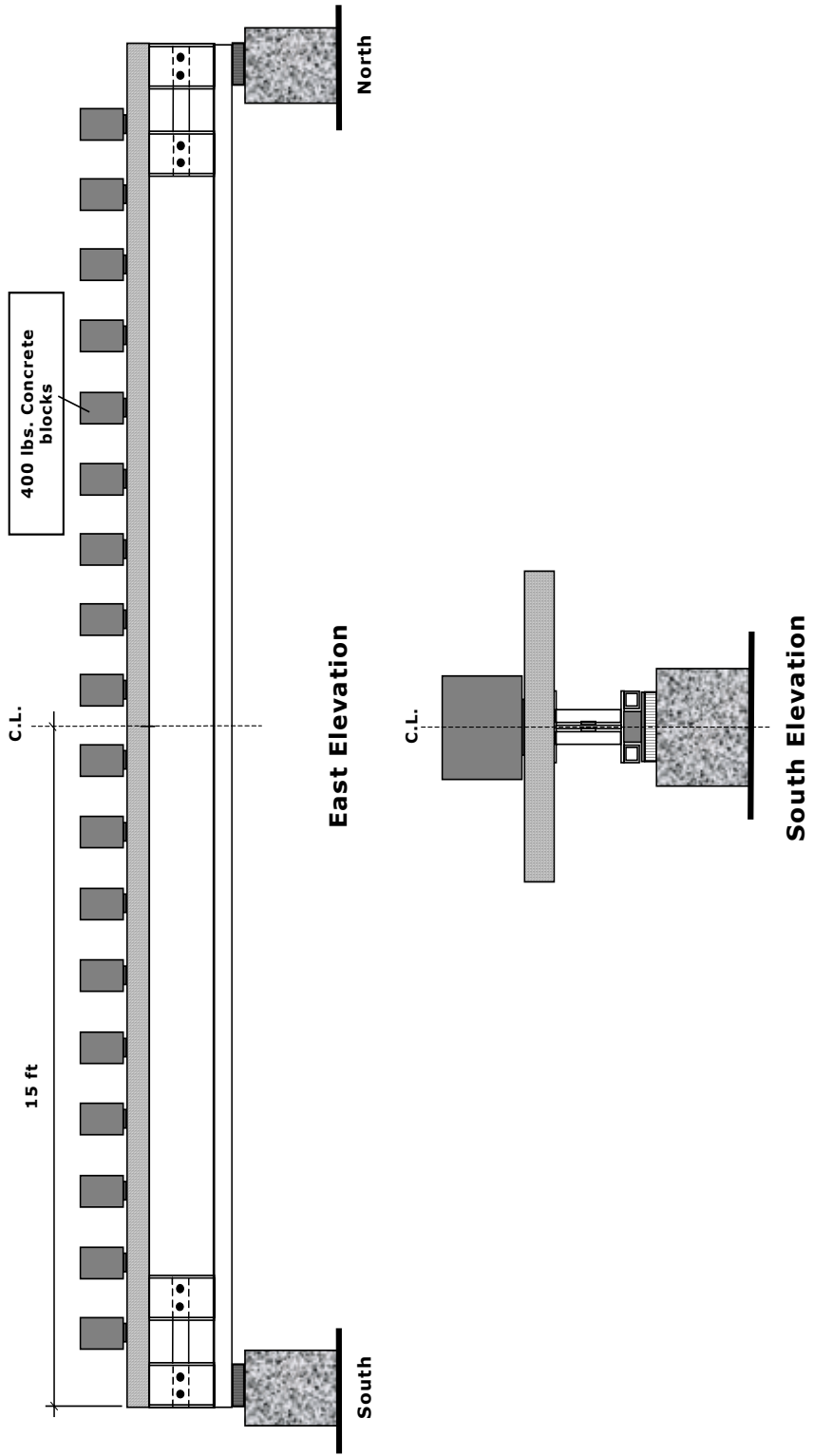


**Figure 6.26.** Specimen IKG1 Loading.

The number of concrete blocks was increased as the test developed. The specimen was initially loaded with five blocks as shown in Figure 6.27. A month later the number of blocks was increased up to a total of nine blocks as shown in Figure 6.28; three months after the initial loading was placed on, the number of blocks was doubled up to 18, as shown in Figure 6.29. This load was left on for a period of three and a half months. After this period, the loading was finally removed, and the specimen began a slow process of recovery. Each time the number of blocks was increased, the specimen was unloaded, and then reloaded. In all, specimen IKG1 was tested for a period of 228 days. During this period strains and deflections were continuously recorded. AE data was also periodically recorded.

Figure 6.30 shows the specimen after the load has been removed. Specimen IKG1 had a midspan permanent deflection of 1¼ in.



**Figure 6.27.** Specimen IKG1 - First Level of Loading.



**Figure 6.28.** Specimen IKG1 - Second Level of Loading.



**Figure 6.29.** Specimen IKG1- Third Level of Loading.



**Figure 6.30.** Specimen IKG1 – After Loading Removed.

## 6.7 Test Results

The specimen midspan deflection as a function of time is shown in Figure 6.31. It can be observed on this figure the development of creep with time and level of loading. Initially only five blocks were loaded on the specimen; after a month four additional blocks were put on; finally, after three months this number was doubled up to a maximum of eighteen blocks. The specimen was then subjected to this level of loading for an additional three and a half months. At the end of this period, the loading was removed. As it is shown in Figure 6.31, only a small amount of recovery was observed. This behavior can be explained if we consider that the deck-girder interface experienced slippage during the test, the recovery then was prevented by friction at this interface. Non-recoverable permanent deformations on the RC deck were observed at its midspan; the FRP girder on the other hand did recover back to its initial configuration after a few hours.

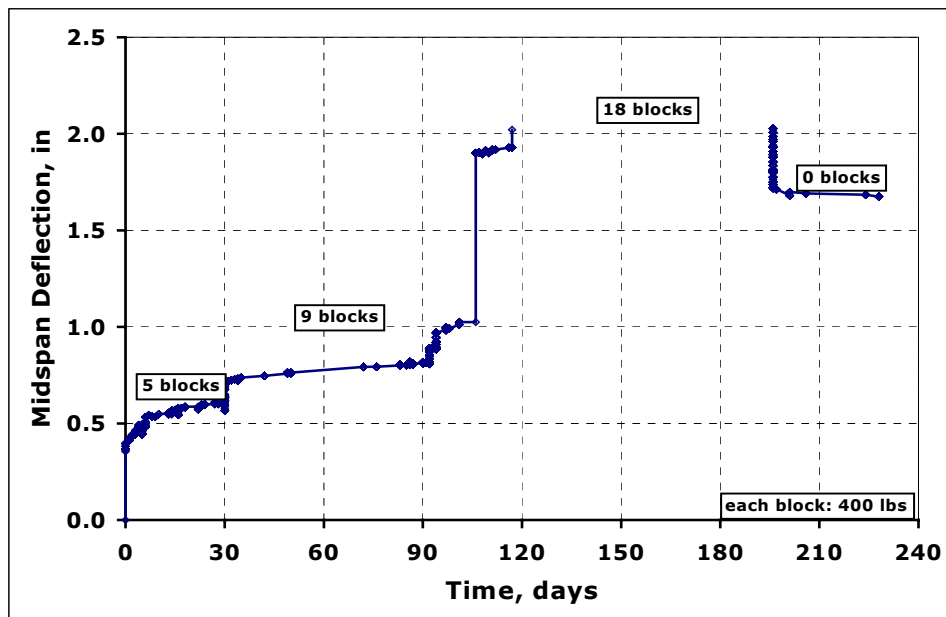


**Figure 6.31.** Midspan Deflection vs. Time.

Due to a malfunctioning of the DAS, experimental data from day 120 through day 192 was lost. Figure 6.31 shows this gap in the data.

The calculated stress acting on the midspan section at the FRP tube as a function of time is shown in Figure 6.32. The corresponding measured strain distribution at the same position is shown in Figure 6.33. It is observed that the strain follows a similar pattern as the midspan deflection shown in Figure 6.31.

The Findley model described in Chapter 10 was used to fit the data collected from the test. The Findley model also known as the power law, has been applied extensively in predicting the viscoelastic behavior of composite materials (Structural Plastics Design Manual, Vol. 1, 1984). The results from the Findley model are shown in Figure 6.34. It is observed that the correlation is very acceptable.

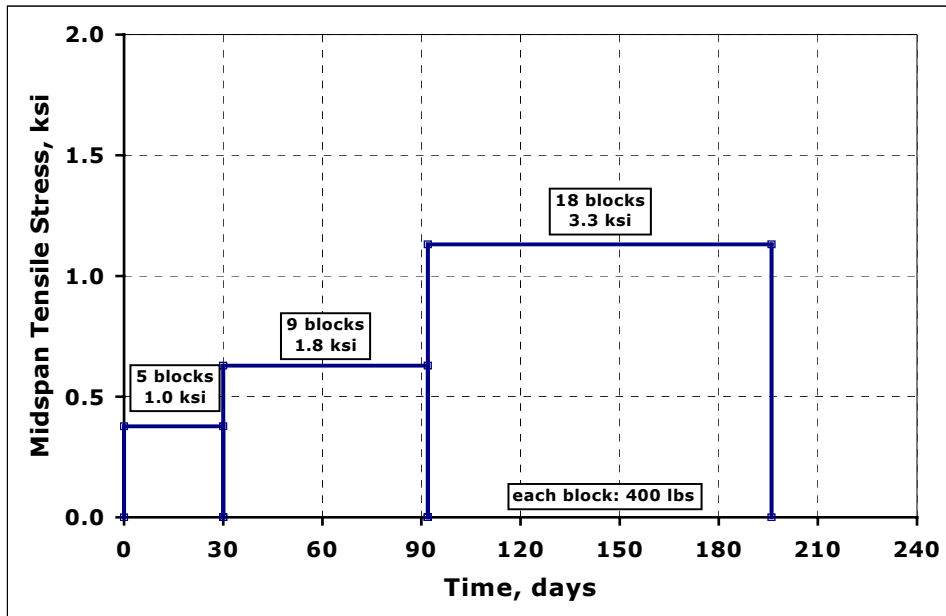


Figure 6.32. Midspan Stresses vs. Time.

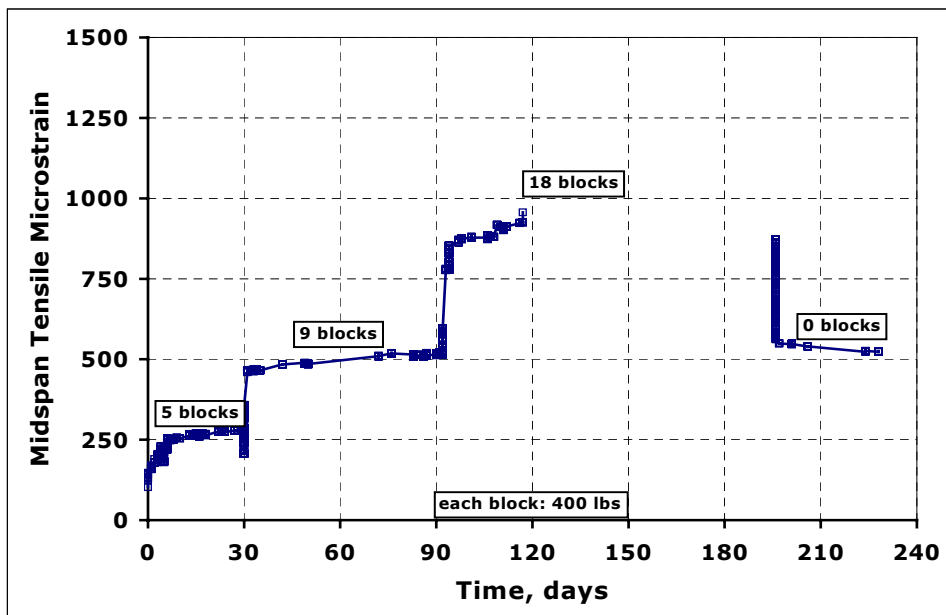
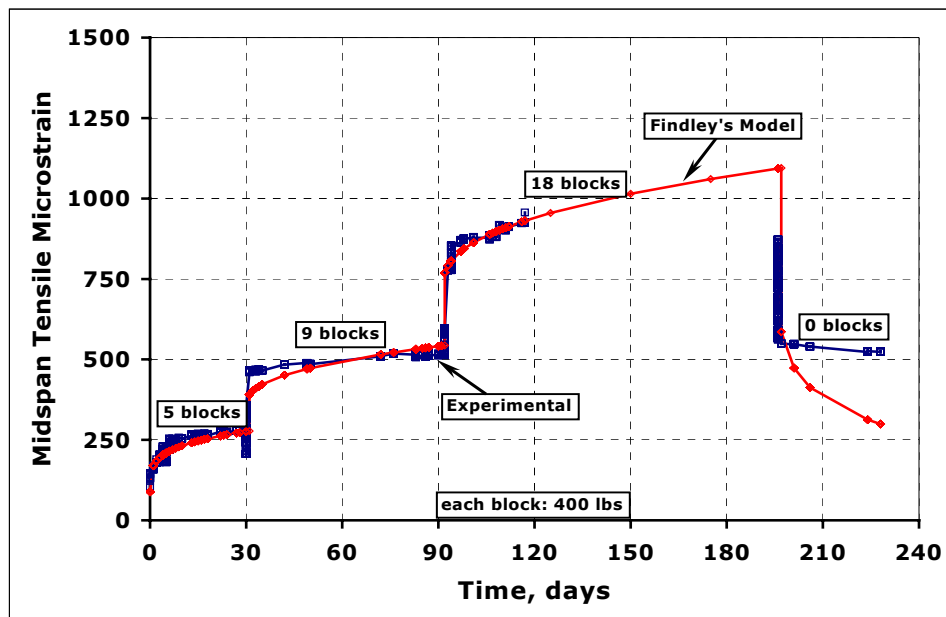


Figure 6.33. Midspan Strains vs. Time.



**Figure 6.34.** Midspan Strains predicted by Findley's Model.

The Findley model is described in detail in Chapter 10. The behavior of the concrete was assumed to be linear with a modulus of elasticity equal to the initial calculated modulus of  $E_{\text{concrete}} = 4110$  ksi.

## 6.8 Significant Findings

Specimen IKG1 behaved as expected. The bonding of the bottom tubes and the shear connectors was not an issue with this specimen.

The viscoelastic behavior of the structural system under study is very important. The Findley model for viscoelastic behavior of structural plastics appears to work particularly well in predicting the behavior of the structural system.



## **6.9 Summary**

This chapter described specimens IKG1 and IKG2, and testing performed on both specimens. Specimen IKG1 was tested under long-term loading to study the viscoelastic behavior of the specimen. Once the experimental data was analyzed to account for the viscoelastic behavior of the structural system, it was found that the Findley model worked particularly well in predicting its viscoelastic behavior. This confirms that it is possible to use data from a relatively short-term sustained load test and then apply Findley's model to predict the behavior of FRP materials in the long-term.

Specimen IKG2 was tested under several different conditions to find mechanical properties of the FRP girder. Buckling of the compression flange controlled the behavior of the FRP girder.

## **Chapter 7**

# **Vinyl Ester Pultruded Hybrid Fiber Reinforced Plastic Girder**

### **7.1 Overview**

This chapter describes experimental work performed on specimens SW1 and SW2. Each specimen used a pultruded hybrid FRP girder with a unique double-web design and internal flange stiffeners that provide the structural shape with stability against buckling. These girders were fabricated with a mix of carbon and glass fibers hence the name hybrid. The resin was vinyl ester. The structural system considered for Specimen SW1 consisted of an FRP girder and an RC deck, whereas Specimen SW2 consisted of the FRP girder alone. Specimen SW1 was subjected to a long-term loading to study its viscoelastic (creep) behavior, whereas Specimen SW2 was exclusively tested under short-term loading to determine its bending, shear, and buckling capacities.

### **7.2 General Description**

Specimen SW1 had a nominal length of 30 ft., with a clear span between supports of 28.5 ft. It was designed to carry load by means of composite action between its components the FRP girder and the RC deck. The FRP girder had special features in both its material and geometry configurations. The girder cross section featured a vinyl ester resin, and glass and carbon reinforcement. The name hybrid refers to the mixed carbon and glass fibers.

These FRP girders were developed and commercialized by Strongwell Corporation, Bristol, Virginia. The overall dimensions of the cross section are

6 in. width, and 8 in. depth, with an average thickness of ½ in, the length for the girders is 30 ft. The reinforcement in the flanges was mainly carbon with a lesser amount of glass. The webs had more glass reinforcement than the flanges. The double web feature stiffened the web against buckling by means of internal stiffeners. Figure 7.1 shows a pair of these FRP hybrid girders and Figure 7.2 shows the cross section dimensions.



**Figure 7.1.** FRP Hybrid Girders Laid Sideways.

Similar FRP girders had been previously used in a bridge rehabilitation program as reported by Hayes (1998), their use though varied significantly from the structural system researched as part of this project. In this project the girders work in composite action with an RC deck, resulting in an increase of stiffness for the structural system. In the project reported by Hayes, not composite action was considered.

In previous chapters the deficiencies of pultruded sections based on steel wide flange and I beam shapes have been discussed. The design of

these hybrid girders is intended to address some of the deficiencies. The biggest problem with conventional FRP shapes is the low modulus of elasticity, which shows as large girder deflections and compression flange and web buckling. The addition of carbon fibers increases the modulus of elasticity. The double web provides additional stiffening of the compression flange and the internal stiffeners provide restraint against web buckling.

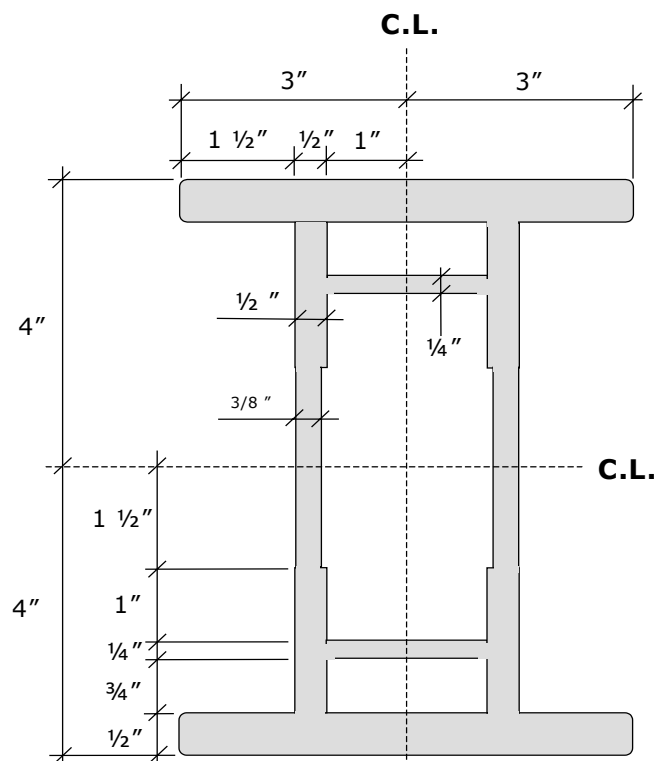


**Figure 7.2.** FRP Hybrid Girder Cross Section (Strongwell, 2000).

### 7.2.1 Specimen SW1

Specimen SW1 was composed of a hybrid FRP girder and an RC deck. This structural system was intended to have the girder and the deck working under composite action. To achieve this, shear connectors similar to the ones used in specimen FG1, FG2, and IKG1 were used. They were bonded and dowelled to the top flange following the same procedures detailed in Chapter

4. Fabrication was performed at the University of Texas. A picture of the girder with the shear connectors on the top flange is shown in Figure 7.3.



**Figure 7.3.** FRP Hybrid Girder and Shear Connectors.

The RC deck had a 3 ft. width, 6 in. thickness and 30 ft. length. Number 4 Grade 60 rebars were used 12 in. apart both longitudinally and transversely. Figure 7.4 shows the specimen dimensions, and Figure 7.5 shows the finished specimen. The specimen clear span was 28.5 ft.

### **7.2.2 Specimen SW2**

Specimen SW2 was composed of a hybrid FRP girder only. This specimen was tested to find the mechanical properties of the girder. The specimen was subjected to various types of loading to determine the girder's bending, shear, and buckling capacities. Specimen SW2 is shown in Figure 7.3.

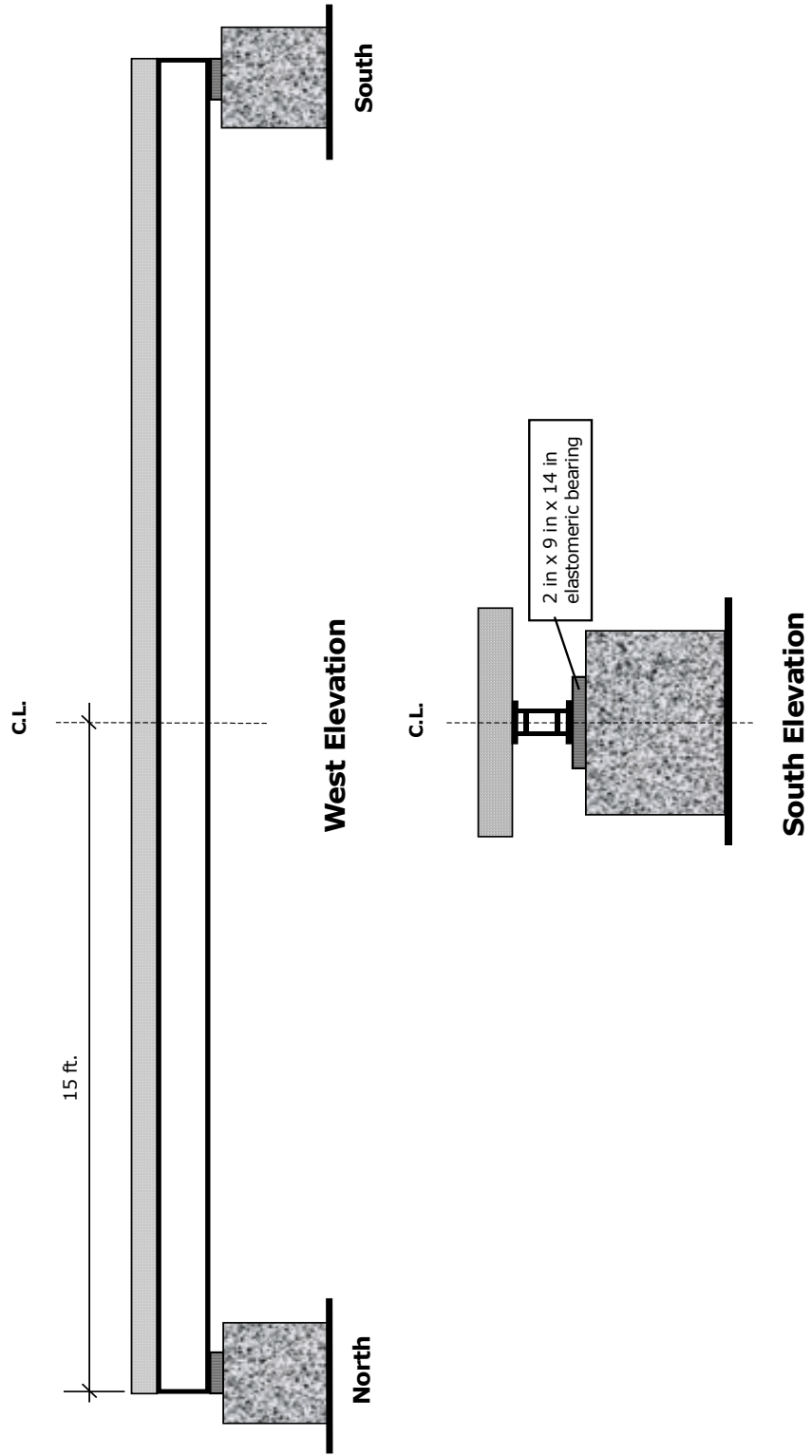


Figure 7.4. Specimen SW1.



**Figure 7.5.** Finished Specimen SW1.

### **7.3 Material Properties**

The resin utilized was Dow Chemical Derakane 411-350; the manufacturer also typically adds styrene and additional fillers during the pultrusion process. Glass Roving  $[0^\circ/90^\circ]$  and  $\pm 45^\circ$  fabric, and continuous strand mat are utilized throughout the section, while carbon fiber tows are dispersed in the flanges to provide greater flexural rigidity. The carbon fiber utilized is either Hercules AS4 36k or AKZO 50k, and the glass fiber is E-glass. The targeted fiber volume fraction (both carbon and glass) is around 55% by weight. The manufacturer quoted a unit weight of 11.2 lbs/ft. (Hayes, 1998). Actual material properties were found by testing samples taken from the FRP girder (Specimen SW2) and the RC deck.

### 7.3.1 FRP Pultruded Girder

Specimen SW2 is shown in Figure 7.6. The first test performed on Specimen SW2 was a flexural test. The specimen was subjected to a four point bending loading with a span of 59 in. for the constant moment span. Longitudinal and transverse strains were measured on sections at midspan, and at 22 in. from the south end of the specimen. Deformations were measured at midspan, and at points close to both ends. Figure 7.7 shows the instrumentation on this specimen, Figure 7.8 shows details of the loading. Figures 7.9, and 7.10 show the specimen before testing and during testing respectively.

As seen in Figures 7.10 and 7.11, Specimen SW2 experienced large deflections and end rotations, the specimen nonetheless behaved linearly elastic for loads below 10 kips (9 in. midspan deflection), beyond this point some level of nonlinearity developed. This is shown in Figure 7.12, which shows the load-deflection curve at midspan for both experimental and analytical responses. The analytical response made use of the elastic modulus calculated from the strain profile at the midspan section, as described in the following paragraph. The analytical response only considered bending deflections since at midspan only bending stresses are acting on the specimen.

The strain measurements at midspan were used to calculate a longitudinal elastic modulus. The longitudinal strain distribution through the cross section depth at midspan is shown in Figure 7.13. Based on this distribution and considering that the strains at midspan are purely caused by a known bending moment, the longitudinal elastic modulus was found to be  $E_{FRP} = 6500$  ksi. On the other hand, at the south end of the specimen, shear strains are predominant, and the strain profile there is very nonlinear and different from the one at midspan.



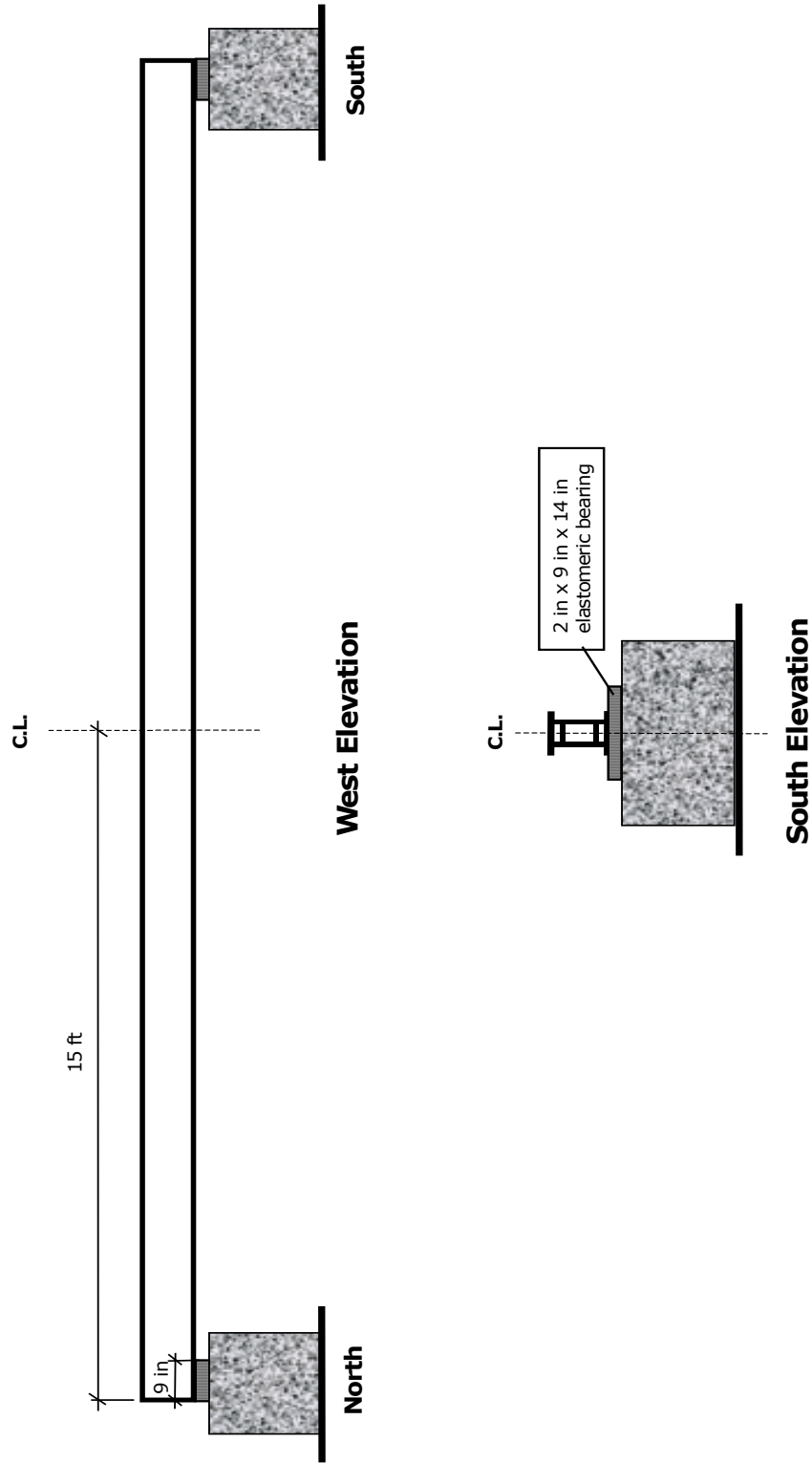


**Figure 7.6.** Specimen SW2.

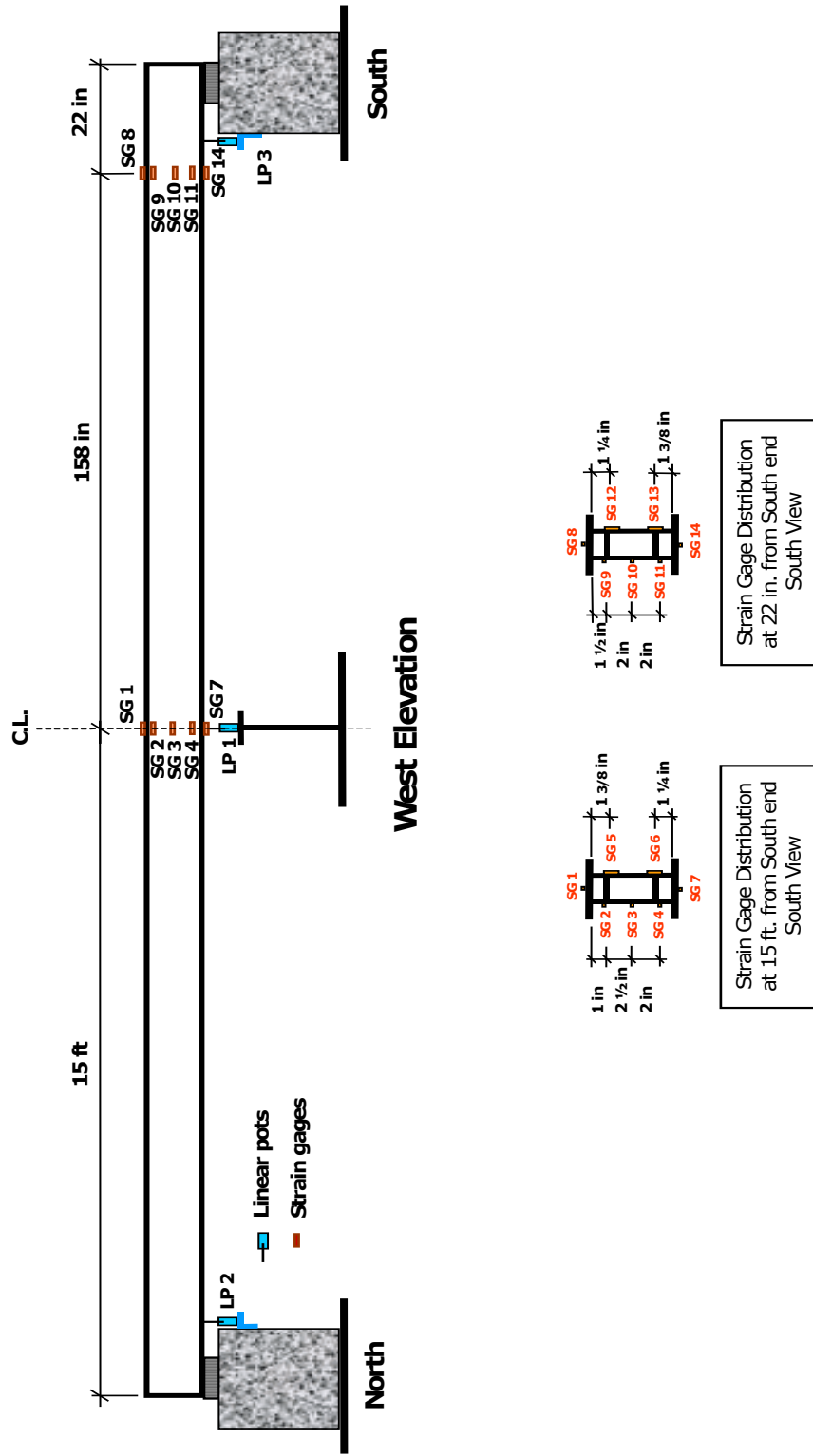


**Figure 7.7.** Specimen SW2, Strain Gages and Linear Pots.

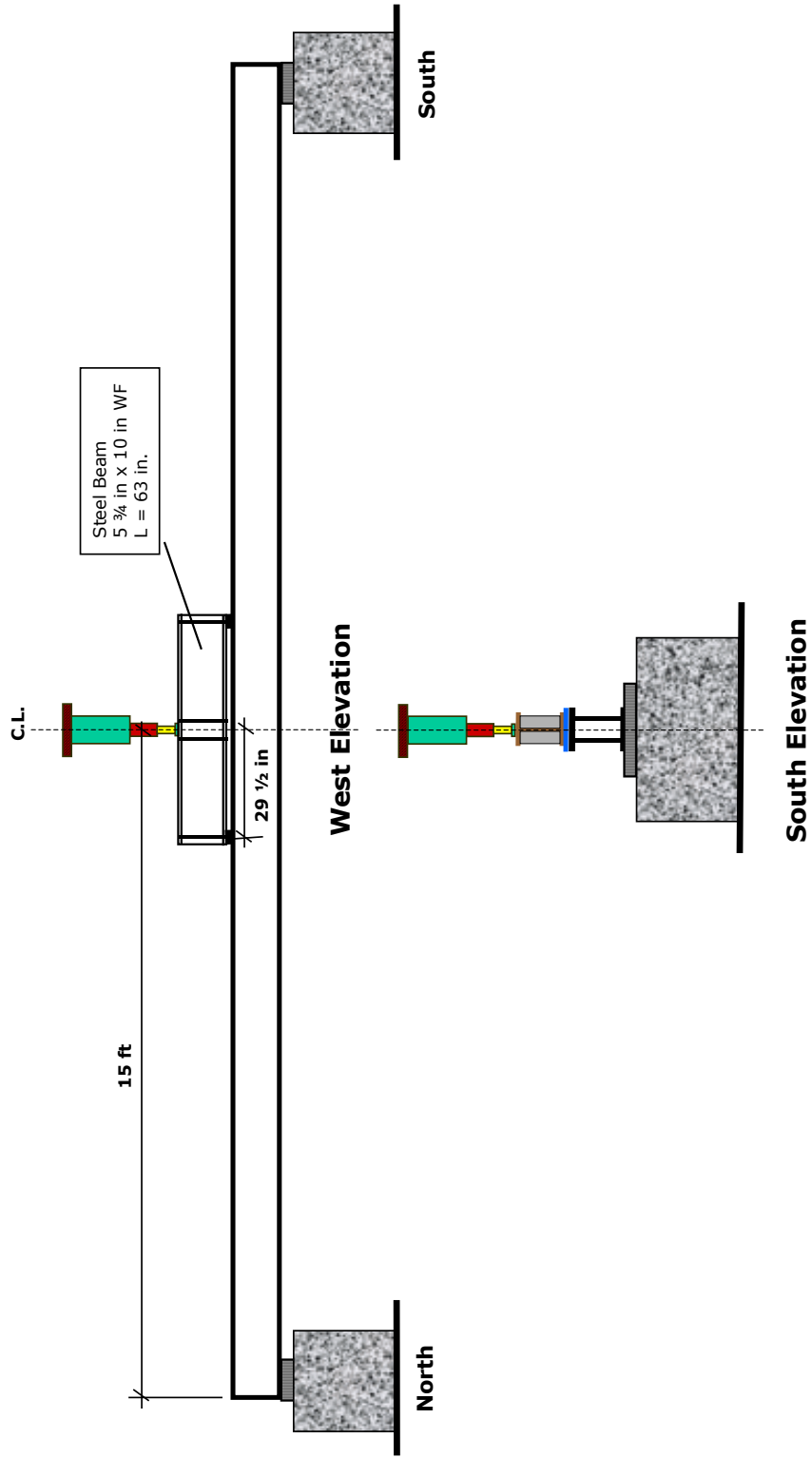


**Figure 7.8.** Loading Arrangement for Specimen SW2.



**Figure 7.9.** Specimen SW2 Before Testing.



**Figure 7.10.** Specimen SW2 During Testing.

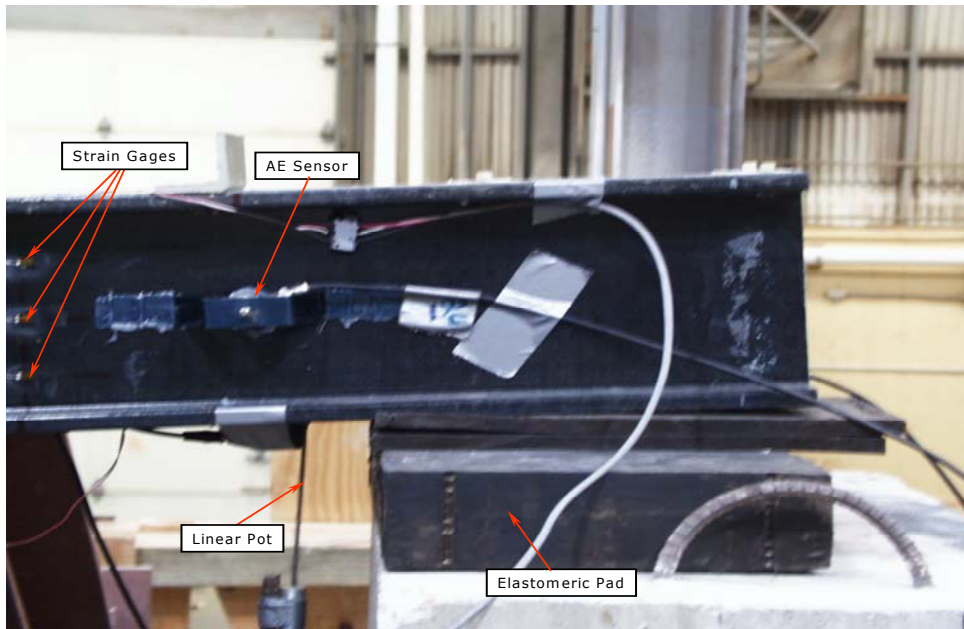


**Figure 7.11.** Specimen SW2 Large Rotations at South End.

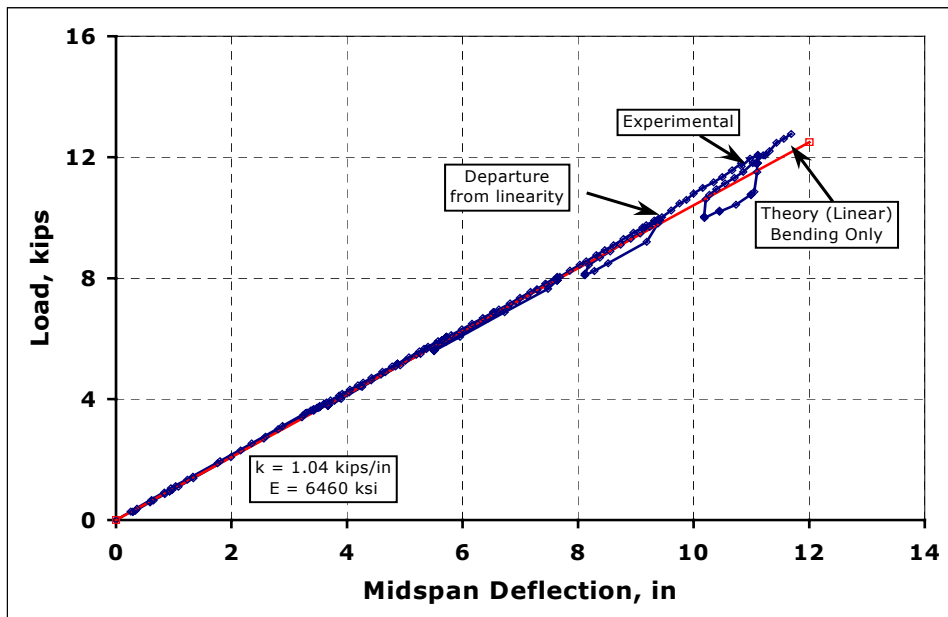


**Figure 7.12.** Specimen SW2 Load-Deflection Response.

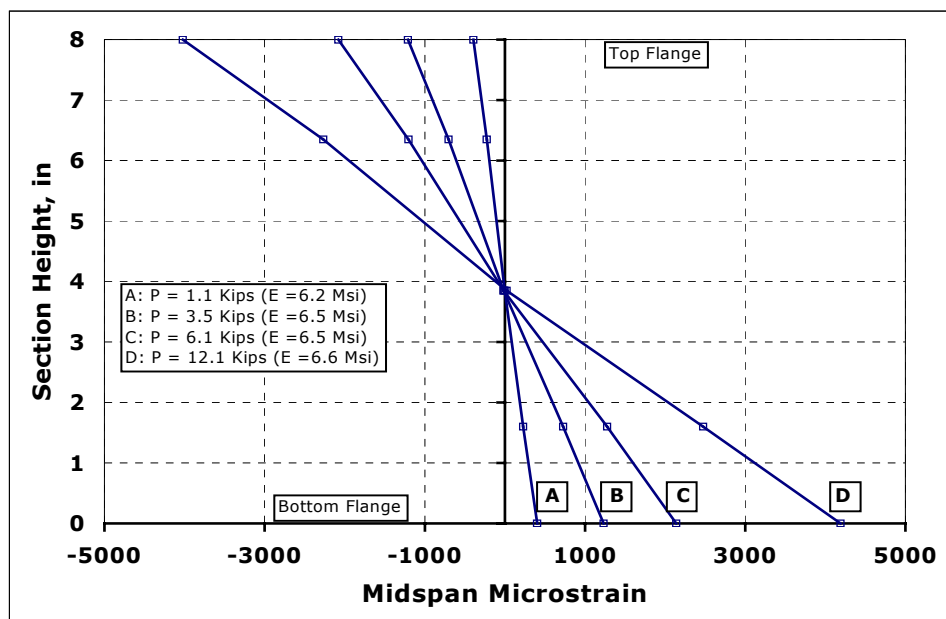


Figure 7.13. Specimen SW2 Linear Strain Distribution at Midspan.

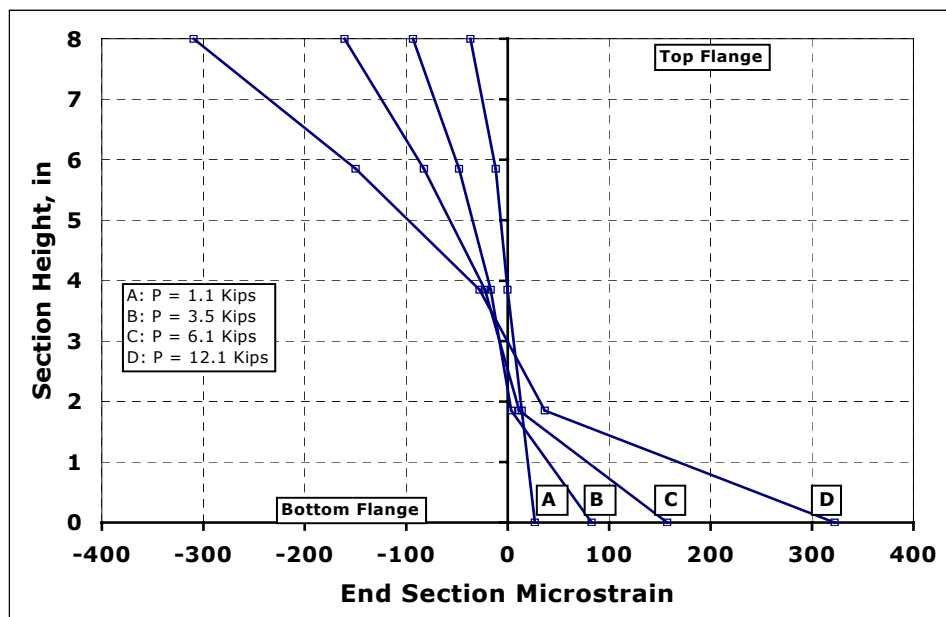


Figure 7.14. Specimen SW2 Nonlinear Strain Distribution at South End.

This behavior is similar to the behavior observed in Specimen FG1 (See Section 4.38 and Figure 4.39). Since the reinforcement in the FRP is provided only in the longitudinal direction, the shear stresses in the cross section are carried primarily by the resin. This results in the behavior shown in Figure 7.14.

Specimen SW2 failed by delamination of the top flange at a load of 12.8 kips. The corresponding compressive strain was 4260 microstrain. Delamination of FRP materials is caused by interlaminar shear stresses, which tend to slide one lamina over adjacent laminae. Figure 7.15 shows early delamination taking place on the top flange of the girder close to its midspan. Figures 7.16, and 7.17 show the top flange of the girder at midspan at failure, delamination had caused buckling of the fibers and as a result the flange at this area has been completely delaminated.

The phenomenon of delamination is highly dependant on the laminate stacking sequence and it can be prevented by a proper design of the same. For example, in some cases a tensile interlaminar stress, can be transformed into a compressive stress by simply rearranging the layer sequence (Daniel, Ishai, 1994).

Additional testing on samples from Specimen SW2 was performed. A shear test on smaller specimens resulted in a type of failure similar to the flexural test, that is, the top flange delaminated and buckled. Also smaller samples were tested to determine the buckling capacity of the double web cross section. Three similar samples were tested. Figure 7.18 shows the dimensions and instrumentation for the three specimens. Figures 7.19 and 7.20 show the samples before and after testing. The failure type was similar to the flexural test, in this case delamination of the web as shown in Figure 7.20. This behavior may be caused by the rather low transverse strength, particularly in the web where the reinforcement is mainly glass.



**Figure 7.15.** Specimen SW2 Top Flange Early Delamination.



**Figure 7.16.** Specimen SW2 Top Flange Delamination.



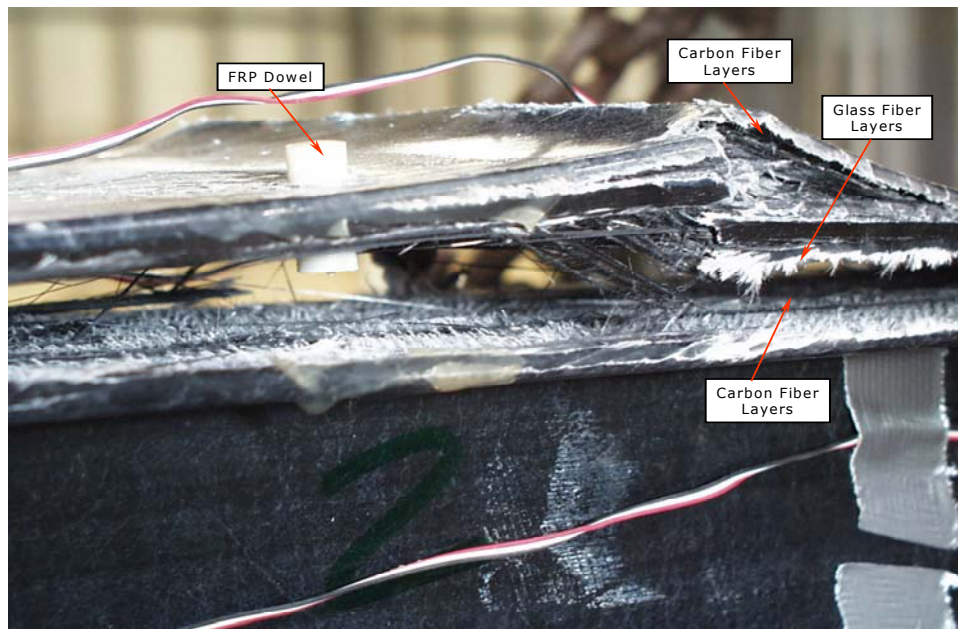


**Figure 7.17.** Specimen SW2 Top Flange Delamination.

Figures 7.21 through 7.23 show that the behavior of the web of Specimen SW2 is linear elastic. The buckling tests on these specimens confirm it can sustain a maximum compressive strain of 5000 microstrain; at this level of strain, delamination will take place.

Tensile tests were also performed on coupons taken from Specimen SW2 flanges. Two dog-bone shaped coupons were tested. The orientation of the specimens was such that the test was performed in the longitudinal direction. The dimensions of the coupons were 2 ft. long, 6 in. wide at each end, and the gage length was 4 in. with a width of 3 in. The thickness of the specimen was ½ in. Figures 7.24 through 7.26 show a specimen before and after testing. Figure 7.27 shows the stress-strain response for this tensile coupon. The response is essentially linear, except for the range of loading (deformation) before failure. The modulus of elasticity  $E_{FRP} = 7460$  ksi, is higher than  $E_{FRP} = 6460$  ksi measured for the entire cross section in bending (Figure 7.12) and reflects the concentration of carbon fibers in the flanges.

A very important conclusion can be drawn from this results, the ultimate tensile strain for this specimens is almost twice the ultimate compressive strain. Thus, the behavior of this kind of girders will be, mostly controlled by the buckling and delamination of its compressive flange, unless the girder is utilized as part of a composite design.

### **7.3.2 RC Deck**

Concrete cylinder samples taking during casting of the RC deck were tested at 3, 7, 14, 21, and 28 days, to determine the compressive strength of the concrete. The nominal 28 days strength was 5000 psi, whereas the actual compressive strength from testing was 4925 psi. The corresponding elastic modulus using the ACI formula for normal weight concrete was found to be  $E_{\text{concrete}} = 4000$  ksi.

## **7.4 Structural Analysis and Design**

Specimen SW1 was designed for AASHTO HS20 loading. The resulting structural system consisted of an FRP hybrid girder and an RC deck, both working under composite action.

With this loading a linear elastic structural analysis was carried out to determine the bending moments, and shear forces developed in the structure. The software used was LEAF (1996). The maximum bending moments, and shear forces developed in the structure where  $M_{\text{max}} = 91.6$  k-ft, at the girder midspan, and  $V_{\text{max}} = 12.8$  kips, close to the girder supports. Both these values were used for design.

As described in previous chapters a composite design between the RC deck and the FRP girder was considered to control the level of deflections caused by the low elastic modulus of the FRP girder.

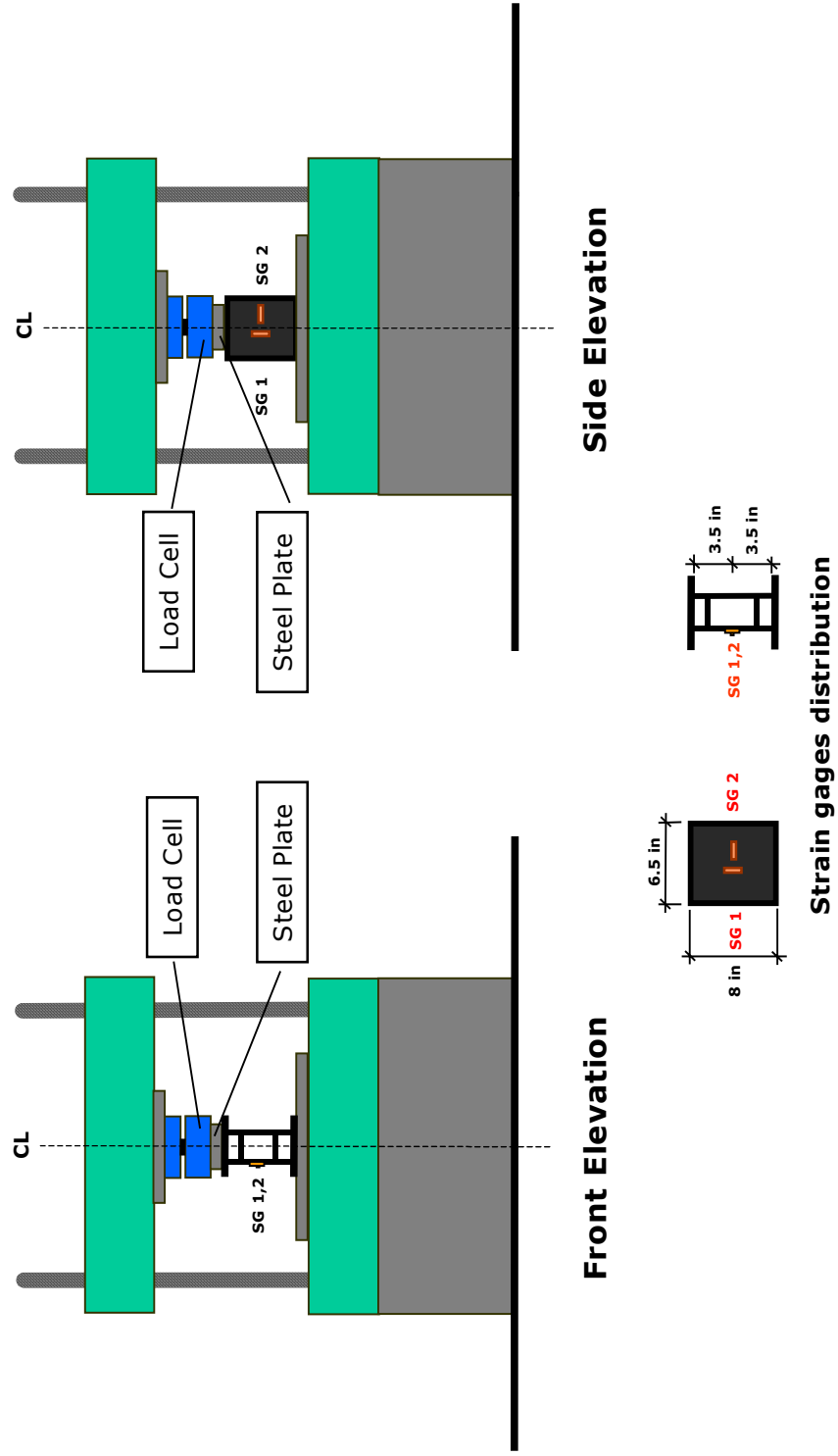


**Figure 7.18.** Specimen SW2 Web Buckling Test.

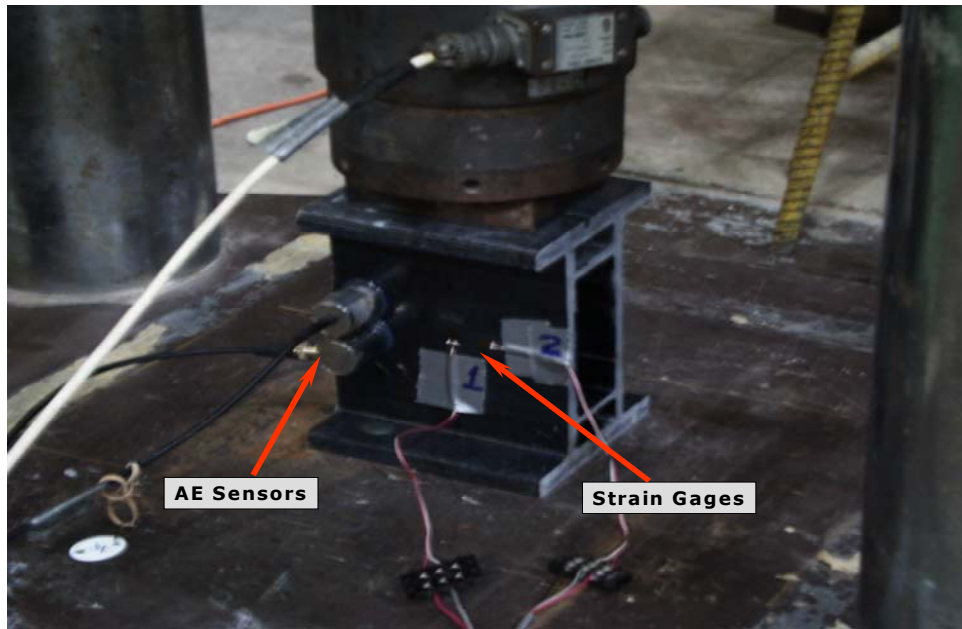


**Figure 7.19.** Specimen SW2 Web Buckling Test Sample.



**Figure 7.20.** Specimen SW2 Web Buckling Test Failure.

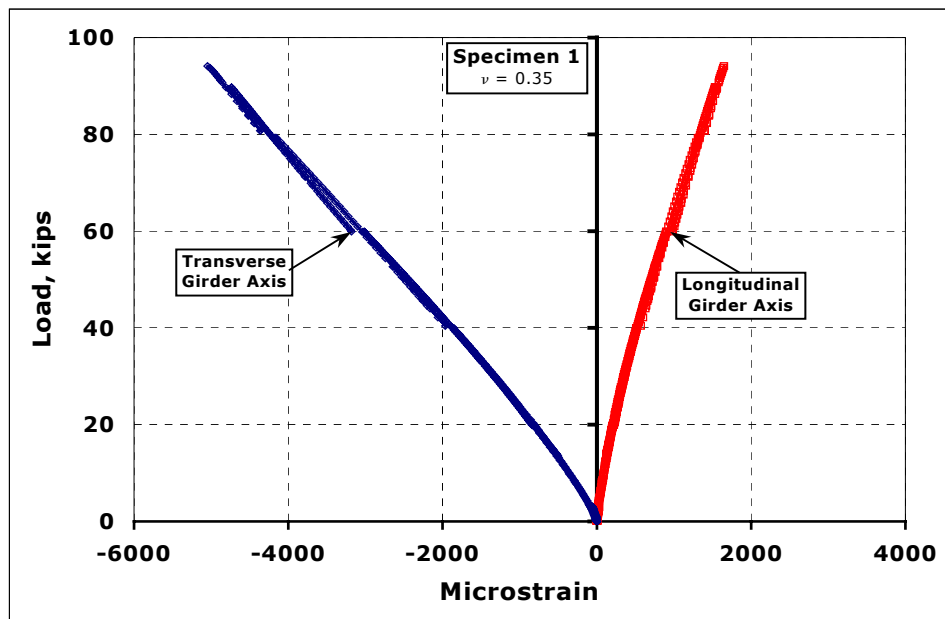


**Figure 7.21.** Web Buckling Test Specimen 1 Load-Strain Curve.

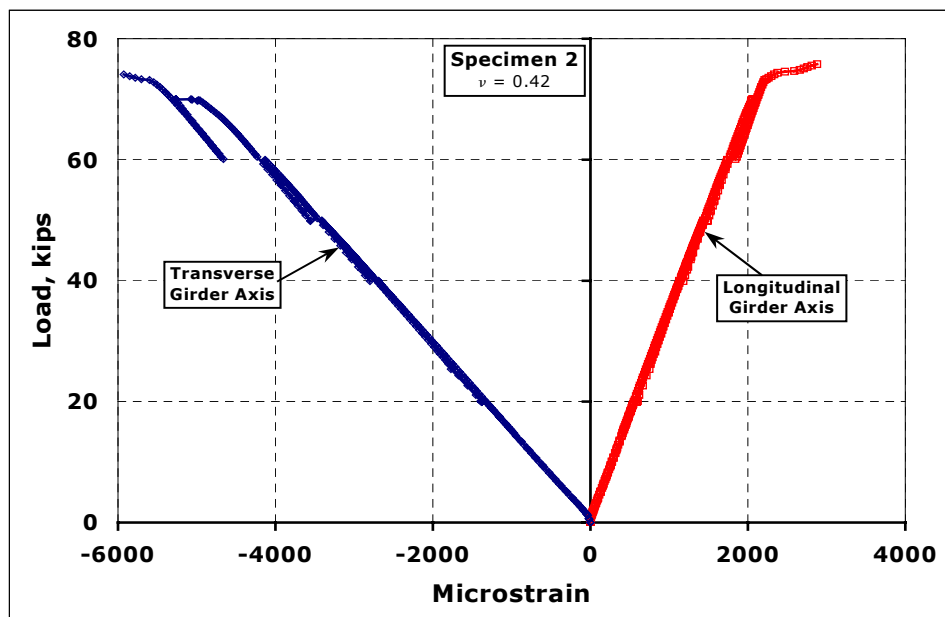


**Figure 7.22.** Web Buckling Test Specimen 2 Load-Strain Curve.

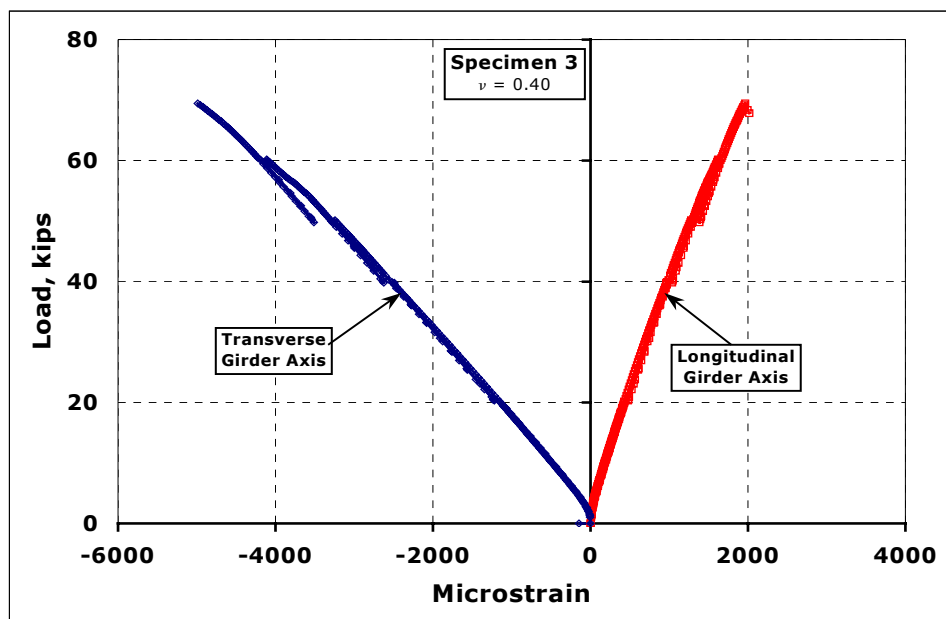


**Figure 7.23.** Web Buckling Test Specimen 3 Load-Strain Curve.

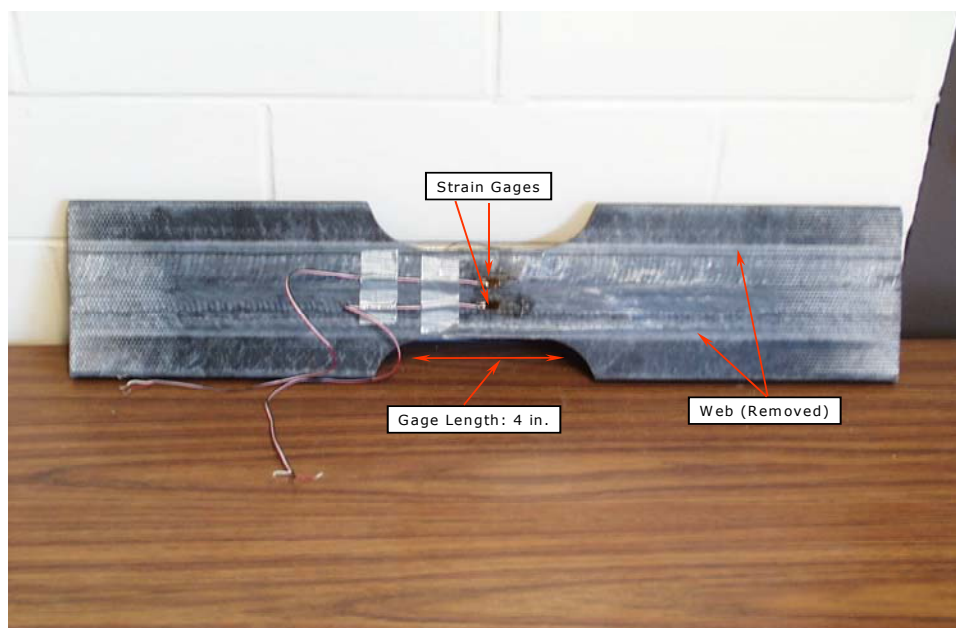


**Figure 7.24.** Specimen SW2 Tensile Coupon Before Test.



**Figure 7.25.** Specimen SW2 Tensile Coupon After Test.



**Figure 7.26.** Specimen SW2 Tensile Coupon After Test (Side View).

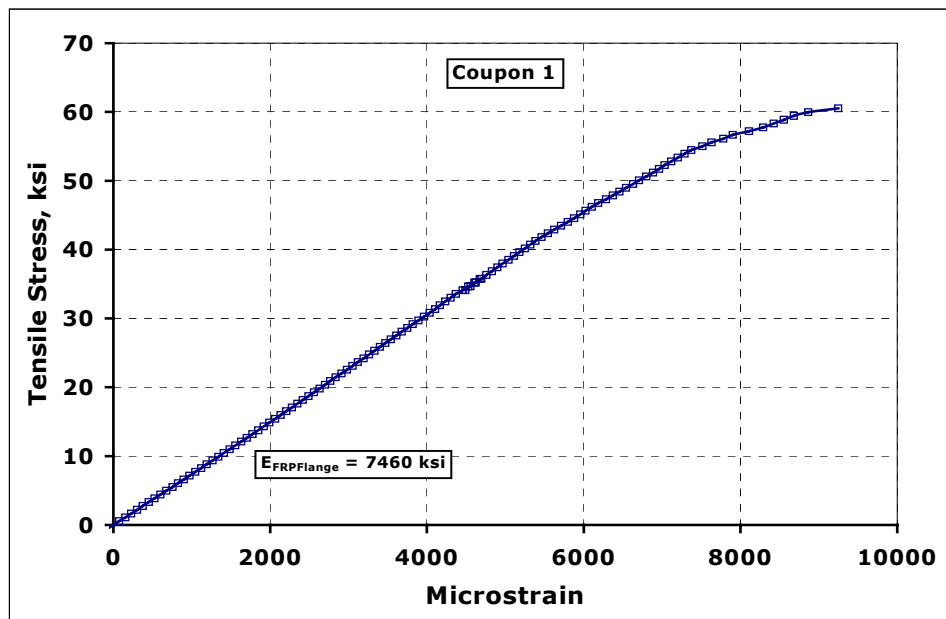


**Figure 7.27.** Specimen SW2 Tensile Test Stress-Strain Curve.

By considering composite action the stiffness of the system increases from  $EI = 3.5 \cdot 10^6 \text{ k-in}^2$  to  $EI = 13.4 \cdot 10^6 \text{ k-in}^2$ , 3.8 times. Hence, the level of deflections is reduced by the same factor. Furthermore the use of an RC deck enhances the behavior of the FRP girder, since in this case the RC deck will be carrying the bulk of compressive stresses.

Another potential problem caused by the low FRP elastic modulus is buckling. Buckling of the cross section web can occur due to shear stresses acting on it, and diagonal compression (strut action) near the supports, whereas buckling of the top flange is caused by the normal compressive stresses acting on the cross section. For this particular specimen the FRP girder's design considers both of these situations by featuring a double web, and horizontal stiffeners symmetrically placed with respect to mid height. This is shown in Figure 7.1 and 7.2.



## **7.5 Instrumentation**

Strain gages (SG) were placed on the FRP girder at sections 6 in., 4 ft., and 8 ft. from the south end, and at midspan on the FRP girder. SG were also placed on the RC deck at the same sections, except at the section 6 in. from the south end. All sections considered for instrumentation had SG longitudinally oriented except the section at 6 in. from the south end. The sections at midspan and at 6 in. from the south end had SG oriented in the transverse direction

Linear potentiometers (LP) were used to measure the deflections at both ends of the girder near the elastomeric bearings, and at midspan. Horizontal displacement between the girder-deck interface close to each end was also measured.

The specimen was supported at each end as shown in Figure 7.26. As it is seen on this figure an elastomeric bearing 2 in. thick, 9 in. wide and 14 in. long was used to support the specimen. The specimen clear span was 28.5 ft. Figure 7.28 shows the instrumentation for this specimen.

## **7.6 Loading**

Specimen SW1 was subjected to long-term loading. The loading was created by a number of concrete blocks uniformly placed along its length. The concrete block dimensions were 12 in. x 16 in. x 23 in., and it weighted 400 pounds. The blocks were placed on top of the RC deck resting on elastomeric bearings 1 in. thick as shown in Figures 7.30, 7.31, and 7.34.

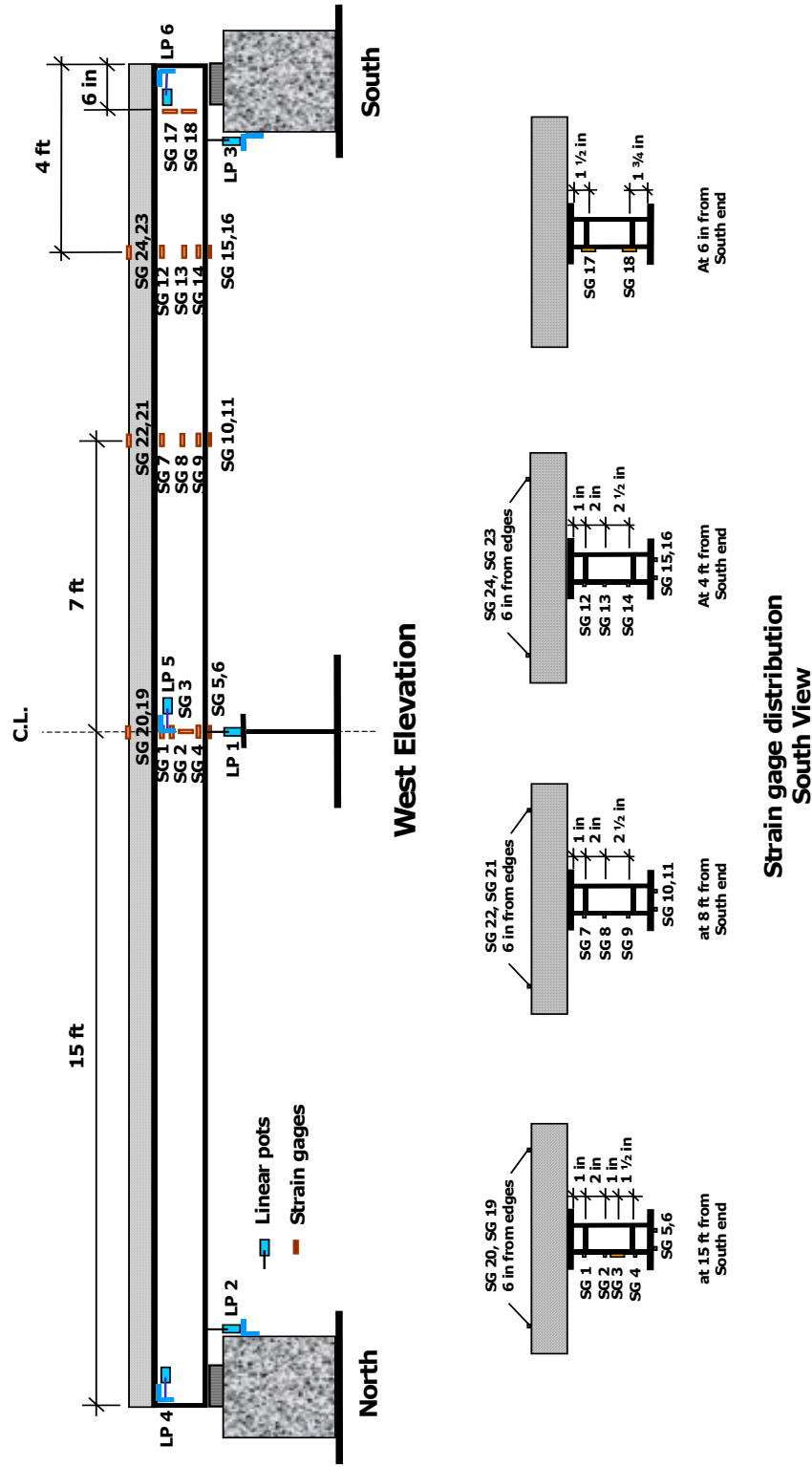


**Figure 7.28.** Specimen SW1, Strain Gages and Linear Pots.

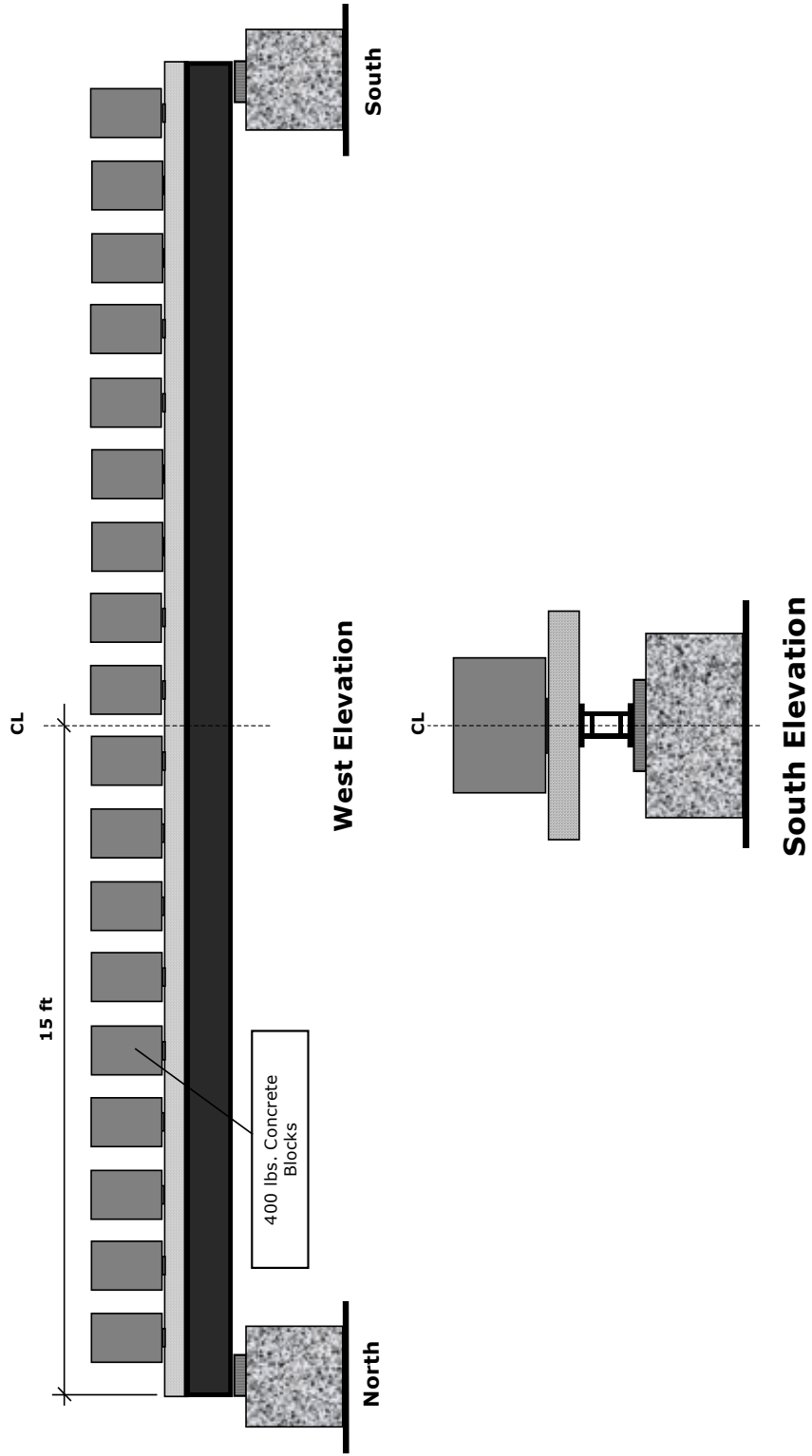


**Figure 7.29.** Specimen SW1, Loading.



**Figure 7.30.** Specimen SW1 Before Loading.

The number of concrete blocks was increased as the test developed. The specimen was initially loaded with five blocks as shown in Figure 7.31. A month later the number of blocks was increased up to a total of nine blocks; thirty days later the number of blocks was doubled, see Figure 7.32. Each time the number of blocks was increased, the specimen was unloaded, and then reloaded. Three months later all the blocks were removed. The specimen was reloaded again a week later, this time using 37 blocks for a period of a week as shown in Figure 7.33. After this period, the loading was finally removed.

After removing the loading, the specimen began a slow process of recovery. In all, specimen SW1 was tested for a period of 210 days. During which strains and deflections were continuously recorded. AE data was also periodically recorded.



**Figure 7.31.** Specimen SW1 - First Level of Loading.



**Figure 7.32.** Specimen SW1 - Third Level of Loading.



**Figure 7.33.** Specimen SW1- Fourth Level of Loading.



**Figure 7.34.** Specimen SW1 - After Load Removal.

Figure 7.34 shows Specimen SW1 after the load was removed. Specimen SW1 had a midspan permanent deflection of 1¼ in.

## 7.7 Test Results

The specimen midspan deflection as a function of time is shown in Figure 7.35. It can be observed on this figure the development of deflection with time and level of loading. The behavior was similar to that of Specimen IKG1 (Figure 6.31). As it is shown in Figure 7.35, only a small amount of recovery was observed. This behavior can be explained if we consider that the deck-girder interface experienced slippage during the test, the recovery then was prevented by friction at this interface. Non-recoverable permanent deformations on the RC deck were observed at its midspan; the FRP girder on the other hand did recover back to its initial configuration after a few hours.

It was also observed that some cracks developed in the RC deck at the interface with the girder. This final condition of the deck means that the deck suffered some damage during testing, most likely after the second month of loading. As the loading increased, the damage in the deck developed and the concrete around the shear connectors became 'loose' due to cracking. The lack of recovery for the specimen can be attributed to permanent deformation and damage in the RC deck, which even after the loading was removed, suffered visible permanent deformations. The deformation of the concrete is permanent non-recoverable and works against the viscoelastic recovery of the FRP.

The viscoelastic behavior of Specimen SW1, will be discussed by taking as reference its midspan section. On this section, the normal stresses were the highest for each loading considered as the test progressed. Figures 7.36 and 7.37 show the normal calculated stresses and measured strains acting on the bottom of the specimen cross section at midspan as a function of time.

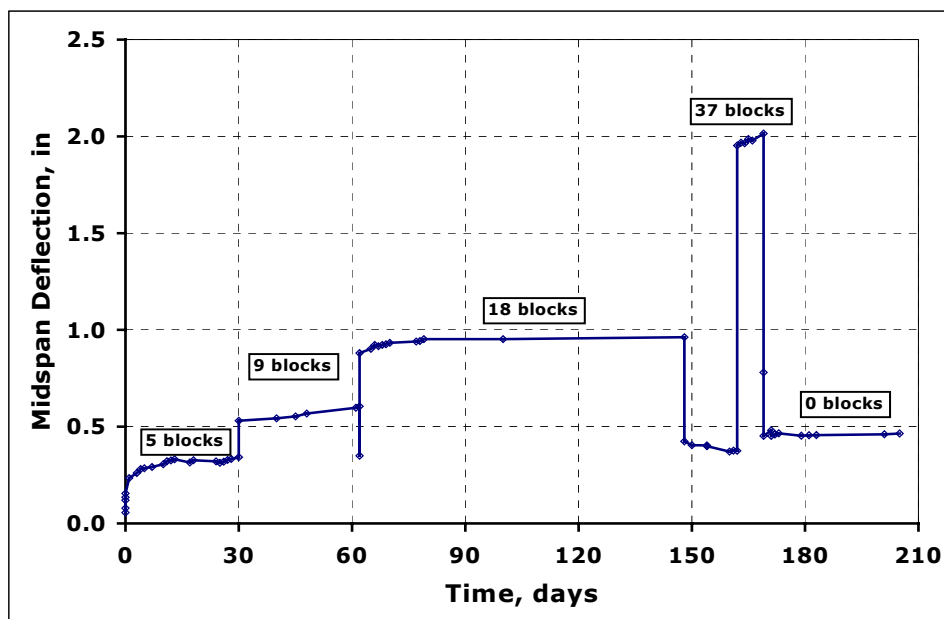


**Figure 7.35.** Specimen SW1 – Midspan Deflection vs. Time.

Based on the strain measurement at midspan shown in Figure 7.38, the longitudinal elastic modulus as a function of time can be obtained using the Findley model. Findley's model has proven to be very accurate in predicting the viscoelastic behavior of FRP materials. It essentially reduces to a power function of time. The Findley model was used to model the strain history at the bottom flange of the midspan section of the specimen. The model was based on data obtained during the first loading step. Figure 7.38 shows the data in Figure 7.37 and the results from the Findley model curves for each load increment. It is seen the model predicts quite accurately the strain history of the specimen under study.



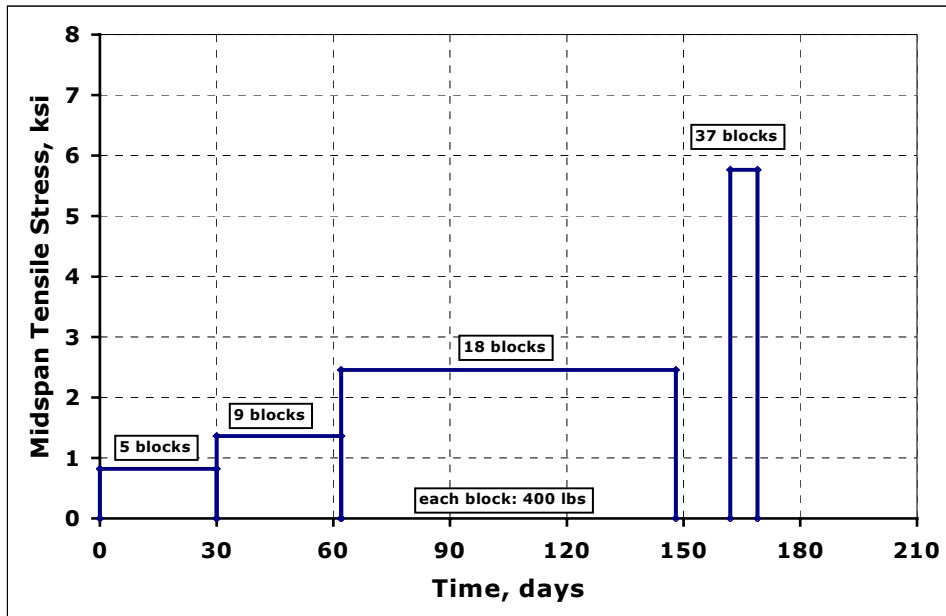


**Figure 7.36.** Specimen SW1 – Midspan Stress vs. Time.

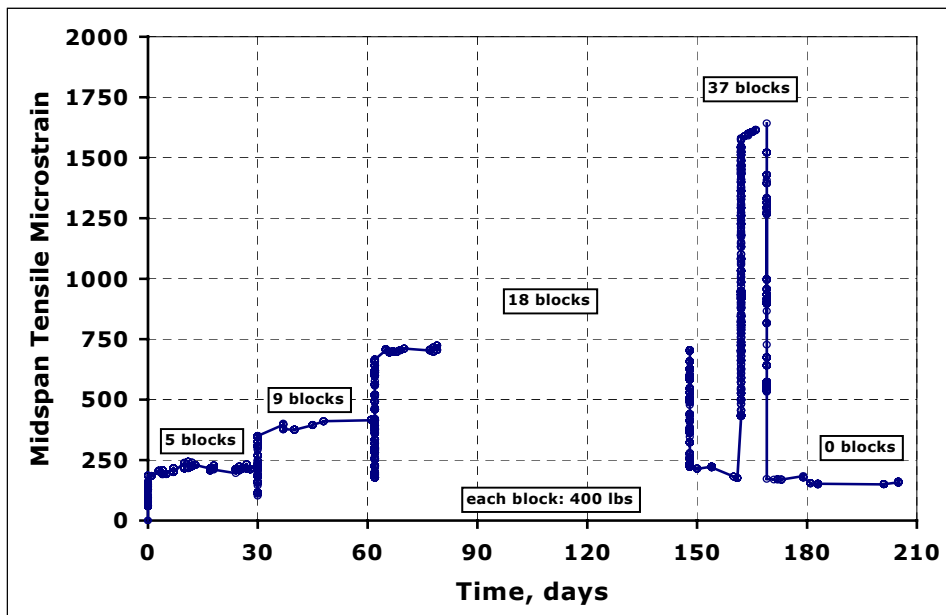


**Figure 7.37.** Specimen SW1 –Midspan Strain vs. Time.

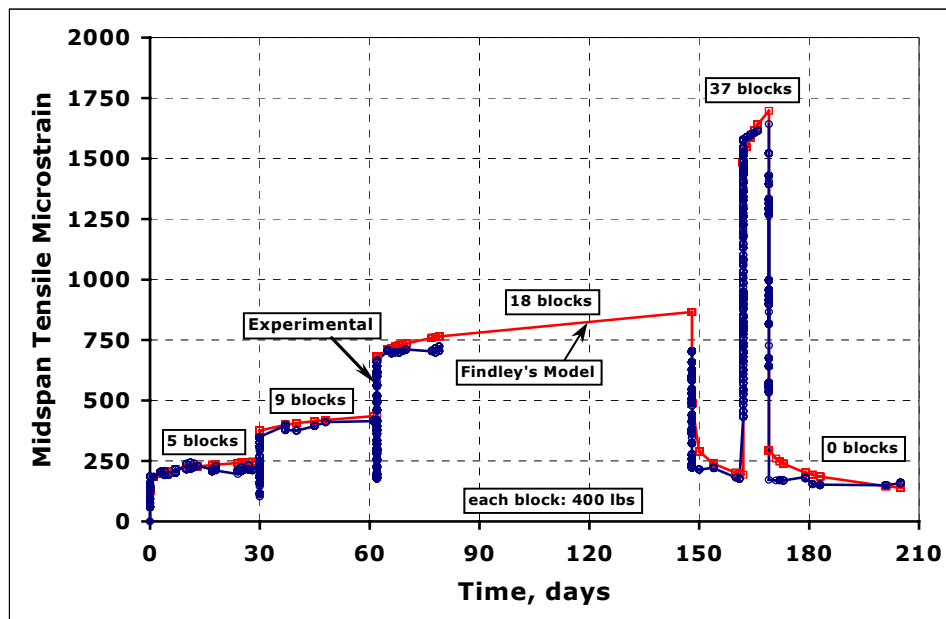


**Figure 7.38.** Specimen SW1 – Midspan Strain vs. Time (Findley's Model).

## 7.8 Significant Findings

The findings from the test on Specimen SW1, reinforced the findings from Specimen IKG1. Again, the Findley model worked particularly well in predicting the viscoelastic behavior of the structural system.

## 7.9 Summary

This chapter described specimens SW1 and SW2, and testing performed on both specimens. Specimen SW2 was tested under several different conditions to determine the mechanical properties of the FRP hybrid girder. It was found that the compressive stresses in the top flange caused it to delaminate and buckle, even when some tensile capacity was still available on the bottom flange. On average, compression buckling took place at a 50% of the tensile capacity of the FRP girder, hence controlling the overall behavior

of the specimen. Specimen SW1 was tested under long-term loading aimed at studying the viscoelastic behavior of the FRP and the creep behavior of the concrete. It was found that the behavior of this structural system followed the general pattern for creep and viscoelastic behavior of systems involving FRP materials. The Findley model worked particularly well in predicting the behavior of Specimen SW1. Due to its practicality this model should be adopted to predict the behavior of structural systems involving FRP materials. Also, the data collected shows that time dependant deformation is very significant for FRP materials, and should be considered during the design of any structural system involving FRP materials.

## **Chapter 8**

# **Vinyl Ester Fiber Reinforced Plastic Contact Molded Girder**

### **8.1 Overview**

This chapter describes specimen TK1. This specimen is composed of a fiber reinforced plastic (FRP) girder and a reinforced concrete (RC) deck. The resin for the FRP girder was vinyl ester. The FRP girder used in this specimen was one of the FRP girders specifically fabricated for this research project and was fabricated by a contact molded process.

### **8.2 General Description**

Specimen TK1 had an overall length of 30 ft., and a clear span between supports of 28.5 ft. It had as structural components an FRP contact molded girder and an RC deck. Specimen TK1 was designed to sustain the applied loads by means of deck-girder composite action.

The FRP girder was fabricated by Tankinetics Inc. Harrison, Arkansas. This company specializes in the fabrication of fiberglass vessels used by the process industries. Tankinetics Inc. was certified by the American Society of Mechanical Engineers (ASME) to fabricate Section X, Class II FRP pressure vessels (ASME Code). Tankinetics Inc. was also an ASME certificate holder for RTP-1 (ASME RTP-1), a standard for the fabrication of FRP tanks and vessels operating at low pressure.

The FRP girder had a 30 ft. length and featured a trapezoidal cross section with an overall constant depth of 18 in. The central 10 ft. of the

girder had a constant cross section, 18 in. clear width at the top, 16 in. outside width at the bottom. The 10 ft. long portions of the girder at each end were tapered from the middle towards the ends. The girder was tapered because at each end the flexural stresses were much less than at midspan. The girder dimensions were selected so that the cross section would be to sustain the level of stresses from the corresponding loading. At both ends the dimensions of the cross section were 10 in. clear width at the top and 8 in. outside width at the bottom. The thickness of the web walls was  $\frac{1}{2}$  in. and the bottom flange was 3 in. thick. Details are shown in Figures 8.1 and 8.2.

Shear connectors were incorporated into the top flanges spaced at 32 in. center to center. Their size and shape were determined based on the stress distribution at the deck-girder interface. Each connector was fabricated integral with the girder's flange and was  $4\frac{1}{2}$  in. width, 8 in. length, and 1 in. thick, as shown in Figures 8.1 and 8.2.

Additionally, web connectors were used to hold the deck and the girder together. They were designed to prevent the RC deck from lifting off the FRP girder, which would prevent the shear connectors from working. It was not intended that they carry any shear. These web connectors consisted of a # 4 steel Grade 60 rebar running across the section and extending outside the web walls by approximately 1 in. and were placed along the length, symmetrically with respect to the midspan as shown in Figure 8.3. These bars were completely embedded in a 6 in. x 6 in., unreinforced concrete block cast integral with the RC deck. The design of these connectors was based on the stress needed to lift the RC deck from the FRP girder

The RC deck was 4 ft. wide and had a thickness of 6 in. for the entire 30 ft. length of the girder. The reinforcement layout was similar to that for the other specimens. Shoring was left in place until removal just prior to testing.

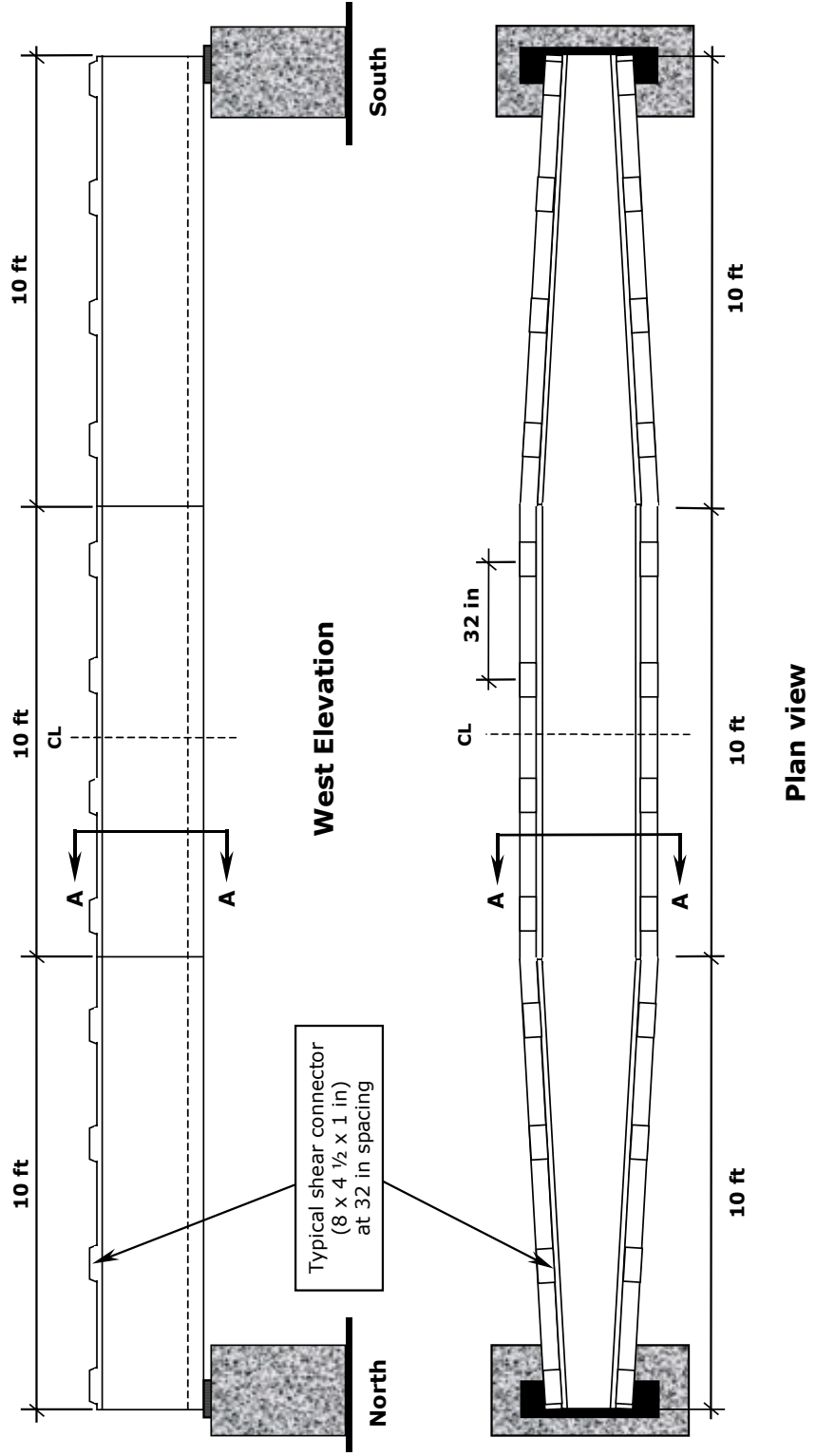


**Figure 8.1. FRP Contact Molded Girder.**

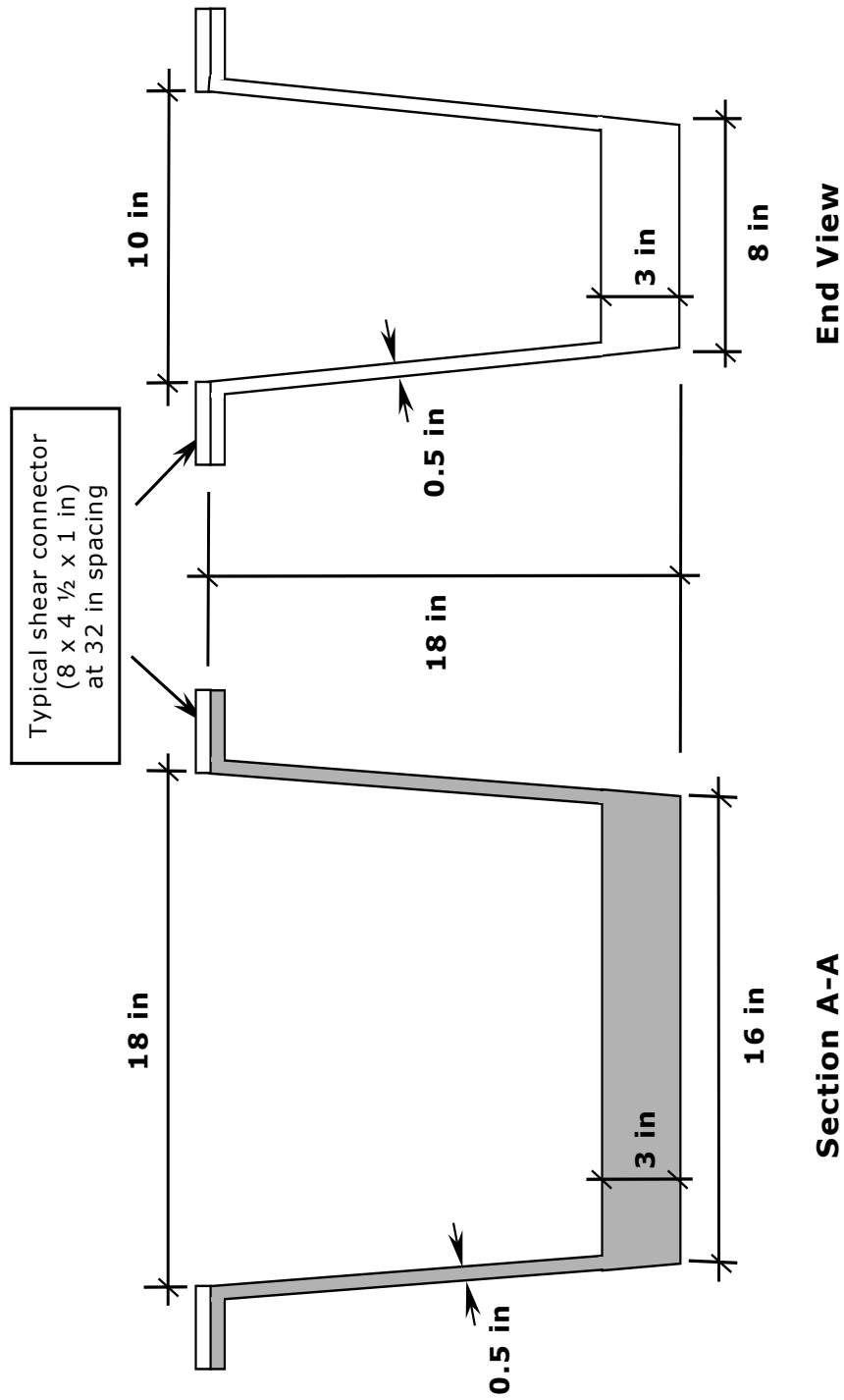


Figure 8.2. FRP Girder Cross Section.

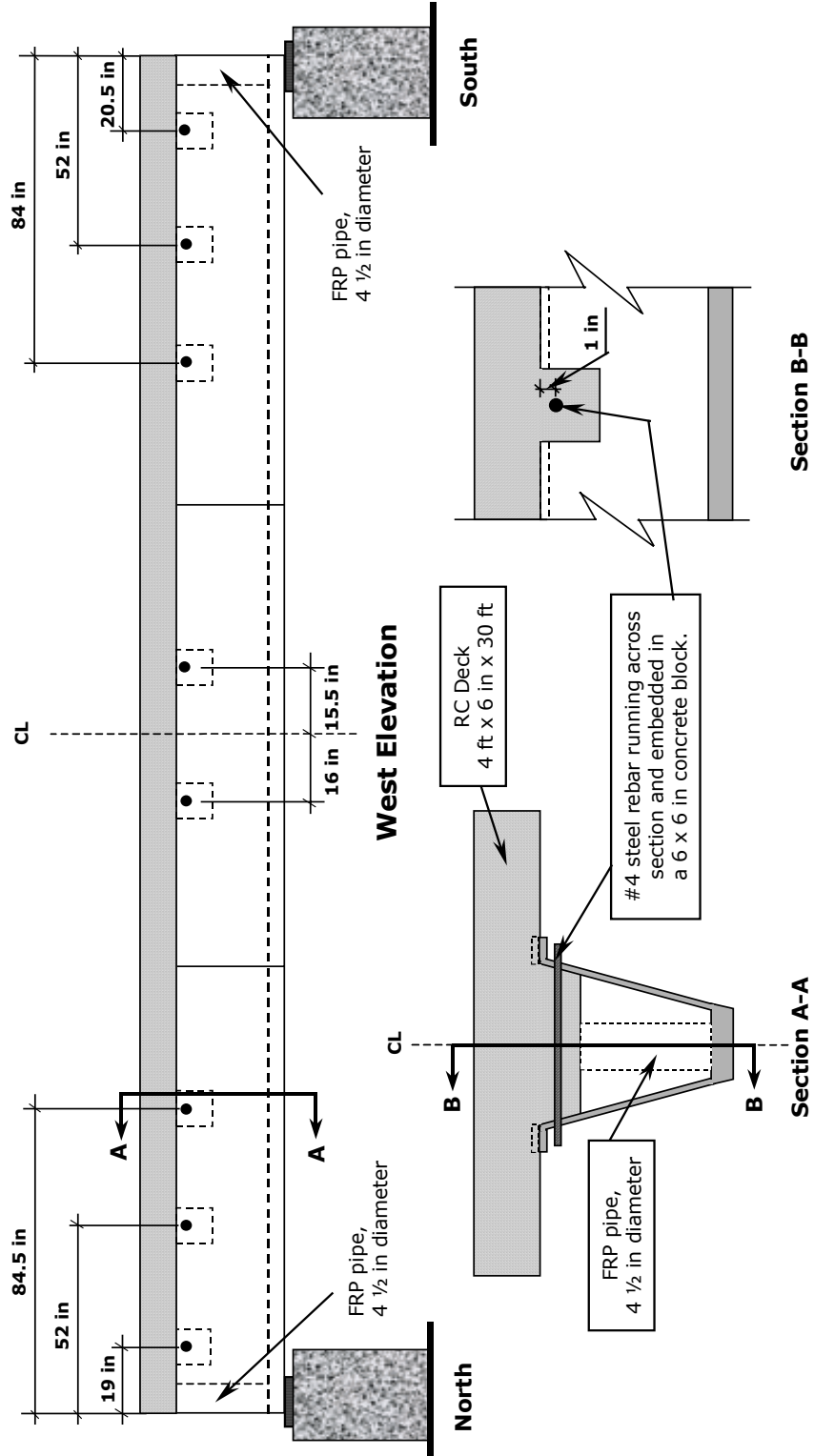


Figure 8.3. Web Connectors.



At the end of each girder a piece of FRP pipe 13 ¼ in. length was placed vertically between the girder bottom flange and the deck as shown in Figure 8.3. These pipes were filament wound series 1500 line pipes, fabricated by Fiber Glass Systems, Inc., San Antonio, Texas. The pipes had an outside diameter of 4 ½ in. (nominal), 4 3/8 in. (actual), and a thickness of ½ in. (nominal), 3/16 in. (actual). A more detailed description of these FRP pipes is given in Chapter 9. Two layers of Teflon sheets 1/32 in. thick each, were placed at each end of the pipes to provide proper fitting between the girder's flange and the deck. The purpose of these pipes was to prevent local buckling of the FRP girder webs at each end, hence acting as web stiffeners.

The specimen was supported at each end on elastomeric bearings whose dimensions were approximately 3 in. thick, 11 in. wide, and 20 in. long, with a clear span of 28.5 ft. The bearing was oriented with the 11 in. dimension parallel to the axis of the girder. Lateral support for the specimen was provided at midspan by means of steel triangular frames attached to the ground as shown on Figures 8.4, and 8.8. The elastomeric bearings and the triangular frames were described in detail in Chapter 3.

Prior to casting the RC deck, the girder cross section was filled with Styrofoam to provide a form for the concrete. The Styrofoam was left in place after the other forms were removed. The Styrofoam was cut to form the concrete blocks at each connector, and also at each end where the pieces of FRP pipe were placed.

A picture of the FRP girder is shown in Figure 8.4. Figure 8.5 shows a close-up of a web connector, and Figure 8.6 shows the end of the TK1 specimen prior to testing. Figure 8.6 also shows the FRP pipe as well as the Styrofoam filling the girder cross section.



**Figure 8.4.** FRP Girder.



**Figure 8.5.** Web Connector.



**Figure 8.6.** FRP Pipe Web Stiffener at South End.

### **8.3 Material Properties**

The materials in the fabrication of the FRP girder were Dow Derakane™ 411-350 epoxy resin (Dow, 1999), and E-Glass reinforcement. The fabricator reported an amount of 28% reinforcement by weight. Actual material properties were found by testing samples from both components: the RC deck and the FRP girder.

#### **8.3.1 FRP Pultruded Girder**

The FRP girder was tested alone under a load applied at midspan, the clear span between supports was 28.5 ft. The girder was loaded up to 3 kips, unloaded and reloaded up to 3.5 kips. The load deflection curve is shown in Figure 8.7. Based on this test a value for the elastic modulus of the FRP was found to be  $E_{FRPgirder} = 2200$  ksi. The fabricator reported an ultimate tensile strength of 25 ksi.

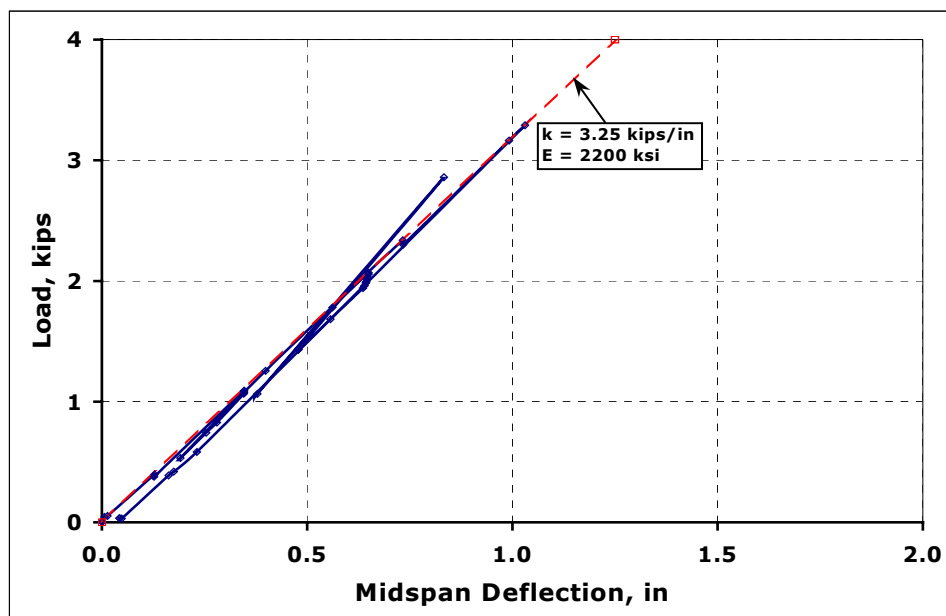


Figure 8.7. FRP Girder Load Deflection Curve.

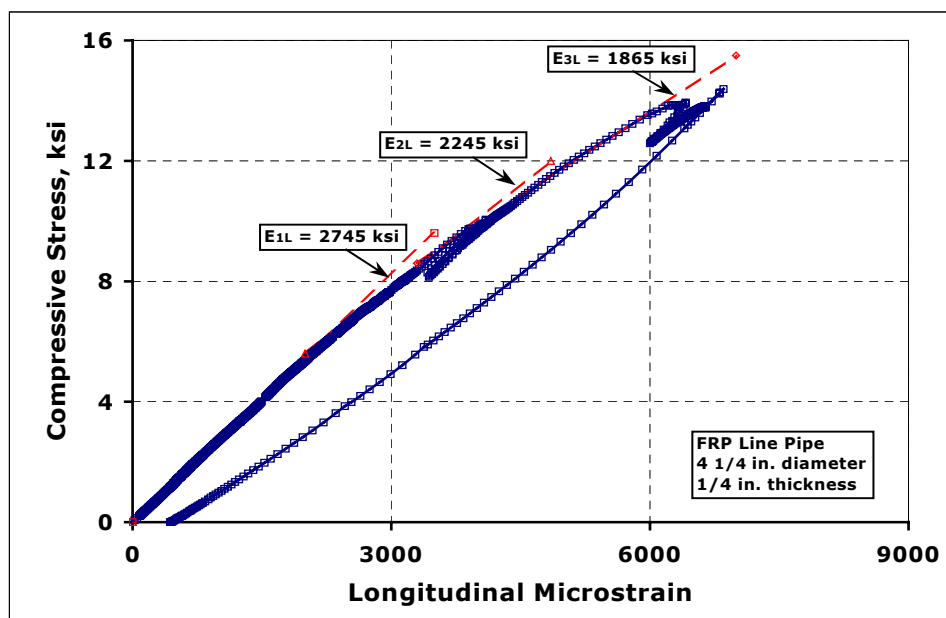


Figure 8.8. FRP Pipe Stress-Strain Curve. Compression Test.

### 8.3.2 FRP Pipe

FRP pipes samples were also tested under compression loading. A thorough discussion of the results from tests on these FRP pipes will be given in Chapter 9. Results from a compression test are given in Figure 8.8. Each of these samples was 1 ft. long, and had a 4 ½ in. outside diameter, and ¼ in. thickness. From Figure 8.8, an elastic modulus  $E_{FRPpipes} = 2745$  ksi was determined. It is also interesting to note the nonlinear behavior of these pipes. A compressive strength of 15 ksi (100 kips) was determined for these pipes.

### 8.3.3 RC Deck

The 28 day compressive strength of the concrete for the RC deck was 5000 psi (nominal), 5250 psi (actual). The corresponding elastic modulus using the ACI formula for normal weight concrete was  $E_{concrete} = 4130$  ksi.

## 8.4 Structural Analysis and Design

Specimen TK1 was designed for AASHTO HS20 loading. The resulting structural system consisted of an FRP girder and an RC deck, both working under composite action.

Considering this load a linear elastic structural analysis was carried out to determine the bending moments, and shear forces developed in the structure. The software used was LEAF (1996). The maximum bending moments, and shear forces developed in the structure where  $M_{max} = 91.6$  k-ft, at the girder midspan, and  $V_{max} = 12.8$  kips, close to the girder supports. Both these values were used for design.

A preliminary design for the FRP girder assumed an overall thickness of ¾ in., an overall constant depth of 18 in., and a bottom flange thickness of

2 in. These dimensions were refined as the process of design developed, finally the design settled on the dimensions given earlier.

A way of overcoming the low elastic modulus of the FRP is to consider composite action between the RC deck and the FRP girder. By considering composite action the stiffness of the system increases from  $EI = 6.0 \times 10^6 \text{ k-in}^2$  to  $EI = 40.5 \times 10^6 \text{ k-in}^2$ , 6.75 times. Hence, the level of deflections is reduced by the same factor.

Another potential problem caused by the low FRP elastic modulus is buckling. Of particular interest is buckling of the web walls and top flanges. Buckling of the web walls can occur due to shear stresses acting on it, and diagonal compression (strut action) near the supports, whereas buckling of the top flanges is caused by the normal compressive stresses acting at the deck-girder interface.

The RC deck was described in Chapter 3. Also, it should be noted that casting of the deck also included the casting of the concrete embedding the web connectors.

The design also relied on the capacity of the shear connectors at the top flanges to take care of the shear stresses developed at the deck-girder interface. This part of the design was key, since the shear connectors were considered fundamental to the behavior of the system for both, sustaining the load and reducing the level of deflection of the whole structural system.

The final geometry of the cross section at midspan and at each end, had the dimensions shown in Figure 8.2.

## **8.5 Instrumentation**

Strains and deflections were measured at selected points. Since the specimen was symmetric, only a quarter of it was instrumented.

Strain gages (SG) were placed at midspan, at 8 ft., and 8 in. from the south end of the FRP girder; and at midspan, and 8 ft. from the south end on the RC deck.

The SG on the FRP girder's web were oriented on both longitudinal and transverse directions, whereas on the RC deck only the longitudinal direction was monitored. Additional gages were used on both FRP pipes at each end, longitudinally oriented with respect to the pipe.

Linear potentiometers (LP) were used to measure the deflections at both ends of the girder closer to the elastomeric bearings and at midspan. Relative horizontal displacement between the girder and deck interface close to each end was also measured. Details of the SG and LP were given in Chapter 3.

Figure 8.9, is a sketch showing the position of all the instrumentation for this specimen, Figure 8.12 shows instrumentation at the North end.

Load was measured with a load cell (LC) having a capacity of 50 kips. Figure 8.10 shows a sketch of the specimen and loading.

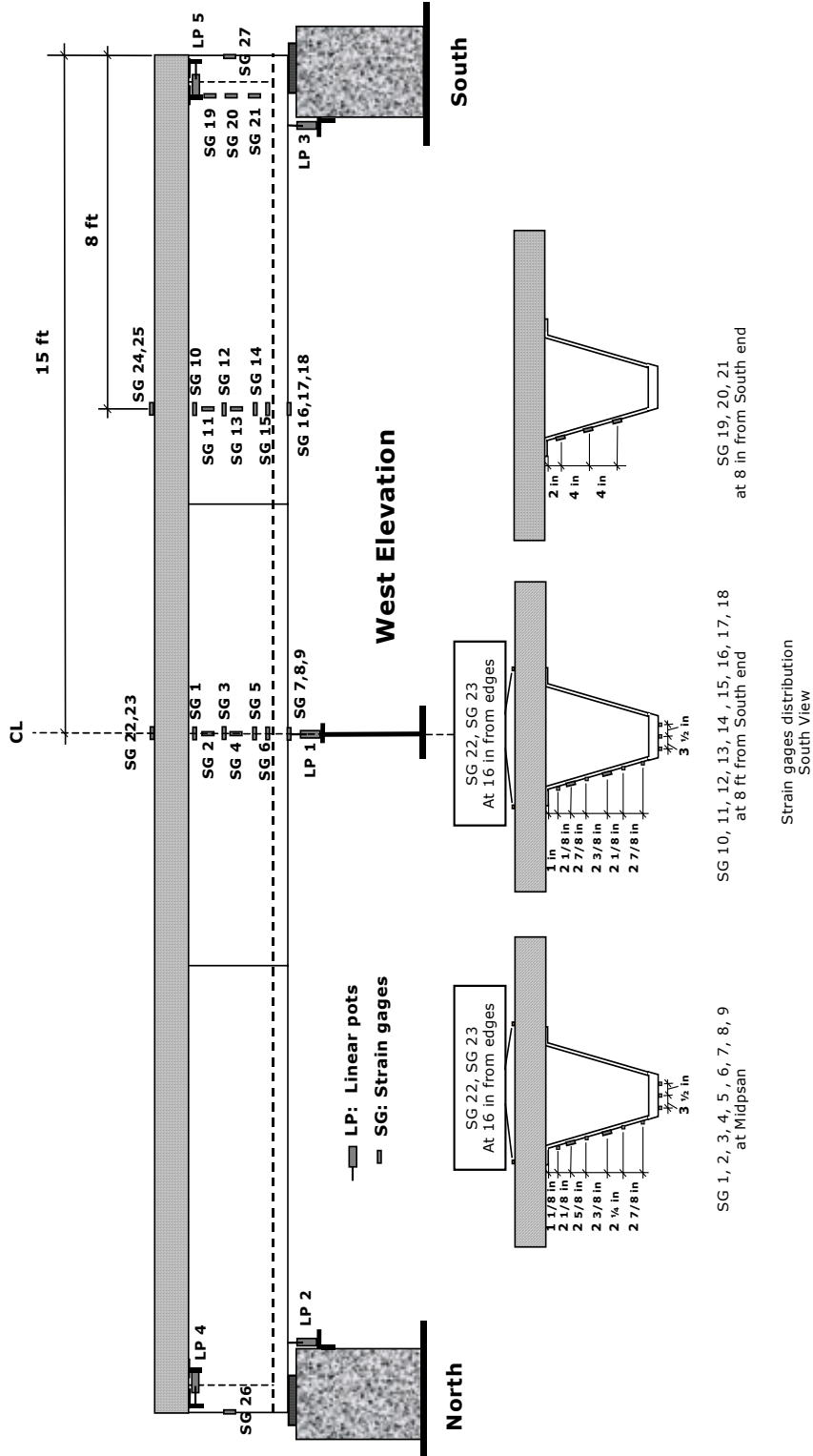


**Figure 8.9.** Specimen TK1, Strain Gages and Linear Pots.



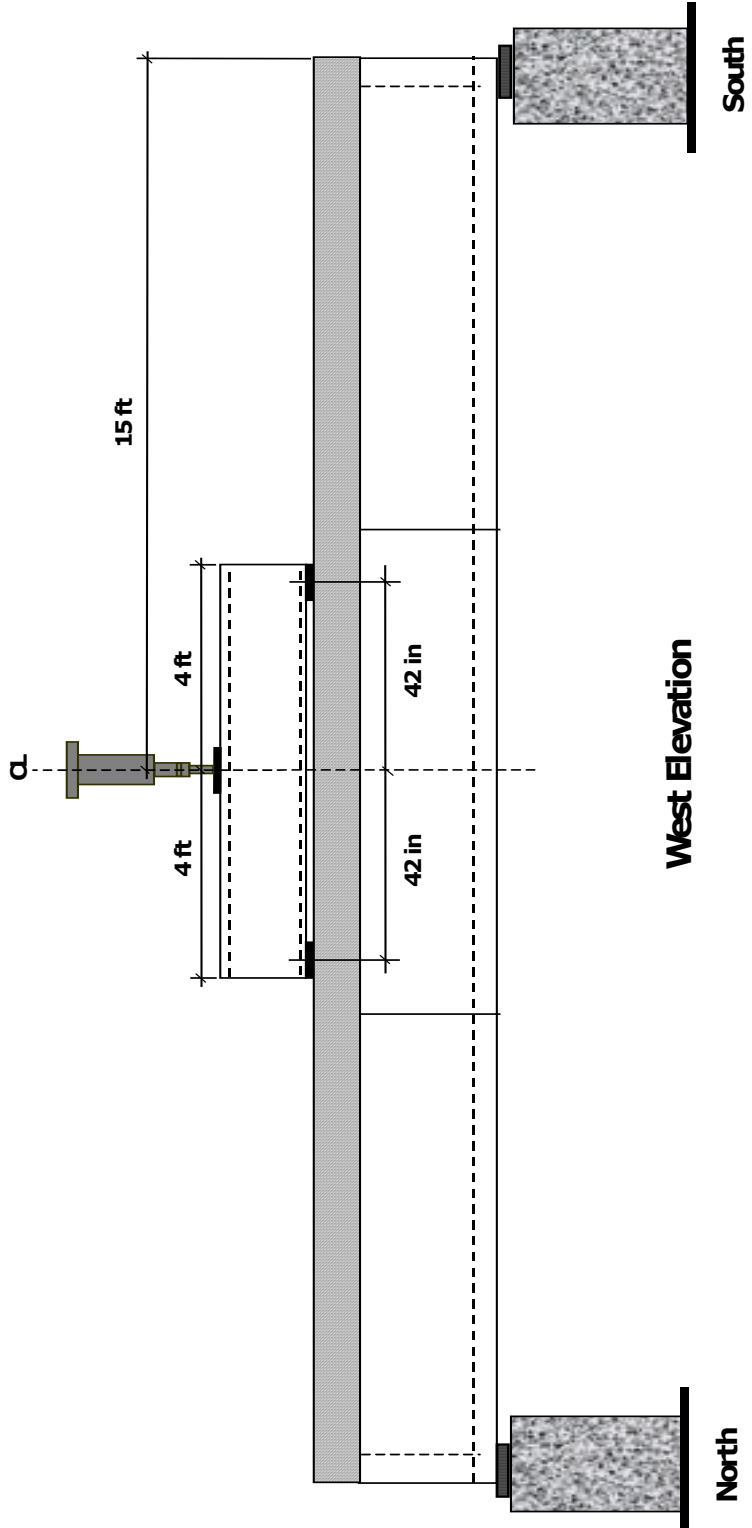


Figure 8.10. Loading.

## 8.6 Loading

Load was applied to the specimen through an 8 ft. long spreader beam placed on top of the deck, causing the specimen to be loaded in four point bending loading. The effective distance between loading points was 7 ft. Elastomeric bearings were used under the loading points as shown in Figure 8.11. The specimen ready for testing is shown in Figure 8.12.

The load was gradually applied to the spreader beam in increments of 3 kips. Since AE data was being collected simultaneously for each increment of load a loading-unloading cycle was performed, with a waiting period in between increments. For instance the specimen was initially loaded up to 4 kips total load, then unloaded to 1 kip, next it was loaded to 7 kips, and then unloaded to 4 kips and so forth. The actual loading schedule is shown in Figure 8.13.

## 8.7 Results and Discussion

### 8.7.1 Load Deflection Behavior

Figure 8.14 shows the experimental load deflection curve at midspan for this specimen. This deflection already subtracts out the deflection of the elastomeric bearings at each end of the specimen. On this figure also are shown theoretical lines corresponding to a full composite action and partial composite action, which assumes that the north half of the specimen is working under full composite action and that there is no composite action on the other half. Also shown are the design loads for this structural system cross section due to bending  $M_{\max} = 91.6$  k-ft ( $P = 14.4$  kips).

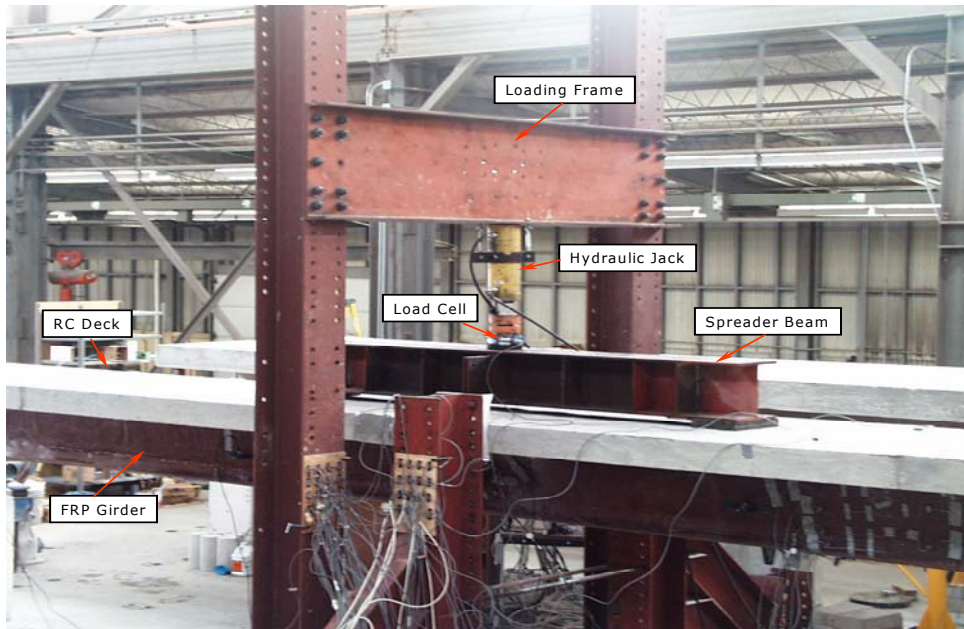


**Figure 8.11.** Loading frame.

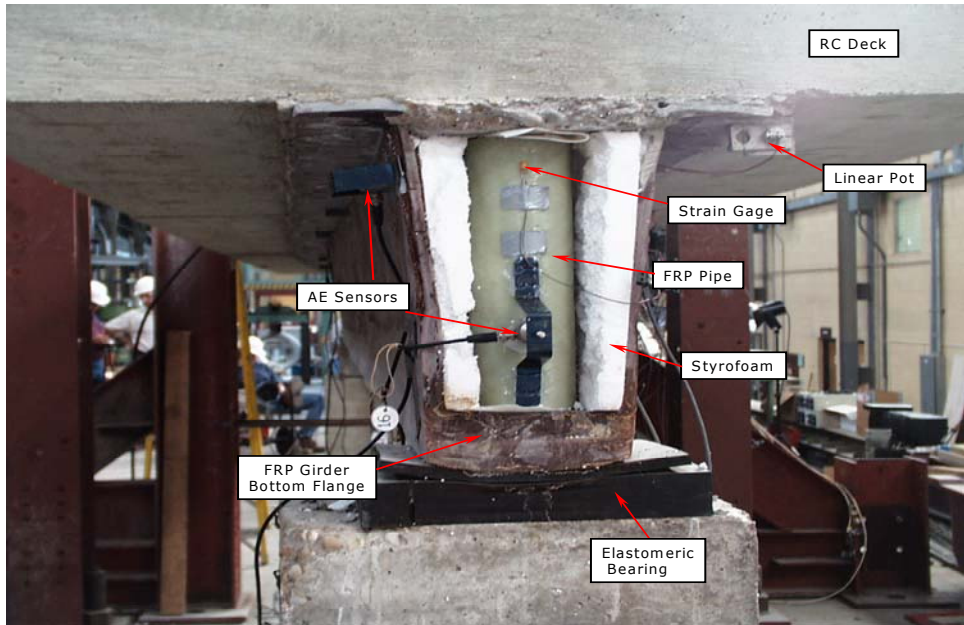


**Figure 8.12.** Specimen TK1 Instrumented Prior to Test.

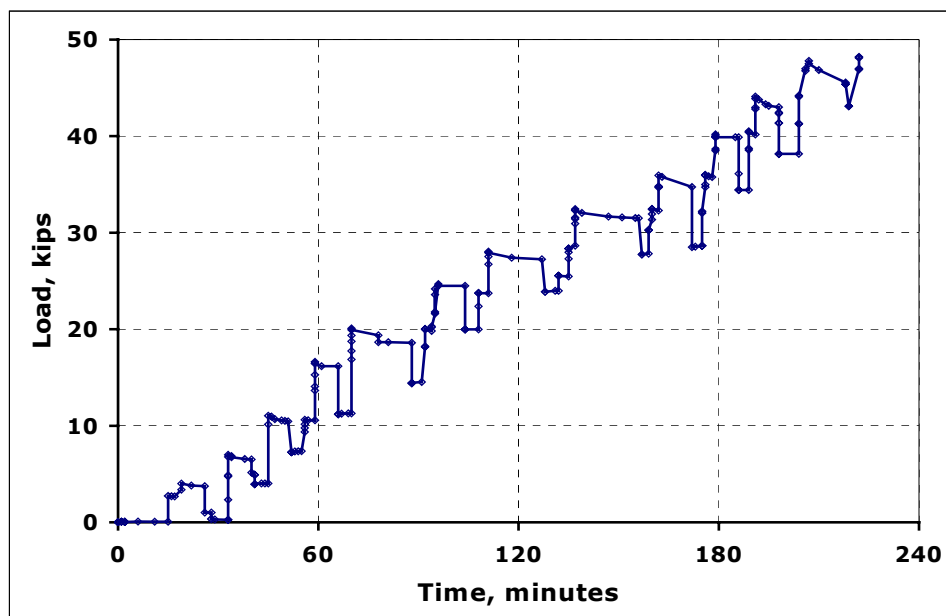


**Figure 8.13.** Load schedule.

Figure 8.14 shows the specimen load-deflection curve at midspan. Figure 8.15 shows a plot of the horizontal relative displacement at the deck-girder interface, the values plotted correspond to measurements near both ends.

The predicted response matched the experimental data at levels of load under 10 kips, with a stiffness of about 44 kip/in. As the applied load increased over 10 kips the system stiffness began to degrade. For levels of load between 10 and 30 kips a nonlinear response is observed. The average stiffness of the system is now about half of the initial stiffness 24 kips/in. Figure 8.15 shows the deck-girder relative displacement developing almost at a constant rate although of very small magnitude. Figure 8.15 also shows that most of the relative displacement took place at the south end of the specimen. No measurable relative displacement was recorded at the north end indicating full composite action.

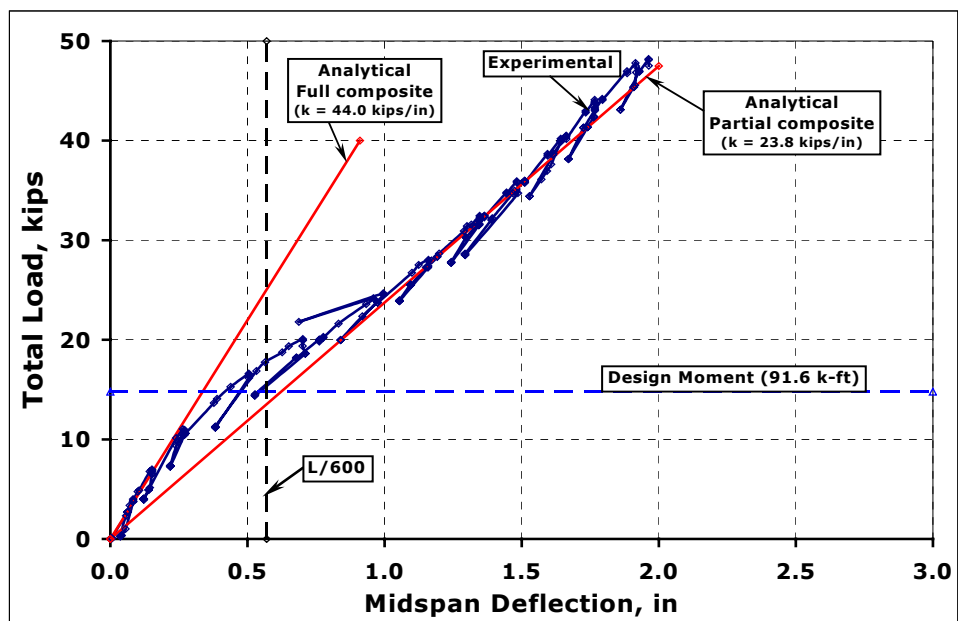


Figure 8.14. Load Deflection Curve at Midspan.

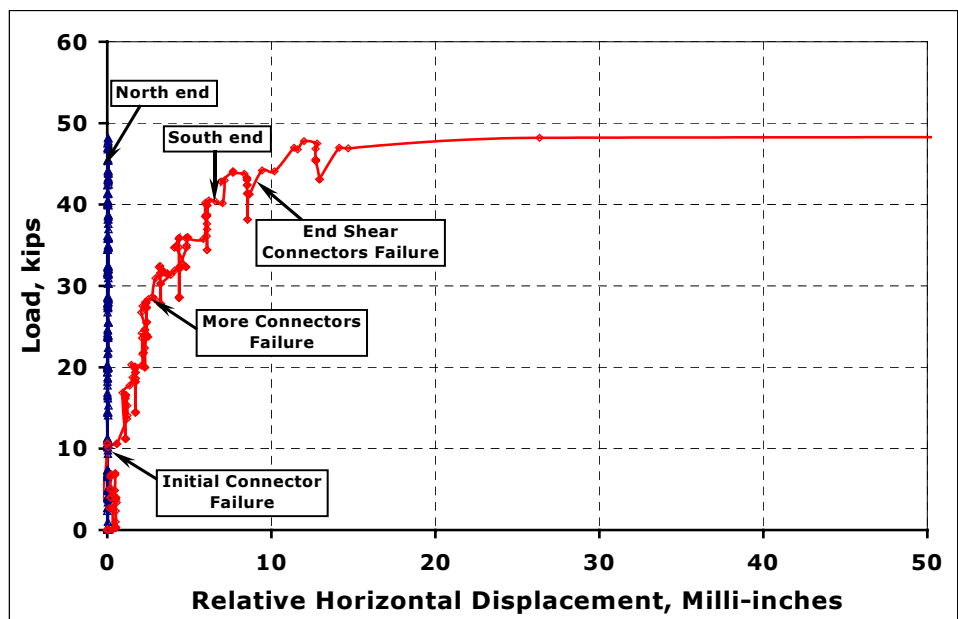


Figure 8.15. Deck-Girder Interface Horizontal Displacement at each End.

As the applied load approached 30 kips the system was still working under composite action, although, it was no longer a full composite action state, instead the cross section carried the load through partial composite action, as some shear connectors (specifically the ones close to south end), stopped transferring the shear stresses at the deck-girder interface. Also, the concrete blocks embedding the web connectors reached their tensile capacity.

As the load increased, the stiffness remained constant all the way up to failure, which took place at 50 kips, with a corresponding midspan deflection of about 2 in. Failure occurred when the concrete block embedding the web connectors (rebars) split open. Once this happened the system composite action was seriously compromised. At this point, the system still had some load carrying capacity, and as seen in Figure 8.14, it actually stiffened up.

Specimen TK1 sustained 3.25 times the design load before failure. This is consistent with the design factor of 4 recommended in Chapter 10.

### **8.7.2 Failure**

As stated earlier, failure started at the south end. Figures 8.16, and 8.17 show the specimen after failure. These figures show that the FRP girder separated almost completely from the RC deck. The design of the shear connectors caused the deck to lift from the FRP girder. When this occurred the amount of shear force transmitted between the deck and the girder was reduced. However, some shear continued to be transmitted.

Figures 8.18 and 8.19 show the FRP girder after failure with the RC deck removed. The areas of concrete around the connectors split open. No damage was found during a follow-up visual inspection of the FRP girder. In other words the FRP girder retained its original strength.



**Figure 8.16.** Shear Failure at Deck-Girder Interface at South End.



**Figure 8.17.** Shear Failure at Deck-Girder Interface at South End.

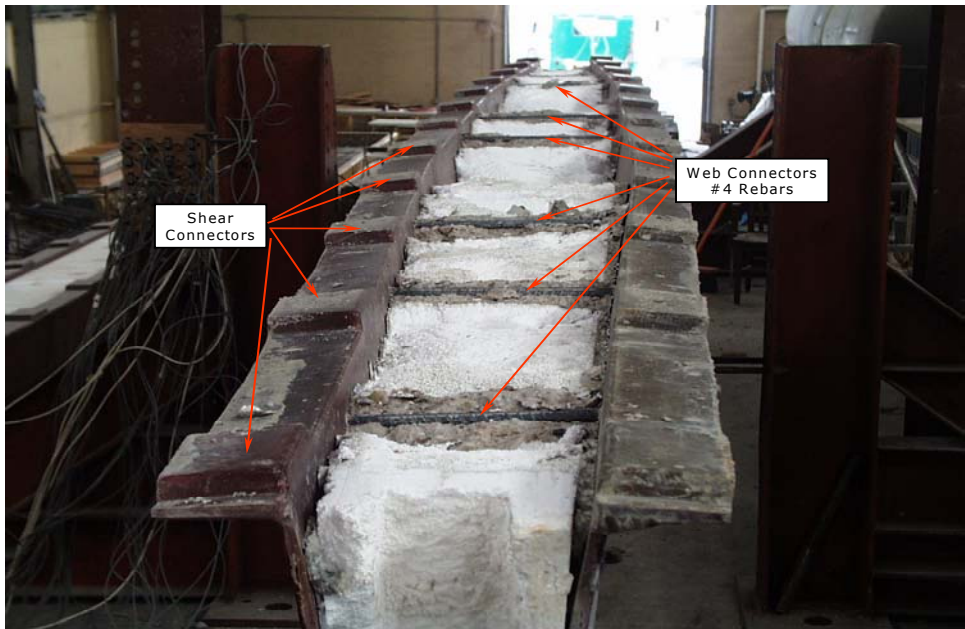


**Figure 8.18.** Girder with RC Deck Removed.

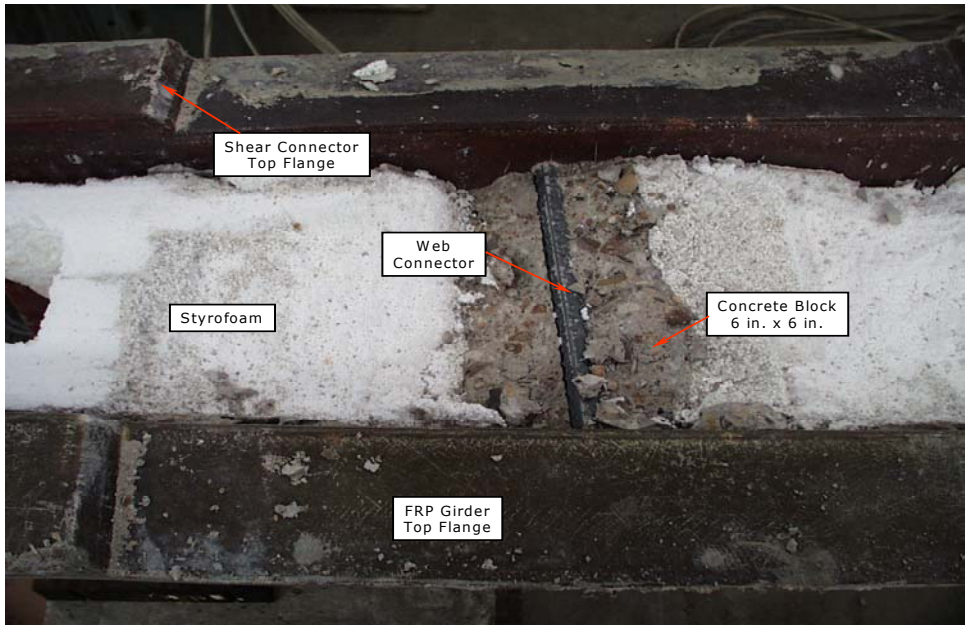


**Figure 8.19.** Web Connector with RC Deck Removed.





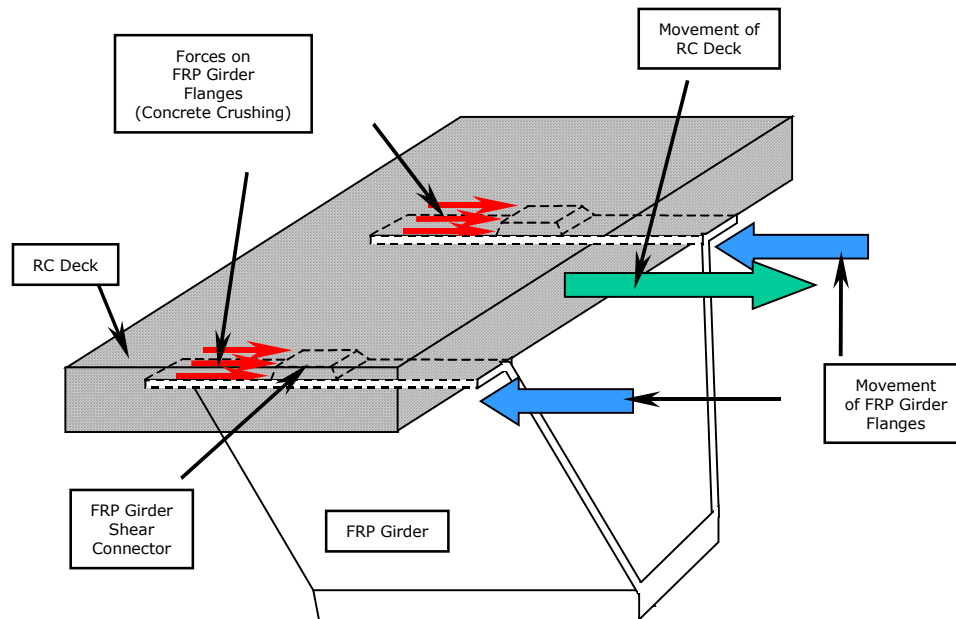
**Figure 8.20.** RC Deck Removed with Rebar Impression.

Figure 8.20 show a close-up of the RC deck at a location of a connector. It clearly shows the traces left by the web connector.

An explanation of what might have happened is as follows. Initially the system developed composite action effectively. As the loading increased the flange shear connectors began bearing against the surrounding RC deck to transfer the shear stresses at the interface. Eventually, the concrete in these zones began crushing causing the system to readapt to a new configuration by means of the slippage or horizontal relative displacement at the interface, especially in the south half of the specimen. The result was a gradual loss of composite action. Figure 8.21 shows a sketch of this development.

As the loading increased, composite action at the south end continue to deteriorate and the deck and girder were kept together only by the action of the web connectors. So the structural system switched from a fully

composite system, into a partially composite system with only the north half working under composite action; in the south half the RC deck and the FRP girder sustained the load independently. This hypothesis seems to agree with the experimental data as shown in Figure 8.14.



**Figure 8.21.** Deck-Girder Slippage Sketch.

The sloping face of the shear connectors resulted in an upward component load on the RC deck. Eventually, the concrete embedding the web connectors reached its tensile capacity and failed. Calculations show that a load  $P = 48$  kips applied on the specimen causes the midspan section at the deck-girder interface to be subjected to a tensile stress of 1 ksi. The steel rebars in the deck prevent the concrete at the interface from splitting open in the longitudinal direction, however the lack of reinforcement in the vertical direction causes the concrete to split open in this direction at a stress of 0.5 ksi. When this happened composite action at this half was completely lost causing the stiffness of the whole system to be substantially reduced. Even

then the system still had load carrying capacity left and the FRP girder was not visibly damaged.

Throughout the test no signs of web buckling were observed. This includes each end of the girder where high shear stresses developed. The reason is attributed to the FRP pipes acting as web stiffeners. The distribution of the applied load on these web stiffeners (FRP pipes) is shown in Figure 8.22. It is seen that the FRP pipes were subjected to small values of axial compressive loads. This fact can be explained by the fact that the FRP pipes only carry a large load if the FRP girder web begins to unload before buckling otherwise, the FRP girder web is the stiffer load path.

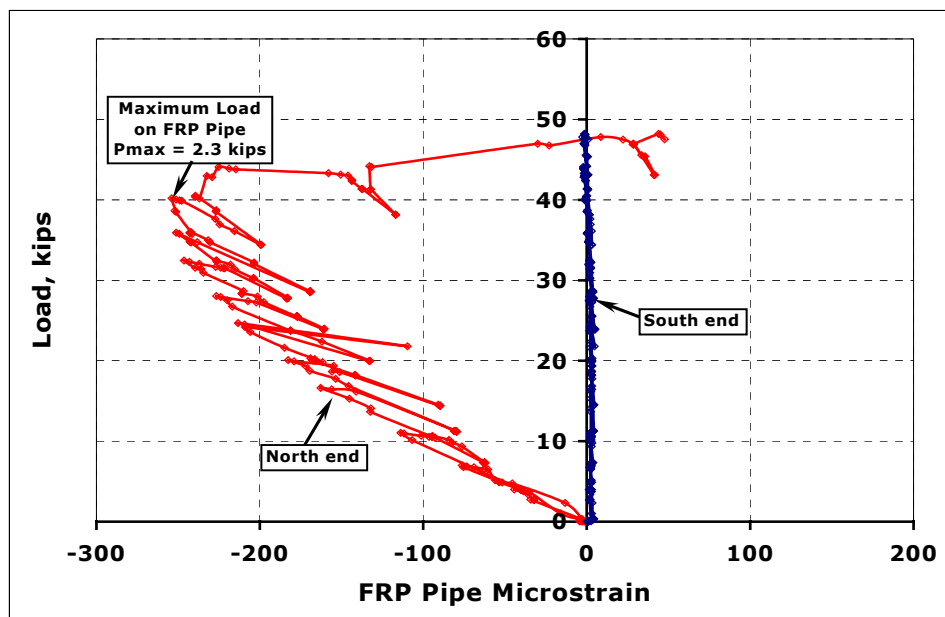


**Figure 8.22.** Load on Web Stiffeners (FRP Pipes).

The lack of axial load transferred to the FRP pipe stiffener at the south end, which is the half that split from the FRP girder, suggests that the RC deck is lifting off the girder at this end at very low loads. As the RC deck lifted from the FRP girder the FRP girder flanges showed some local buckling

as shown in Figures 8.23 and 8.24 under a load of 40 kips. This buckling was probably triggered by the early deterioration of the shear connectors, which caused the flanges to switch from being subjected under tensile stresses to being subject to compression stresses.

### **8.7.3 Strain Behavior**

Strains were found to vary linearly with the applied load. Most FRP materials are linear in nature. This behavior is shown in Figures 8.25 through 8.29. The values correspond to the strain distribution in both the longitudinal and transverse directions at midspan, at sections 8 ft. and 8 in. from the south end.

Of special interest is Figure 8.29, which shows the transverse strains at three locations at a section 8 in. from the south end. It is observed that the response is linear all the way up to 44 kips of load, where the strains have a sharp deviation from linearity, the explanation here is that at this level of load composite action at this section (and its vicinity) was lost. The sharp increment of strains indicates the girder's web undergoing large deformations.

The strain distribution along the depth of the cross section is also of interest. Accordingly, these distributions are shown in Figures 8.30 through 8.32. The strains appear to vary linearly, except for a departure from linearity at the 12 in. height of the girder's web. It is believed that this is caused by lateral deflection of the web (bulging) that was observed during testing. This is more visible at the midspan section, Figure 8.30. The other portions of the web follow a more linear pattern. The departure from linearity of the transverse strains 8 in. from the South end is believed to be due to the high shear stresses at the end of the girder. However, because the fiber reinforcement is not unidirectional, this effect is not as marked with this specimen as with the pultruded girders discussed in Chapters 4 and 5.

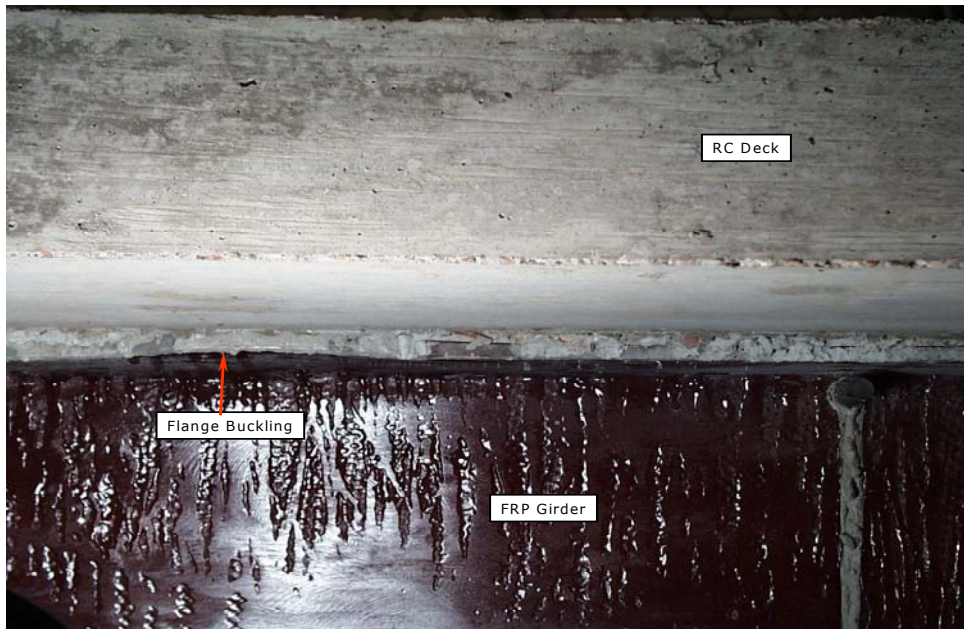


**Figure 8.23.** FRP Girder Flange Buckling.

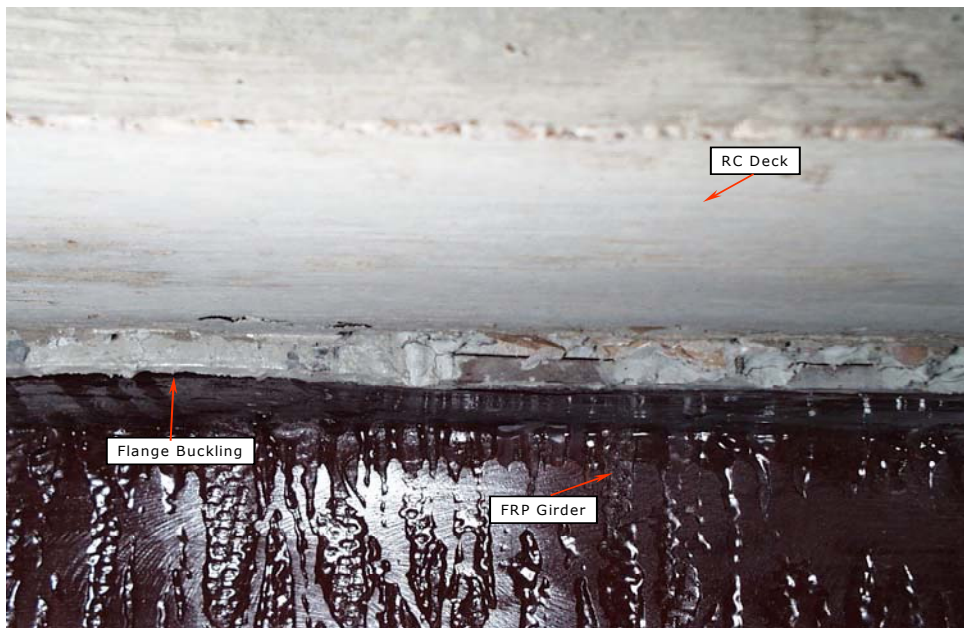


**Figure 8.24.** FRP Girder Flange Buckling.

Overall, the specimen was subjected to a maximum longitudinal tensile strain of  $\epsilon_{Tmax} = 0.0025$ , which took place on the FRP girder's bottom flange, and which corresponds to a maximum tensile stress of  $\sigma_{Tmax} = 5$  ksi, again 20% of the  $\sigma_{Tu} = 25$  ksi. The maximum compressive stress took place on the RC deck and had a value of  $\sigma_{Cmax} = 1$  ksi, 20 % of the  $\sigma_{Cu} = 5$  ksi. That is, the specimen experienced stresses well below the strength capacity of both components: RC deck and FRP girder, by a factor of 5. This means that with a more adequate shear connectors, and proper reinforcing of the web connectors in the transverse direction the specimen will be able to sustain much higher values of load.

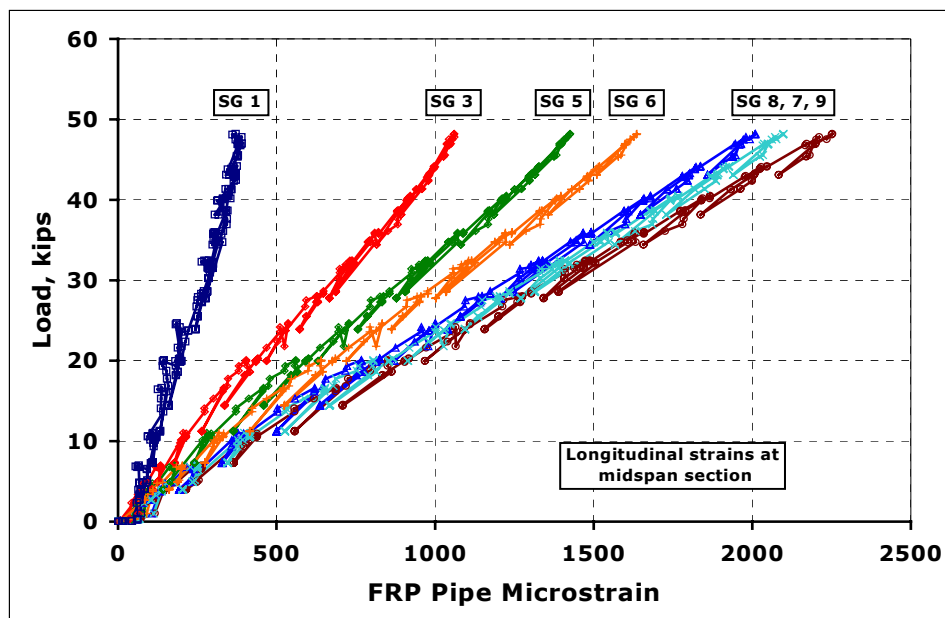


**Figure 8.25.** Longitudinal Strain Distribution at Midspan Section.

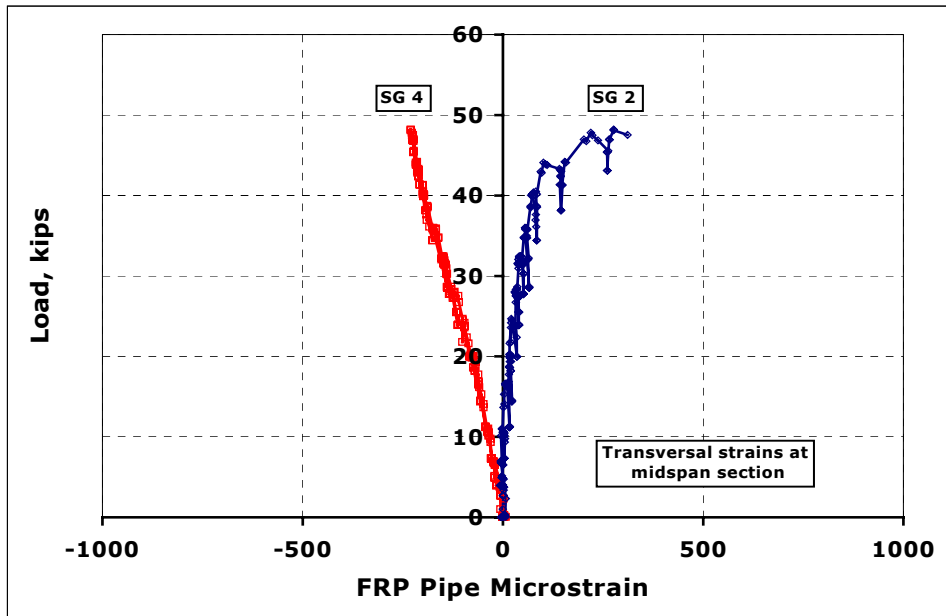


**Figure 8.26.** Transverse Strain Distribution at Midspan Section.

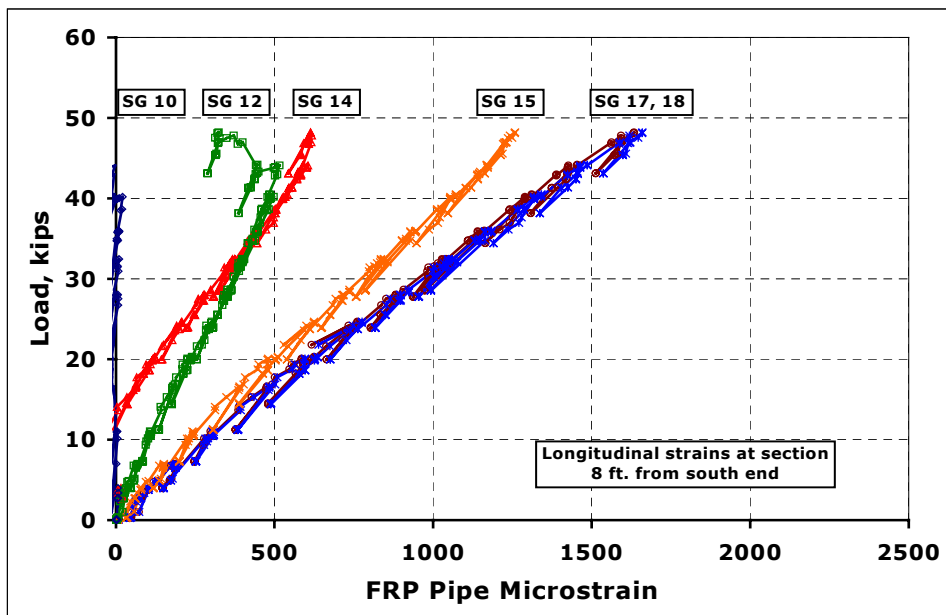


**Figure 8.27.** Longitudinal Strain Distribution at 8 ft. from South End.

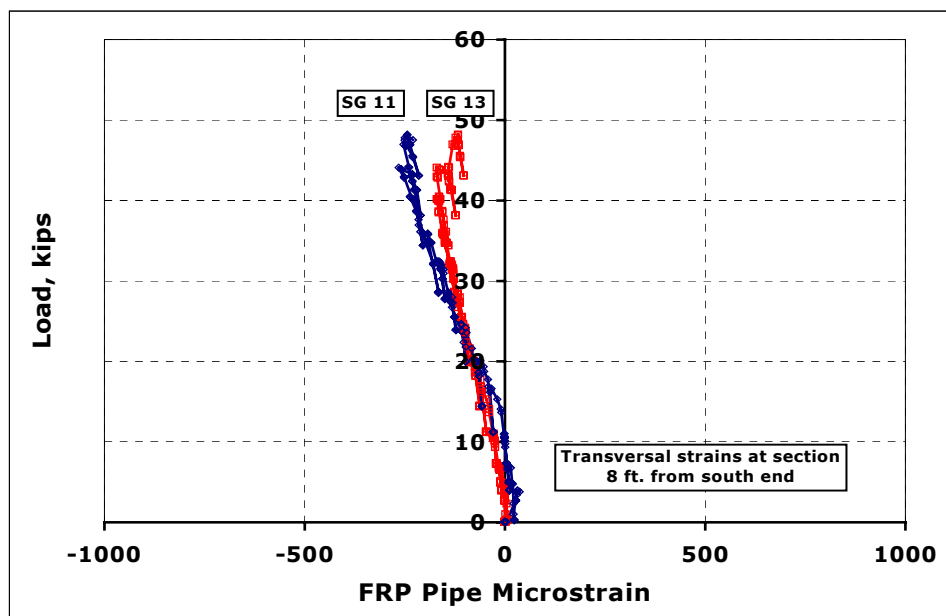


**Figure 8.28.** Transverse Strain Distribution at 8 ft. from South End.

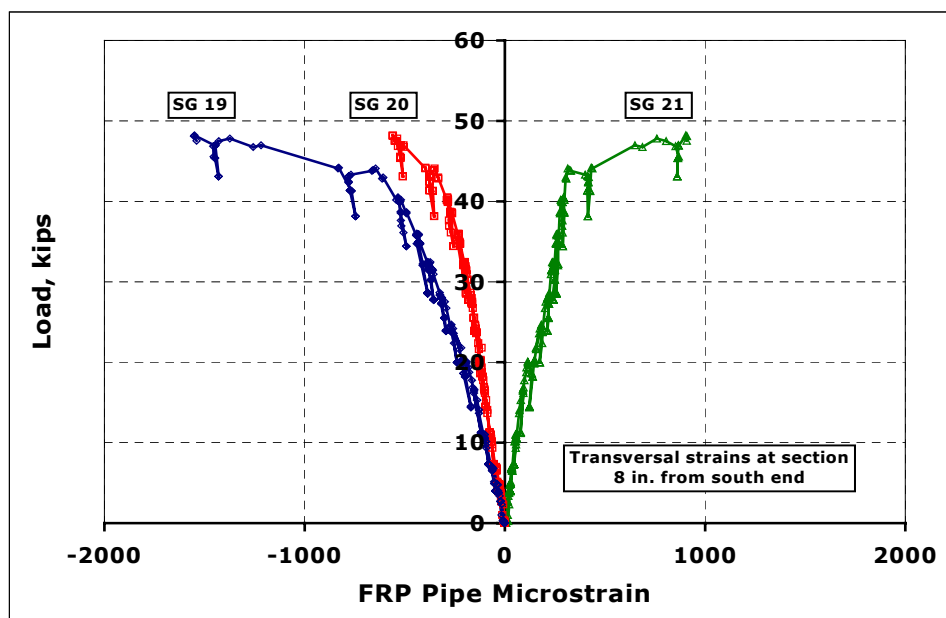


**Figure 8.29.** Transverse Strain Distribution at 8 in. from South End.



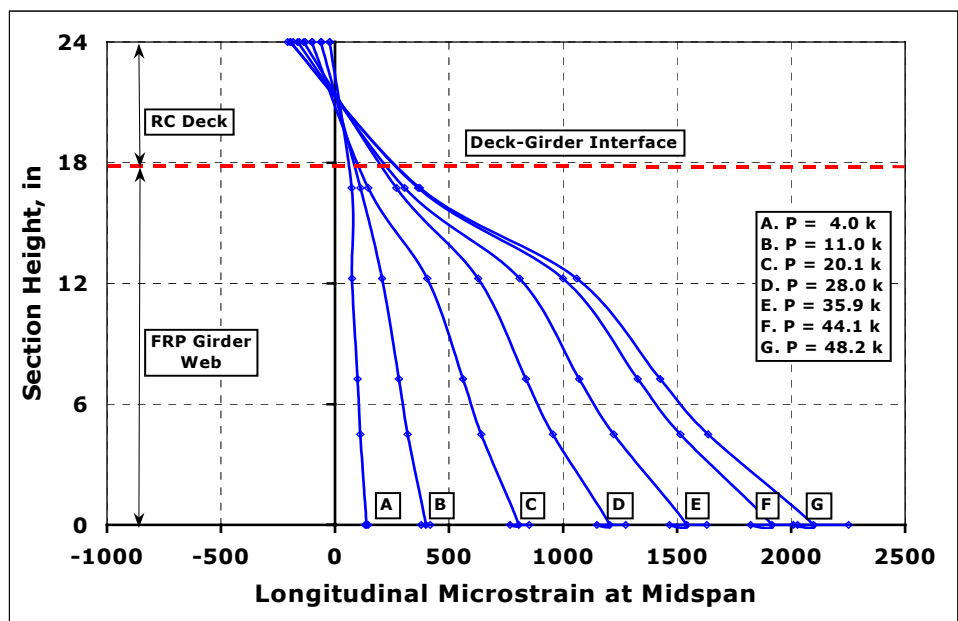


Figure 8.30. Longitudinal Strain vs. Section Height at Midspan.

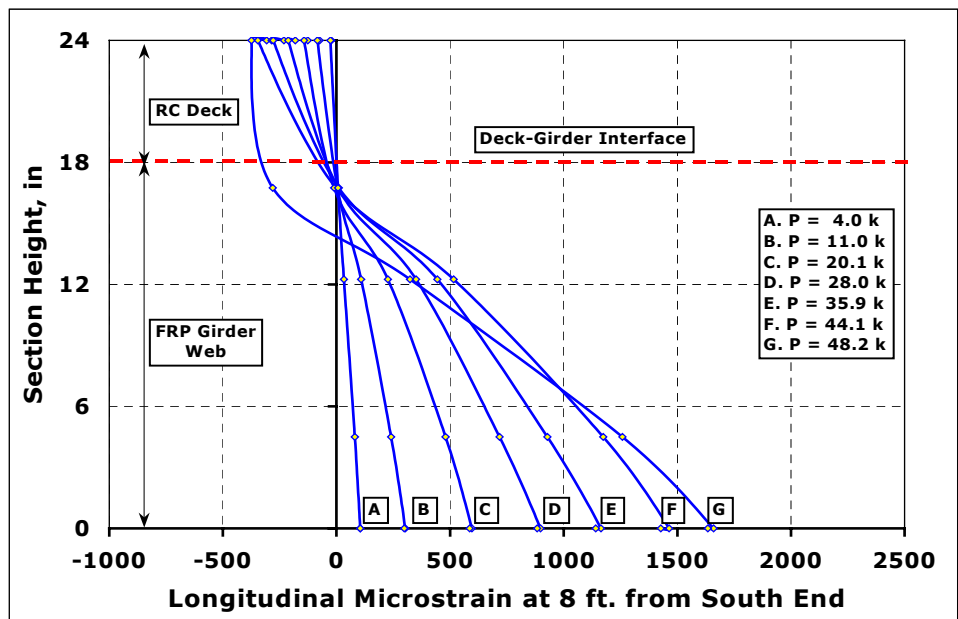
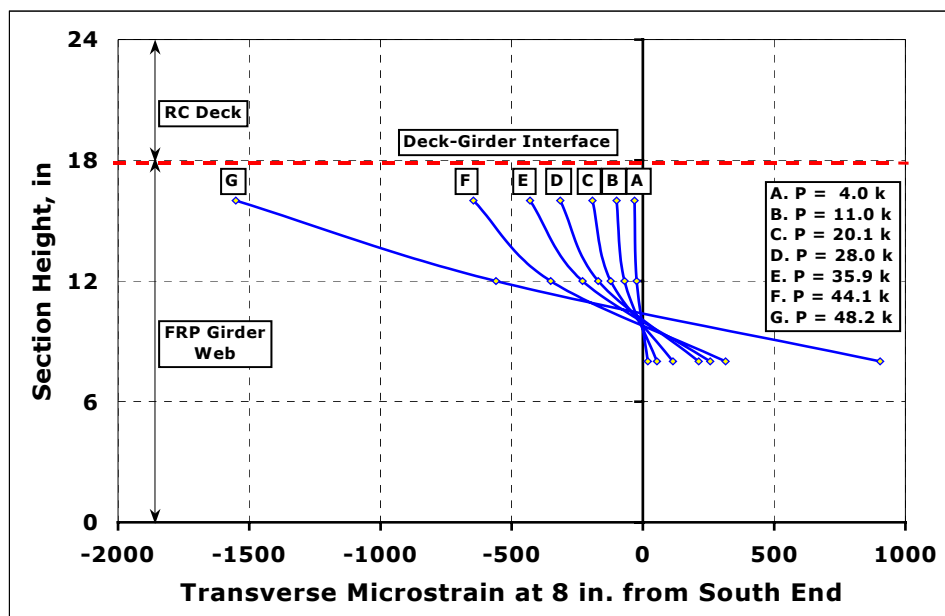


Figure 8.31. Longitudinal Strain vs. Section Height at 8 ft. from South End.



**Figure 8.32.** Transverse Strain vs. Section Height at 8 in. from South End.

An additional test was performed on two coupons taken from the web of the FRP girder. The purpose of this test was to investigate the behavior of the girder web under the bearing stress caused by the web connectors. The coupons were 2 ft. long and 6 in. wide. Coupon 1 had a linearly varying thickness with an average of  $\frac{3}{4}$  in. This variation in thickness was observed along the web wall of the element. Coupon 2 had a more uniform thickness of  $\frac{1}{2}$  in. Two  $\frac{7}{8}$  in. diameter holes, 1 ft. apart were symmetrically located about both the length and width as shown in Figure 8.33.

Steel plates and bolts were used to attach the coupons onto the testing machine. The steel plates sandwiched the coupons, and an A325,  $\frac{7}{8}$  in. diameter bolt held both the plates and the coupon together. The bolts were hand tight to prevent friction from reducing the bearing stresses on the holes. The steel plates then were clamped into the testing machine. Tensile load was applied along the longitudinal axis of the specimen as shown in Figure 8.34.

Coupon 1 failed when it was transversely torn apart at one of the bolt holes as shown in Figure 8.35. Coupon 2 failed by bearing at one of the bolt holes; the bolt hole elongated as shown Figure 8.36. Both coupons had a sudden failure.

Bolt hole elongation was measured by subtracting the elongation of the plate from the relative displacement of both bolts. Tensile stress vs. longitudinal bolt hole elongation (sum of both holes) curves for both coupons are shown in Figure 8.37, the response was linear as it is seen. Coupon 1 sustained a maximum tensile stress of 6.2 ksi, and a bearing stress around the holes of 36.3 ksi; similarly, Coupon 2 sustained a maximum tensile stress of 7.1 ksi, and a bearing stress around the holes of 41.7 ksi.

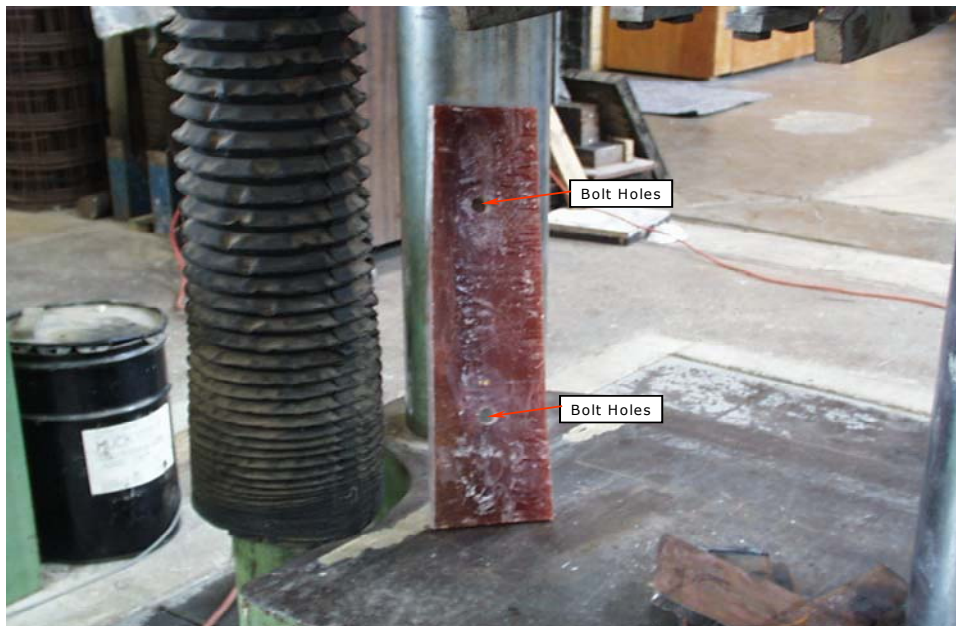


**Figure 8.33.** Coupon 1.

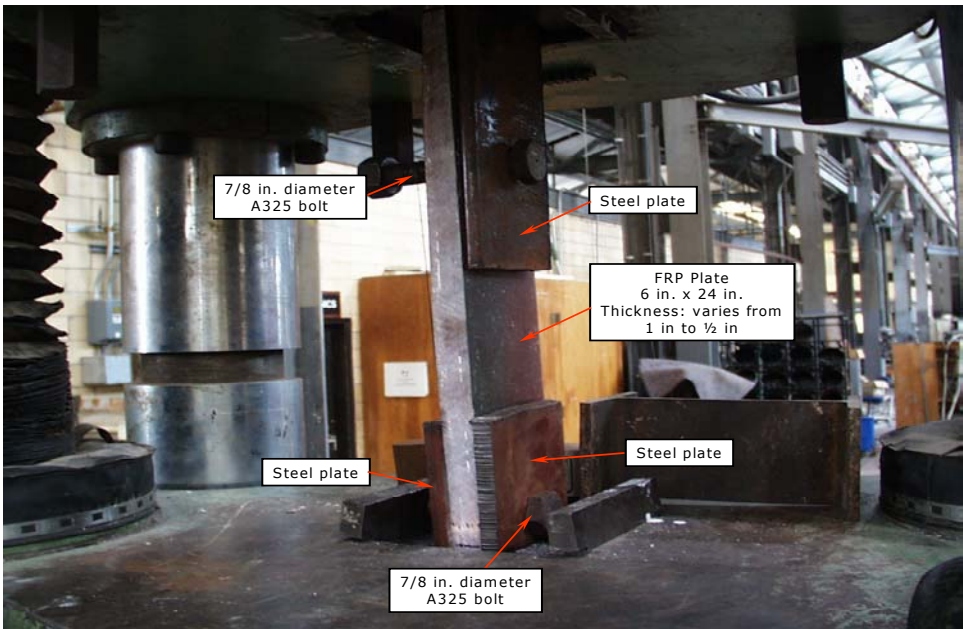


**Figure 8.34.** Coupon 1 during testing.



**Figure 8.35.** Coupon 1 after testing.



Figure 8.36. Coupon 2 after testing.

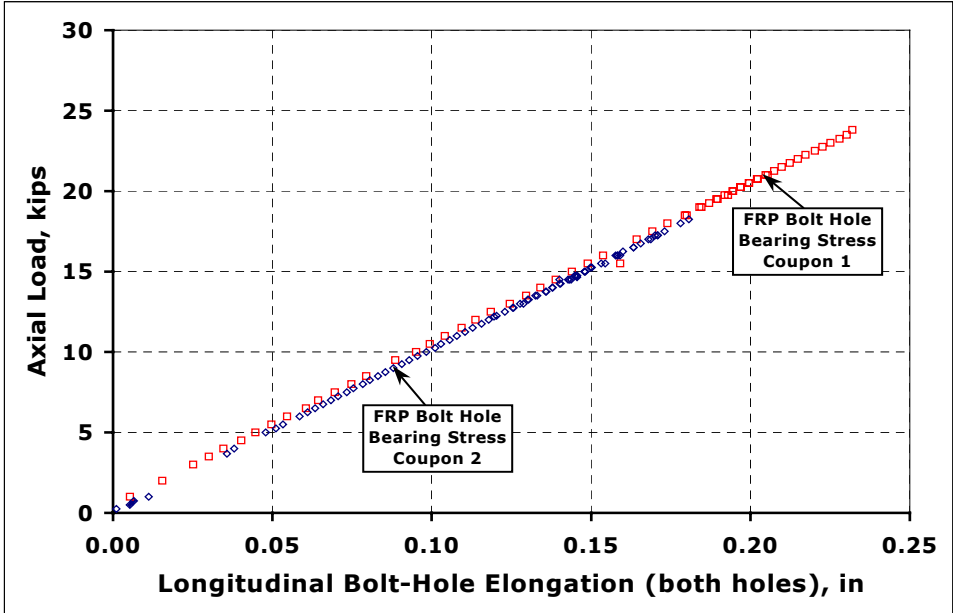


Figure 8.37. Tensile Stress – Bolt Hole Elongation (Sum of both holes).

## **8.8 Significant Findings**

Based on the experimental results, a structural design based on a contact molded FRP section is feasible for short span bridge construction. The structural design was appropriate.

Integrally molded shear connectors were able to transfer shear but a greater number is required.

It is possible to prevent lifting of the RC deck from the FRP girder by using the web connectors. However, for these connectors to perform properly it is necessary to tie them to the steel reinforcement in the RC deck. The use of stirrups is recommended.

The geometry of the FRP girder was appropriate. The thickness of the bottom flange could have been reduced.

The web stiffeners at each end worked satisfactorily. In a field application this stiffener could be made of concrete and be made an integral part of the RC deck.

## **8.9 Summary**

This chapter covered the experimental work on specimen TK1. Specimen TK1 was designed for an AASHTO HS20 loading, and had as structural components a contact molded FRP girder, and an RC deck both working under composite action.

Composite action was fundamental to ensure an appropriate behavior of the structural system. To achieve a proper response the system relies entirely on shear connectors distributed along the top flanges as integral part

of them. Additional web connectors in the form of steel rebars are also needed to ensure that the RC deck and the FRP girder remain together helping composite action to develop accordingly.

The most vulnerable zone of the system is located at the deck-girder interface, since it is there where the maximum shear demand takes place. Based on the test results, it is noted that the failure was progressive, and did not take place suddenly. In fact from Figures 8.14 and 8.15, it is inferred that failure gradually began to develop at about 25% of the maximum load.

Also it should be noted that as with the previous specimens, after failure the specimen still was able to sustain additional load; and stability of the structural system was not an issue.

The structural system in Specimen TK1 showed great potential as a method of dealing with the FRP girder's low elastic modulus. It is expected that an adequate shear capacity will significantly improve the overall performance of this structural system. The resulting structural system then can become the basis for an actual field application.

## **Chapter 9**

### **Tied Arch Fabricated From FRP Pipes**

#### **9.1 Overview**

This chapter describes specimen FGS12 and the experimental work performed on it. Specimen FGS12 consisted of an RC deck and two FRP tied arches FGS1 and FGS2. The glass reinforced pipes were standard off the shelf pipes used for oil industry applications; the resin was epoxy. RC deck rested as a simply supported deck on top of the two FRP arches. The behavior of the structural system is presented and discussed.

#### **9.2 General Description**

Specimens FGS1 and FGS2, were fabricated with FRP pipes manufactured at Fiber Glass Systems, San Antonio, Texas. This company specializes in the fabrication of fiberglass pipes, which have wide application in the oil industry. These pipes use aliphatic amine cured epoxy resin, and premium twistless fiberglass reinforcement. The fabrication process used on these pipes is filament wound. Representative pipes as delivered to the FSEL are shown in Figure 9.1.

The pipes have a nominal length of 30 ft., with diameter sizes ranging from 1 ½ in. through 9 5/8 in., and a thickness ranging from 1/16 in. through 11/16 in. Each pipe has both ends threaded, so that threaded coupling can be used to connect several pipes together to fit a desired length. These pipes are manufactured to withstand temperatures up to 200°F. In addition, they perform extremely well in corrosion prone environments caused by carbon dioxide, hydrogen sulphide and salt water (Star Fiber Glass Systems, 1997).





**Figure 9.1.** FRP Pipes (Downhole and Line types).

Fiber Glass Systems manufactures the following types of pipes, API design line pipe, standard design line pipe, and downhole tubing (Star Fiber Glass Systems, 1997). For this project only the standard design line pipe and downhole tubing types were used.

The term "line pipe" means that the primary use of the pipe is for surface lines that convey oil from the well head to the storage tanks in an oil field, or convey injection chemicals from tanks to the well head. These pipes can be above ground or buried. The primary load on this type of pipe is flexural (spanning between supports) and internal pressure. Fiber reinforcement for these pipes is filament wound at an angle to the axis of the pipe. On the other hand the primary use of "downhole tubing" is as the stringer in an oil well or injection well. The primary loading in this case is axial tension and high internal or external pressure. Fiber reinforcement consists of axial fibers and filament wound fibers, which are wound at a large angle relative to the axis of the pipe. Downhole tubing is used in highly

corrosion applications. Examples are oil wells in sour crude oil fields, and for secondary and tertiary recovery.

Using these FRP pipes two specimens similar to the one shown in Figure 9.2 were assembled. The 6 in. diameter, standard design line pipes were used for the members in the arch, each with an average length of 6 ft., and  $\frac{5}{16}$  in. thickness. The vertical members were also standard design line pipes, with a 4  $\frac{1}{4}$  in. diameter,  $\frac{1}{4}$  in. thickness, and various lengths. The bottom chords were made out of downhole tubing pipes, with a 4  $\frac{1}{4}$  in. diameter,  $\frac{1}{4}$  in. thickness, and 30 ft. length.

The design of the arches was carried out by fogeometry of the arches was determined such the loading on the structural system be carried app

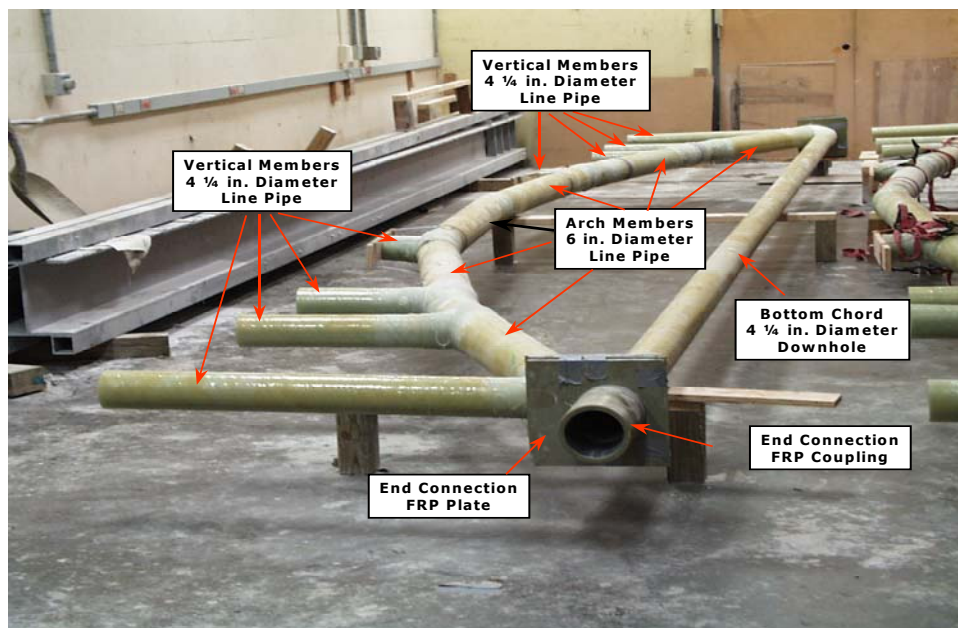


**Figure 9.2.** Finished Assembled Arch.

Except as noted otherwise the pipes were cut to length and/or modified and then assembled at the University of Texas. Three types of connections, which are discussed below were used:

- type 1, was primarily used to join the components in the arch,
- type 2, was used to join the vertical members onto the arch, and,
- type 3, was used to join the bottom chord to the arch with the vertical members already attached to it.

See Figures 9.2 and 9.3 for details of the arch.

Connection type 1 is sketched in Figure 9.4. The fitting was machined from a ½ in. thickness pipe by Fiber Glass Systems; accordingly, the fit-up of these connections was good. It used a "black paste" specially designed for this kind of joining. The name is related to the final appearance of the mix, which is rather a deep dark color. The paste used 40% epoxy, and 60% of solids (ceramic spheres and graphite) by weight. In addition, amine was also added in an amount of 13.5 pph (parts per hundred). Before applying the paste, the exterior coating on the surfaces was ground off and cleaned thoroughly. After the mix was applied all the pieces were fitted in place and left for curing. The process of curing took some time, and external heating was needed for proper cure. Heating was applied by means of a heating sheet, which was wrapped around each connection. Figure 9.5 shows the components for this connection, and Figure 9.6 shows an assembled connection prior to wrapping. After the joint had properly cured, it was further reinforced by means of an external FRP wrapping applied a week later. The connection is designed to resist local moments in the arch caused by the concentrated loads from the vertical members.

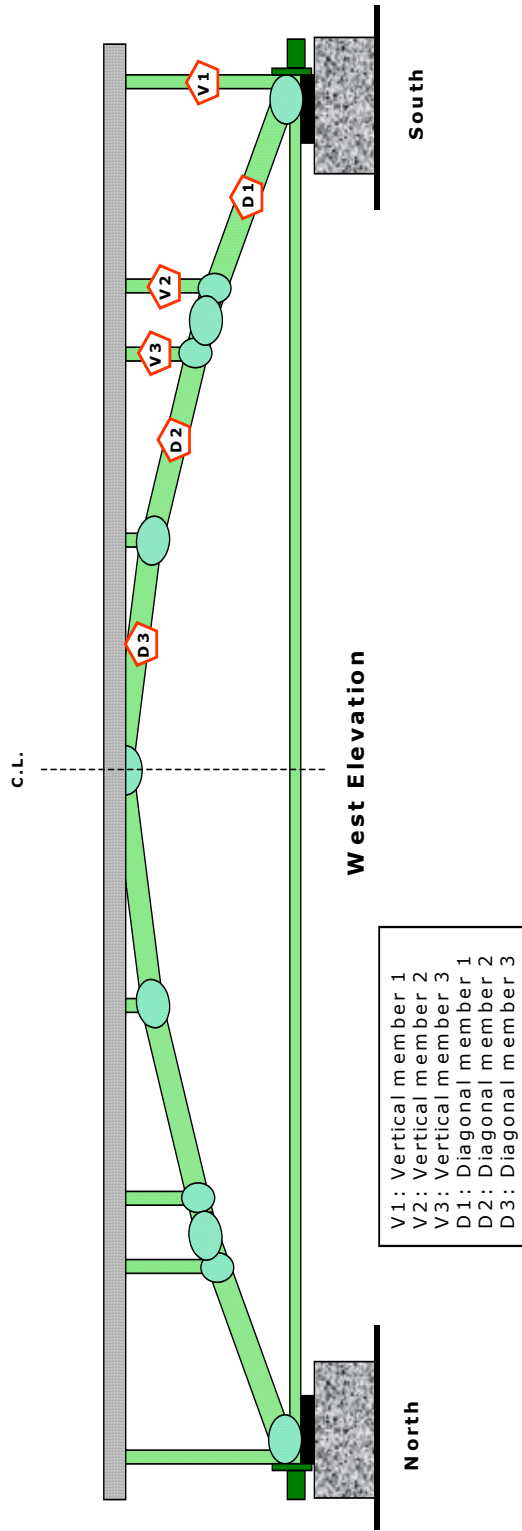
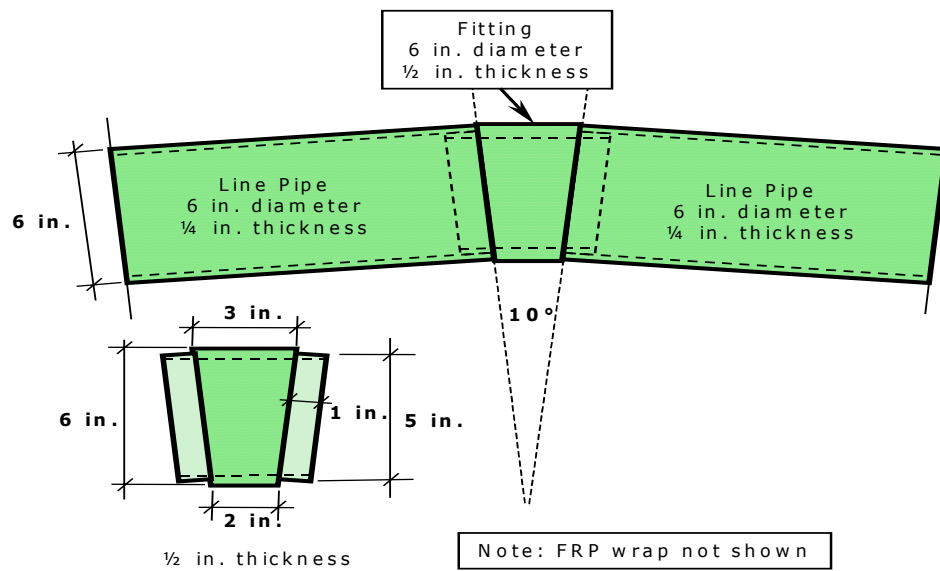


**Figure 9.3.** West View of Specimen FGS12.



**Fitting Detail**

**Figure 9.4.** Connection Type 1 Detail.

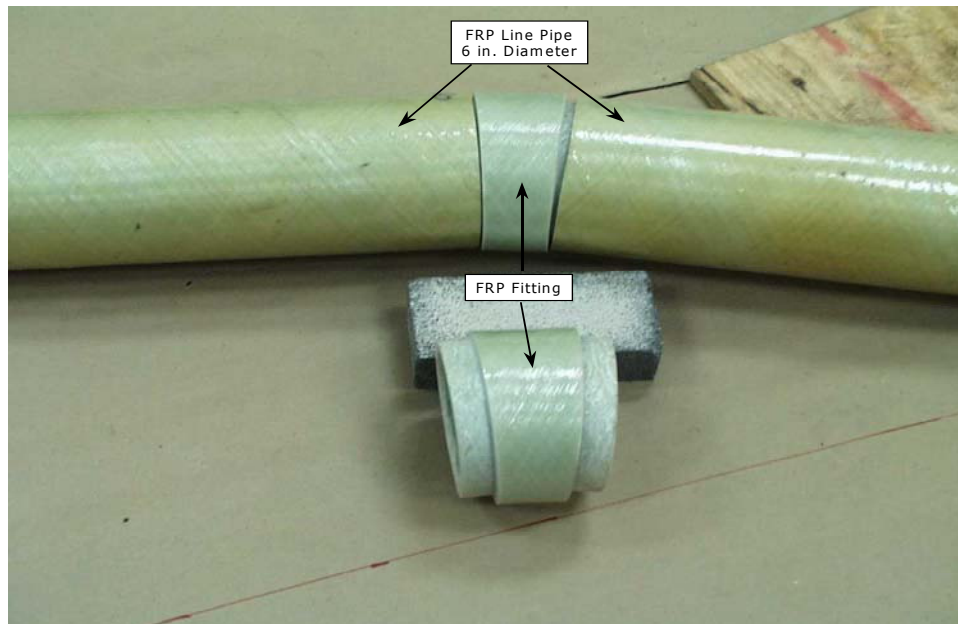


**Figure 9.5.** Connection Type 1 Detail.



**Figure 9.6.** Assembled Connection Type 1 Prior to Final Wrap.

Connection type 2 is sketched in Figure 9.7. As standard practice, the exterior coating of the surfaces of the pipes being joined were ground off and thoroughly cleaned. A joint prepared in this way is shown in Figure 9.8. The members being joined were fitted together and the wrapping applied. The wrap consisted of fiberglass fabric in pieces of 6 in. width and 3 ft. length, in average 4 to 5 pieces were used at each connection. The mix was pure epoxy plus 13.5 pph of amine. The fabric was thoroughly soaked in the mix as shown in Figure 9.9. The wet fabric then was wrapped around the members being connected. The process of curing took two days at room temperature. The same wrapping was used as an additional reinforcement on connection type 1. Figure 9.10 shows the finished type 2 connection.

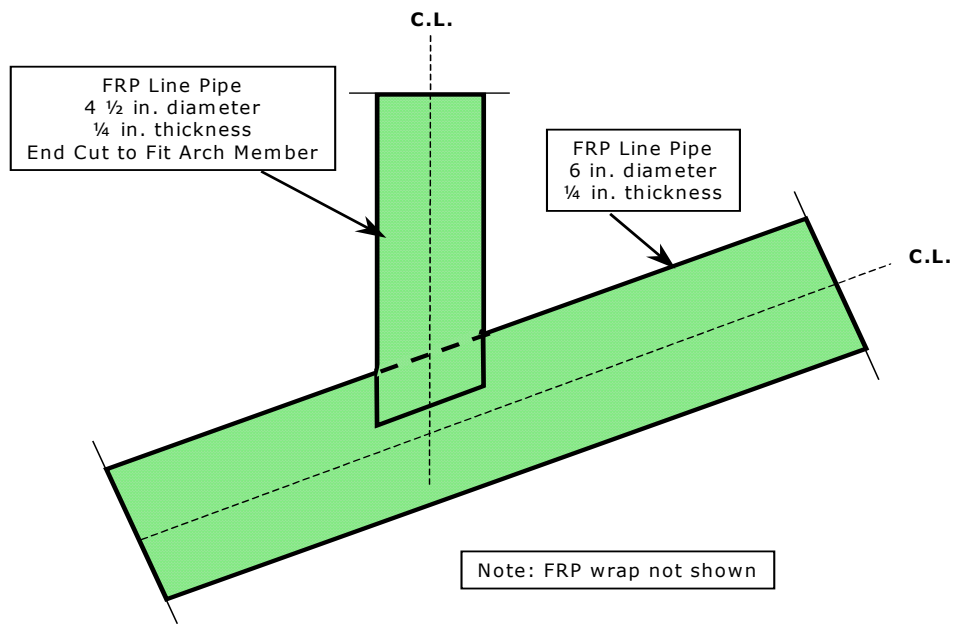


**Figure 9.7.** Schematic of Connection Type 2.

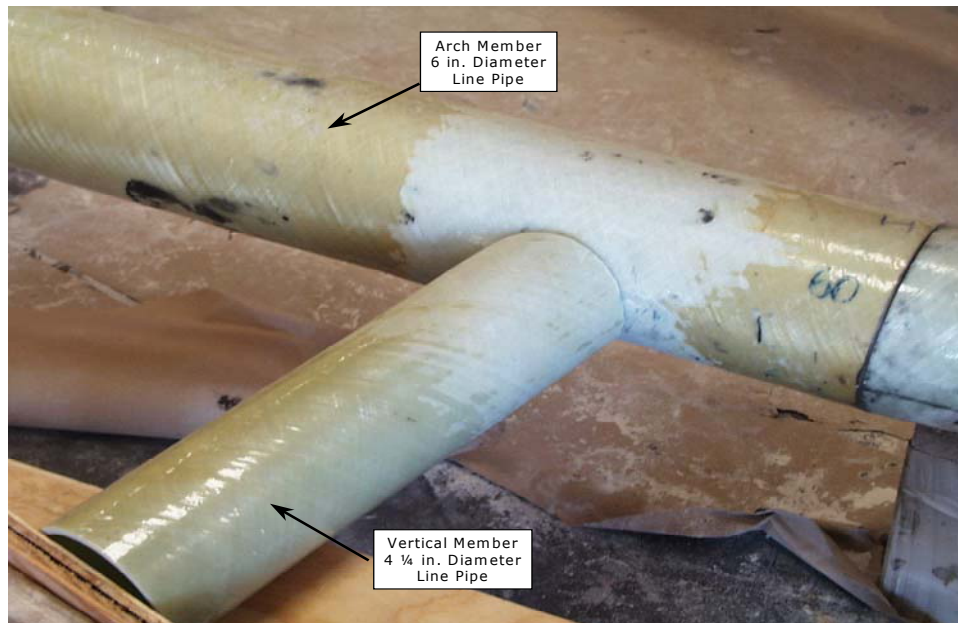


**Figure 9.8.** Detail of Connection Type 2 before Wrapping.



**Figure 9.9.** Wetting Fiberglass Fabric for Connection Type 2.



**Figure 9.10** Finished Connection Type 2.



Connection type 3 is sketched in Figure 9.11. This connection was used at the ends of each arch. Its main function was to hold all the arch components together hence its behavior was crucial to the overall integrity of the structural system. The connection joined the bottom chord, to the arch. In addition four FRP square plates 12 in. x 12 in. x 1/2 in. were bonded together and placed at each end. The plates bore against the threaded end couplings, which were attached to each end of the bottom chord as shown in Figures 9.11 and 9.12. The surfaces of the pipes at the connection were thoroughly cleaned after grinding off the exterior coating as seen in Figure 9.12. A similar mix as used in connection type 2 was also used for this type of connection. The components of the connection were fitted together and then the wrapping was applied. All the connections were handled following the recommendations in Fiber Glass Systems, Installation and Application Practices (1996). Figure 9.13 shows the finished connection, and Figure 9.14 shows a finished tied arch.

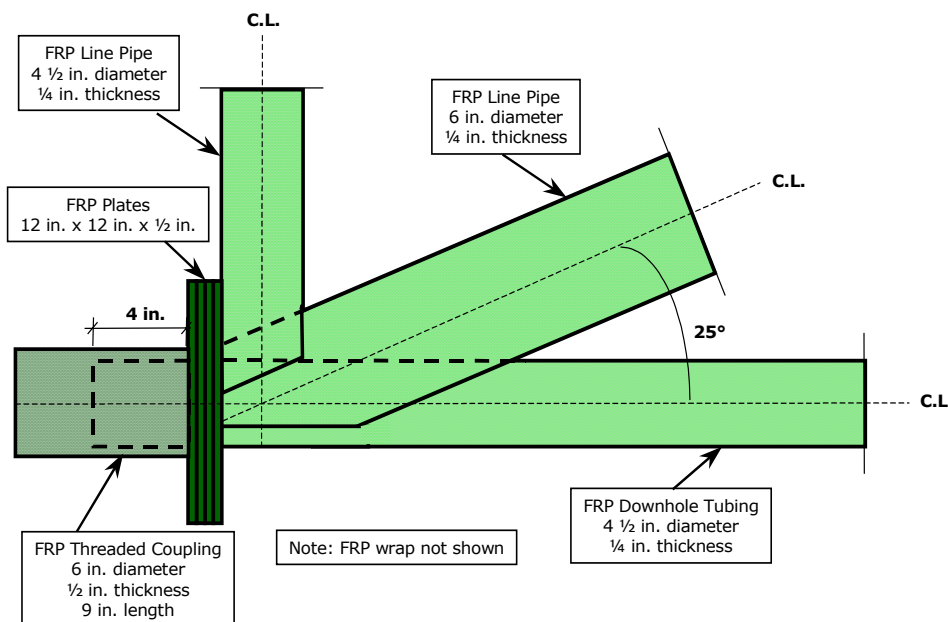


**Figure 9.11.** Schematic of Connection Type 3.

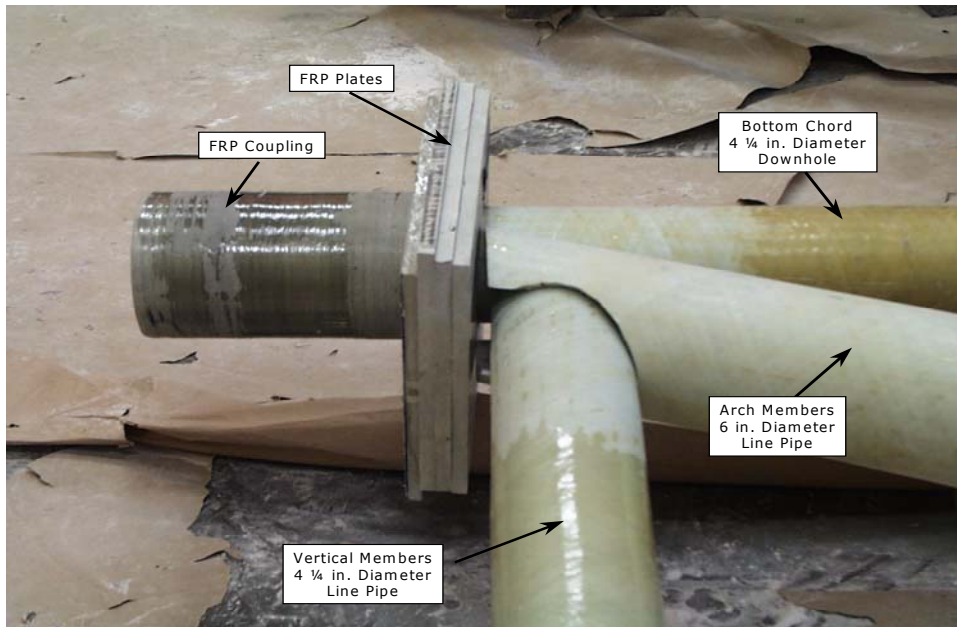


**Figure 9.12.** Connection Type 3, Before Wrapping.



**Figure 9.13.** Finished Connection Type 3.



**Figure 9.14.** Finished Arch.

Once both arches were finished, they were lifted onto the test area as shown in Figure 9.15. Both ends of the arches were supported on a  $\frac{1}{2}$  in. thick elastomeric bearing sitting on the bottom half of a 6 in. diameter FRP pipe, which in turn rested on an elastomeric bearing. Details are shown in Figure 9.16. The arches were placed 30 in. apart center to center. Figure 9.17 shows part of the formwork used for casting the RC deck. The forms were removed 3 weeks after casting. In addition, the arches were tied at each end, to prevent them from moving relative to one another. Details are shown in Figure 9.18. The shoring at midspan was left in place until just prior to testing.

The RC deck had a  $5 \frac{2}{3}$  ft. width, 6 in. thickness, and a length of 30 ft. Reinforcement was provided by # 4 Grade 60 rebars, which were placed at 12 in. spacing longitudinally, and 18 in. It was simply supported on top of the vertical members. No special connections were considered, other than the vertical members running  $\frac{1}{2}$  in. into the deck. An FRP plate was placed at the

top of each vertical member. See Figure 9.19. Figure 9.20 shows the specimen after all formwork was removed. The wood boards shown in Figure 9.19 were used to keep the end of the vertical pipes in place during cast of the RC deck. They were left in place permanently, after the forms were removed. The specimen clear span was 28.5 ft.

### 9.3 Material Properties

The materials used in the fabrication of the FRP pipes were aliphatic amine cured epoxy resin, and premium twistless E-Glass reinforcement. Actual material properties were found by testing samples from both components: the RC deck and the FRP pipes.

#### 9.3.1 FRP Pipes

Compression tests on short lengths of the FRP pipes were performed. The lengths of these pipes were 12 in. The average thickness for both the 6 1/8 in. and 4 1/4 in diameter samples was 1/4 in.



**Figure 9.15.** Arch Being Carried to Test Area.

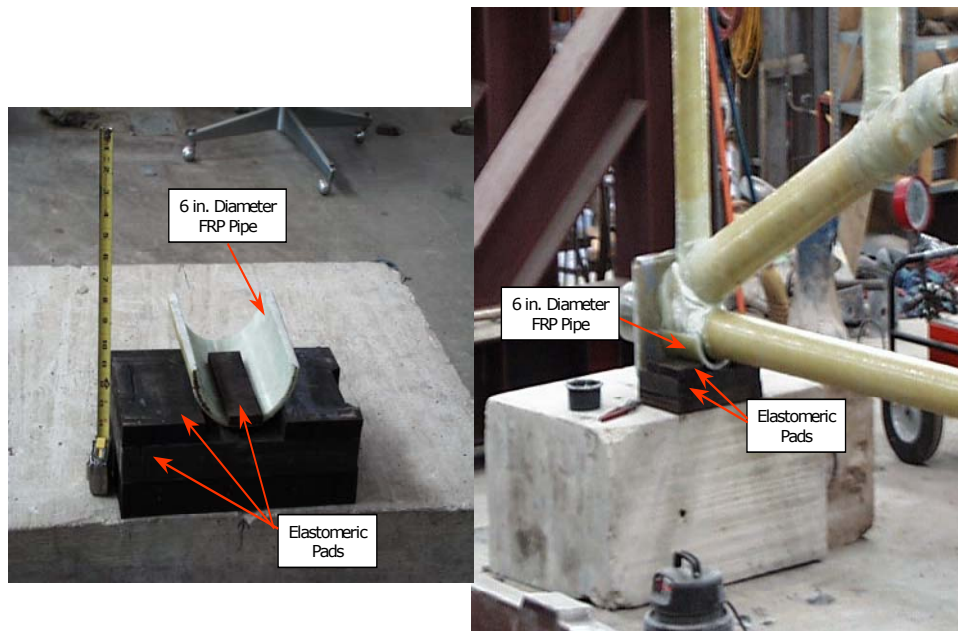


**Figure 9.16.** Support Detail Before and After Placing of Arch.



**Figure 9.17.** Arches in Place Prior to Completing Formwork for RC Deck.

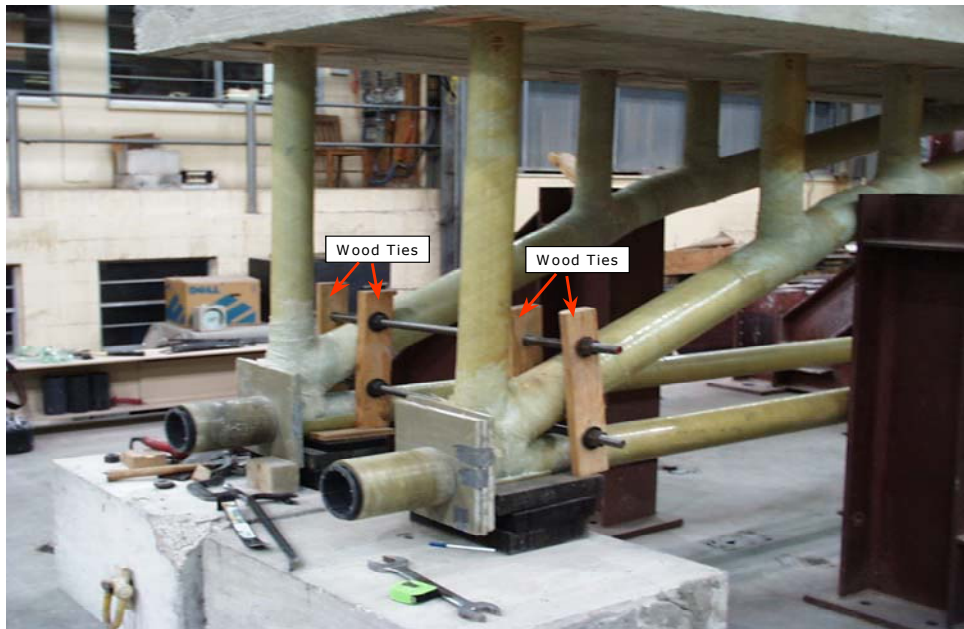


**Figure 9.18.** South End View.

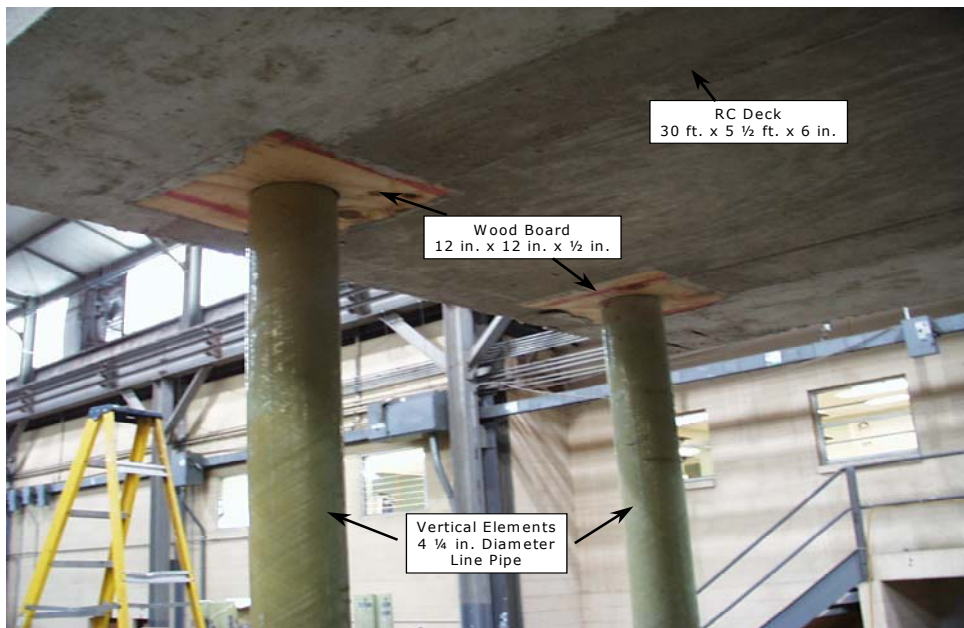


**Figure 9.19.** RC Deck Simply Supported on Vertical FRP Members.



**Figure 9.20.** Specimen After Formwork Removal.

Six strain gages (SG), paired on diametrically opposed areas at midheight were used to monitor the strains during testing, two strain gages were oriented parallel to the loading direction, two transverse to the loading, and the last two oriented at 45°. See Figure 9.21.

Both these samples were subjected to axially applied compressive stresses as shown in Figure 9.21. Each sample had thermoplastic caps placed on both ends to prevent early damage or delamination. These caps deformed as the load was increased in such a way that they provided some level of restraint to the edge of the pipes, hence preventing early delamination, and acted to distribute the load causing a uniform stress distribution at midheight where the strains (stresses) were measured.

The stress-strain curves for both specimens are shown in Figures 9.22 and 9.23 respectively. From these tests the maximum compressive stress for both samples is set to  $\sigma_{\text{cmax}} = 14$  ksi. The effective axial initial elastic

modulus is calculated as  $E_{FRP} = 2745$  ksi for the 4 ¼ in. diameter pipes (vertical members), and  $E_{FRP} = 2500$  ksi for the 6 ¼ in. diameter pipes (arch members). The Poisson ratio for these two specimens were determined as  $\nu = 0.38$ , and  $\nu = 0.42$  respectively.

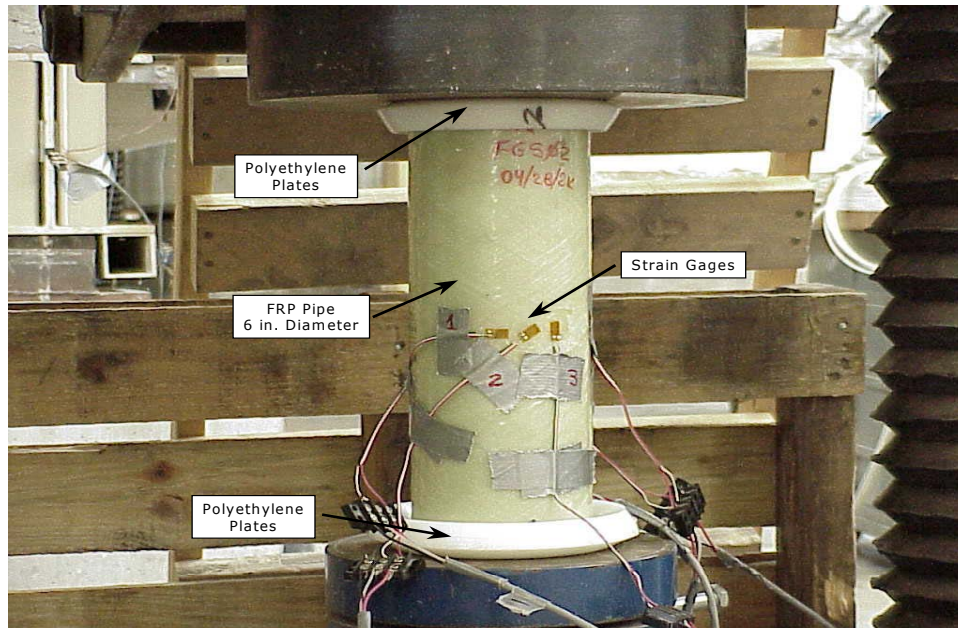


**Figure 9.21.** 6 in. Diameter Sample Under Compressive Load.

The values for the stresses were determined from the maximum load applied onto the specimen. The specimen did not actually crush or fail, and although no visible damage was observed it was not possible to load it any further. This was probably because of yield strength of the thermoplastic caps in bearing had been reached.

Star Fiber Glass Systems, 1997, lists a nominal coefficient of thermal expansion of  $8.7 \times 10^{-6}$  in/in/°F, an axial and hoop elastic modulus of 2000 ksi and 3300 ksi respectively, and a Poisson ratio of 0.39 for the line pipes (Star Fiber Glass Systems, 1997). This is the kind of pipe used for the arch and vertical members. As is to be expected, the measured value of elastic



modulus is greater than the “book” value. For this type of product, the latter value is typically the “guaranteed minimum”. The actual and nominal Poisson ratios are in agreement.

For the downhole pipes used to tie the arch, the fabricator catalogue lists a nominal coefficient of thermal expansion of  $8.7 \times 10^{-6}$  in/in/°F, an axial and hoop elastic modulus of 3000 ksi and 4500 ksi respectively, and a Poisson ratio of 0.39 (Star Fiber Glass Systems, 1997).

### 9.3.2 RC Deck

Concrete cylinder samples taking during casting of the RC deck were tested at 3, 7, 14, 21, and 28 days, to determine the compressive strength of the concrete. The nominal 28 days strength was 5000 psi, whereas the actual compressive strength from testing was 5150 psi. The corresponding elastic modulus using the ACI formula for normal weight concrete was  $E_{\text{concrete}} = 4093$  ksi.

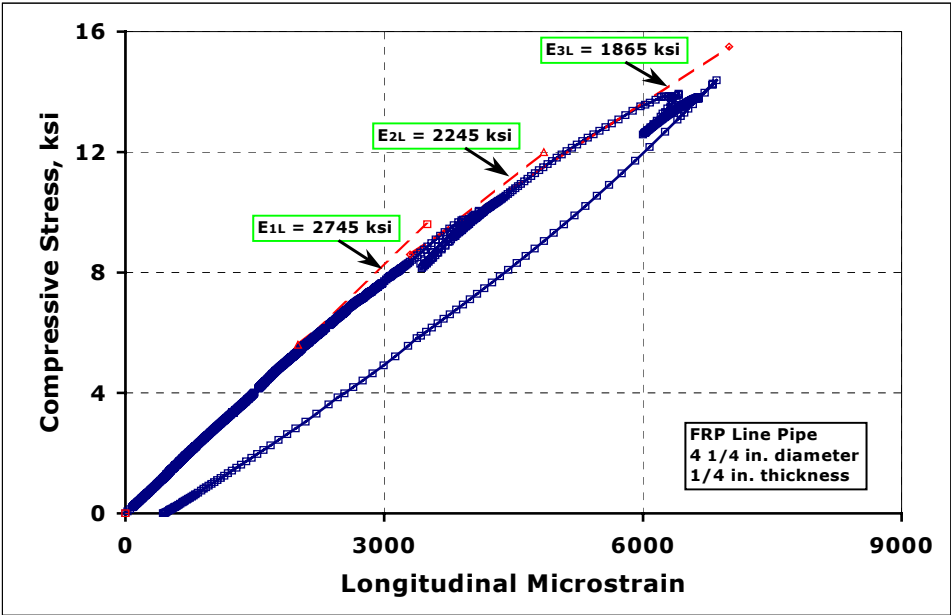
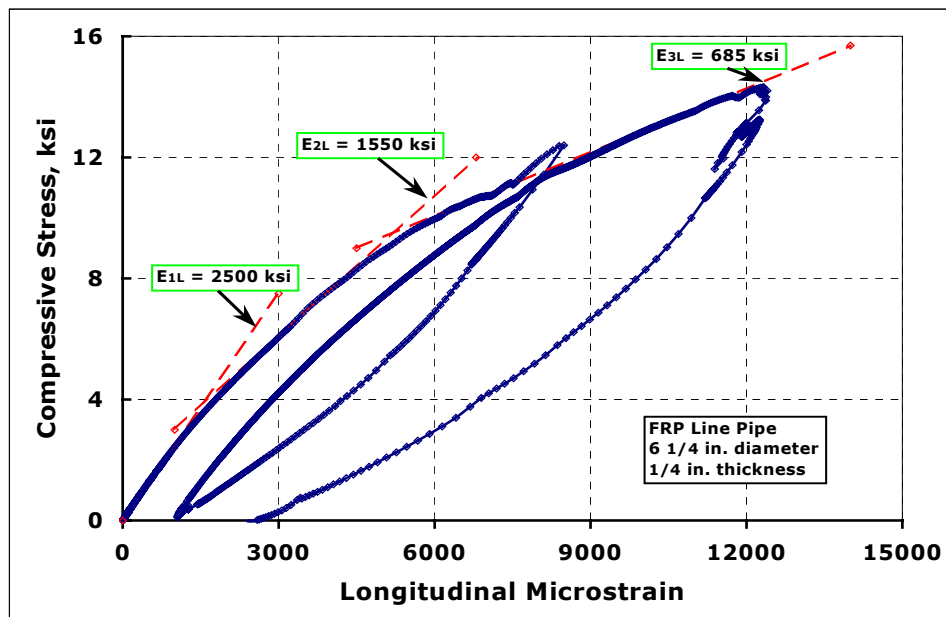


Figure 9.22. 4 ¼ in. Diameter Pipe (Vertical Members) Stress-Strain Curve.



**Figure 9.23.** 6 ¼ in. Diameter Pipe (Arch Members) Stress-Strain Curve.

## 9.4 Structural Analysis and Design

Specimen FGS12 was designed for AASHTO HS20 loading. The resulting structural system consisted of an FRP girder and an RC deck; the RC deck simply rested on top of the FRP arches. The maximum bending moments developed in the structure where  $M_{max} = 91.6$  k-ft, at the girder midspan.

With this load a linear elastic structural analysis was carried out to determine the stresses developed in the different components of the structural system. The software used was LEAF (1996). The maximum stresses developed were below the capacity of each component, that is, the RC deck and the FRP pipes.

## 9.5 Instrumentation

Instrumentation of the specimen began immediately after the formwork was removed. Since the arches were virtually symmetric, only one half (south half) of each arch was instrumented. Details of the SG, LP, and LC were presented in detail in Chapter 3.

All strain gages (SG) placed on the pipes were aligned axially. The location of the SG was as follows: (See Figures 9.24 and 9.25)

- Each 6 ft. long piece had two SG diametrically opposed at midplane, except for SG7 and SG8, which were placed on the bottom.
- The vertical members also had two SG on opposite sides of the pipe, except for the small piece of pipe at the first joint from midspan.
- The bottom tying chords had three SG, one on each side, and one on the top. All SG were placed at the mid-length of the member.
- Additional SG were placed on the concrete deck, bonded to the top surface, at distances 4, 8 and 15 ft. from the South end.

The location of the linear pots (LP) was as follows: (See Figures 9.24 and 9.25)

- Center of RC deck.
- Center of a bar connecting the center of the two bottom ties so as to obtain the average vertical deflection of the ties at midspan.
- In a similar way additional LP were placed near to each support to measure the elastomeric bearings deflections, and at the two outer connections on the arches.

Load was measured with a load cell (LC) having a capacity of 50 kips.

## 9.6 Loading

Once the instrumentation was finished, standard safety devices as described in Chapter 3 were placed on each side of the specimen to prevent them from turning over. The safety devices were placed close to both ends as shown in Figure 9.26. It should be emphasized that at no time during testing were these frames in contact with the specimen. They were designed to stop any significant lateral movement of the structural system should a stability failure occur.

Load was applied to the specimen through two loads points from an 8 ft. long spreader beam placed on top of the deck midway between the arches. Thus the specimen was loaded in four point bending. The effective distance between loading points was 7 ft. Elastomeric bearings were used under the loading points. The loading frame is shown in Figure 9.27, and the specimen ready for testing is shown in Figure 9.28.

The load was gradually applied to the spreader beam in increments of 3 kips. Since AE data was being collected, for each increment of load a loading–unloading cycle was performed, with a waiting period in between increments. For instance, the specimen was initially loaded up to 4 kips total load, then unloaded to 1 kip, next it was loaded to 7 kips, and then unloaded to 4 kips and so forth. See Figure 9.29 for details on the load schedule.

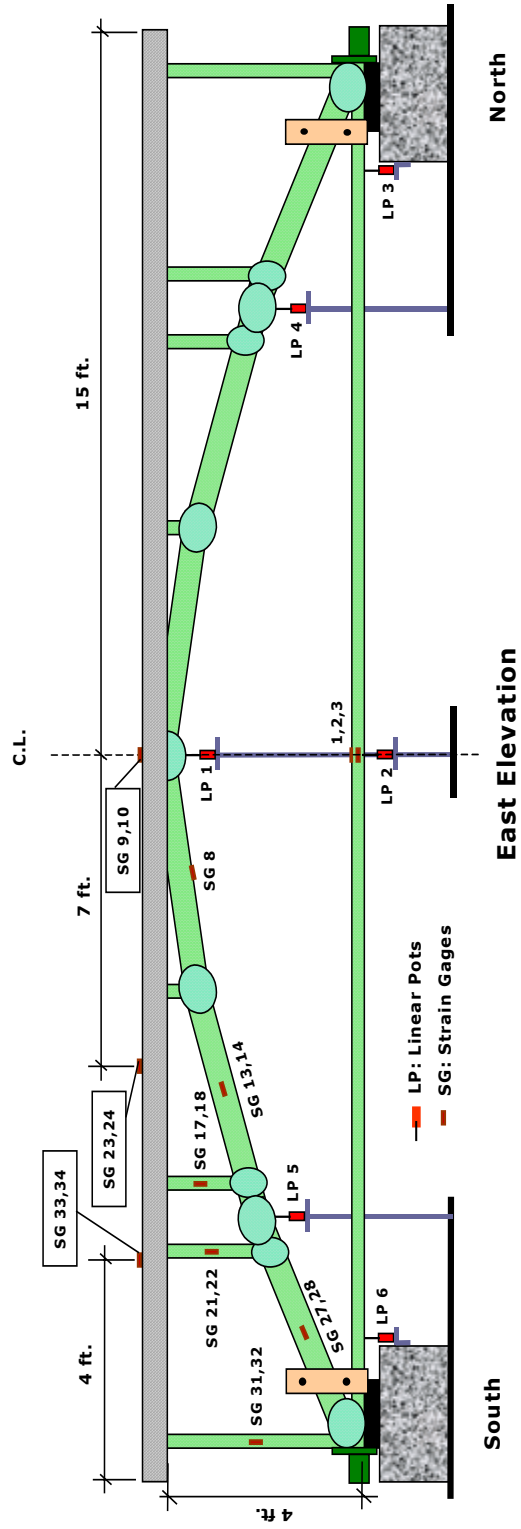


Figure 9.24. Specimen FGS12, Strain Gages and Linear Pots.

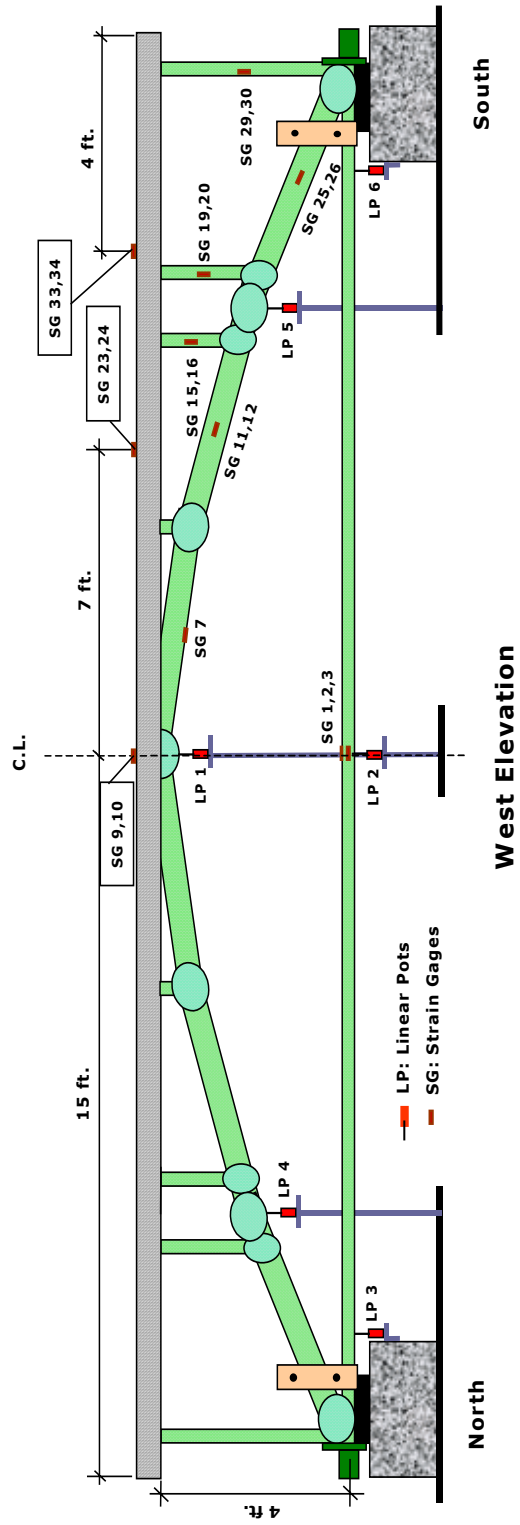
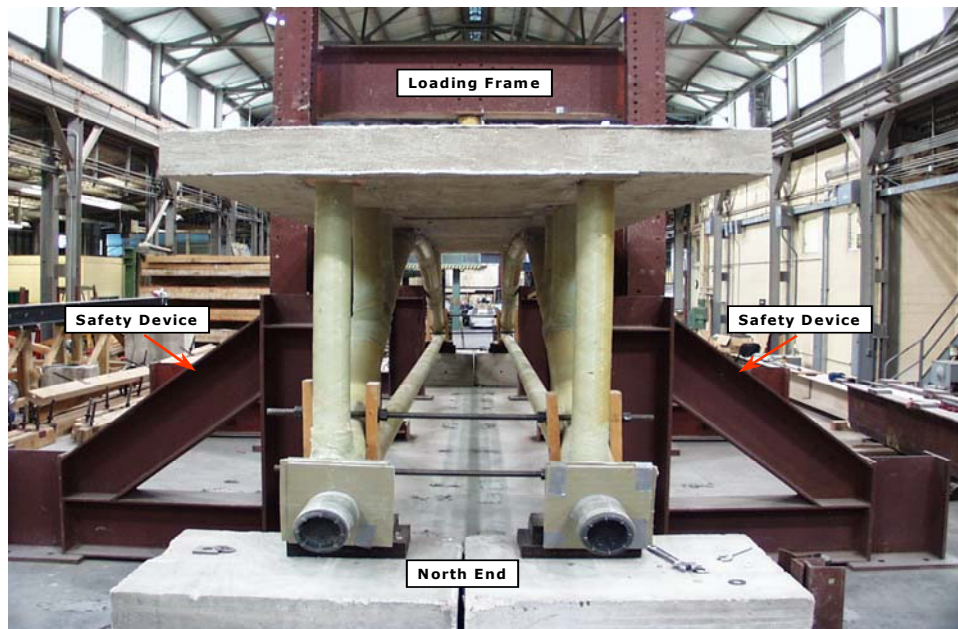


Figure 9.25. Specimen FGS12, Strain Gages and Linear Pots.



**Figure 9.26.** Safety Devices Against Lateral Collapse.

## 9.7 Results and Discussion

The specimen was subjected to a four point bending loading. The response of the specimen is shown in Figure 9.30. The system has an initial stiffness of 22.5 kips/in. This stiffness is valid for load under 20.0 kips. For loads greater than 20.0 kips but less than 30.0 kips, the tangent stiffness is 19.2 kips/in, a reduction of 15%. For loads greater than 30 kips the stiffness is 14.0 kips/in, an overall 38% stiffness reduction.

The experimental initial stiffness of 22.5 kips/in is larger than the analytically predicted stiffness of 20.0 kips/in. This difference can be explained as follows. First, connections type 1, 2, and 3, in both arches were considered as rigid in the analytical model, however, in the actual specimen the rotational stiffness provided by the FRP wrapping was not rigid enough to yield a perfectly rigid connection. This effect would tend to reduce the measured stiffness, especially for large values of load.

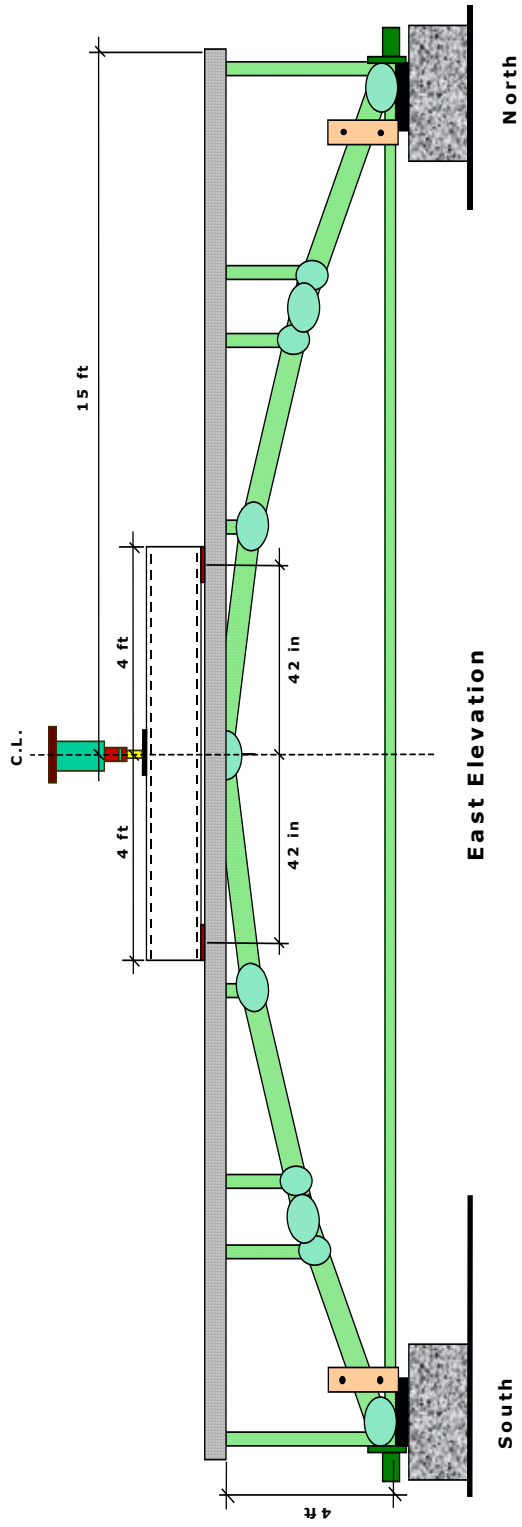


**Figure 9.27.** Loading Frame.





**Figure 9.28.** Loading Frame.

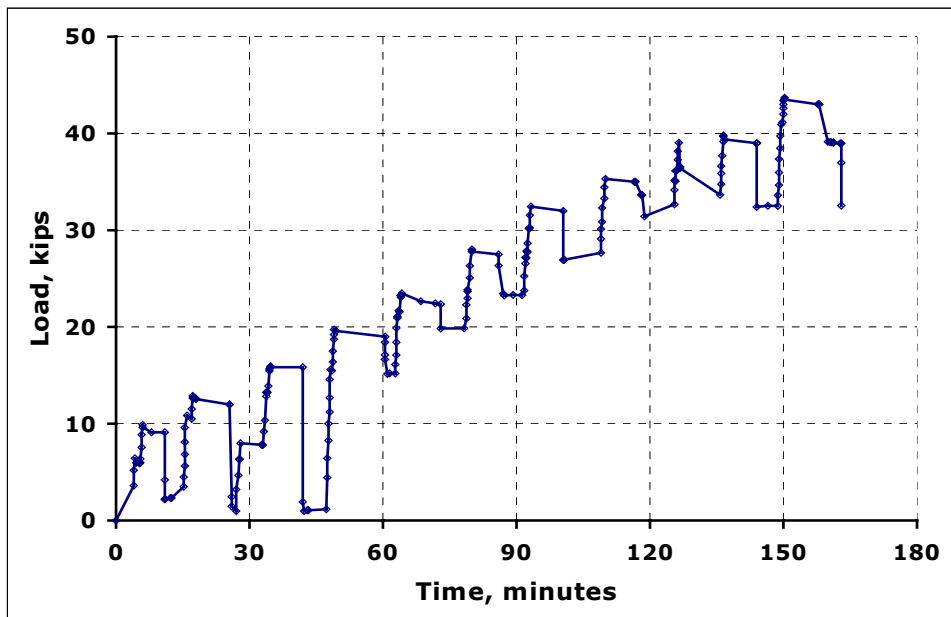


**Figure 9.29.** Load Schedule.

On the other hand and as discussed in Section 9.3.1 the measured axial stiffness of the line pipes were greater than the “book” values. For the analysis, the measured values were used. However, for the donwhole pipes the book value was used instead (experimental data was not available). Using a “book” value would tend to underestimate the actual stiffness of the structural system. This is reflected in Figure 9.30.

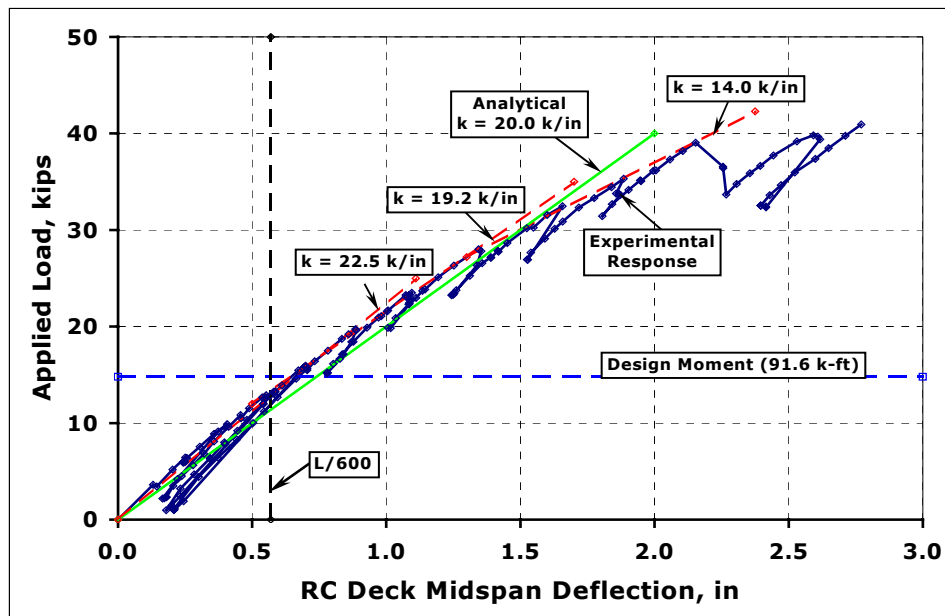


**Figure 9.30.** Load-Deflection Curve at Midspan.

The RC deck simply rested on the FRP vertical members, since no special links between the RC deck and the FRP pipes was provided there was the possibility of some vertical members slipping off the RC deck. This slippage also could be caused by fit-up problems during assemblage of the arches and construction of the structural system.

The type 3 connections discussed in Section 9.2 were the most critical since they were designed to hold the whole structural system together. They depended on the capacity of the FRP wrapping to hold the arch end, the

vertical member, and the tying chord together; and on the bearing capacity of the FRP plates and the FRP couplings to take the axial loads. As discussed previously the joints were fabricated in the laboratory by workers with no experience or training in handling this kind of materials, accordingly there were some fit-up problems due to machining inaccuracies. Figure 9.12 shows a fit-up gap corresponding to an end joint.

The stiffness was reduced by shear cracking of the type 3 end joint of the east arch at the south end at a load of 20 kips. Figure 9.31 shows the magnitude of this crack. This shear crack caused a reduction in stiffness of 23% of the initial stiffness.

As the load increased the next failure took place at the north end of the east arch, by shear cracking in a similar fashion as the earlier failure at the south end of the same arch. The load on the system was 28 kips. This shear crack is shown in Figure 9.32. The stiffness was greatly reduced down to 56% of its initial value.

As the loading continued, the vertical member at the south end of the arch on the west side slipped off the RC deck at a load of 39 kips. See Figures 9.33 and 9.34. This slippage was caused by the loss of symmetry of the structural system, since the arch on the east side was weakened by the shear cracking of the south end joint; it caused the RC deck to rest unevenly on top of both arches as shown in the sketch in Figure 9.35. The RC deck then just rotated around its longitudinal axis, causing the vertical member to come off. At this point the test was stopped, although the system still was able to sustain additional load, certainly its own weight. Specimen FGS12 sustained 2.8 times the design load before failure.



**Figure 9.31.** Wrap Shear Cracking at the South End Joint, East Arch.

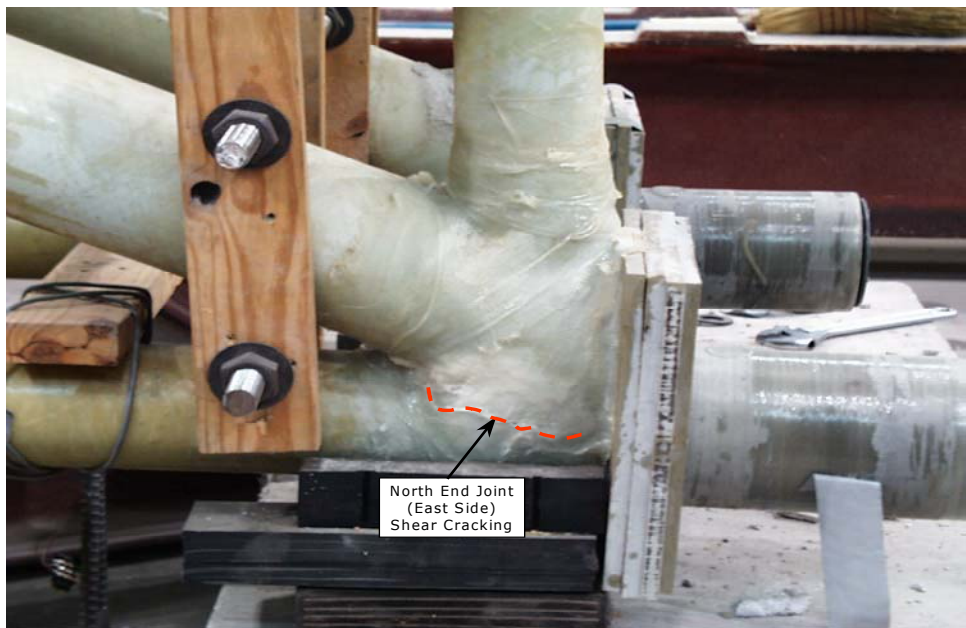


**Figure 9.32.** Wrap Shear Cracking at the North End Joint, East Arch.



**Figure 9.33.** Slippage of Vertical Member at South End of East Arch.



**Figure 9.34.** Close Up of Figure 9.33.

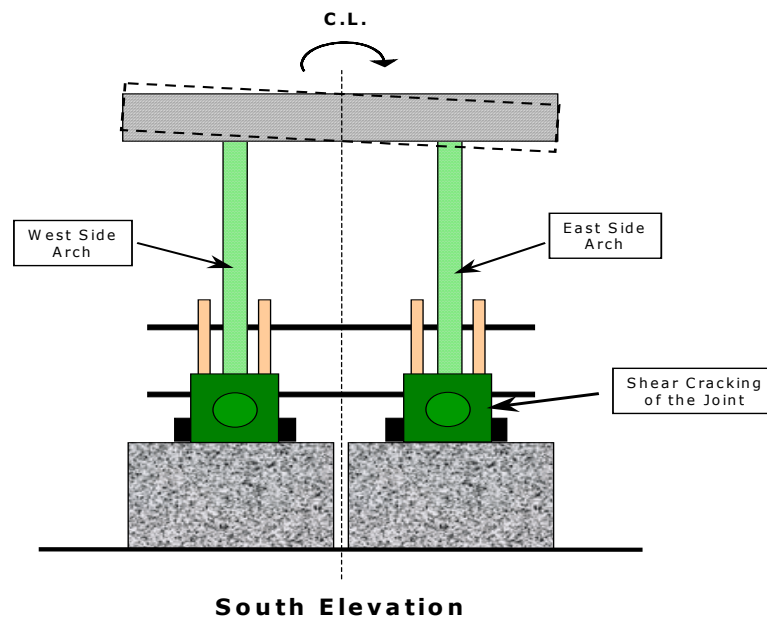


**Figure 9.35.** Rotation of RC Deck Caused by Shear Cracking.

The experimental strain distribution on the vertical members Vertical 1, 2, and 3 (see Figure 9.36 for nomenclature) as the structural system was loaded is shown in Figures 9.37 through 9.39. The straight lines show the strain distribution from the analytical model.

As noted previously, the members for specimen FGS12 were machined and fabricated at the University of Texas and except for type 1 connections, the quality of fit-up and wrapping was not good. Emphasis was placed on the arch members and no particular care was taken with the vertical members. Load was transferred to these members through and FRP plate placed on top of each member. Accordingly, it is likely that the load was not concentric for these members and that significant bending is induced. This is shown in Figures 9.37 through 9.39 were the strain gages on opposite sides of each member show different values of strain. Further, the stiffness of the RC deck is significant compared to the arches and this contributes to an unequal distribution of vertical loads between the members. For example, Vertical 1

on the West arch picks up much more load than the Vertical 1 on the East arch. In contrast, Vertical 2 on the West arch picks up less load than Vertical 2 on the East arch. As a result of the poor fit-up of these vertical members, the experimental and analytical values for the strain distribution on the vertical members shown in Figure 9.37 through 9.39 have a poor correlation.

Figures 9.40 through 9.42 show the strain distribution for the arch members (diagonals) as the test developed. The straight lines show the strain distribution from the analytical model. The values for the arch member Diagonal 2 and 3 have a good correlation. Some bending is present. Unfortunately, the data from the East side of the East arch is not available because of an instrument malfunction. The correlation for Diagonal 1 is not good, particularly for the East arch. This member ends at the joint that failed first at the South end of the East arch. It is likely that the inadequate stiffness of this joint resulted in a redistribution of load, and prevented the Diagonal 1 from carrying the full analytically predicted load.

The strain distribution on the bottom chord is shown in Figure 9.43. As with the previous figures the straight lines are the values from the analytical model. The strains from the gages on the exterior top of the pipes are shown on the left of the origin, whereas, the values from the gages on the midplane of the pipe cross sections are given on the right of the origin. The correlation of the analytical and experimental values, is very good for the strains on the exterior top of the pipe (curves on the left). The correlation of the strains at the midplane though is not as good. The reason for this discrepancy is that the analytical model uses a nominal elastic modulus, and nominal cross section dimensions. As discussed previously, the elastic modulus of the pipe is probably significantly higher than the nominal value, which results in a lower measured strain. A better correlation is expected if actual values for these parameters were used instead.

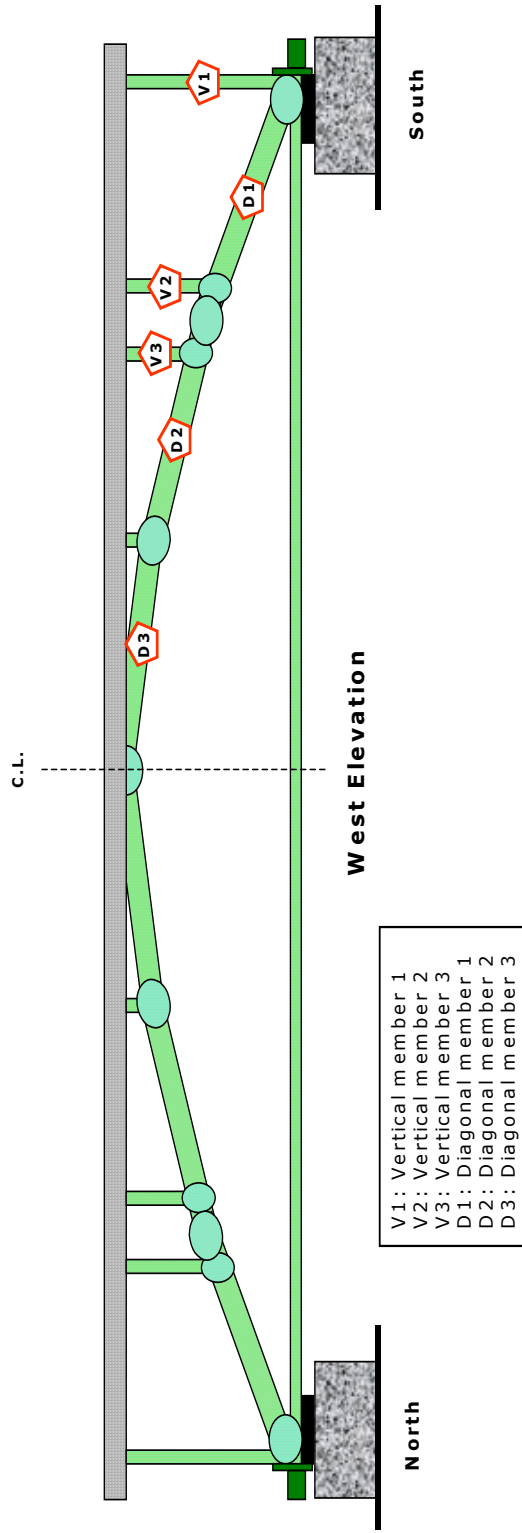


**Figure 9.36.** Specimen FGS12 Member Notation.



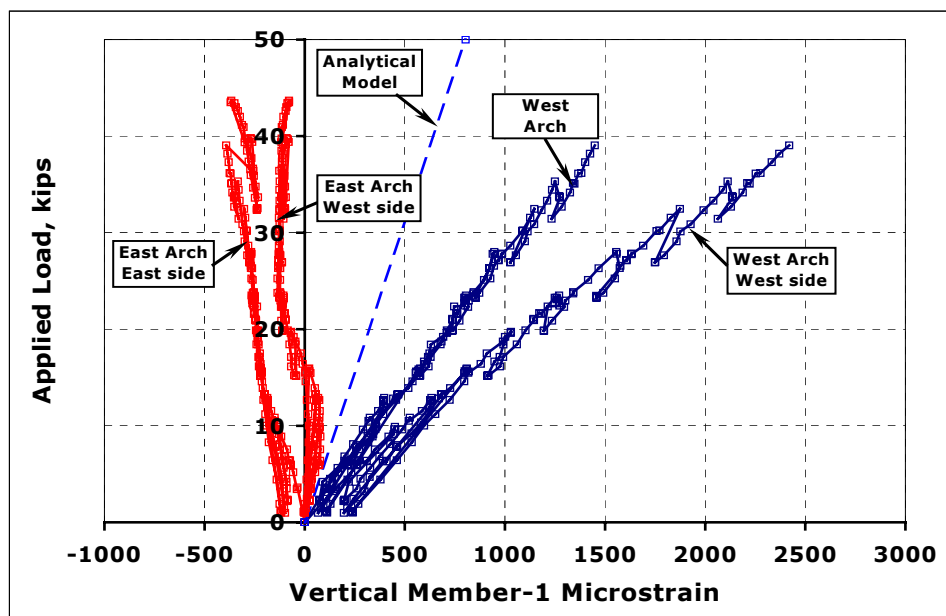


Figure 9.37. Vertical 1, Strain Distribution.

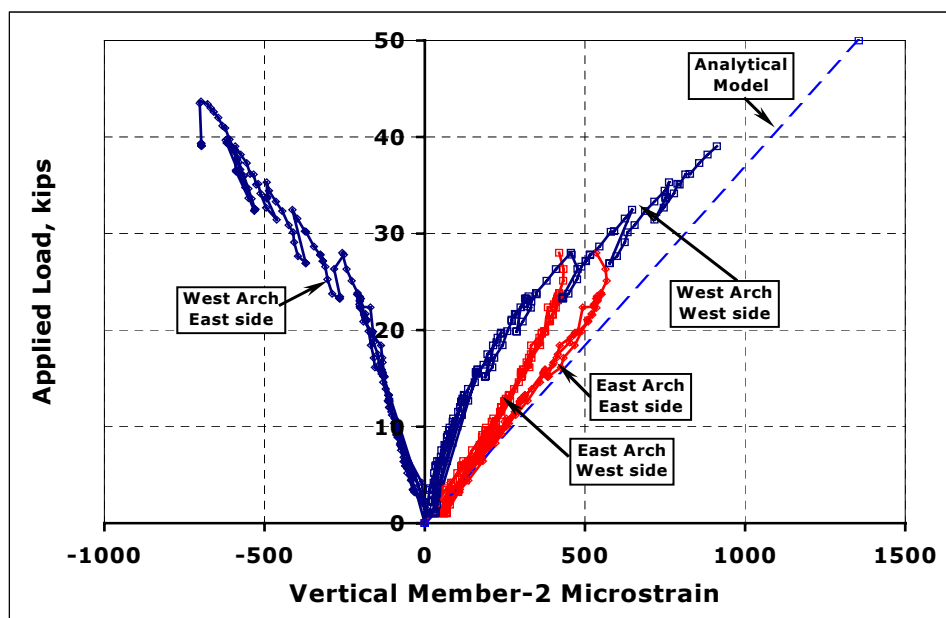


Figure 9.38. Vertical 2, Strain Distribution.

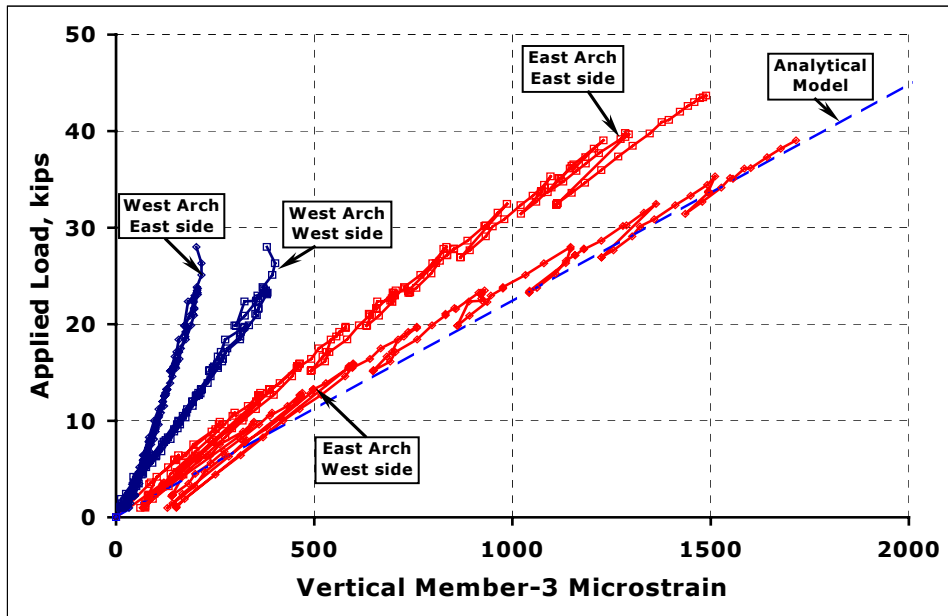


Figure 9.39. Vertical 3, Strain Distribution.

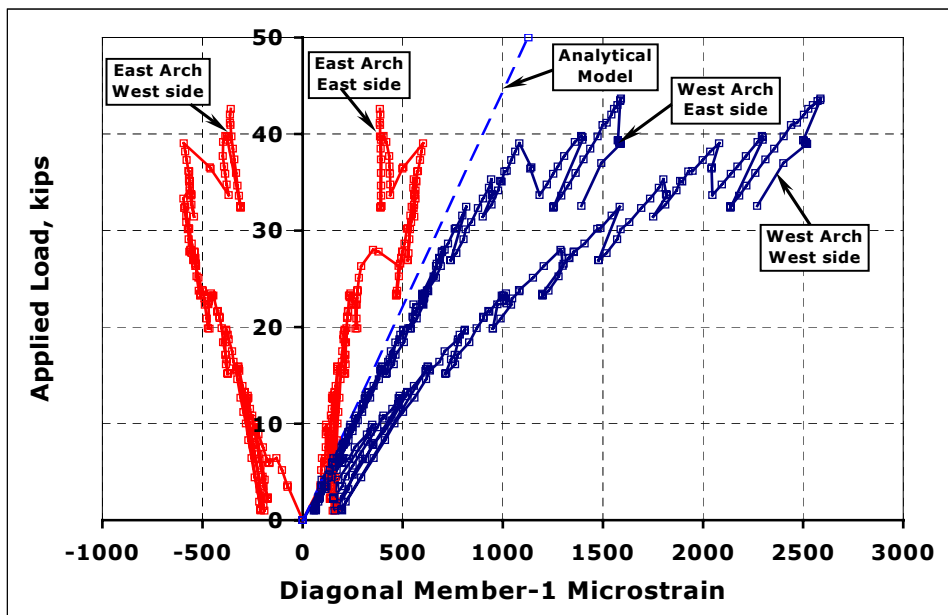
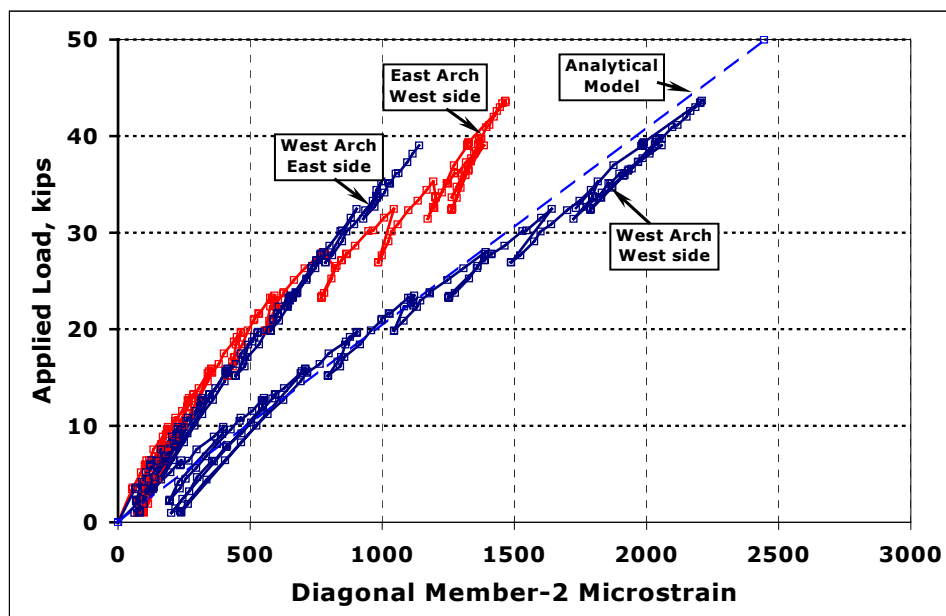
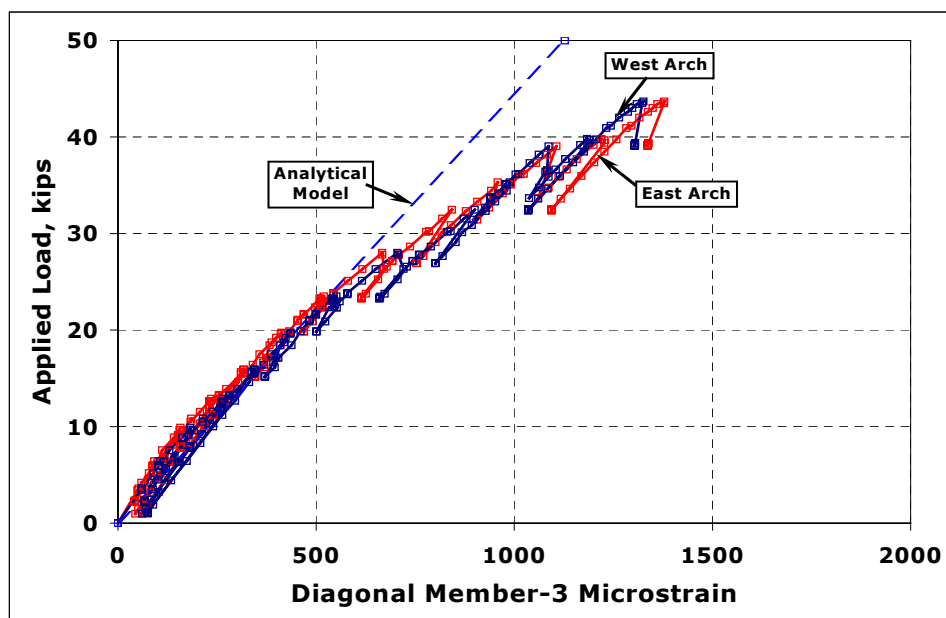


Figure 9.40. Diagonal 1, Strain Distribution.



**Figure 9.41.** Diagonal 2, Strain Distribution.



**Figure 9.42.** Diagonal 3, Strain Distribution.

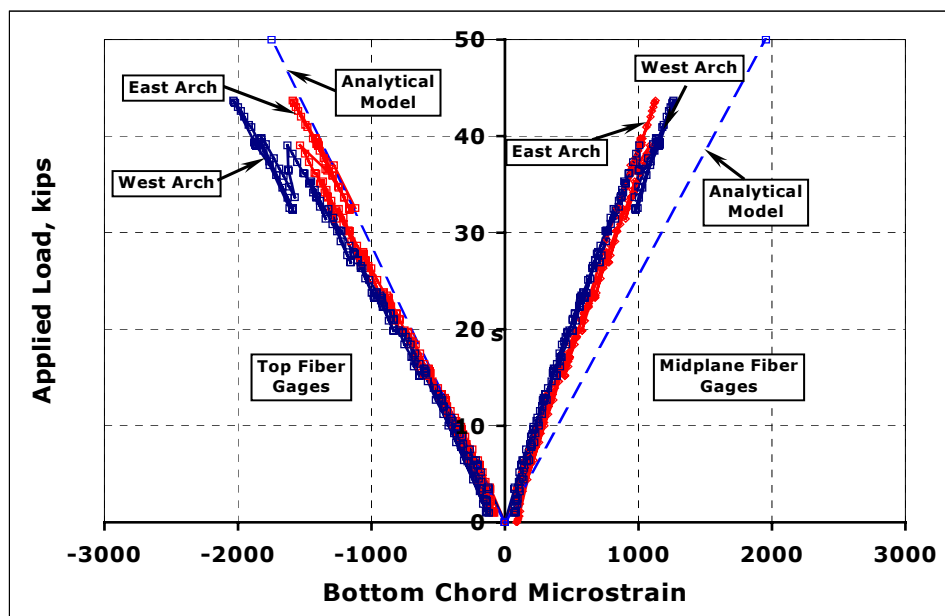


**Figure 9.43.** Bottom Tying Chords, Strain Distribution.

It should be noted that as shown in Figures 9.22 and 9.23 the FRP line pipes used in assembling both arches exhibit a nonlinear behavior, especially the pipes with a larger diameter, which were used as the arch members. For the level of load applied in the test however, both the vertical and arch members did not get into the nonlinear range as can be seen in Figures 9.37 through 9.43, in fact the maximum stresses in the vertical and arch members were below 50% and 25% of their capacity respectively. Experimental data for the pipes used as tying chords in both arches was not available, and there is no way of actually quantifying a similar ratio. Based on the catalogue values, the level of stress is less than 25% its capacity.

## **9.8 Significant Findings**

The structural arch system used in this test performed as expected and construction of short and medium span bridges is feasible with this system.

Machining, assembly, and connection details are important and must be carefully controlled in order for the system to perform satisfactorily. Defects in the joints had a strong influence on the behavior of the FRP arches, and the structural system as a whole.

Wrapping of the joints is also important. The wrappings for Specimen FGS12 performed acceptably, but for a field application, a more reliable wrapping technique is needed. Wrapping is what determines the effectiveness of the joint and so special attention should be paid to its design and fabrication.

## **9.9 Summary**

This chapter covered specimen FGS12, which consisted of two arches made of FRP pipes (FGS1 and FGS2), and an RC deck simply resting on top of both arches. No special connections between the RC arches and the RC deck were considered. The FRP pipes are commercially available and are used mainly in the oil industry.

The resulting structural system was loaded up to failure. Failure occurred when the two end joints on the same arch cracked due to shear. The shear cracking was not of the catastrophic kind, and the specimen still was able to sustain additional load and stability of the structural system was not compromised.

Finally, the effectiveness of the wraps on each connection of the arch was only estimated during the design and fabrication of the arches. There was not experimental data available on the behavior of this kind of wrap that would allow for a better assessment of its mechanical properties. It ended up working out much better than expected. For future applications, it is recommended that experimental work be conducted to determine the mechanical properties of this kind of wrap. A better understanding of the wrap behavior will not only significantly allow for a better analysis and a more optimal design of the joints in the arch, but it also will help in a better prediction of the structural system response, making it a much more reliable load carrying structure.

# **Chapter 10**

## **Design of Fiber Reinforced Plastic Structural Members**

### **10.1 Overview**

This chapter presents design recommendations for fiber reinforced plastic (FRP) structural members. Recommendations for structural analysis, failure criteria, viscoelastic analysis, stability, ASTM tests, resin and design factors are included.

### **10.2 Structural Analysis**

The study of the mechanics of composite materials can be divided into Micromechanics and Macromechanics.

Micromechanics provides an understanding of the behavior of the fiber and resin constituents, and how their combination affects composite behavior. It has some limitations in predicting some composite mechanical properties.

Macromechanics uses the lamina level as the building block for analyzing composite laminate behavior. Laminate theory is used to accurately predict laminate properties. These analysis methods address:

- Stress-strain relationships.
- Thermal and moisture effects.
- Inelastic Behavior.
- Strength and failure.
- Interlaminar stresses.

Structural analysis is the next level beyond laminate analysis. It addresses loading and geometry for a given structure. For composites, it is more complex than for traditional materials. Analysis strategies can be divided as follows:

- **Detailed Analysis:** Rigorous stress analysis to obtain a full picture of the stresses generated for a given loading. Results from this kind of analysis allow for a reduction of factors of safety and weight. Aerospace industry, ASME Section X class II pressure vessels, and the automotive industry make extensive use of this type of analysis. A detailed analysis often involves an in depth finite element analysis. The expense is justified by weight savings in the part, which have a significant impact on the operating cost and performance of an aircraft, or the cumulative cost of a component, which will be produced with thousands of copies.
- **Prototype Testing:** stress analysis followed by extensive prototype testing. ASME Section X class I pressure vessels, sports equipment, and the pipe industry, make extensive use of this type of analysis. Extensive prototype testing is used when multiple copies of a component are manufactured, but is not practical for bridge structures, which are generally one of a kind.
- **Conventional Analysis:** a comprehensive structural analysis but relatively simple macrolevel stress analysis, with higher factors of safety and non-destructing examination (NDE). ASME Section X class II pressure vessels, FRP tanks, and FRP stacks, make extensive use of this type of analysis. This type of analysis is typical for conventional structural engineering with steel, concrete, and timber, which relies on ductility and high safety factors to overcome the harmful effect of stress concentrations.



**Recommendation:** A conventional analysis is recommended for structural engineering applications.

**Recommendation:** This conventional analysis should be complemented by comprehensive NDE similar to that required by ASME Section X Class II pressure vessels, including visual inspection and acoustic emission testing. A complementary NDE research program is being sponsored by TxDOT (project 0-1892) at Texas A&M and the University of Texas. The objective of the program is to specify appropriate NDE methods for FRP highway structures.

### **10.3 Failure Criteria**

Failure criteria for composites are more elaborate than for metals due to the non homogeneity of the material. Furthermore, the modes of failure of a composite lamina are numerous in contrast to metals where yielding is the only mode of failure. A lamina can fail under one of the following mechanisms: fiber breakage, fiber pull-out, matrix cracking, and micro-buckling.

There are basically three failure criteria for lamina: Maximum Strain, Maximum Stress, and Tsai-Wu. Some other variations of the Tsai-Wu also exist (most notably Tsai-Hill and Hoffman), but these are particular cases of the general case given by the Tsai-Wu formulation. For some cases these criteria is also applied for the entire laminate, for these cases the criteria is based on destructive tests other than theoretical considerations.

#### **10.3.1 Maximum Strain Criterion**

In this criterion failure is predicted when any principal material axis strain component exceeds its ultimate strain. The criterion then can be expressed as follows:

$$\begin{aligned} \varepsilon_{Lu}^c < \varepsilon_1 < \varepsilon_{Lu}^t \\ \varepsilon_{Tu}^c < \varepsilon_2 < \varepsilon_{Tu}^t \quad (10.1) \\ \gamma_{12} < \varepsilon_{LTu} \end{aligned}$$

where:

$\varepsilon_{Lu}^c, \varepsilon_{Lu}^t$ : longitudinal maximum strain compression, tension.

$\varepsilon_{Tu}^c, \varepsilon_{Tu}^t$ : transverse maximum strain compression, tension.

$\varepsilon_{LTu}$ : in-plane maximum shear strain.

The failure envelope is a rectangle in the  $\varepsilon_1$ - $\varepsilon_2$  plane. In the  $\sigma_1$ - $\sigma_2$  plane, however, the envelope is a skewed parallelogram as shown in Figure 10.1. The 1 and 2 directions are the principal directions of the FRP material. The simplicity of the criterion makes it very attractive, however, its main drawback is that it does not account for interaction between the stress components, hence there is a poor correlation between experimental data and predicted failure, especially when the principal stresses do not align with the fiber directions.

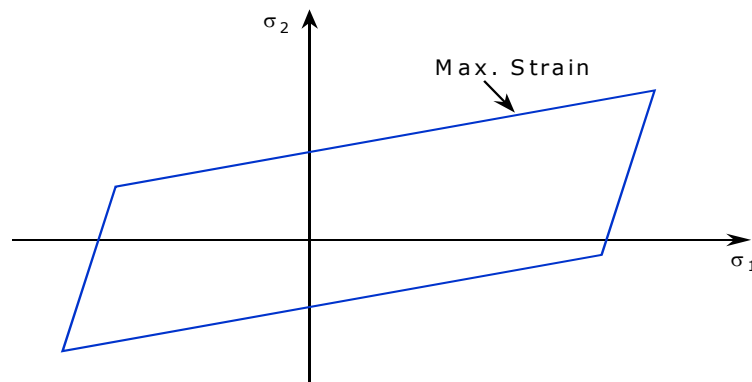


**Figure 10.1.** Schematic of Maximum Strain Criterion.

### 10.3.2 Maximum Stress Criterion

In this criterion failure is predicted when any principal material axis stress component exceeds its ultimate stress. The criterion then can be expressed as follows:

$$\begin{aligned}\sigma_{Lu}^c < \sigma_1 < \sigma_{Lu}^t \\ \sigma_{Tu}^c < \sigma_2 < \sigma_{Tu}^t \quad (10.2) \\ \tau_{12} < \sigma_{LTu}\end{aligned}$$

where:

$\sigma_{Lu}^c, \sigma_{Lu}^t$ : longitudinal strength compression, tension.

$\sigma_{Tu}^c, \sigma_{Tu}^t$ : transverse strength compression, tension.

$\sigma_{LTu}$ : in-plane shear strength.

The failure envelope is a rectangle in the  $\sigma_1$ - $\sigma_2$  plane as shown in Figure 10.2. As with the maximum strain criterion, the simplicity of the criterion makes it very attractive, however, both criteria share the same drawback, in that they do not account for interaction between the stress components, hence there is a poor correlation between experimental data and predicted failure for biaxial loading.

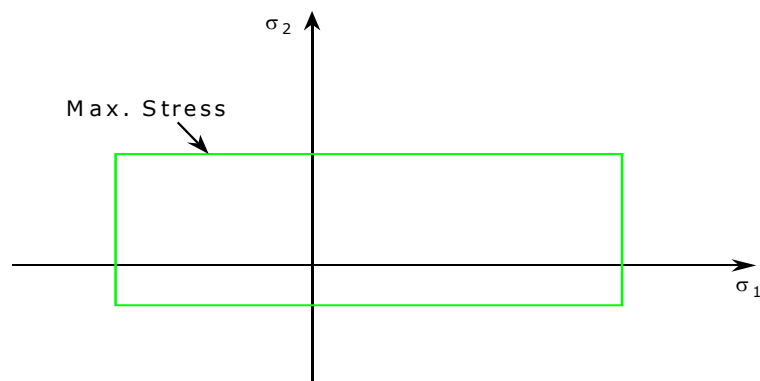


**Figure 10.2.** Schematic of Maximum Stress Criterion.

### 10.3.3 Tsai-Wu Criterion

It is the most general of the quadratic interaction criteria. In its most general form the criterion can be expressed as follows:

$$F_i \sigma_i + F_{ij} \sigma_i \sigma_j = 1, \quad i, j = 1, \dots, 6. \quad (10.3)$$

For the case of a 2D problem, the criterion reduces to:

$$F_{11} \sigma_1^2 + F_{22} \sigma_2^2 + F_{66} \sigma_6^2 + F_1 \sigma_1 + F_2 \sigma_2 + 2 F_{12} \sigma_1 \sigma_2 = 1 \quad (10.4)$$

Each of the constant  $F_{ij}$ , can be determined by specializing (10.4) to a particular set of stresses  $\sigma_i$ . Accordingly,  $F_{ij}$ , and the  $F_i$ , take the following form:

$$\begin{aligned} F_{11} &= 1/\sigma_L^t \sigma_L^c, & F_1 &= 1/\sigma_L^t - 1/\sigma_L^c \\ F_{22} &= 1/\sigma_T^t \sigma_T^c, & F_2 &= 1/\sigma_T^t - 1/\sigma_T^c \\ F_{66} &= 1/\tau_{LT}^2 \end{aligned} \quad (10.5)$$

The remaining coefficient  $F_{12}$  can be computed from:  $F_{12} = (F_{11} F_{22})^{1/2}$ .

where:

$\sigma_L^t$ : longitudinal tensile strength.

$\sigma_L^c$ : longitudinal compressive strength.

$\sigma_T^t$ : transverse tensile strength.

$\sigma_T^c$ : transverse compressive strength.

$\tau_{LT}$ : in-plane shear strength.

A schematic of this criterion is shown in Figure 10.3, and Figure 10.4 shows a schematic comparison of these three criteria.

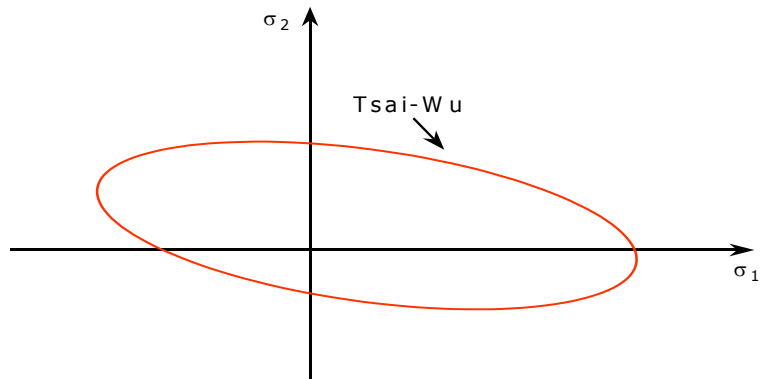


**Figure 10.3.** Schematic of Tsai-Wu Criterion.

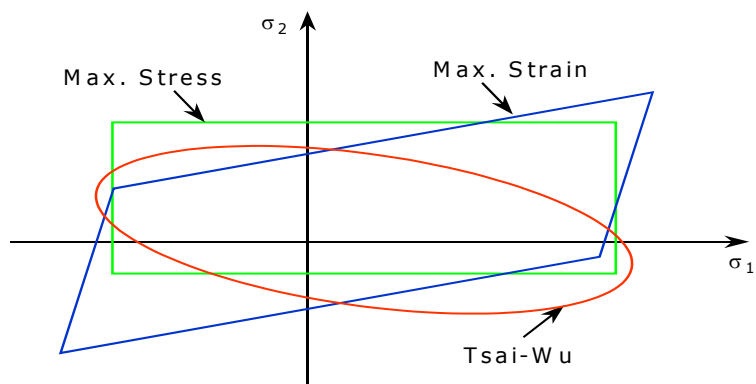


**Figure 10.4.** Schematic Failure Criteria Comparison.

**Recommendation:** The Tsai-Wu failure criterion is recommended to evaluate the safety of a FRP structural member under a given state of stress. However, in cases where the stresses are primarily oriented in a material principal direction, the maximum stress criterion can be used.

## **10.4 Viscoelastic Behavior**

The term viscoelasticity stands for all aspects of time dependent response of stress to strain apart from failure. It is the characteristic that contrasts the behavior of plastics from the behavior of metals. Viscoelasticity does not apply to chemical aging.

Depending on the conditions, a viscoelastic material may be under creep, relaxation and recovery. Creep is the strain response to a stress that is constant with time. Relaxation is the stress response to an applied constant strain. Recovery is the strain response to a stress that has been removed.

### **10.4.1 Creep**

Creep is usually defined as the increase in strain with time in response to a constant applied stress, at a constant temperature. The creep strains in plastics do not increase indefinitely, and approach a final value asymptotically. Given enough time, they also recover completely upon the removal of the load.

The ratio of the instantaneous strain to the constant applied stress is called the creep compliance. Creep compliance is a very important factor in the time dependent design of plastics.

### **10.4.2 Relaxation**

Relaxation is the counterpart of creep. It is usually defined as the decline in stress with time, in response to a constant applied strain, at constant temperature.

The ratio of the instantaneous stress to the constant applied strain is called the relaxation modulus.

### 10.4.3 Viscoelastic Models

It is apparent that a simple constitutive relation such as Hooke's law cannot describe the different time dependent behaviors. A formulation taking into account the time-dependent behavior of the material is needed. There are two approaches that achieve this (Krishnamachari S.I., 1993).

- **Spring-Dashpot Models:** This approach is also called the differential representation of viscoelasticity. The models consist of using an arrangement of springs and dashpots in parallel and/or series. The load and displacement in the arrangement is time dependent.
- **Boltzmann's Superposition Principle:** This approach is also called the integral representation of viscoelasticity. This principle simulates the creep, relaxation, recovery, and other dynamic behavior of a given material.

#### 10.4.3.1 Spring-Dashpot Models

The following spring dashpot models are frequently used when describing the time dependent behavior of viscoelastic materials. See Figure 10.5.

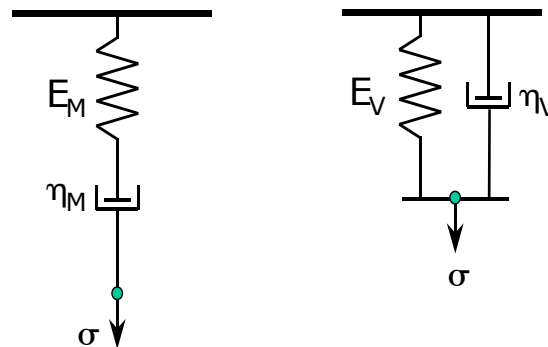


**Figure 10.5.** Basic Viscoelastic Models, Maxwell (left) and Voigt (right).

The equations defining the Maxwell model response are given below for the case in which the model is subject to a stress  $\sigma$ .

$$\begin{aligned}
 \sigma &= \sigma_{spring} = \sigma_{dashpot} \\
 \varepsilon &= \varepsilon_{spring} + \varepsilon_{dashpot} \\
 \varepsilon(t) &= \frac{\sigma}{E_M} + \int_0^t \frac{\sigma}{\eta_M} d\tau
 \end{aligned} \tag{10.6}$$

In a similar fashion the equations defining the Voigt model response under similar loading are:

$$\begin{aligned}
 \varepsilon &= \varepsilon_{spring} = \varepsilon_{dashpot} \\
 \sigma &= \sigma_{spring} + \sigma_{dashpot} \\
 \sigma(t) &= E_V \varepsilon + \eta_V \frac{d\varepsilon}{dt}
 \end{aligned} \tag{10.7}$$

If these responses are further specialized for the case in which the applied stress is constant, i.e.  $\sigma = \sigma_0$ , we obtain for the Maxwell model:

$$\begin{aligned}
 \sigma_{spring} &= \sigma_{dashpot} = \sigma_0 \\
 \varepsilon(t) &= \frac{\sigma_0}{E_M} + \frac{\sigma_0}{\eta_M} t = D(t) \sigma_0 \\
 D(t) &= \frac{1}{E_M} + \frac{1}{\eta_M} t
 \end{aligned} \tag{10.8}$$

where,  $D(t)$  is the creep compliance. This response is linear as shown in Figure 10.6.



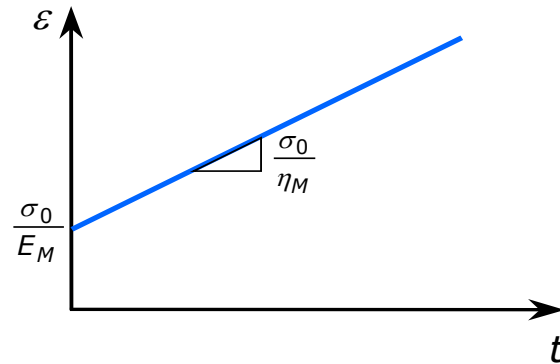


**Figure 10.6.** Maxwell Model Responses Under a Constant Stress  $\sigma_0$ .

Similarly, under the same conditions the Voigt response is given by:

$$\begin{aligned} \sigma_{spring} &= \sigma_{dashpot} = \sigma_0 \\ \eta_V \frac{d\epsilon}{dt} + E_V \epsilon &= \sigma_0 \\ \epsilon(t) &= \frac{\sigma_0}{E_V} (1 - e^{-\frac{t}{\tau_V}}) = D_{(t)} \sigma_0 \quad (10.9) \\ D_{(t)} &= \frac{1}{E_V} (1 - e^{-\frac{t}{\tau_V}}), \quad \tau_V = \frac{\eta_V}{E_V} \end{aligned}$$

where again,  $D_{(t)}$  is the creep compliance, and  $\tau_V$  is the retardation time. The response this time however, is nonlinear (exponential) as shown in Figure 10.7.

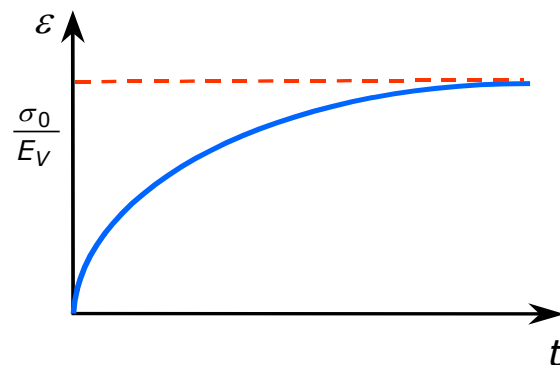


**Figure 10.7.** Voigt Model Responses Under a Constant Stress  $\sigma_0$ .

The Maxwell and the Voigt viscoelastic models do not accurately describe viscoelastic behavior of FRP materials. However, these models form the basis for more complex models such as the Kelvin model shown in Figure 10.8. The Kelvin model is a combination in series of the two basic models, the Maxwell and the Voigt models. More complex arrangements exist, where several Maxwell and Voigt models are combined in order to achieve a better prediction of the actual response of the material in hands.

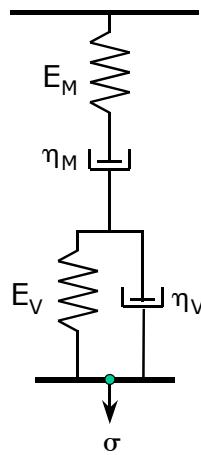


**Figure 10.8.** Kelvin Viscoelastic Model.

#### 10.4.3.2 Findley's Model

Due to the complexity of modeling creep, the most favored approach is to develop a model based on data from experimental work. One of the most widely applied laws for creep is Findley's power law given in its most general form (Hollaway, 1993):

$$\varepsilon(t) = \varepsilon_0 + m \left( \frac{t}{t_0} \right)^n \quad (10.10)$$

where,  $\varepsilon_0$  and  $m$  are functions of stress,  $t$  is time duration,  $t_0$  is a constant and  $n$  is independent of stress.

The parameters can be represented by hyperbolic functions (Findley, 1951), equation 10.10 then can be written as:

$$\varepsilon_{(t)} = \varepsilon_0 \sinh\left(\frac{\sigma}{\sigma_0}\right) + \varepsilon_t \left(\frac{t}{t_0}\right)^n \sinh\left(\frac{\sigma}{\sigma_t}\right) \quad (10.11)$$

For linear and moderately nonlinear behavior, and for relatively small stresses, equation 10.11 can be expressed as follows:

$$\frac{1}{E_{(t)}} = \frac{1}{E_0} + \frac{1}{E_t} t^n \quad (10.12)$$

where  $E_{(t)}$  is the viscoelastic modulus.

Equation (10.12) is also known as the Findley model or the power law model, and although it is an approximate equation, its simplicity and practicality makes it the ideal choice when predicting the time dependent behavior of viscoelastic materials. Findley's equations are particularly useful in problems of sustained applied loads.

Equation 10.12 is completely defined if the constants  $E_t$  and  $n$  are known.  $E_0$  in this equation is the initial elastic modulus of the material and is a known parameter. For FRP materials of the type used in this study,  $E_t$  can be determined using ASTM D638 or D 5083 tests.

The way the values for  $E_t$  and  $n$  are calculated is as follows. First, select two values of time  $t$  at which the values for  $E_{(t)}$  are known, once these values are set, then  $E_t$  and  $n$  can be calculated by simply solving the resulting equation system. Practical values for time  $t$  are:  $t = 1$  hour, and  $t = 100$  hours, but any other pair of values will do. For these two values of time the constants  $E_t$  and  $n$  are given by:

$$\log\left(\frac{1}{E_{(t)}} - \frac{1}{E_0}\right) = n \log(t) - \log(E_t)$$

$t = 1 :$

$$E_t = \frac{1}{\frac{1}{E_{(1)}} - \frac{1}{E_0}} \quad (10.13)$$

$t = 100 :$

$$n = \frac{1}{2} \left[ \log(E_t) + \log\left(\frac{1}{E_{(100)}} - \frac{1}{E_0}\right) \right]$$

In this study, strains and deflection at the specimen midspan section were measured (see Chapters 6 and 7). This data then was used to calculate the viscoelastic modulus at a desired time. By using the viscoelastic modulus at times:  $t = 1$  hour, and  $t = 100$  hours, equation 10.13 can be used to determine the values for  $E_t$  and  $n$ .

One of the valuable features of this approach is the ability to predict long term viscoelastic response based on a 100 hour load test.

#### 10.4.3.3 Boltzmann's Superposition Principle

The Boltzmann's superposition is a way of describing viscoelastic response under different loading condition. The principle is summarized in Figure 10.10. In this figure the actions are shown on the left column, and the corresponding responses on the right column. Initially the system is under a stress  $\sigma_0$ , which has a response as shown in the right column.

The same response can be applied to a different time  $t_m$ , as shown on the second row on Figure 10.9. If these two states of loading were superimposed, their responses also will be superimposed as shown in the third row of Figure 10.9. The fourth row of Figure 10.9 shows response when a specimen is unloaded, by using superposition of a negative load equal to the current load. For a typical creep test, the time dependent strains are

recorded for a different level of stresses. The Boltzmann's principle can then be applied to model the response of the specimen with time. The simplicity yet reliable accuracy makes this method a powerful tool for viscoelastic analysis of FRP structural members.

**Recommendation:** It is recommended that the viscoelastic behavior of a FRP structural member be modeled using the Findley model and the Boltzmann's superposition principle.

**Recommendation:** It is recommended that the constants in the Findley model be computed based on the times:  $t = 1$  hour and  $t = 100$  hours.

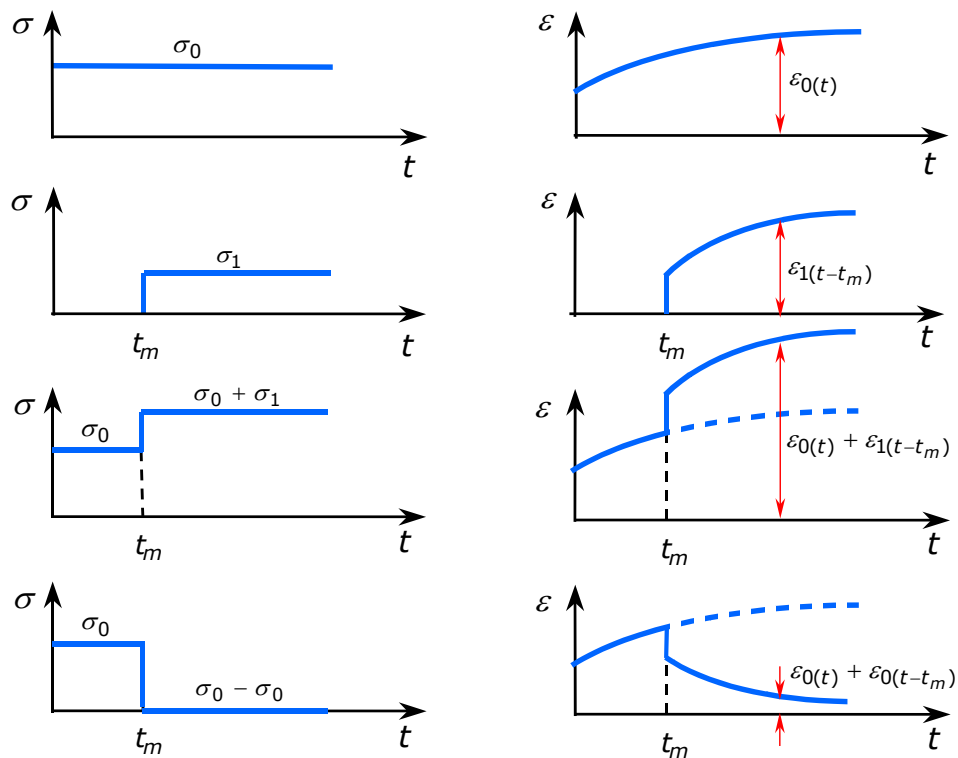


**Figure 10.9.** Schematic of the Boltzmann's Superposition Principle.

## **10.5 Stability**

### **10.5.1 Overall**

The analysis of stability for FRP composite materials is largely based on theoretical developments for isotropic materials. Indeed, much of the progress in understanding stability of composites has occurred by rederiving the isotropic results while taking into account all the additional stiffness terms that can be present for a composite. While the additional terms greatly increase the length and complexity of the equations, the fundamental mechanics largely remains the same (ASM Handbook, 2001). An extensive review of literature is given by Leissa (1985), and excellent references include Whitney (1987), Iyengar (1988), Reddy (1997), Jones (1998), Barbero (1999).

**Recommendation:** Analytical methods, which take into account the non homogeneity of the composite, should be used for determining overall buckling.

### **10.5.2 Creep Buckling**

This type of buckling is especially important in FRP components, since in this kind of materials viscoelastic behavior becomes important. The creep buckling can be analyzed by performing a viscoelastic analysis in conjunction with a conventional buckling analysis on the FRP component.

**Recommendation:** Long-term deflection should be calculated using a viscoelastic model and these deflections should be used in the buckling analysis.

### **10.5.3 Local Buckling**

Thin walled structural shapes usually display buckling of the walls without the overall deflection of Euler buckling. Testing is very important and

it is to be performed on specific components to detect planes of delamination. Regarding a buckling analysis the whole cross section should be considered to obtain accurate results, a finite element analysis is usually performed.

**Recommendation:** Sections of a component subject to compression loading should be tested under uniform compression to determine buckling mechanisms, behavior, and failure loads. The testing program should be complemented by conventional local buckling analysis.

## 10.6 ASTM Testing Methods

Testing is important to determine material properties and must be performed for a particular laminate. Subject to the results of compression tests on specific sections of the member, the compression strength is normally considered as equal to the tensile strength.

**Recommendation:** The ASTM tests listed in Table 10.1 are recommended.

**Table 10.1.** Recommended ASTM Tests for FRP Mechanical Properties.

FRP Mechanical Property	ASTM Test Method
Tensile strength in longitudinal direction	D 638 or D 5083
Tensile modulus of elasticity in longitudinal direction	D 638 or D 5083
Tensile strength perpendicular to longitudinal direction	D 638 or D 5083
Tensile modulus of elasticity perpendicular to longitudinal direction	D 638 or D 5083
Compressive strength	(*)
In-plane shear strength	D 3846
Bearing strength	D 953
Glass content, weight percent	D 2584

(\*) Compression loading test of a local section of the component as described in Section 10.5.3.

## 10.7 Allowable Design Factors

Currently, there is not a defined stress ratio for the design of FRP structural components. As a reference, the stress ratio used in pressure vessel design is 6 (Ziehl, 2000). This value is well on the conservative side, as an attempt to keep the lamina in the relatively undamaged state of service. In contrast, ASME RTP-1 for FRP tanks uses stress ratios as low as 1.6 for the structural layers. The draft ASCE standard on FRP stacks (FRP Stacks Standard, 2001) uses factors ranging from 2.6 for short-term loads in tension to 7.7 for long-term loads in tension.

Since the failure criterion recommended in Section 10.3 is based on the ultimate failure values of the lamina, laminas made with more flexible resins, which have a lower failure strength but greater elongation to failure are penalized. For loading perpendicular to the fibers, laminas made with flexible resins have similar ultimate strength to laminas made with brittle resins. However, the stress at onset of damage is significantly higher for laminas with flexible resins (Ziehl, 2000).

Based on test results from the specimens tested as part of this research, it was observed that none of the specimens' FRP components reached their ultimate strength. In several cases, the maximum stress on the component at design loads was around 20-25%, of its ultimate nominal strength. Also, for civil engineering applications, the structures rarely experience high cycle fatigue, and structures are subjected to maximum load only for short periods of time.

A stress ratio of four is recommended together with resins having an elongation to failure of five percent.

Table 10.2 (Ziehl, 2000) lists a variety of commercially available resins used in the manufacturing of FRP components. From this table it is seen that



a number of vinyl ester resins meet the criteria including Hetron 922, Derakane 411-350, and Derakane 8084. Although not listed in the table, a number of epoxy resins will also meet this criterion.

Figures 10.10 through 10.12 (Ziehl, 2000) show the behavior of specimens monitored with acoustic emission subjected to bending, with three different fiber orientations and several types of resin. It is clear from these Figures that the flexible resins, Derakane 411-350 and Derakane 8084 perform best. A separate study by Ramirez (1999) showed that the stress at onset of emission is an indication of the endurance limit of the FRP. The studies by Ziehl and Ramirez confirm that unidirectional or knitted fabrics perform better under long term loading than woven roving.

**Recommendation:** Use a design factor of four.

**Recommendation:** Use matrix resins with an elongation of at least five percent.

**Recommendation:** Do not use woven roving reinforcement.

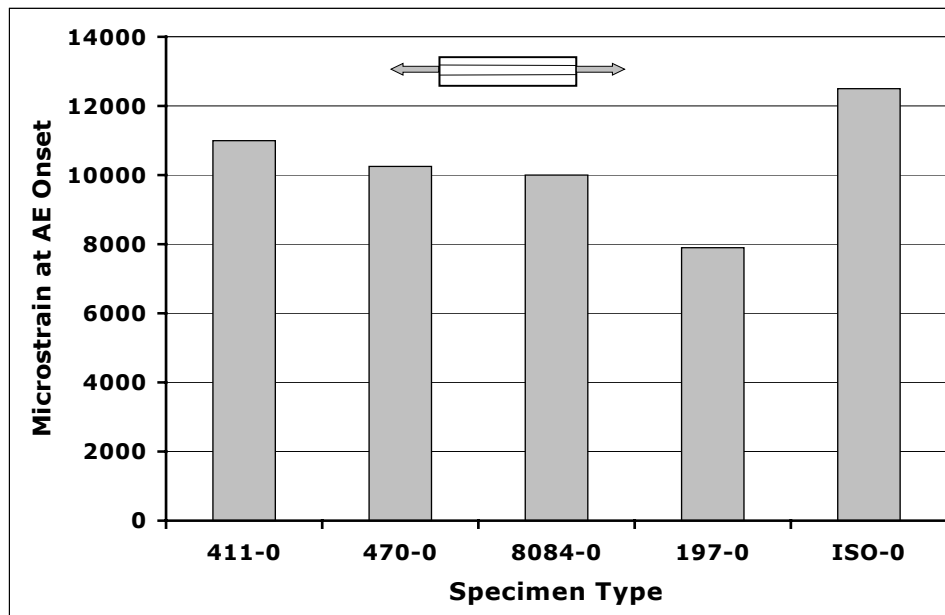


**Figure 10.10.** Strain at AE Onset, Fiber Orientation 0°.

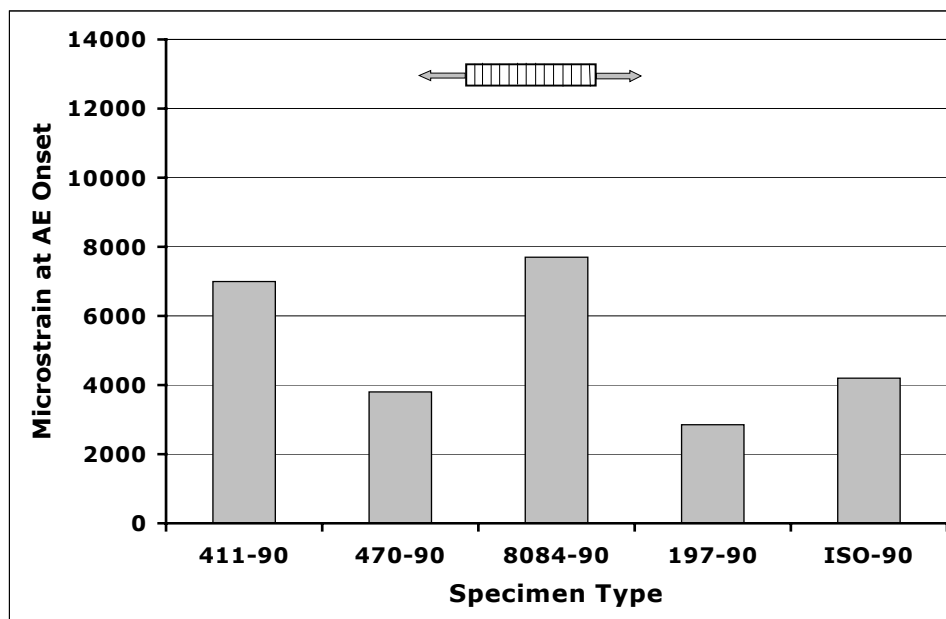


**Figure 10.11.** Strain at AE Onset, Fiber Orientation 90°.

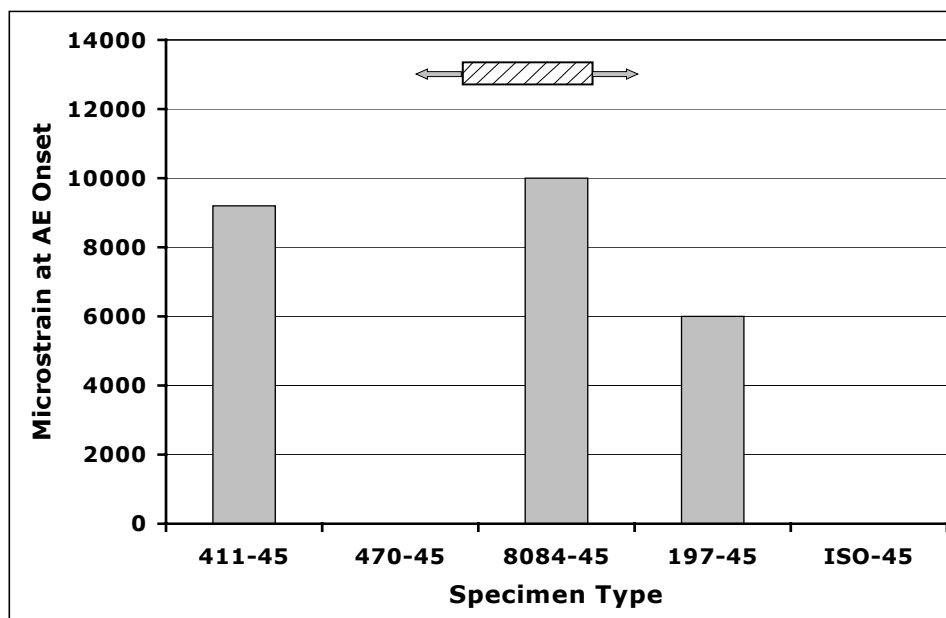


**Figure 10.12.** Strain at AE Onset, Fiber Orientation 45°.

**Table 10.2.** Published Mechanical Properties of Resins.

	Type	Manufacturer	Tensile Strength (ksi)	Compressive Strength (ksi)	Tensile Modulus (ksi)	Compressive Modulus (ksi)	Tensile Elongation (%)
Derakane 470-300	Vinyl Ester	Dow	12.4	-	520	-	3-4
Derakane 411-350	Vinyl Ester	Dow	11.5	16.5	490	350	7-8
Derakane 8084	Vinyl Ester	Dow	10.5	-	460	-	10-12
Hetron 197-3	Polyester	Ashland	5.5	29.3	510	510	1.1
Aropol 7241T-15	Polyester	Ashland	10.7	-	540	-	2.4
Hetron 922	Vinyl Ester	Ashland	12.5	-	460	-	6.7

Source: (Ziehl, 2000).

## **10.8 Summary**

Design recommendations are given for FRP components that can be used for structural members in short span bridges. Also, the design recommendations can be applied to FRP components of other structural systems.

Probably the most important recommendation on the materials selection is the requirement on the resin component of the FRP. It is very important that the requirement on elongation is satisfied, as otherwise the FRP may fail earlier than anticipated and in undesired brittle way.

# **Chapter 11**

## **Summary, Conclusions, and Recommendations**

### **11.1 Overview**

This chapter summarizes the research reported on this dissertation. The experimental program consisted of the study of a structural system composed of a reinforced concrete (RC) deck and a fiber reinforced plastic (FRP) girder, designed to be used in short span bridge superstructures.

### **11.2 Objective of Research**

Investigate by literature review and experimental studies the technical feasibility of utilizing structural plastic materials for the primary structural members in an economically viable short span highway bridge.

### **11.3 Experimental Program Summary**

In all six full-scale specimens were tested. Five specimens having an RC deck and the FRP girder working under composite action, and the remaining specimen was designed to have the RC deck and the FRP girder working independently.

Typically, the RC deck was 4 ft. wide, 30 ft. long, and 6 in. thick. Steel reinforcement was provided in both directions by #4 rebars spaced a 12 in. and 18 in. Normal concrete was used with a nominal compressive strength of 5 ksi at 28 days.

The FRP component had two configurations. The five specimens designed to work in composite action utilized an FRP girder, and the remaining specimen utilized a pair of tied arches made from FRP pipes. The FRP girders used various combinations of resins and reinforcement, and were fabricated by means of pultrusion and contact molded processes.

The specimens had an overall length of 30 ft., with a typical clear span between supports of 28.5 ft.

Long and short term loading was considered. Four specimens were tested under short term loading, and the remaining two were tested under sustained loading. The short term load specimens were loaded in four point bending. The sustained loading was necessary to study the viscoelastic behavior of the proposed structural system. Sustained load was applied by a number of concrete blocks evenly spaced along the length of the specimen, simulating a distributed load.

## **11.4 Conclusions and Recommendations**

The following conclusions and recommendation are drawn from this study:

### **General**

- Construction of a short span highway bridge with structural plastic primary members is technically feasible.

### **Materials**

- For reasons of economy, glass fiber reinforced thermoset plastic (FRP) is the recommended material of construction for the structural plastic components.

- Carbon or graphite may be used to supplement the glass fibers where additional stiffness is required. The high cost of these fibers requires that they be used sparingly.
- Widely used thermoset resins such as vinyl ester and epoxy with high elongation to failure are recommended.
- Self-extinguishing resins with ultraviolet (UV) protection should be used.

### **Advantages**

- Adequate strength is easily achieved.
- Large deflections will accompany initial structural failure providing warning of impending collapse.

### **Disadvantages**

- Connections between FRP composites and other components (FRP and conventional materials) are difficult.
- Low elastic modulus leads to high deflections. Choice of structural system such as composite girder/deck or tied arch can help overcome this problem. This will remain a problem with long span bridges.
- Low elastic modulus leads to stability problems. Choice of structural system can help overcome this problem.
- Fabrication process has a major influence on the resulting structural system and its overall performance.

### **Design**

- Design recommendations are given in Section 11.5.

### **FRP Members**

#### **Pultruded Members**

- Structural shapes based on steel shapes are inefficient.

- Fiber orientation is primarily in the direction of pultrusion. This results in planes of weakness parallel to the fibers, which affect shear and local buckling performance.
- This process is suitable for manufacture of a large number of components of any length.
- Structural shape must have a constant cross section.
- Very expensive for non-standard shapes.
- Structural shapes familiar to structural engineers are available and suitable for small structural applications in corrosive environments such as loading docks, cooling plants and grating.

#### **Contact Molded Members**

- Members can be shaped and fiber arranged to meet structural requirements.
- Poor fabrication quality.
- Low glass content, which means low strength and low modulus.
- Manufacturing process slow and expensive for large number of components.
- Low cost for small number of components.
- Members fabricated with this process are likely to be suitable for short span bridge applications.

#### **Infusion Molded Members**

- Members can be shaped and fiber arranged to meet structural requirements.
- Difficult to mold a flexible resin.
- Expensive for a small number of components.
- Preferred over contact molding because of better fabrication quality and high glass content.



### **Filament Wound Members**

- Limited to shells of revolution.
- Fibers can be arranged to provide axial, transverse and shear strength.
- Good quality of fabrication with high glass content.

## **11.5 Design Recommendations**

The following design recommendations are based on the experimental results from this study:

- Use a design factor of four.
- Use resins with an elongation of at least five percent.
- Do not use woven roving reinforcement.
- The Tsai-Wu failure criterion is recommended to evaluate the safety of a FRP structural member under a given state of stress. However, in cases where the stresses are primarily oriented in a material principal direction, the maximum stress criterion can be used.
- It is recommended that the viscoelastic behavior of a FRP structural member be modeled using the Findley model and the Boltzmann's superposition principle.
- It is recommended that the constants in the Findley model be computed based on the times:  $t = 1$  hour and  $t = 100$  hours.
- Analytical methods, which take into account the non homogeneity of the composite, should be used for determining overall buckling.
- Long-term deflection should be calculated using a viscoelastic model and these deflections should be used in the buckling analysis.
- A conventional analysis is recommended for structural engineering applications.

- This conventional analysis should be complemented by comprehensive NDE similar to that required by ASME Section X Class II pressure vessels, including visual inspection and acoustic emission testing. A complementary NDE research program is being sponsored by TxDOT (project 0-1892) at Texas A&M and the University of Texas. The objective of the program is to specify appropriate NDE methods for FRP highway structures.
- The ASTM tests listed in Table 10.1 are recommended.

### **11.6 Other Observations**

The following observations are based on the experimental program:

- Resin suppliers have developed extensive data on the effect of water, environmental contamination, freeze-thaw performance, and corrosive fluids for the long-term performance of structural plastics. This data is available to the design engineer and should be considered as part of the materials selection process.
- The Federal Highway Administration and many State Highway Departments are concerned about the long-term corrosion and deterioration issues affecting highway bridges built of timber, steel, and concrete.
- The Federal Highway Administration and many State Highway Departments are interested in the use of structural plastics as a way of overcoming the long-term corrosion problem.
- Repair of local damage (impact, vandalism, cracks) can be easily performed in the field.
- Short- and long-term corrosion resistance.
- Light weight makes them easy to install with minimum traffic and environmental disruption. Heavy machinery is not needed for

installation, an important issue in rural areas or developing countries.

- Initial cost: optimization, design experience, construction volume and fabrication process improvements will reduce cost. However, initial cost is likely to be more than for conventional materials.
- Life cycle cost: reduced maintenance and increased life may offset higher initial cost.
- Lack of standardization.
- Lack of design and field experience in the structural engineering community.
- Stress concentrations at sharp corners and holes are a problem.

### **11.7 Future Research**

The structural system developed in this research by no means is the most efficient alternative for short span bridge design. There are still some issues that need to be addressed, among them:

- Development of design standards.
- Development of more reliable connections.
- Research appropriate structural systems for different spans and loading.
- Optimize the design to reduce the initial cost.
- Developed improved shear connectors between the RC deck and the FRP girders.
- Use of recently developed infusion molding manufacturing process.

## References

### Chapter 1

Saadatmanesh H., M. Ehsani M., Fiber Composites in Infrastructure, edited by Saadatmanesh H., Ehsani M.. Second International Conference on Composites in Infrastructure, ICCI '98. Vol. II, 1998.

Structural Plastics Research Council, ASCE Manual No. 63.

Structural Plastics Research Council, ASCE Manual No. 66.

A Report on Current Practice in Structural Plastic Connections.

### Chapter 2

American Society of Civil Engineers, Structural Plastics Design Manual, ASCE Manuals and Reports on Engineering Practice NO. 63, New York, 1984.

ASCE Manuals and Reports on Engineering Practice, No. 47. Selected Abstracts on Structural Applications of Plastics, 1967.

American Society of Mechanical Engineers, Reinforced Thermoset Plastic Corrosion Resistant Equipment, ASME RTP-1, New York, 1992.

American Society of Mechanical Engineers, Fiber-Reinforced Plastic Pressure Vessels, Reported by ASME Biler and Pressure Vessel Committee, New York, 1998.

Breña S.F., Strengthening Reinforced Concrete Bridges Using Carbon Fiber Reinforced Polymer Composites, Ph.D. Dissertation, Dept. of Civil Engineering, The Univeristy of Texas at Austin, December 2000.

Bridge demonstrates advantages of composites. MMFG profile. Winter 1996.

Broutman L., Krock R., Composite Materials Vol. 3, 1969.

Busel J., Lindsay K., On the road with John Busel: A look at the world's bridges. Composite Design and Application. 1997.

CFI, Composites for Infrastructure: A Guide for Civil Engineers, Vol. I, Ray Publishing, Inc., 1998.

Chajes M., Finch W., Rehabilitation of Foulk road bridge #26 (Wilmington, Delaware) using ACM: First full scale use of CFRP sheets for bridge rehabilitation in US. FRP International. April 1995, Vol. III, Issue 2.

Composites Bridges. Lightweight composite bridges installed in Maui. Composites technology. January/February 1996.

Composites for infrastructure, A guide for Civil Engineers. A ray publishing publication, 4891 Independence St., Suite 270, Wheat Ridge, CO 80033.

Dial S., Smokestack rescue. Civil Engineering / May 1998, pp. 62.

Dietz A., Plastics for Architects and Builders, The MIT Press, 1969.

Dufton P.W., Polymers in Building and Construction, RAPRA Industry Analysis Report, 1997.

FHWA's Scanning Program, FHWA Study Tour for Advanced Composites in Bridges in Europe and Japan. U.S. DOT, Federal Highway Administration, December 1997.

Fowler, T.J., Private Communication.

Heger, F.J., Design of FRP Fluid Storage Vessels, Journal of the Structural Division, Proceedings of the ASCE, November, 1970.

Herakovich C.T., Mechanics of Fibrous Composites, John Wiley& Sons, Inc. 1998.

Hull D., Clyne T., An Introduction to Composite Materials. Cambridge University Press, Cambridge, 1996.

Hybrid composite beams used in Park bridge. Hetron newsletter, Winter 1997.

IPWEA, Application of FRP Composites in Bridge Engineering. Institute of Public Works Engineering Australia, IPWEA Conference paper, October 2001.

Infrastructure: Project looks at hybrid fibers for concrete reinforcement. Composite Design and Application. Winter 1995.

Johansen E., ACM Bridges help environment. FRP International. April 1995, Vol. III, Issue 2.

Kaw K., Mechanics of Composite Materials. CRC Press, 1997.

Khalifa M., Kusha S., Krieger J., Bridges constructed using fiber reinforced plastics. Concrete International. June 1993

Lindsay K., Hybrids a new class of construction materials. Composite Design and Application. 1995.

Liu X., Silva P.F., Nanni A., Rehabilitation of Steel Bridge Members with FRP Composite Materials. Proc., CCC 2001, Composites in Construction, Oct.10-12, 2001.

Mallick P.K., Fiber-Reinforced Composites: Materials, Manufacturing and Design, 2<sup>nd</sup> Ed., Marcel Dekker, Inc., 1993.

McCormick F.C., Field Study of a Pedestrian Bridge of Reinforced Plastic. Final Report, Virginia Highway and Transportation Research Council, 1985.

McCormick F.C., Fatigue Study of a GRP Pedestrian Bridge. Final Report, Virginia Highway and Transportation Research Council, 1986.

Modern Plastics, "U.S. pavilion in Moscow", Vol. 37, NO. 4, Dec. 1959.

Phair M., Bridges. Polymer composites to replace span's steel and concrete deck. ENR/MAY 1997.

Ramirez G., Ph.D. Dissertation, Dept. of Civil Engineering, The University of Texas at Austin, 1999.

Rebar for concrete. Owens – Corning.  
<http://www.owenscorning.com/owens/composites/applications/infra/concrete.html>

Researchers use space-age composites to bolster concrete bridge, make repairs easier. University of Dayton News. Nov. 27, 1995.  
<http://www.udayton.edu/news/nr/112795a.html>

ICCI '98. Vol. I, Fiber Composites in Infrastructure, edited by Second International Conference on Composites in Infrastructure, Editors Saadatmanesh H., Ehsani M., 1998.

ICCI '98. Vol. II, 1998, Fiber Composites in Infrastructure, edited by Second International Conference on Composites in Infrastructure, Editors Saadatmanesh H., Ehsani M.

Schwartz M., Composite Materials, Properties, Nondestructive Testing, and Repair. Vol. I, 1996.

Schwartz M., Composite Materials, Properties, Nondestructive Testing, and Repair. Vol. II, 1997

SPI Composites Institute, Composites Design & Applications Winter 1996, pp. 12-14.

Southfield, MI, to build composite/concrete bridge. Composite Design and Application, 1996.

State of the art bridge provides link for National forest. MMFG profile. Winter 1997.

Teng J.G., FRP-strengthened RC structures, Wiley, NY, 2000.

Tom's creek bridge reopens with composite beams. Strongwell profile. Fall 1997.

West Virginia bridge constructed with plastic rebar. Civil Engineering / February 1997, pp. 11.

Where composites meet the road. Civil Engineering / February 1997.

Whittier R.P., Design and Evaluation of Plastics House of Future, ASME Report 57-A212, December 1957, 13 pp.

WTEC, World Technology (WTEC) Monograph, Editor Karbhari V.M., 1999. Loyola College.

Glossary of FRP Composites & Other Related Terms

<http://www.mdacomposites.org/Glossary.htm#CTE>

<http://www.netcomposites.com/glossary.asp?letter=m>

### **Chapter 3**

Building Code Requirements for Structural Concrete (ACI 318-95) and Commentary (ACI 318R-95), American Concrete Institute.

FSEL-DAS, Data Acquisition Systems, Ferguson Structural Engineering Laboratory, The University of Texas at Austin, 1993.

(Instruction Bulletin B-127), Strain gauge test data, TML, Tokyo Sokki Kenkyujo Co., Ltd., 1997.

Measurements Group, Inc, Precision Strain Gages, Engineering data sheet, Measurements Group, Inc., 1997.

#### **Chapter 4**

Fibergrate Composite Structures, Inc., Technical Design Data.  
<http://www.fibergrate.co.uk/dynaform.htm>

LEAF, Linear Elastic Frame Analysis, Computer program for the analysis of frame structures. CFI Scientific Software, Austin, Texas, 1996.

#### **Chapter 5**

Fibergrate Composite Structures, Inc., Technical Design Data.  
<http://www.fibergrate.co.uk/dynaform.htm>

Isis Report, Structural Composites, Inc., CFRP Laminates for Bridge Strengthening, October, 2000.

LEAF, Linear Elastic Frame Analysis, Computer program for the analysis of frame structures. CFI Scientific Software, Austin, Texas, 1996.

#### **Chapter 6**

ASCE Manuals and Reports on Engineering Practice No. 63, Structural Plastics Design Manual, Volume 1, 1984.

LEAF, Linear Elastic Frame Analysis, Computer program for the analysis of frame structures. CFI Scientific Software, Austin, Texas, 1996.

#### **Chapter 7**

DERAKANE: <http://www.dow.com/derakane/fabricat/tech/pultrus.htm>

Hayes, M.D., Characterization and modeling of a fiber reinforced polymeric composite structural girder and bridge structure for use in the Tom's creek bridge rehabilitation project. Master thesis, 1998.

LEAF, Linear Elastic Frame Analysis, Computer program for the analysis of frame structures. CFI Scientific Software, Austin, Texas, 1996.

Mosallam, Chambers; Design Procedures for Predicting Creep and Recovery of Pultruded Composites, 50<sup>th</sup> Annual Conference, Composite Institute, The Society of the Plastics Industry, Paper 6-C, 1995.



Strongwell; Development of a design guide for Strongwell's double web I-beam, 2000.

Strongwell structural shapes,  
<http://www.strongwell.com/pult/pultrusion.htm>

The Tom Creek bridge,  
<http://filebox.vt.edu/eng/esm/jlesko/tcb/coverpage.html>

Zureick, A., "Development of large hybrid composite shapes", Georgia Institute of Technology, 1996.

## **Chapter 8**

Dow Chemical Company, DERAKANE Epoxy Vinyl Ester Resins, Technical product information. Form No. 125-00016-396X SMG.

Fiber Glass Systems, Inc., <http://www.onr.com/star/>

LEAF, Linear Elastic Frame Analysis, Computer program for the analysis of frame structures. CFI Scientific Software, Austin, Texas, 1996.

Tankinetics, Inc., <http://www.tankinetics.com/advanced.html>

## **Chapter 9**

LEAF, Linear Elastic Frame Analysis, Computer program for the analysis of frame structures. CFI Scientific Software, Austin, Texas, 1996.

LLAMA, Linear LAMinar Analysis of composite laminates, Computer program for the analysis of composite laminates. CFI Scientific Software, Austin, Texas, 2000.

Star Fiber Glass Systems, Inc., Installation and Applications Practices, Line Pipe, 1996.

Star Fiber Glass Systems, Inc., Installation and Applications Practices, Tubing, 1996.

Star Fiber Glass Systems, Inc., Tubing, Casing, Line Pipe, Fittings, 1997.

## **Chapter 10**

Ambartsumyan, S.A. Theory of Anisotropic Plates, Technomic, Lancaster, PA, 1970.

ASM Handbook Vol. 21 Composites, The Material Information Society, Material Park, OH, 2001.

ASME Boiler and Pressure Vessel Committee, Subcommittee on Fiber-Reinforced Plastic Pressure Vessels, Section X: Fiber Reinforced Plastic Pressure Vessels, 1998, Edition with 1999 Addenda and 2000 Addenda.

ASME, Reinforced Thermoset Plastic Corrosion Resistant Equipment, ASME RTP-1, 1995 Edition, with Addendums ASME RTP-1a, 1995; ASME RTP-1b, 1997; ASME RTP-1c, 1998; ASME RTP-1d, 1998; and ASME RTP-1e, 1999.

Barbero, E.J., Introduction to Composite Materials. Taylor & Francis, 1999.

Findley W.N., Worley W.J., Some static fatigue and creep tests of a glass fiber laminated with a polyester resin AF, Technical Report NO 6389, Engineering Experimental Section, University of Illinois, April, 1951.

FRP Stacks Standard, 2001, ASCE Codes & Standards, Final 4/23/01.

Hollaway L., Polymer Composites for Civil and Structural Engineering, Chapman & Hall, First Edition, 1993.

Iyengar, N.G.R., Structural Stability of Columns and Plates, Chichester, England, 1988.

Jones, R.M., Mechanics of Composite Materials, 2<sup>nd</sup>. ed., Taylor and Francis, NY, 1998.

Krishnamachari, S.I, Applied Stress Analysis of Plastics, A Mechanical Engineering Approach. V.N. Reinhold, 1993.

Leissa, A.W., Buckling of Laminate Composite Plates and Shell Panels, AFWAL-TR-85-3069, Air Force Wright Aeronautical Laboratories, 1985.

Project 0-1892, Inspecting FRP Composite Structures with Nondestructive Testing, joint research project, Texas A&M and The University of Texas at Austin.

Ramirez, G, Monitoring and Prediction of Damage in Filament Wound Composite Pipes Under Pressure Loading, Ph.D. dissertation, Dept. of Civil Engineering, The University of Texas at Austin, 1999.

Reddy, J.N., Mechanics of Laminated Composite Plates-Theory and Analysis, CRC Press, Boca Raton, FL, 1997.

Timoshenko, S.P., Gere, J.M., Mechanics of Materials, 3<sup>rd</sup> ed., PWS-Kent, Boston, MA, 1990.

Ziehl, P.H., Development of a Damage Based Design Criterion for Fiber Reinforced Vessels, Ph.D. dissertation, Dept. of Civil Engineering, The University of Texas at Austin, 2000.

Vinson, J.R., The Behavior of Sandwich Structures of Isotropic and Composite Materials, Technomic, Lancaster, PA, 1999.

Whitney, J.M., Structural Analysis of Laminated Anisotropic Plates, Technomic, Lancaster, PA, 1987.